UCRL-5829
Nuclear Rocket &
Ramjet Engines, C-86
M-3679 (23rd. Ed.)
This document contains 197 pages.
This is copy 104 of 148 Series A.

UNIVERSITY OF CALIFORNIA
Lawrence Radiation Laboratory
Livermore, California

Contract No. W-7405-eng-48

PLUTO QUARTERLY REPORT NO. 2

(October – December 1959)

By

The Nuclear Propulsion Division Staff

January 8, 1960

DISCLAIMER

DISTRIBUTION
Series A

	Copy No.
LRL Livermore,	
Information Division	1 - 15
Edward Teller	16
John S. Foster	17
C. M. Van Atta	18
Gerald W. Johnson	19
Theodore C. Merkle	20 - 24
Harry L. Reynolds	25
Richard P. Connell	26
William M. Pierson	27
Roger E. Batzel	28
Albert J. Kirschbaum	29
Henry C. McDonald, Jr.	30
W. Blake Myers	31
Albert J. Rothman	32
LRL Mercury, Nevada, Dale Nielsen	33
LRL Berkeley,	
Wallace B. Reynolds	34
Hayden S. Gordon	35
Division of Military Application, Washington	
Brig. Gen. A. D. Starbird	36
AFPR, North American, Downey	37
Air Force Special Weapons Center	38
Air Research and Development Command (RDRAP)	39
Air Research and Development Command (RDZN)	40
Air Technical Intelligence Center	41
Albuquerque Operations Office	42
Argonne National Laboratory	43
Army Ballistic Missile Agency	44 - 45
Assistant Secretary of Defense, R & D (WSEG)	46
Atomic Energy Commission, Washington	47 - 58
Atomics International	59
Battelle Memorial Institute	60

DISTRIBUTION (Contd.)

Series A

	Copy No.
Brookhaven National Laboratory	61
Bureau of Aeronautics	62
BAR, Chance Vought, Dallas	63
Bureau of Ordnance	64
Bureau of Ordnance (AD-1B)	65 - 66
Bureau of Ships	67
Chicago Operations Office	68
Defense Atomic Support Agency, Sandia	69
Defense Atomic Support Agency, Washington	70
duPont Company, Aiken	71
General Electric Company (ANPD)	72
General Electric Company, Richland	73 - 74
Lockland Aircraft Reactors Operations Office	75
Los Alamos Scientific Laboratory	76 - 77
Marquardt Aircraft Company	78
National Aeronautics & Space Adm., Cleveland	79 - 80
National Aeronautics & Space Adm., Washington	81 - 82
New York Operations Office	83
Oak Ridge Operations Office	84
Office of Naval Research	85
Office of the Assistant for Operations Analysis DCS/O	86
Office of the Chief of Naval Operations	87
Patent Branch, Washington	88
Phillips Petroleum Company (NRTS)	89
Pratt & Whitney Aircraft Division	90
San Francisco Operations Office	91
School of Aviation Medicine	92
Union Carbide Nuclear Company (ORNL)	93
USAF Project RAND	94 - 95
U.S. Naval Postgraduate School	96
Warfare Systems School	97
Wright Air Development Center	98 - 103
Technical Information Service Extension	104 - 148

PLUTO QUARTERLY REPORT NO. 2

Table of Contents

PLUTO QUARTERLY REPORT NO. 2*

(October – December 1959)

Lawrence Radiation Laboratory, University of California
Livermore, California

CHAPTER I. TORY II-A

SECTION I. NEUTRONICS

Reactivity Worth of Control Vanes and Vernier Rods

Several ANGIE R-θ calculations have been performed to determine the dependence of the Tory II-A reactivity on control vane angle. Figure I-1 illustrates the results. The reactivity swing is: $\Delta k_{eff} = 0.095$. The curve has been normalized to unit reactivity at a control vane angle of 64° from full-in position, which is a design point for high temperature, high power operation. The average fuel loading was assumed to be 8.38% by weight of OyO_2 in the fueled BeO. This latter value is expected to be reduced in the actual loading distribution in the core, but the change should affect the curve of Fig. I-1 only slightly.

Experimental data from a critical assembly with similar control vanes have appeared in the literature.[1] Their curve was normalized to the computed one at the two extremes. The deviation between them at any vane angle is only ~ 1% in reactivity. Therefore, the ANGIE curves gain added credence.

Figure I-2 shows the reactivity worth of a typical vernier rod as a function of control vane angle. Although only three ANGIE problems were run, the curve describing the full variation was entered, and so must be considered

---

* Pluto Quarterly Report No. 1 is UCRL-5699.

[1] J.R. Stehn, ed., The Physics of Intermediate Spectrum Reactors (U.S. Government Printing Office, 1959), Chapter 15.

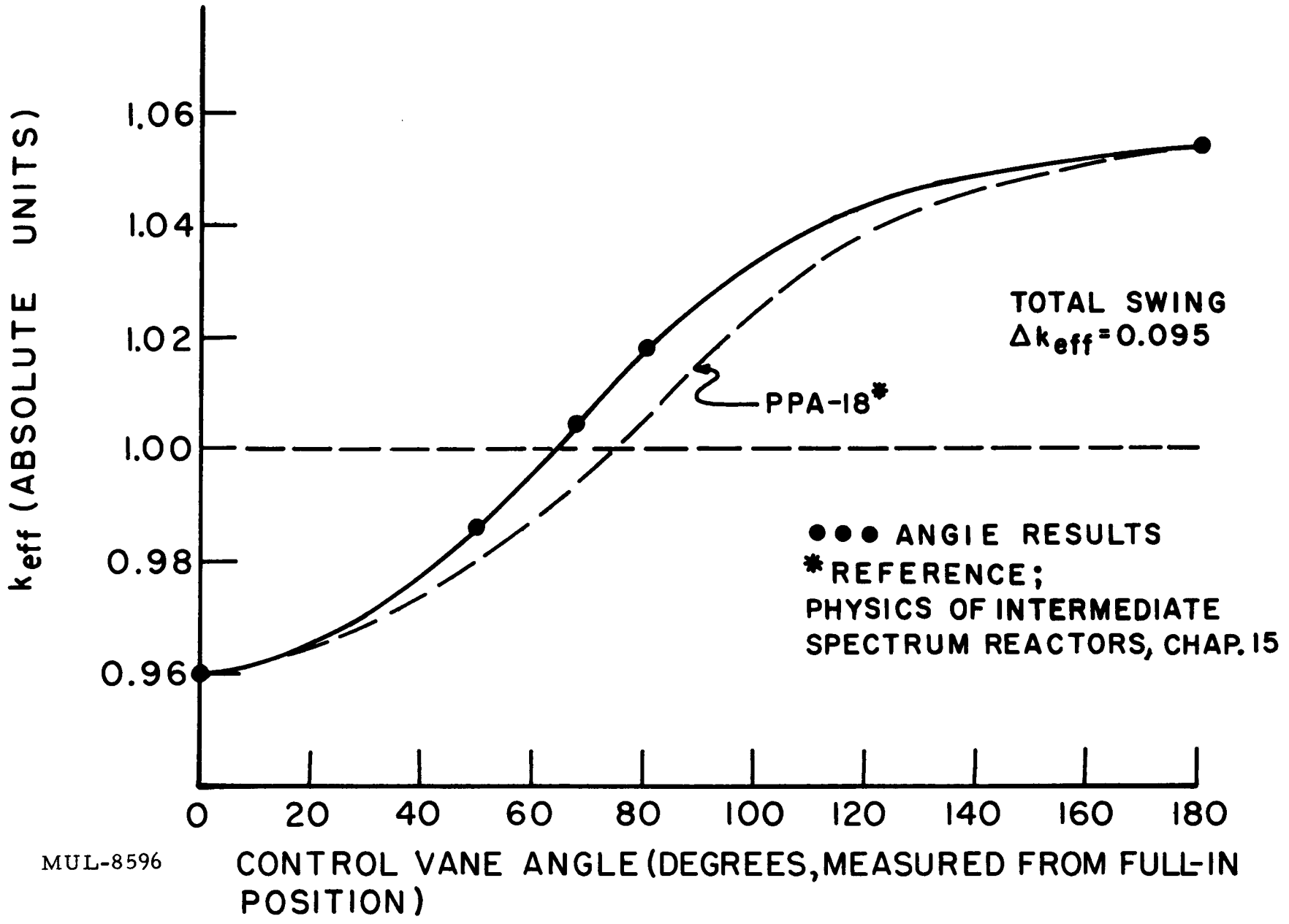

Fig. I-1. Variation of k_{eff} with control vane angle; vernier rods withdrawn.

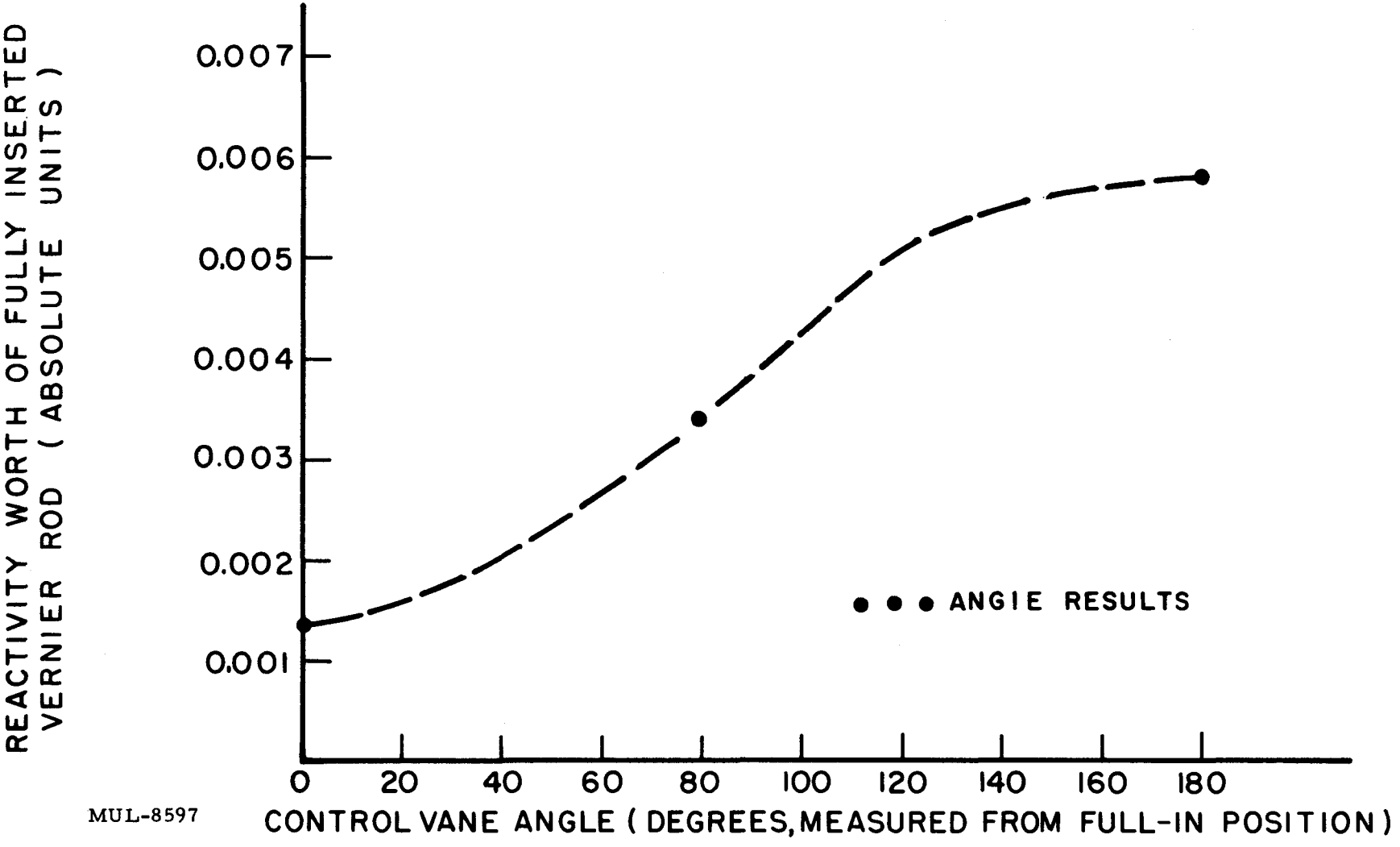

Fig. I-2. Variation of reactivity worth of a vernier rod with control vane angle.

as approximate. At the two extreme angles, the slopes must be zero. It is pertinent to note that at no vane angle is a vernier rod worth more than $1.00. Here, $\beta \simeq 0.0065$. Also, at θ (vane) = 0°, a rod has only 23% of its maximum value.

SPADE – Molybdenum

Since the last Quarterly Report, experimental data on the molybdenum resonance absorption integral has been released by a Harwell group.[1] The results of the SPADE experiments which were given in the previous report are found to be in good agreement. A comparison is shown in Fig. I-3. The resonance integral, extrapolated to zero thickness is shown by the English group to be 19 ± 2.5 barns.

On the same figure (I-3) are shown the theoretical curves based on published resonance parameters.[2] Corrections for foil self-shielding were made for individual resonances.[3]

The parameters describe molybdenum resonances below 700-ev neutron energy. The contribution from unresolved resonances above this energy can be estimated on the basis of the spacing of resonances in the region below 700 ev, and is found to be 1-2 barns. The latter value should be considered suggestive rather than quantitative, since it is in reality a prediction based on a crude extrapolation. Figure I-3 demonstrates a need to postulate ~7 barns from the unresolved resonances in order to bring experiment and theory into accord.

It may be recalled that the use of molybdenum tension rods was rejected because of adverse neutronic effect of the rods. This effect was inferred from the SPADE experiments. It is gratifying to observe very satisfactory agreement between the SPADE results and the Harwell data.

Revised Tory II-A Fuel Loading Distribution

The fuel loading pattern was specified for Tory II-A, where the fueled tubes had a flat-to-flat dimension of 0.295 inch and internal hole diameter of 0.2145 inch. Since its release, the above fuel tube dimensions have been

---

[1] Tattersall, Rose, Pattenden, and Jowitt, AERE-R2887.

[2] Phys. Rev. 99, 10 (1955); also BNL-325, Second Edition.

[3] G. M. Roe, KAPL-1241 (1954).

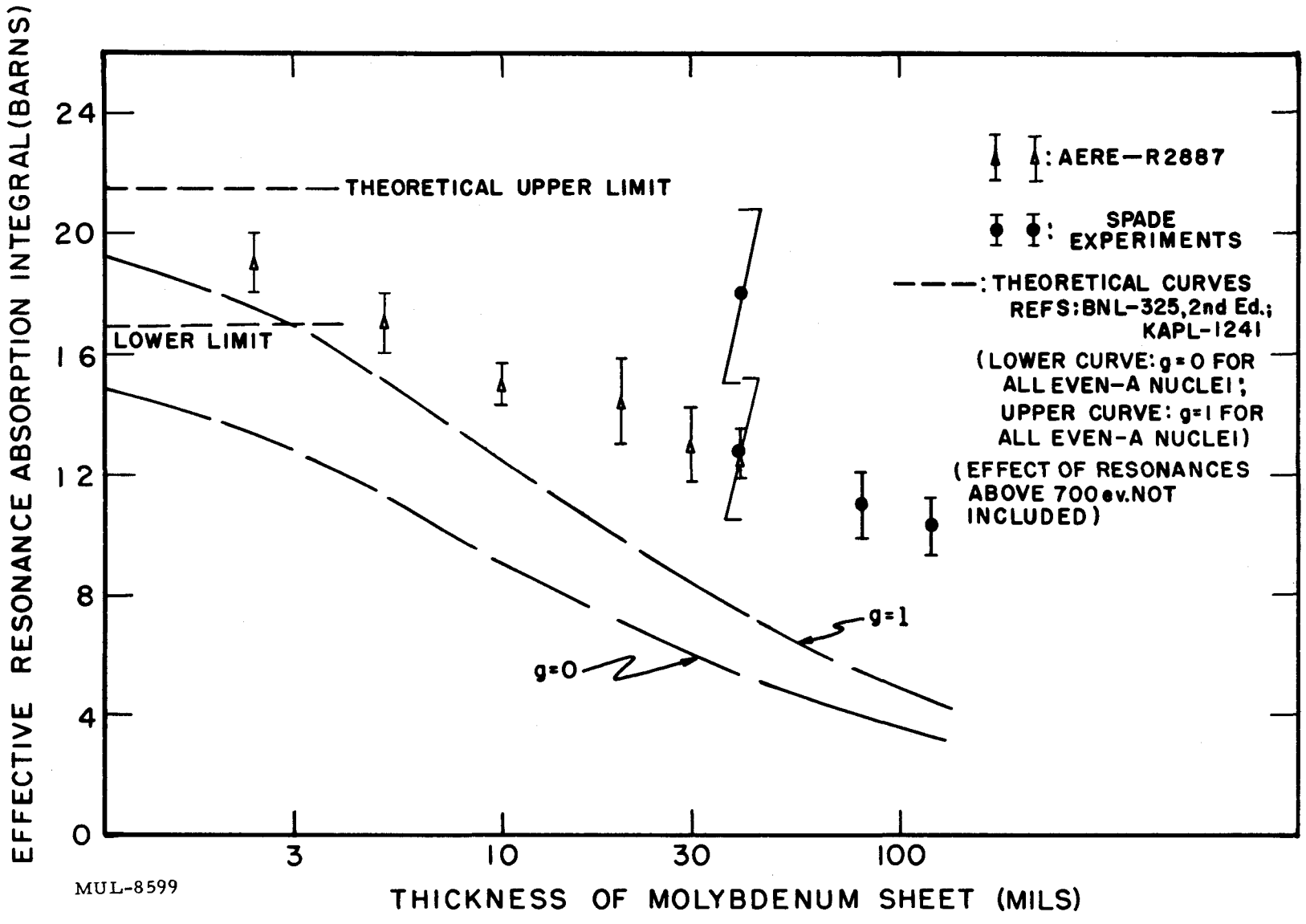

Fig. I-3. Effective resonance absorption integral of molybdenum vs thickness of molybdenum sheet.

changed to 0.297* and 0.2005 inch, respectively. Inasmuch as this has a profound neutronic effect, all important calculations were repeated to determine the most suitable loading pattern for Tory II-A.

The design point was chosen to be criticality at an average core temperature of 1350°K, and control vane angle of 64° from the full-in position with rods withdrawn. The latter value was chosen from considerations of dependence of radial power density on vane angle and uncertainty in prediction of the actual value of reactivity that will be encountered. The nominal active core length is 44.5 inches.

It was found from two-dimensional ANGIE calculations that local cell effects alter power density by about 1%. The dogbones cause a slight rise in power density in their immediate vicinity, while the tension rods act as poisons. Because of the magnitude of the perturbation, the issue was ignored when determining the revised fuel loading distribution. On the other hand, azimuthal variations in power density at the radial periphery of the core were found to be as much as ± 3%. The present distribution takes this into account.

The one-dimensional ZOOM code was employed in determining the proper fuel loading variation for constant radial power density. Figure I-4 shows that weight percent of OyO_2 in the loaded BeO varies from 4.16% to 9.10%. The average in the core is, according to the ZOOM calculation, 7.14%. If one sums over all fueled elements in the actual core as represented by the loading chart, the average fuel loading is 7.16%, which is in very good agreement.

The class assignments were made such that power density variations at any axial station are within ± 2.5% of the average. At the core radial periphery, the radial power density variation across an individual fuel tube could be as much as 15%. The loading was chosen so that the average power density in the tube was within the prescribed limits.

Table I-1 lists the number of tubes in each class. One finds that the mass of OyO_2 is 61.7 kg, 50.7 kg of which is U^{235}. The oralloy contains 93.2% U^{235}.

It must be understood that the present loading distribution will very likely be revised as issues which affect the neutronic picture are clarified. As an example, the 2-mil difference in the flat-to-flat dimension between supplier's and LRL tubes account for $\Delta k \sim 1.6\%$, or a 10% change in fuel content. Other factors when combined create a much greater uncertainty.

---

* This value of 0.297 inch is a supplier's tube specification. LRL tubes have a dimension of 0.295 inch.

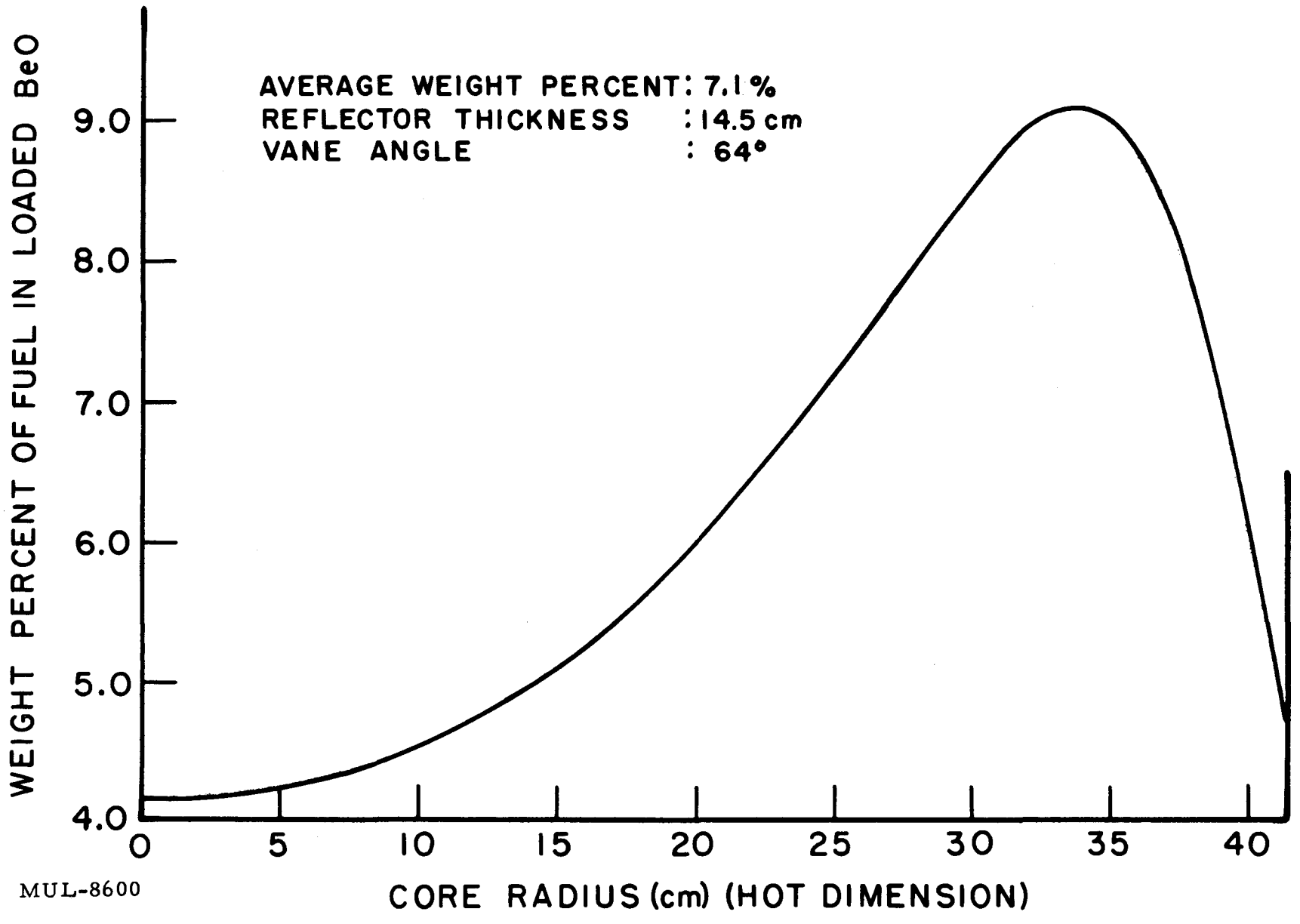

Fig. I-4. Fuel loading pattern for constant radial power density.

TABLE I-1. FUEL LOADING CLASSES

Class No.	Wt% OyO_2	Total density*	No. holes / Class	No. fuel tubes / Class
00	4.25	2.982 g/cc	283	3113
0	4.47	2.986	240	2640
1	4.70	2.991	288	3168
2	4.93	2.996	310	3410
3	5.17	3.001	371	4081
4	5.41	3.007	308	3388
5	5.68	3.013	373	4103
6	5.95	3.019	279	3069
7	6.25	3.025	343	3773
8	6.52	3.032	456	5016
9	6.87	3.040	477	5247
10	7.16	3.047	574	6314
11	7.49	3.055	565	6215
12	7.88	3.064	580	6380
13	8.27	3.072	852	9372
14	8.70	3.080	1048	11,528
15	9.12	3.094	1276	14,036
16	9.53	3.104		
17	10.00	3.115		
		Av: 3.047	Tot: 8623	Tot: 94,853

* $\rho = 0.96 \Big/ \left(\frac{x}{10.9} + \frac{1-x}{3.01} \right)$, where x is the weight percent of OyO_2.

Temperature Effects on Tory II-A

The Tory II-A core will operate with a peak temperature of approximately 2300°F. The effect on reactivity is expected, therefore, to be measurable. The temperature effect is conventionally separated into two parts. One is called the nuclear effect and relates to the change in nuclear parameters because of an alteration of the neutron spectrum in the thermal region. The second is the geometric effect, and is simply due to reactor expansion with a resultant increase in neutron leakage. These will be dealt with separately.

Nuclear Temperature Effect

Since Tory II-A is an epithermal reactor, conventional one- or two-group calculations which assume thermalization of neutrons cannot be employed. Instead, a procedure which involves a multigroup approach is appropriate. Therefore, the ZOOM code was used to generate information on dependence of reactivity on temperature.

The nuclear transfer coefficients which are temperature dependent are computed on the basis of assuming a neutron spectrum which is Maxwellian at low energies and which varies as E^n at higher energies. Experiments on other systems[1] suggest that such a spectrum is in error and that the Maxwellian peak should be reduced in magnitude and shifted to higher energy. However, out of ignorance of the actual spectrum that will be found in Tory II-A, the simple picture is retained and the resultant transfer coefficients were employed.

Figure I-5 illustrates the calculated effect of temperature on k_{eff} for various bare BeO systems of different fuel loadings. In one case (i.e., $BeO/U^{235} = 247$) a reflected system is treated in which the 9-in.-thick cylindrical reflector is maintained at room temperature. One observes a considerable temperature effect for the more thermal systems whereas for $BeO/U^{235} = 120$, $\Delta k_{eff} = 0.25\%$ for passage of the system from 300°K to 1350°K. This value of Δk_{eff} is appropriate to Tory II-A insofar as the nuclear effect is concerned. It is seen to be comfortably small.

Comparison to Hot Box Result

Several BeO systems have been studied at the Hot Box facility. One of these is a bare BeO system with U^{235} and a BeO/U^{235} ratio of ~530:1. Preliminary results appear in UCRL-5699 (Pluto Quarterly Report No. 1). When the geometric effect is removed from the data of the hot run, the results are gratifyingly close to the prediction from ZOOM calculations. The points shown on Fig. I-5 have been corrected for the reduction in self-shielding of fuel as the assembly is heated up.

The value of Δk_{eff} was found in essentially one way. The change in critical buckling due to temparature (and only nuclear effects) is determined. It is necessary to take into account the reduction of foil self-shielding with

[1] A. M. Weinberg and E. P. Wigner, The Physical Theory of Neutron Chain Reactors (University of Chicago Press, 1958).

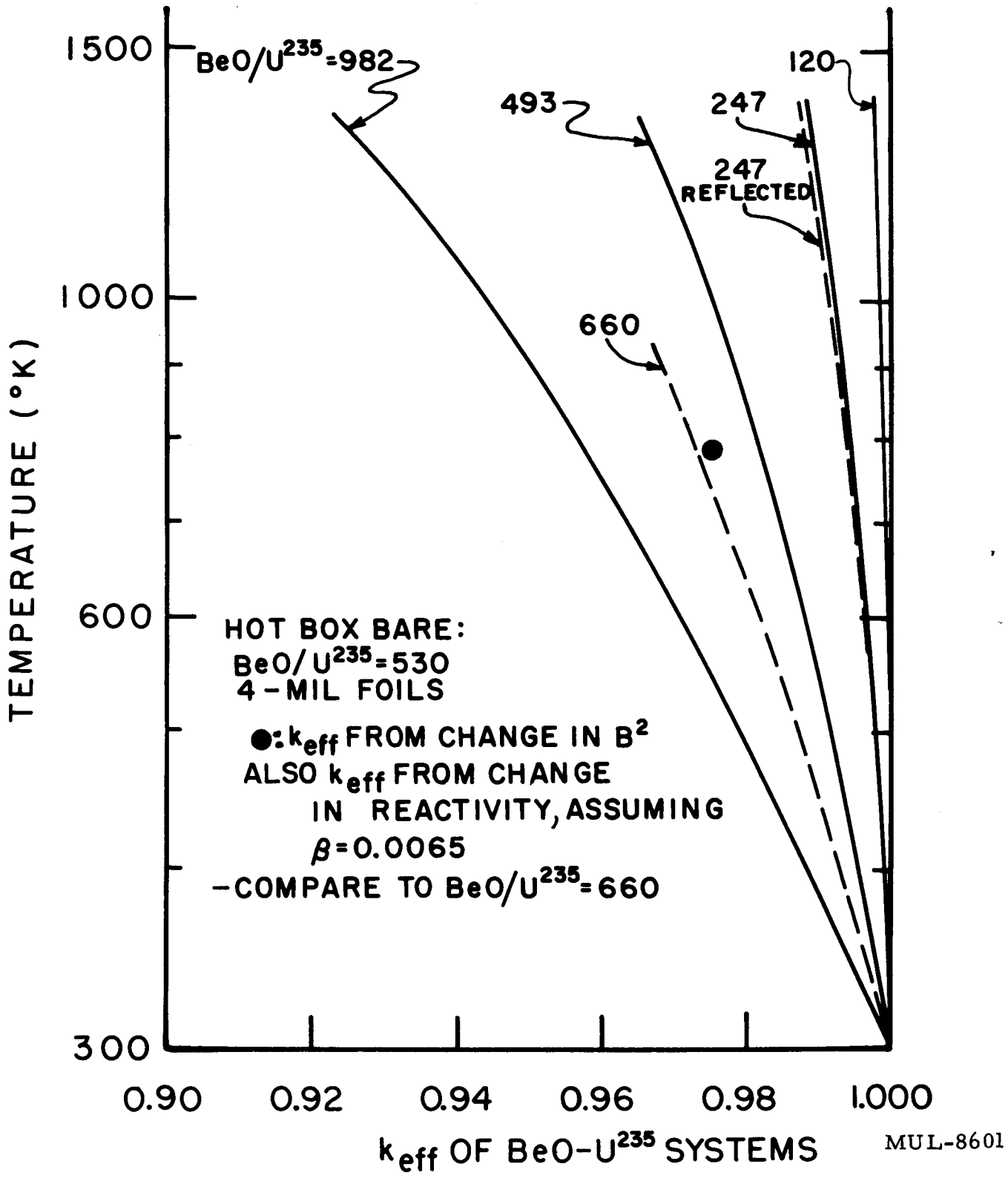

Fig. I-5. Nuclear effect of temperature on criticality of bare BeO systems. Results of ZOOM calculations.

increase in temperature. (This increases the magnitude of the negative effect in the range: 90°-950°F by ~ 0.5 - 0.6% in k_{eff}.)

Also, removal of the geometric effect is straightforward in the case of an assembly which is a rectangular parallelepiped. Given an assembly of dimensions a, b, c, if mass is conserved while dimensions are altered to $a + \delta a$, $b + \delta b$, $c + \delta c$, the neutronic effect is such as to create an assembly of the original density but shortened in the a dimension by:

$$\left[\frac{b(a+2\Delta)^3}{a(b+2\Delta)^3} + \frac{c(a+2\Delta)^3}{a(c+2\Delta)^3}\right] \delta a + \left[\frac{a}{b} + \frac{c(a+2\Delta)^3}{b(c+2\Delta)^3}\right] \delta b$$

$$+ \left[\frac{a}{c} + \frac{b(a+2\Delta)^3}{c(b+2\Delta)^3}\right] \delta c \ .$$

This is derived by application of the rule of constancy of mean-free-paths for criticality. In the present case the overall reactivity change is 3.0% after accounting for reduction in foil self-shielding. Of this, 22% is due to geometry and 78% is due to the nuclear effect. Therefore, Δk_{eff} (nuclear) = −0.0234 for $\Delta T = 860°F$.

Another related approach involved calibration of vanes and determination of the change in criticality in dollars. Here, also, estimates must be made for reduction of foil self-shielding and geometric effects. They are essentially those outlined in the previous paragraph. In UCRL-5699, the nuclear effect, before the self-shielding reduction correction was made, was shown to be $3.04.

The two methods are not truly independent, for the determination of change in reactivity is based on the assembly length. However, during a hot run, the variation of supercriticality with temperature can be determined at intermediate temperatures. Nevertheless, the two methods are related through the value for β. The value derived which brings the two values for Δk (nuclear) into agreement is: $\beta \simeq 0.0065$. It was hardly necessary to perform a hot run to find β. One could, with a cold assembly, find it by calibrating a fine vane both in dollars and in terms of ΔH_c (i.e., change in critical height). Then with ZOOM, one can find $\Delta k_{eff}/\Delta H_c$ which immediately leads to β. It is gratifying to find a value of β which is so reasonable. The relative worth of delayed neutrons with respect to fission neutrons tends to raise β to ~0.0070 but the (n, 2n) effect should reduce it to ~0.0064.

The Hot Box value for Δk_n, shown in Fig. I-5, is 10% below the value predicted by ZOOM. The experimental value is accurate to ~ ± 15%. In addition, extensive calculations are required to appraise effects of such perturbing objects as the stainless steel sheets which enclose the foils, the low-mass table, and the vane guide system. The comparison is therefore preliminary.

Geometry Effect

Tory II-A is expected to operate at an intermediate vane angle of 64° from the full-in position. This is neutronically equivalent to a graphite reflector of 14.5 cm thickness. An equivalent bare cylindrical reactor can be found by fitting ZOOM's radial power density near the center to a power density appropriate to a bare cylinder (i.e., $J_0(2.405\ r/R_b)$). One finds $R_b \simeq 55$ cm. Also, $Z \simeq 130$ cm, as found from ANGIE two-dimensional comparisons to ZOOM results. It is shown that the effective change in length, Z, is:

$$\delta Z_{eff} = -\left[2Z/R + 0.587\left(\frac{Z+2\Delta}{R+\Delta}\right)^3\right]\delta R - 0.587\ \frac{R(Z+2\Delta)^3}{Z(R+2\Delta)^3}\ \delta Z\ .$$

The value for δZ is easily determined. With a temperature coefficient of expansion of $5.2 \times 10^{-6}\ °F^{-1}$,(*) and $\Delta T \simeq 2000°F$, $\delta Z = 1.35$ cm. The value for δR must be qualified. First, the radial expansion occurs by virtue of front and rear support structure expansion. Also the radial expansion varies with axial position. In addition, the BeO structural members are free to move radially by ~20 mils. A reasonable estimate for δR is ~155 mils or 0.39 cm; however, the core-reflector gap is reduced as the core expands radially, so that streaming losses are reduced. As a consequence, the closing of the gap reduces the cost in reactivity of core radial expansion. The calculation will proceed, disregarding the gap effect, and then the latter effect will be considered independently.

The expression for δZ_{eff} becomes:

$$\delta Z_{eff} = -12.3\ \delta R - 3.2\ \delta Z = -4.7 - 4.3 = 9.0\ \text{cm} = 3.5\ \text{in.}$$

ZOOM calculations show that:

$$\delta k_{eff}/\delta Z_{eff} \simeq 0.0053\ \text{inch}^{-1},$$

so the above effect implies:

$$\Delta k_{eff}\ (\text{geometry}) = -0.019.$$

---

* That is, for BeO.

The closing of the gap will now be considered. SPADE experimental results, after analysis with ANGIE and ZOOM, indicate that for Tory II-A, the cost in reactivity, per inch of radial gap, is:

$$\delta k_{eff}/\delta R_{gap} \simeq 0.030 \text{ inch}^{-1}.$$

In the present case, $\delta k_{eff}^{gap} \simeq + 0.0047$. As a consequence,

$$\Delta k_{eff} \text{ (geometry)} \simeq - 0.019 + 0.005 \simeq - 0.014.$$

The overall temperature effect, therefore, is expected to be:

$$\Delta k_{eff} \text{ (nuclear + geometry)} = - 0.017.$$

In light of approximations made, a suggested uncertainty would be:

$$\Delta k_{eff}^{temp} = - 0.017 \pm 0.009.$$

Results from ZOOM and ANGIE Calculations

The codes should be expected to predict reasonably the nuclear temperature effect, since the comparison to Hot Box data was satisfactory. ZOOM-Tory II-A results give: Δk_{eff} (nuclear) $\simeq - 0.006$ which, although it is small, is about twice the size of the predicted value. Since the discrepancy in absolute units is small, there is no great need for concern. However, it deserves further attention.

The geometry effect is not treated satisfactorily by the codes because of the failure to handle radial gaps properly. It is surprising that the ZOOM and ANGIE codes give $\Delta k_{eff}^{temp} \simeq - 0.009$, which is a reasonable value.

Conclusion

The effect on reactivity of Tory II-A in going from room temperature to 1350°K (average core temperature) is:

$$\Delta k_{eff}^{temp} = - 0.017 \pm 0.009.$$

Of this, $- 0.0025$ is due to the nuclear effect. The remainder is attributed to geometric expansion of the core. The closure of the gap acts to compensate the core expansion by adding $\Delta k_{eff} \simeq 0.005$ to the gross geometry effect of $\Delta k_{eff} \simeq - 0.019$.

SECTION II. AIR FLOW CONTROL SYSTEM

Introduction

The Tory II-A air flow control system must provide the capability of performing all steady-state and transient studies which are anticipated during reactor operations. As outlined in UCRL-5465,[1] during a typical full power run the air flow control system must be capable of scheduling the reactor air flow rate such that:

(1) The reactor can be brought to equilibrium at full design temperature with power level in 10 Mw range.

(2) The reactor power level can be programmed from 10 Mw to full design power level while maintaining core temperature constant at full design temperature.

(3) The core fuel element temparature can be maintained constant to within several percent at full design temperature while holding full design power level.

(4) The reactor power level can be programmed from full design power to 10 Mw in 15 seconds while holding core temperature constant.

To fulfill the above specifications, it is required that the air flow control system be capable of doing at least the following:

(1) Take the air flow rate up to approximately 50 lb/sec under manual control in a period of several minutes (using the high pressure air supply).

(2) Take the air flow rate from 50 lb/sec to full design flow rate in a period of 15 seconds under automatic control.

(3) Take the air flow rate from its full design value to 50 lb/sec in a period of 15 seconds under automatic control.

(4) Hold flow rate constant to within 1% of the demanded value at full design flow rate.

When considering a "typical" Tory II-A full power run, the above specifications represent somewhat of an overdesign; however, during emergency shutdowns or in accident situations, these "fast" programs are actually quite realistic.

In addition to the specifications listed above, a general requirement is that the frequency response of the air flow control system must be at least a

[1] R.E. Finnigan, Control Concepts for Nuclear Ramjet Reactors, UCRL-5465, Feb. 1959.

decade below that of the power control system in order to eliminate interactions between the two control loops. This selection of values has not been chosen arbitrarily. It is necessary that the power control system have a fairly fast small-signal response in order that

(1) it may maintain the desired power level in the face of fast reactivity perturbations,

(2) it will be insensitive to process changes, i.e., variation in reactor parameters or reactor power level.

On the other hand, it is desirable to have a relatively slow responding flow control system. It will be shown that there exists in the flow control process a sizeable transportation lag which presents a stability problem if one attempts to get a fast responding closed-loop system. Examination of the transient requirements listed above show that a fast transient response is not required in this system, since the normal input is a relatively slowly varying ramp function. Since the small-signal frequency response of the power control system is approximately 10 cycles/second, it is required that the small-signal frequency response of the flow-control system be 1 cycle/sec or less. It will be shown that a closed-loop frequency response of about 1.0 cycle/sec is easily obtained and satisfies all specifications given above.

Description of the Tory II-A Air Supply System

Figure I-6 shows in simplified schematic form the Tory II-A air supply system. Included in this system are the following major components:

(1) Tank Farm – This facility is capable of holding approximately 120,000 lb of air at 3600 psia.

(2) Compressors – Two compressors are used to charge the tank farm to the desired pressure.

(3) Blower – Two blowers are provided which can continuously deliver low pressure air at rates up to 25 lb/sec.

(4) Shut-off Valves – Two gate-type, electrically actuated shut-off valves (AV-1, AV-2) shut off the air supply upstream of the pressure control valves during charging and prior to blowdown.

(5) Pressure Control Valves – Two electro-hydraulically actuated pressure control valves (AV-3 and AV-4) are used to control the air flow rate delivered by the air supply system. AV-3 is a plug-type valve which has an open area of 100 in^2 when fully opened. AV-4 is a globe-type valve which has an open area of 6 in^2 when fully opened.

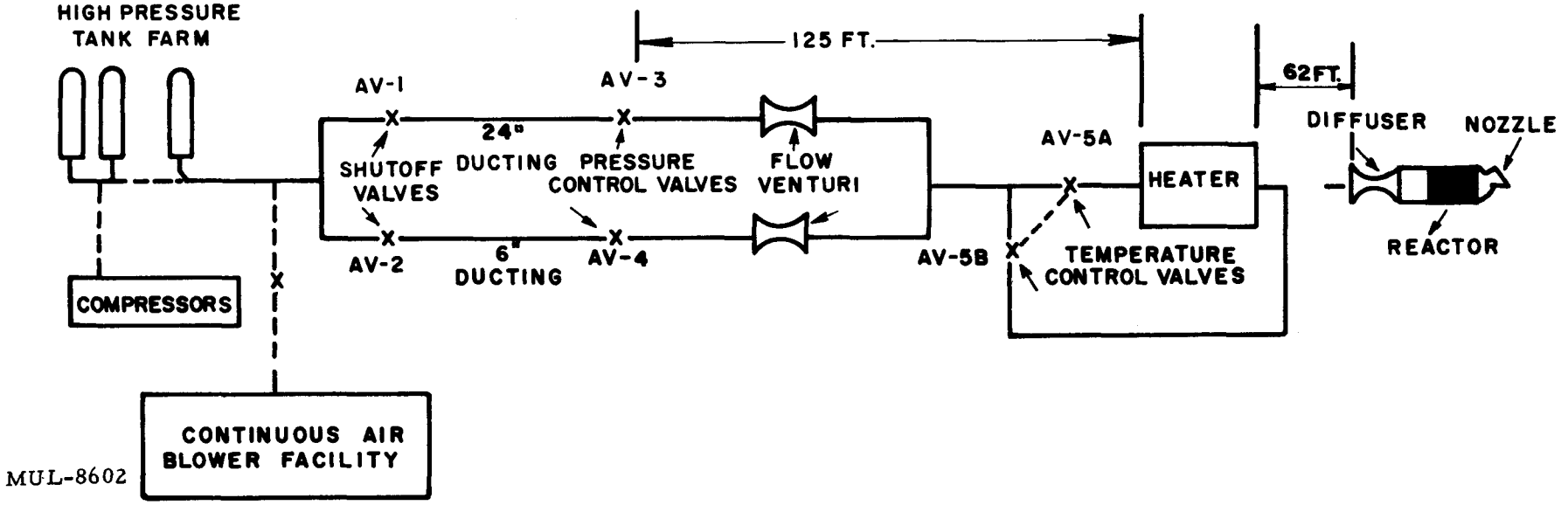

Fig. I-6. Schematic of Tory II-A air supply facility.

(6) Temperature Control Valves — Two electro-hydraulically actuated, butterfly-type valves (AV-5A and AV-5B) maintain control of the air temperature at the reactor inlet by controlling the percentage of the air which passes through the heater. These valves have been sized so that they do not load the pressure control valve upstream (AV-3 or AV-4) nor change the overall air flow rate established by that valve.

(7) Heater — An oil-fired, stored-energy type heater is used to heat the air going to the reactor. The heater, consisting of a bank of heavy steel tubes suspended in a cell, is brought to temperature prior to use but is not run during blowdown.

(8) Flow-venturi — Following the pressure control valves in each air line is a flow-venturi which is instrumented to provide a continuous air flow rate reading during blowdown. This reading is used to control the flow process during manual control and is used to calibrate the diffuser flow rate indication during automatic operation.

(9) Diffuser — A convergent-divergent nozzle has been placed between the heater and the reactor. The diffuser has two major functions:

(a) It serves to isolate the reactor from the air supply when maintaining choked flow in the diffuser section, effectively preventing interaction between the power level and flow control systems.

(b) It gives a more desirable velocity profile at the reactor inlet, minimizing any tendencies to starve certain sections of the core.

(10) Pressure and Temperature Transducers — Multiple pressure and temperature transducers are mounted at the diffuser inlet to provide signals which can be used for closed-loop control of the flow process.

(11) Exit Nozzle — A convergent-divergent exit nozzle is located at the reactor exit. It serves to raise the reactor exit stagnation pressure and aim the high velocity air stream to an angle of 30° above the horizontal, thereby minimizing site contamination.

(12) Ducting — A considerable amount of ducting is used to connect the components within the control loop. There is 125 ft of ducting between the pressure control valves and the heater and 62 ft between the heater and diffuser inlet. These lengths have significance when considering system stability since they introduce transportation lags in the forward control loop.

(13) Air-bleed Valves — Two pop-off air-bleed valves are provided downstream of the pressure control valves in the 24-in. air line to help prevent over-pressuring the downstream components (ducting, heater, reactor).

Control Philosophy

As with the power level control system the most stringent requirement placed on the air flow control system is that of reliability. Failure of this control system can cause loss of the test facility as well as the reactor itself. It is recalled that the power control system reliability problem was solved to a great extent by providing a number of control elements individually actuated. Then loss of any single control element would not cause a major accident. Such a solution cannot be realistically applied here since there is only one control element (the large pressure control valve) used during high power runs. Malfunction of this element presents serious problems: If the valve were to suddenly fail to the full open position, over-pressurization of the test facility and the reactor inlet would almost certainly follow with the likelihood of major damage to both. If the valve were to fail shut on a high power run, overheating of the core components would occur before the auxiliary pressure control valve can be brought on the line or the power "dumped" to a safe value. It can be seen that this system must, if possible, be at least as reliable as the power control system since it is capable of doing damage not only to the reactor but the facility as well.

Because of the single control element normally used for flow rate control, it has not been possible to entirely solve the reliability problem with this system. However, several features have been included in the control actuation philosophy which help to make the system more reliable:

(1) Use of the larger pressure control valve for normal control of air flow rate with the smaller valve (separately actuated) being kept on standby throughout reactor operations.

(2) Provision of a servo-actuation subsystem for normal control of each pressure control valve with an override actuation subsystem available for backup in the event of servo subsystem component failures (e.g., failure of servo-valve).

(3) Provision of multiple transducers to detect accident situations and fast electronic circuitry to effect a hydraulic holding action in the pressure control valve subsystem when an accident situation has been detected.

Control System Design and Analysis

A. Modes of Control

There are three modes of control of the air flow control system: manual, automatic, and manual override. These modes are next briefly described.

(1) Manual Control Mode — In this mode, control of the air flow rate is maintained by the operator who programs the position demand of either pressure control valve. Actuation of the valve is accomplished by means of an electro-hydraulic servo subsystem which employs position feedback.

(2) Automatic Control Mode — Control of the flow rate is maintained by means of conventional feedback control methods in the automatic control mode. The operator programs the desired air flow rate and the pressure control valve which has been selected is automatically positioned so as to maintain this flow rate. Only pressure control valve AV-3 is intended for use in the automatic control mode.

(3) Manual Override Control Mode — In this control mode the operator is able "manually" to individually open-loop position either pressure control valve using on-off electro-hydraulic actuation methods. The pressure control valve is actuated by the same actuator as in normal servo control, but the actuator is driven by solenoid valves which are capable of overriding the servo-valve normally used. When in the override mode there are three functions that can be performed: (1) close slow, (2) open slow, and (3) hold. With these three functions the operator is capable of attaining and holding (to within several percent) any desired flow rate.

The control system can be placed in the override mode in several ways:

(1) Operator action.

(2) Whenever the error signal of the pressure control valve subsystem indicates an accident situation. During normal transients this error signal has a predictable low value. Sudden movements of the valve could be caused by malfunction of components within the valve subsystem or by noisy or faulty inputs to the subsystem. Either situation is detected by observing the valve error signal.

(3) Whenever the rate of change of pressure at the diffuser inlet exceeds preset variable set points, coincidence (2 of 3) safety circuitry can be used to effect the override action.

B. Control Elements

The air flow control system normally uses the large pressure control valve (AV-3) to maintain the desired air flow rate, except at very low flow rates where the smaller pressure control valve (AV-4) is used. Either valve is capable of being operated in the manual or automatic mode but it is not expected that AV-4 will be used in automatic control and the valve has not been

designed for such operation. It will be used only to attain low flow rates which are not within the resolution of the large valve.

Figure I-7 shows a plot of the stroke vs effective area for control valve AV-3. When maintaining choked flow through the valve, flow rate is proportional to valve area (assuming inlet pressure and temperature constant), so the plot shown indicates the control effectiveness of the valve. Of considerable significance in the design of the flow control system is the known region of operation of this control element. During a typical Tory II-A full power run, the control valve is used over less than 15% of its total stroke and is used a high percentage of the time at displacements around 10% of full stroke. A 1% error in positioning the control valve (0.05 in.) can produce a flow error of 80 lb/sec. Stated differently, the gain of the pressure control valve when operating at full tank pressure is 1600 $\frac{\text{lb/sec}}{\text{in. stroke}}$. When the large nonlinear forces which act on the valve are considered, the arguments for automatic control of air flow rate become quite decisive. This subject will be treated in more detail below.

At the time of writing, neither the valve-flow characteristic (stroke vs effective area), nor the dynamic characteristics are known for the small pressure control valve (AV-4).

C. Design of the Pressure Control Valve Actuation Subsystem

The pressure control valve subsystems are being provided by an outside contractor, built to LRL-approved specifications. Because the specifications had to be written before a comprehensive systems study could be carried out on the flow control system, some changes in the control valve actuation subsystem are planned after delivery of the valve. The design outlined below includes the intended LRL modifications.

1. Large Pressure Control Valve (AV-3)

The following are the requirements which the large pressure control valve actuation subsystem must fulfill, whether used as a simple position feedback system in the manual mode, or as an inner loop of the overall flow control system in the automatic control mode:

(1) Position the pressure control valve such that a linear relationship exists between position demand voltage and valve effective area. It is desirable that the nonlinearity be less than 5% in the range of automatic control, and the resolution better than 0.1% of total effective area.

(2) Possess a small-signal frequency response which is variable from 1 to 3 cps (variable with gain setting).

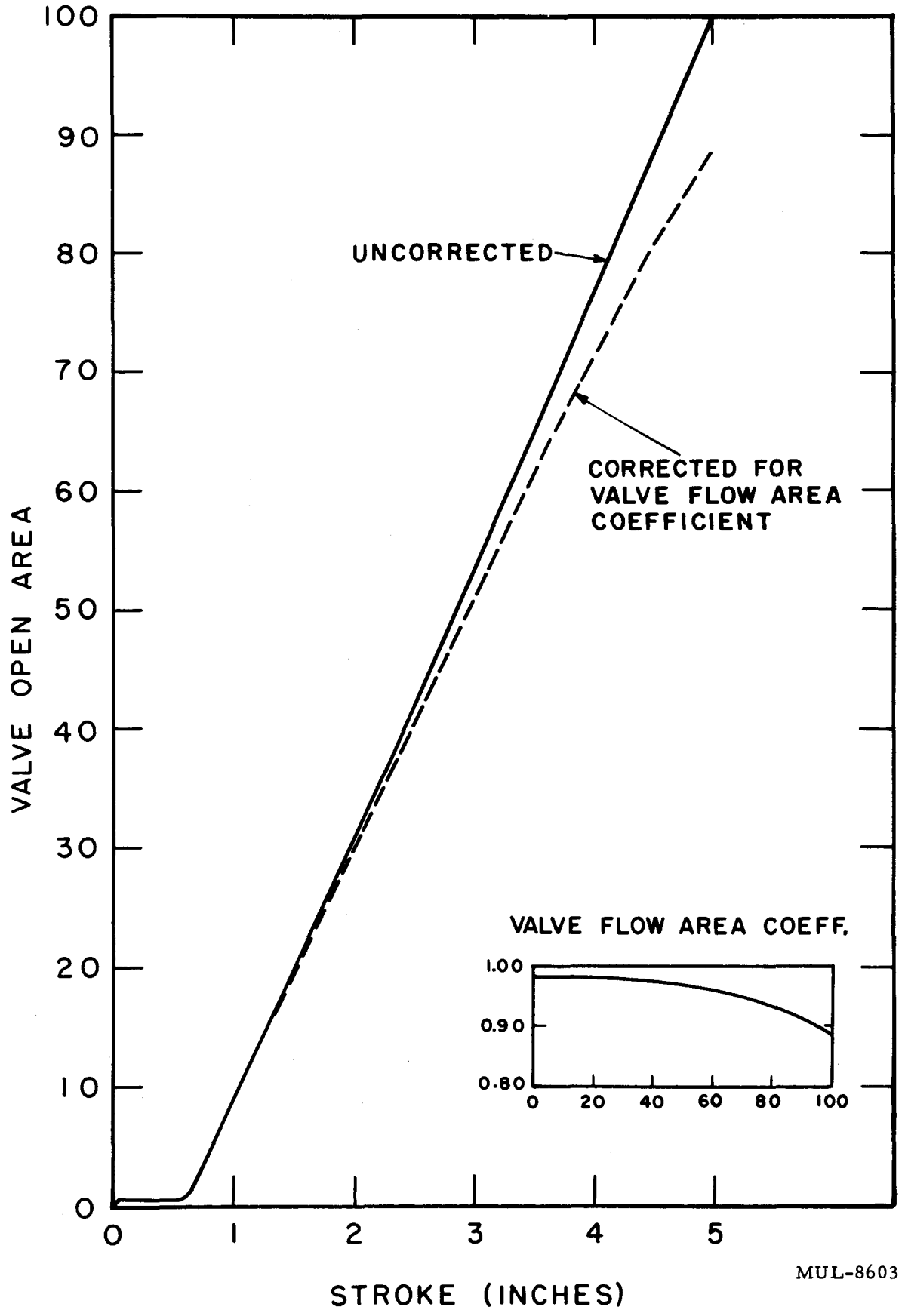

Fig. I-7. Plot of effective area vs stroke for 24-inch pressure control valve.

(3) Show less than 12% overshoot to a step displacement input.

(4) Possess an orifice limited saturation velocity which gives a full stroke period of 8 to 10 seconds (time from full open to full close).

(5) In the manual override mode, it is required that the valve stroking time be 14 to 16 seconds in either direction. In the override-hold function, it is required that the value drift be less than 0.5% full stroke/second with a closing force on the valve of 30,000 lb.

To provide the high stiffness required, a conventional electrohydraulic position servo was selected by the contractor. A three-stage, linear flow control servo valve is used to drive a hydraulic cylinder which actuates the pressure control valve. A linear relationship between actuator position and valve area is obtained by appropriate shaping of the valve contour. A cable-driven, precision-potentiometer is used for position feedback and indication. By appropriate choice of design parameters, the selected system can fulfill all the requirements listed above. The resulting linear numerical transfer function that relates valve effective area A_v (in^2) to the area demand voltage V_D is

$$\frac{A_v}{V_D}(s) = G_V(s) = \frac{4(1+s)}{\left[1 + \frac{1.4s}{12.9} + \left(\frac{s}{12.9}\right)^2\right]\left[1 + \frac{s}{1.12}\right]} . \qquad (1)$$

2. Small Pressure Control Valve (AV-4)

The following are the requirements which the smaller pressure control valve actuation subsystem must fulfill:

(1) Position the control valve in a quasilinear fashion over its entire stroke with a resolution better than 1% of full stroke.

(2) Show less than 20% overshoot to a step displacement input.

(3) Possess an orifice limited saturation velocity which gives a stroking time (full close to full open or vice versa) of approximately 1 second.

(4) In the manual override mode it is required that the valve stroking time be 5-8 seconds. In the override-hold function, it is required that the valve drift be less than 5% full stroke/second with maximum closing force exerted on the valve.

Again, because of the high stiffness requirement, the contractor selected a conventional electrohydraulic position servo similar to that used on the large pressure control valve. The dynamic characteristics of the actuation subsystem are unknown at the time of writing, but are not critical since this system will only be used in the manual mode.

D. Design of the Automatic Control System

The general requirements on the automatic air flow control system were given in the Introduction. They are restated here in a more specific manner:

(1) The flow control system must possess an adequate margin of stability over the flow rate range 50 lb/sec to 1000 lb/sec.

(2) The flow control system should have a small-signal frequency response ($-90°$ phase shift point) of approximately 1 cps.

(3) The system should show less than 10% overshoot to small step functions.

(4) The steady-state error with a 15-second ramp input should be less than 0.5% of full design flow rate.

The basic control system configuration which has been selected is that shown in Fig. I-8 in simplified block diagram form, where

$V_{\dot{W}_{Demand}}$ = voltage proportional to demand air flow rate (volts)

$V_{\dot{W}}$ = voltage proportional to air flow rate at diffuser inlet (volts)

$\epsilon_{\dot{W}}$ = voltage proportional to air flow rate error (volts)

V_D = voltage proportional to pressure control valve area demand (where $V_D = V_D' + V_D''$) (volts)

A_v = effective area of the pressure control valve (in^2)

P_{T_0} = stagnation pressure at the diffuser inlet (psia)

V_A = voltage proportional to valve area demand before linearization (volts)

$V_{i.c.}$ = initial condition for compensation network (volts)

P_0 = tank farm air storage pressure (psia)

T_0 = tank farm air storage temperature (°R)

The various components and subsystems have the linearized transfer functions indicated. The numerical transfer function for the flow process can be shown to be

$$G_P(s) = \frac{P_{T_0}}{A_v}(s) = \frac{0.273P_0}{\sqrt{T_0}} \quad \frac{e^{-0.155s}}{(1 + 2.1s)} \; . \tag{2}$$

The transfer function for the pressure transducer used for feedback of air flow rate is

$$K_f = 0.161 \text{ volts/psia.} \tag{3}$$

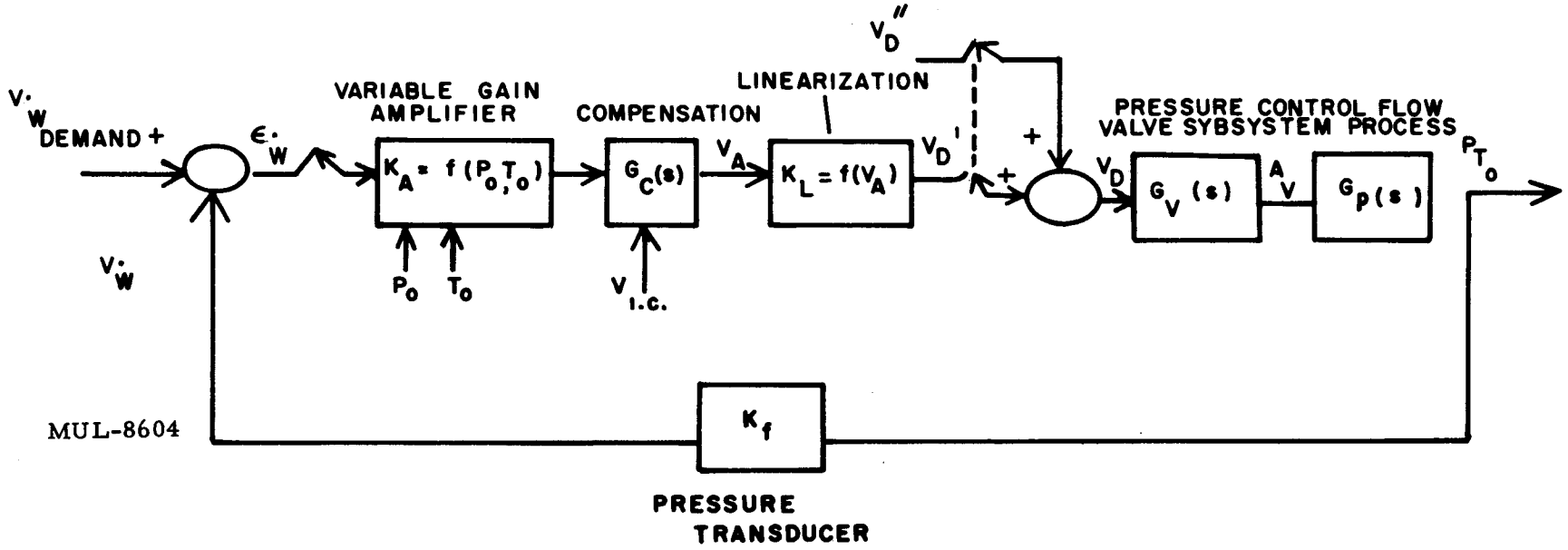

Fig. I-8. Air flow control system block diagram.

Assuming the valve characteristic is linear when delivered, $K_L = 1$ (i.e., no function generator compensation required). V_D'' serves to provide any dc bias required in the linearization process.

The open loop transfer function of the flow control system is

$$G(s) = K_A\, G_c(s)\, K_L\, G_V(s)\, G_p(s). \tag{4}$$

Since $G_p(s)$ contains a $P_0/\sqrt{T_0}$ term, the gain of the loop and the system performance would vary with tank farm pressure and temperature unless compensated for elsewhere. To offset this effect, choose

$$K_A = K\sqrt{T_0}/P_0. \tag{5}$$

Using standard servo techniques the gain term K and the compensation $G_c(s)$ are chosen as follows:

$$K = 45.6 \text{ volts/volt}$$

$$G_c(s) = \frac{6.3}{s}\ \frac{(1 + 2.1s)}{\left(1 + \frac{s}{0.01}\right)}\ \left(1 + \frac{s}{0.5}\right)\ (1 + s). \tag{6}$$

The compensation shown is accomplished by means of a lag-lead network and a proportional plus integral network.

The closed-loop frequency response of the resulting system is shown in Fig. I-9 while the response to a step function input is shown in Fig. I-10. It can be seen that $-90°$ phase shift occurs at $f = 0.9$ cps, and the overshoot to a step function is less than 10%. The synthesized control system has a zero steady-state error to a step change in flow rate demand, but has a finite steady-state error, $\epsilon_{\dot{W}_{ss}}$, to a ramp-type flow rate demand. With a ramp input $V_{\dot{W}_{Demand}}(t) = Rt$, it can be shown that

$$\epsilon_{\dot{W}_{ss}} = \frac{R}{K_0},$$

where

$$K_0 = \lim_{s \to 0} s\, G(s) = 16.1 \text{ sec}^{-1}.$$

For a 15-second ramp function

$$\epsilon_{\dot{W}_{ss}} \cong 3 \text{ lb/sec},$$

which is less than 0.5% of full design flow rate.

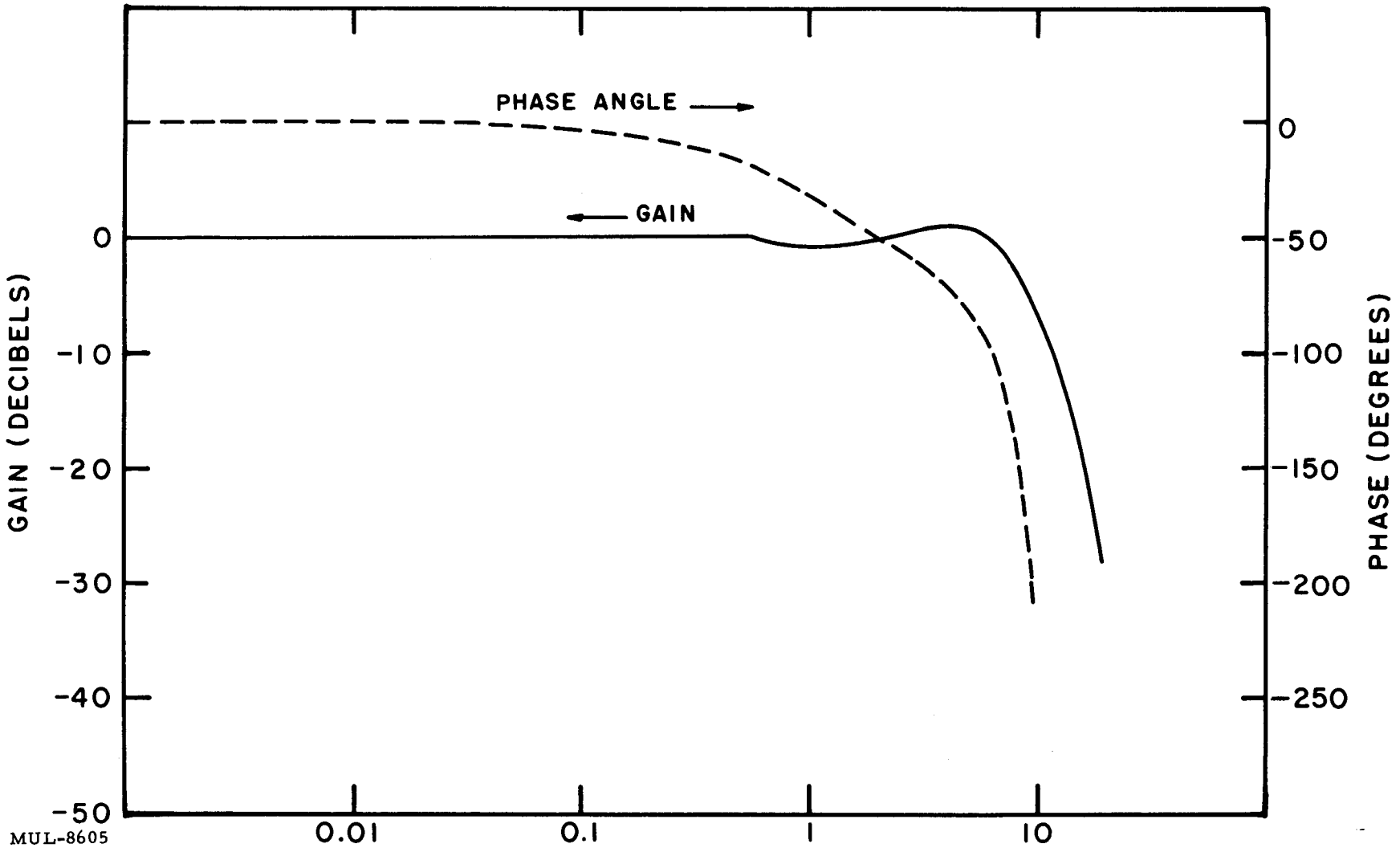

Fig. I-9. Closed loop frequency response of the air flow control system.

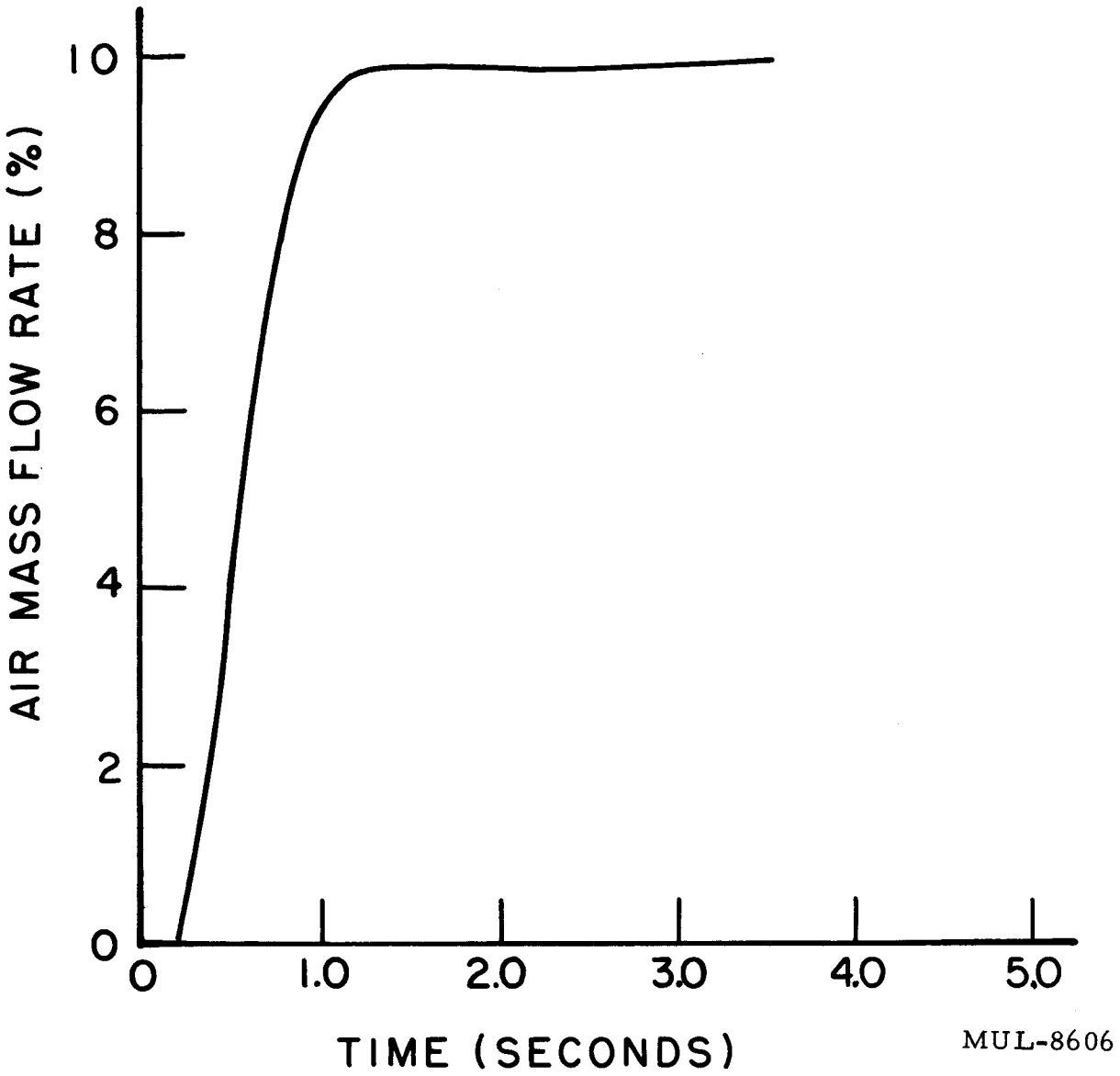

Fig. I-10. Air flow rate control system step response.

SECTION III. INSTRUMENTATION

Introduction

The possibility that the Tory II-A core thermocouple leads might vibrate excessively because of aerodynamic forces has been considered for some time. Until recently it was planned to have webs in the unfueled tubes which carried the thermocouple leads in order to limit the amplitude of these vibrations. Since manufacture of these special webbed dummy tubes might have been somewhat of a problem, it was decided to test for vibration under conditions similar to Tory II-A.

Purpose

(1) To determine whether vibrations could be aerodynamically excited in thermocouples lying in a small air duct.

(2) To determine whether such vibrations, if induced, would interfere with thermocouple life or operations.

(3) To determine the effect of these wires on duct air flow.

Procedure and Results

The results indicate:

(1) That vibrations will not be excited under the conditions we are interested in.

(2) That the wires cause a large flow resistance.

The procedure by which these results were obtained was as follows:

Two 0.067-in.-diam thermocouples were passed in through the wall of an 0.243-in.-i.d. plastic tube, passed through the tube for a distance of 50 inches, and then passed back out through the tube wall. The plastic tube expanded into a plenum chamber containing a metering orifice on one end, and on the other was connected to an air supply. The air flow rate could be controlled by valves upstream and downstream.

One thermocouple junction was connected to a hot plate. Another similar thermocouple, outside the tube, was connected in series opposition to this, and its junction placed at the same position. This compensated for temperature variations in the plate during the test. The null position of a recording potentiometer was placed in the middle of a 10-in. scale, and its sensitivity set to 2.0 mv per 10 inches of deflection. A variation of as little as 10 microvolts, due to possible vibration effects, could thus be detected.

The air was turned on and the flow varied from zero to maximum in about 20 equal steps, and then decreased in a similar number of steps. No vibrations were observed. This procedure was repeated twice more, and in the latter cases the tube was struck with a rubber hammer at each flow rate setting. Vibrations of about one wire diameter were excited by each blow, but were damped out in a fraction of a second.

At no time was any deviation noted in the recorder pen position.

At maximum flow rate a very high pressure drop was noted along the length of the tube. Pressure measurements, under choking conditions, indicated that a Fanning friction factor of 0.00622 could be attributed to the tube alone.

Assuming an isentropic transition across the sections where the couples enter and leave the air stream, the average friction factor along the section containing the couples was computed to be 0.00513.

Conclusions

The results indicate that aerodynamic effects will not interfere with core thermocouples. Vibrations due to external sources could not be sustained for a sufficient length of time to determine whether long term drift, due to externally induced vibrations, will be a problem or not. The low amplitude observed would seem to indicate that cold-work effects will be negligible.

It will be noted that true dynamic similarity was not obtained. This would require both Reynolds number and Mach number ranges held to values expected in the core. However, in this Reynolds number range (10^6), effective dynamic similarity is dependent on Mach number similarity alone for all practical purposes. These results should, therefore, be quite similar to those found in the core.

Maximum Permissible Rod Withdrawal Rate During Manual Startup

Some DANE problems have been run to determine what is a reasonable rate of reactivity insertion for Tory II-A when approaching critical from complete shutdown conditions.

A source strength of 5×10^7 neutrons/sec and a shutdown reactivity of 0.97 was assumed. Several reactivity ramps of various slopes were run. These runs correspond to the physical situation where the operator begins inserting reactivity at a certain rate, and for some reason insertion continues

even though the operator takes his hand off the button. Additional assumptions were (a) no air flow, (b) core at ambient temperature, (c) reactivity temperature coefficient of -1.9×10^{-5} ρ per °K, (d) prompt neutron lifetime of 4.5×10^{-5} sec.

Some of the pertinent information from the DANE outputs is summarized in Table I-2. Because of the negative temperature coefficient the power level vs time curve goes through an early maximum and may be oscillatory in character. "Turn-down" in the table headings refers to this first maximum.

TABLE I-2

Reactivity insertion rate, absolute units/sec	Power level at time of power turn-down (Mw)	Time at which power turn-down occurs (sec)	Core temperature at turn-down (°K)
0.0001	10.9	368	403
0.0005	70.5	75.8	342
0.001	182	38.4	352
0.005	1255	8.1	422

The table shows that for 0.0001 ρ/sec the turn-down occurs 368 seconds after start. This should be ample time to allow the operator to determine that something is wrong.

The manual rod withdrawal system is being designed to allow 0.0001 ρ/sec with the provision of increasing this 3- or 10-fold later if experience with the reactor warrants.

SECTION IV. HEAT TRANSFER

Thermal Stress Compilation

The following is a compilation of expected Tory II-A ceramic part thermal stress loads at design operating conditions. The refinement of analytical techniques and application of more pertinent experimental information are expected to demand modification of some of the listed parameters.

Depending upon the geometry of the element being thermal stress analyzed, classical flat plate or cylindrical elastic theory, with necessary boundary constraints, was applied. It should be obvious to the reader what geometrical and constraint assumptions were used for any specific element.

Since this is a compilation and not a review, the techniques and recipes applied will not be discussed.

The physical properties of BeO that were used in the calculations are as follows:

Young's Modulus, E, $= 45 \times 10^6$ psi

Poisson's Ratio, ν, = 13

Thermal conductivity, $k\left(\frac{\text{watt}}{\text{cm °K}}\right) = -1.3 \times 10^{-4}\left[\bar{T}\,(°F) - 3600\right]$

for 1800°F, $\bar{T}$ = 2400°F

Coefficient of thermal expansion,

$\alpha\,(°F^{-1}), = \left[1.55 \times 10^{-3}\ T\,(°F) + 3.4\right] \times 10^{-6}$

At the Tory II-A design point, the following maximum power densities are expected:

Fuel elements: 19 Mw/ft^3

Inner Links : 1.7 Mw/ft^3

Outer Links : 0.9 Mw/ft^3

The compilation is presented in Table I-3.

It should be noted that the outer links may be the most heavily stressed links in the Tory II-A core. Since it is highly desirable that these elements do not break during operation, further attention will be focused on this problem. It should be possible to develop labyrinth seals which minimize the thermal stress within while balancing pressure across the outer links.

It is obvious that all possible types of elements are not listed in the compilation; however, those that are presented should be representative of the most highly stressed core ceramic components.

TABLE I-3. TORY II-A CERAMIC COMPONENT ELASTIC STRESS

Element	Location (All at X/L = 0.5)	$\bar{T}$ (°F)	ψ	Stress (10^3 psi)
Fuel element	Near center of module	2275	1	20
	Link adjacent, core center	2000	1.2	24
	Link adjacent, core outer row	2000	1	20
	Like above, near rod	2000	1.2	24
	2nd row from core edge, not near rod	2275	1.1	22
Link	Center module (0.180" web)	1900	~0.15	3
	Outer module (0.254" web)	1900	0.28	5.5
Link eye	Center module (0.180" web)	1900	0.7	14
	Outer module (0.254" web)	1900	0.4 - 2.3	11 - 45*

$$\psi = \frac{\text{element elastic stress}}{\text{normal fuel element elastic stress}}$$

* The wide spread of values correspond to uncertainty in adiabatic wall location. The stress is very dependent upon the magnitude of external cooling. With the present design, external radiation and convective cooling indicate that a reasonable stress value is about 15,000 psi.

Thermal Stress in Fuel Tubes Adjacent to Dogbone Links

This work was initiated to study the thermal stresses generated in a fuel tube which is adjacent to one of the links of the core superstructure; the stress in these fuel tubes may be expected to differ from the stress in a fuel tube internal to one of the core modulus, since the outer fuel tubes are convectively cooled on two adjacent hexagonal sides. This convective cooling creates an asymmetrical temperature distribution in these fuel elements and therefore raises the maximum tensile stress at the inner bore of the tube.

The problem was solved analytically for a long circular cylinder with the same inner radius as a fuel tube and an outer radius such as to make the cross-sectional area equal to the area of a fuel tube by finding the asymmetrical temperature distribution and then applying the solutions developed by B.E. Gatewood[1] to find the stresses in such a configuration. This solution

[1] B.E. Gatewood, Thermal Stresses (McGraw-Hill Book Co., New York, 1957), p. 205.

assumes that the heat transferred to the outer edge comes from the inner bore of the tube; the stresses arising from this portion of the solution are then added to the stresses developed in a fuel tube with no outer cooling but with a power density such as to compensate for the heat transferred to the two outer hexagonal faces at steady state. In finding the asymmetrical temperature distribution it is assumed that this distribution is not strongly dependent on the angular coordinate and that the rate of heat transfer at the cooled outer portion is constant. The subsequent analysis is straightforward and follows the equations of Gatewood. Maps of the stress components were drawn from this equation.

The maximum stress is probably of greatest interest. We examine the full power conditions for the Tory II-A reactor.

Inner radius = 0.2748 cm

Outer radius = 0.3924 cm

Power density = 839 watts/cm^3

Coefficient of linear expansion of BeO = $12 \times 10^{-6}/°K$

Coefficient of heat transfer at inner bore = 0.361 watts/cm^2–°K

Coefficient of heat transfer at outer edge

(effective over angle of $2\pi/3$ radians) = 0.284 watts/cm^2–°K

Young's modulus for BeO = 50×10^6 psi

The following value was obtained for maximum tensile stress

$$\sigma = 2.19 \times 10^4 \text{ psi},$$

which can be compared to an equivalent tube with no outer cooling

$$\sigma = 1.61 \times 10^4 \text{ psi}.$$

In conjunction with this study a calculation was made of a tube which was coated with 20 mils of insulation on the outer faces exposed to heat transfer, which gave

$$\sigma = 1.87 \times 10^4 \text{ psi}.$$

In all of the above calculations, the maximum compressive stress was always numerically less than the maximum tensile stress. In the problems with asymmetrical temperature cases, there was a shearing stress $\tau_{r\theta}$ of lower order of magnitude than either the tensile or compressive stress.

All of the above stress numbers must be qualified, of course in terms of the values of the coefficient of linear expansion and Young's modulus; however, the relative values remain unchanged. Also, no account was taken of the variation of thermal conductivity with temperature.

SECTION V. ENGINEERING

Material Selection

Core Support Structure. This structure spans the duct-upstream of the reactor, hence is cooled by air at inlet temperature. Calculations using a conservative value of 0.8 Mw/ft^3 for radiation heating indicate a maximum temperature of 1300°F for the most severe planned operating regimes. The material selected is AM 355. Fabrication is done by welding. Deflection, rather than stress, is the critical design factor, as this component establishes the alignment of the core in the duct.

Tension Rods. A highly conservative calculation has placed the maximum temperature at 1550°F. The material employed is Hastelloy R-235. Deflection is again critical in design because of the beam action of the tubes in supporting the core weight.

Base Plates. The base plates will follow exit gas temperature very closely, remaining a few degrees above it because of radiation heating. To operate in this temperature range (2000°F) the 1/2% titanium-molybdenum alloy has been chosen. Oxidation protection is achieved by a proprietary coating, chromalloy W-2. Plates are 1 in. thick, made by machining a rolled blank. The maximum stress at design conditions, and assuming an unfavorable support condition, is 14,700 psi.

Shroud. The shroud is made of R-235 sheet. The outer cylinder is 0.040 in. thick, reinforced with doublers near the inlet. The inner cylinder and a corrugation between are each 0.015 in. thick. Assembly is by spot welding at the crests of the corrugation. Wiper seals are 0.015-in. R-235, spot-welded to the inner cylinder.

The shroud is well cooled, no part of it exceeding 1400°F. The critical stress is hoop stress occurring near the inlet (the coolest region) and amounts to approximately 50,000 psi.

Experimental Work in Support of Design

Numerous tests and experiments have been performed to investigate design problems and check the performance of prototype parts.

Support Structure. A room temperature test of a geometrically similar mild steel model was performed to measure strains and deflections. Design calculations were substantiated closely, with a few minor modifications indicated.

Base Plates. Stress coat and photoelastic techniques were employed to verify the adequacy of base plate design from the standpoint of strength. An evaluation was made of available protective coating for molybdenum, leading to the selection of W-2 (chromalloy W-2) for use in Tory II-A. Present base plate coating tests are aimed at simulating reactor conditions, i.e., proper geometry, abrasion, fluid velocity, etc.

Tension Rods. Elevated temperature tests of prototype tension rod material have been made by subcontractor. In all cases the Tory II-A conditions were met with a fully adequate margin of safety.

Fuel Element Dimensions. A test assembly was constructed to establish the proper outside dimension for the fuel elements. Fuel elements and structural links were simulated in metal and the problems of tolerance buildup and expansion allowances studied.

Core Assembly

Core assembly procedures have been established and work is under way on the design and fabrication of equipment. Assembly will be done on a modular basis. Each tube module will be built up without structural links or tension rods and the modules subsequently assembled into a core.

The core itself will be assembled in a vertical position, inlet end up. The tension rods are fed upward alongside each module as the structural links are placed in position. After all ceramic parts are assembled, the support structure and shroud are lowered into place. Addition of the pressure vessel with its forward and aft adapter completes the assembly.

Critical Measurements

The first step after core assembly will be a room temperature critical experiment, utilizing the Tory II-A reflector-control assembly.

Procurement Status, Tory II-A-1 Parts

Beryllium Oxide. Contracts are in effect for purchase of raw material and fabricated fuel elements and structural links. UOX grade BeO is employed as the starting material for both components. Dual sources have been established for the fabrication work. In the case of fuel elements one of these sources is the LRL Fuel Element Fabrication Facility.* The first tubes (unfueled) and structural links destined for reactor use are due during December. Evaluation quantities and test parts in both components have already been received.

---

*See Chapter II.

Fuel Element Evaluation

Prototype fuel elements made by the outside supplier are thoroughly tested to check their suitability for Tory II-A conditions. The qualities checked are purity, density, dimensions, physical integrity (cracks, inclusions, etc.), degree and uniformity of fuel loading, high temperature ultimate and fatigue strength, uranium retention and dimensional stability. The supplier has experimented with several different additives and additive concentrations to meet the specific requirements of LRL performance specifications.

A simple three-point modulus of rupture test is used to check mechanical strength. Loading rate is 30 lb/min. Fatigue strength is measured by the same means, employing a 10-minute cycle with 2 minutes at load and 4 minutes at no load. All significant strength tests to date have been run at 2100°F.

Rather severe high density inclusions found in many tubes appear to increase the short-time strength of the material, but are suspected of lowering fatigue strength. One of the objectives in current testing is to evaluate this effect. Data from the strength testing of many lots of material is summarized in Table I-4. Stresses are expressed as calculated by elastic theory though inelastic action may have occurred.

The standard test for fuel retention has been 4 hours at 2732°F in moving dry air. A loss in this test of less than 10% of the uranium present is desired.

TABLE I-4

Loading	Condition	No. of specimens	Mod. rupture, (psi)
Unfueled	Few high density incl.	30	17,730
Fueled	Few high density incl.	88	21,800
Fueled	Severe high density incl.	52	26,200
Fueled	Few high density incl.	52	21,460
Fueled	Severe high density incl.	12	27,150
Fueled	Unknown	9	28,510

Quality Assurance

An inspection line for BeO components is being set up. Nondestructive testing will be performed on 100% of the parts received. Sampling methods for destructive testing are based upon fabrication batches wherever possible. The following operations will be performed.

Nondestructive

Feature inspected	By
Density	Minimum weight
Cracks	Fluorescent penetrant (Zyglo)
Dimensions	Pneumatic gauges
Voids and inclusions	Radiography
Uranium content	DXT
Uranium distribution	DXT

Destructive

Uranium retention	4 hr at 2732°F
Dimensional stability	4 hr at 2192°F
Strength	Mod. of rupture at 2100°F
Purity	Emission spectroscopy

Test Program

Introduction

A program of testing has been planned in support of the Tory II-A core design. The chief purpose of this program is to give prior information about the effect of the physical conditions of operation on the core and adjacent structures. Wherever possible, this information guides core design. Otherwise, it can limit power level, or the rates of change of temperature and pressure during Nevada operations.

The testing problem is to generate the physical conditions to be expected, to apply them to the core components in a controlled manner, and to measure and evaluate the effects. In many instances the work has been done on isolated components of the core. More generally the environment depends on adjacent elements in an unpredictable way and the parts must be tested together in subassemblies. A considerable amount of this work has been done by Marquardt Aircraft Corp. in support of the Tory II-A program.

In addition some materials evaluation work has been done. This work has been done in several places. LRL has undertaken the coordination of the program and the testing that could be done locally. Ceramic modulus of rupture tests at high temperature have been performed.

Some specialized facilities have been developed at LRL, in particular an air atmosphere testing furnace has been built with a 3000°F temperature capability and a 2-foot cubic working space in which parts can be stressed. This furnace has had limited service to the present time because of failures of the molybdenum disilicide heating elements and of the load-transmitting test appurtenances. The furnace is, however, essential for testing parts too big for the ordinary platinum-wound resistance furnaces.

A small amount of testing has been accomplished in support of the Hot Box program.

Tory II-A Testing

A. Structural Tests

1. Shroud Tests

The static cantilever load deflection tests on the core shroud have been completed. The purpose of these tests was to observe the structural performance of the shroud under loading similar to that of the core at room temperature and at 1200°F.

The shroud was subjected to twice the design load while it was heated to 1200°F in the radiant heat facility. The most significant result of this series of tests is that no failure or permanent set could be perceived as a result of this loading.

Due to the type of construction, local strain and deflection data were not intelligible except along the rear periphery. Fortunately, this is the region of greatest interest since this is the portion immediately supporting the core.

The most significant results, copied from the interim test report, are given below.

Run	Load (lb)	Temp (°F)	ΔD_1	ΔD_2	ΔL_1	ΔL_2	ΔT_1	ΔT_2	ΔF
A-2	2600	70	125	-84	125	-84	0	0	7
A-4	1300	70	64	-47	64	-47	0	0	5
A-5	1300	1200	399	64	100	-248	299	312	4.5

(continued)

Run	Load (lb)	Temp (°F)	ΔD_1	ΔD_2	ΔL_1	ΔL_2	ΔT_1	ΔT_2	ΔF
A-6	0	1200	299	312	0	0	299	312	0
A-7	2600	1200	505	5	206	-307	299	312	23
A-8	1300	1200	427	44	128	-268	299	312	14.5
B-2	2600	70	147	-74	147	-74	0	0	7.5
B-4	1300	70	71	-32	71	-32	0	0	0
B-5	1300	1200	392	67	75	-235	317	302	10
B-6	0	1200	317	302	0	0	317	302	0
B-7	2600	1200	514	12	197	-290	317	302	5
B-8	1300	1200	427	47	120	-255	317	302	0.5

The figures above give deflections in mils at the end of the shroud where elliptical springs couple it to the core. The runs tabulated above are consecutive. The subscript "1" refers to that diameter parallel to the direction of loading, and subscript "2" to that diameter orthogonal to this. D is the total increase in mils of the diameter over the cold no-load condition. T is that portion of the increase that can be attributed to thermal effects as determined by the hot no-load condition. L is the remaining portion of this diametral increase that must be attributed to load effects. F is the deflection of the centerline at the free end due to loading, if the deflection curve of the shroud periphery can be assumed symmetrical about both the diameters described above. This has been determined by a process of elimination and is presented here for an order of magnitude verification only. The errors in the readings from which this was determined were of the same order of magnitude.

2. Tie Rod Tests

Three samples of rolled and welded R-235 tie tubes were tested at Marquardt. The principal results of two of the tests are:

Temp, °F	1,500	1,700
Yield strength (psi)	70,900	32,300
Ult. strength (psi)	100,800	49,100
Elong. in 2 in., %	11	24
Young's Modulus, 10^6 psi	23.3	16.6

3. Front Support Structure Test

The testing of the front support structure, a welded N-155 body, is to take place in a large Marquardt furnace. This is to be a proof test of the Tory II-A component. The test item is attached to the forward adapter spool by the clevis lugs. A stiffening flange is added to the adapter spool by means of a Marman clamp. The test temperature is 1050°F and cooling is supplied to the adapter spool. Tensile loading is applied to the 72 support points by means of a large whiffle structure. Moment loading is also supplied by means of loading rods. The load on each support point is 3000 lb and the moment is 86,800 in.-lb. Measurements include temperatures at 12 points on the structure and 15 points in the clevis lug regions, deflections at 16 points on the item and 6 points in the clevis lug regions.

All hardware is ready for the test as supplied by Marquardt. The test is waiting final x-ray inspection of the front support structure. Present scheduled date for the test is January 18, 1960.

B. Aerothermodynamics

1. Core Sector Test

The sector test is a cold flow test to investigate the flow characteristics of the labyrinth annulus with respect to the core. Specific questions to be resolved were finding the best annulus seal configuration, to find the magnitude of the induced pressure drop across peripheral structural links, and to find the magnitude of radial leakage flow.

The model chosen was a 22° "pie-cut" of the core which subtends a standard 6-in. labyrinth seal. The test item was a rectangular pressure vessel in which steatite tubes were stacked in steps separated at various intervals by aluminum slats which represented structural links. The top of the vessel had a removable head in which the annulus is located. Various seal configurations could be located in the head piece.

Measurements included 9 internal static pressures, 7 annulus static pressures, inlet total pressure, exit static pressure, exit total pressure and a rake of total pressures at the rear face of the assembly.

The test item was located on the Marquardt test facility near Saugus, California, in August 1959. Tests were run employing various seal configurations. Modifications to the test were made several times to supplement the information obtained. In November the testing was concluded.

In practically all tests, tube misalignment greater than anticipated in the core was an important factor in contributing to overall pressure drop. Large inlet and exit losses were observed. The following conclusions have been made from the test results:

(1) Transient pressure rises over a period of 10 seconds or less are detrimental to the front seal.

(2) Leakage from the core to the annulus is the most significant means of maintaining annulus and core pressures equal.

(3) With the best annulus seal configuration pressure differences across peripheral links were 8 psi or less in steady state.

(4) The impedance between the last region of the annulus and the exhaust chamber should be as large as possible to eliminate large pressure differences in this region.

Figures I-11 through I-14 show the various aspects of the test item. Figure I-15 is a graph of static pressures from a typical test.

2. Base Plate Test

This is a test of base plate coatings under a combined environment of hot flow, pressure loading, bearing loads between coated parts, and ceramic bearing. A circular coated molybdenum plate (Fig. I-16) with core-type hole pattern is located in a 5-in. duct supported by 3 coated molybdenum pieces and ceramic tubes forward of the plate. The 5-in. duct is part of the Marquardt hydrogen burner facility at Saugus (Fig. I-11). The test item is subjected to 5 lb/sec of flow at 2000°F with a pressure drop load of 150 psi. Total time under these conditions is to be 25 minutes.

The first plate is now undergoing test. Two more plates are slated for testing.

C. Core Mechanical Tests

1. Structural Link Stress Distribution Test

The purpose of this test is to determine the location and magnitude of the maximum stress in an aluminum peripheral structural link with reactor-type loads.

The specimen was covered with stress coat and a specified load was applied. The locations of the maximum stress were then determined by sensitizing the stress coat with cold water. Strain gauges were then placed on several interesting points on the specimen. Various combinations of loads were applied to the specimen and the strains were read. The results for a pure pressure drop load are shown in Fig. I-17.

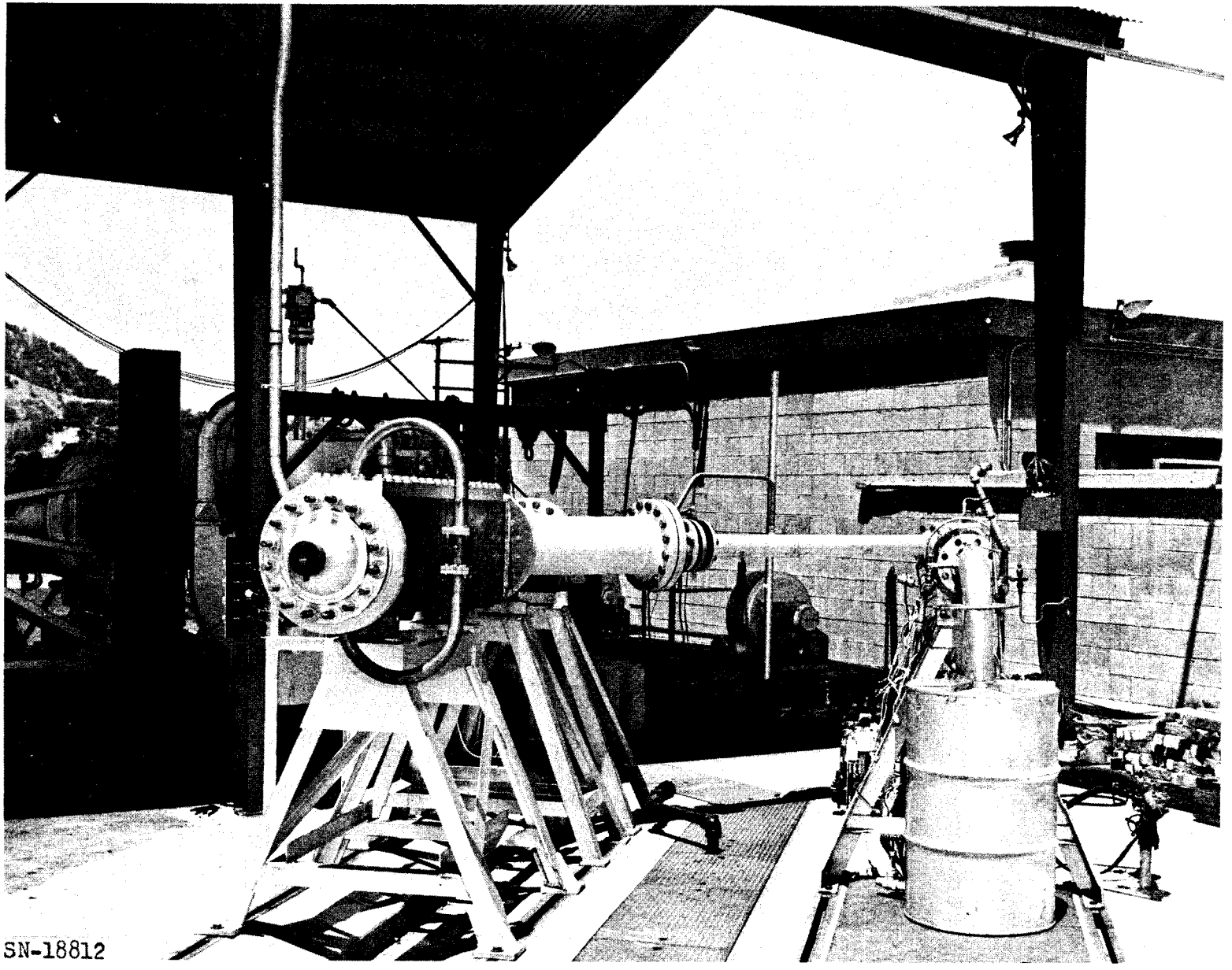

Fig. I-11.

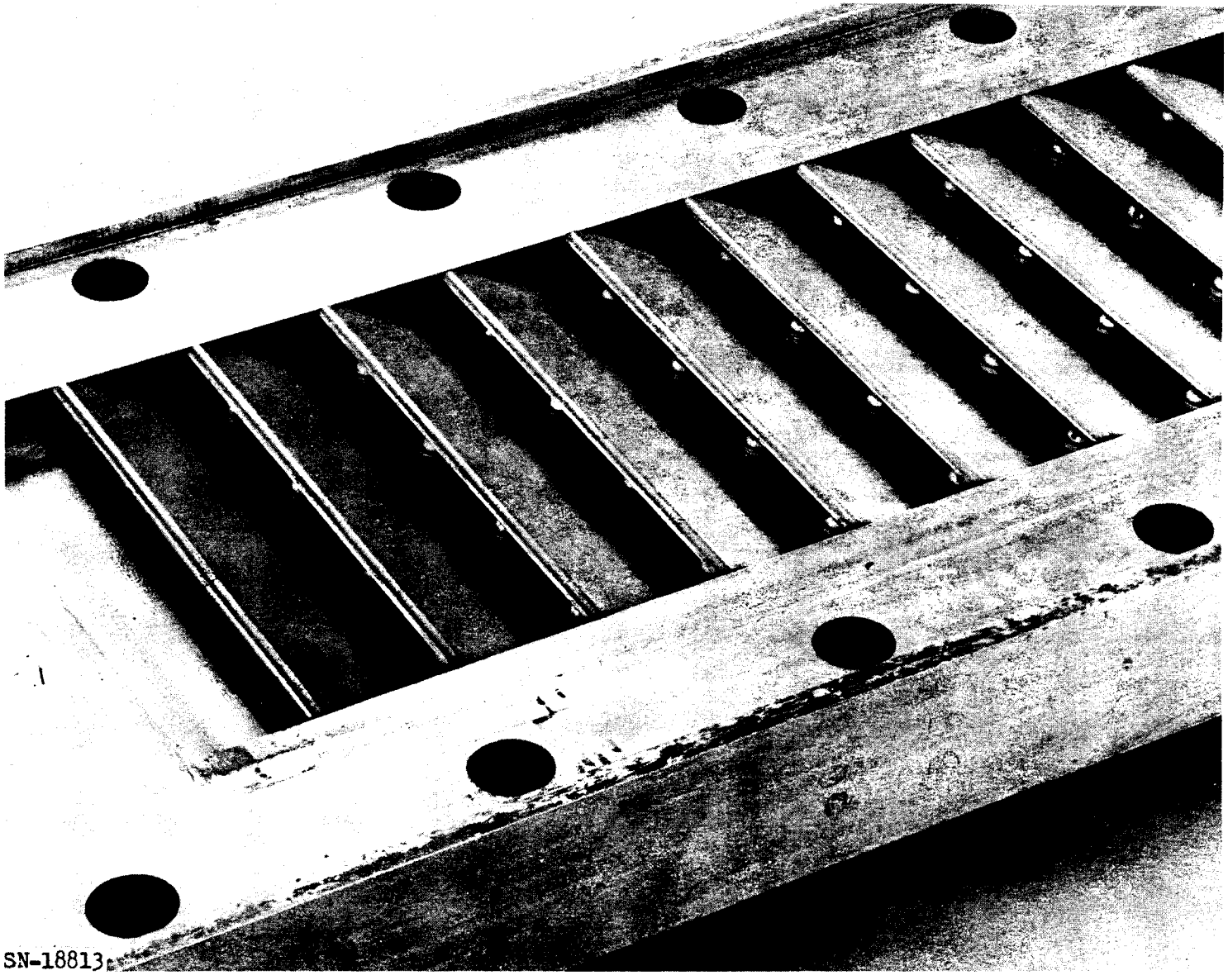

Fig. I-12. Labyrinth seal configuration.

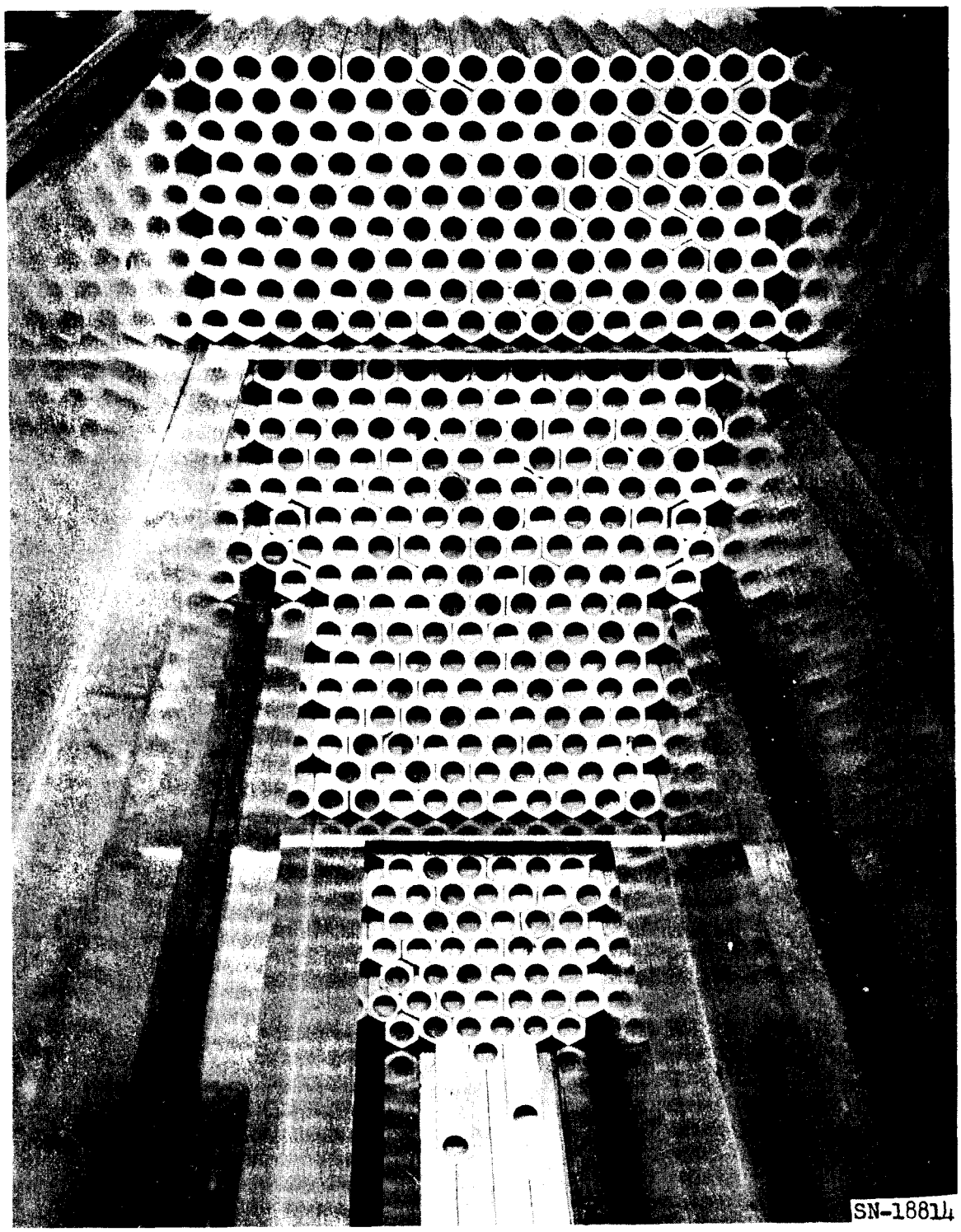

Fig. I-13. Inside of sector — looking upstream.

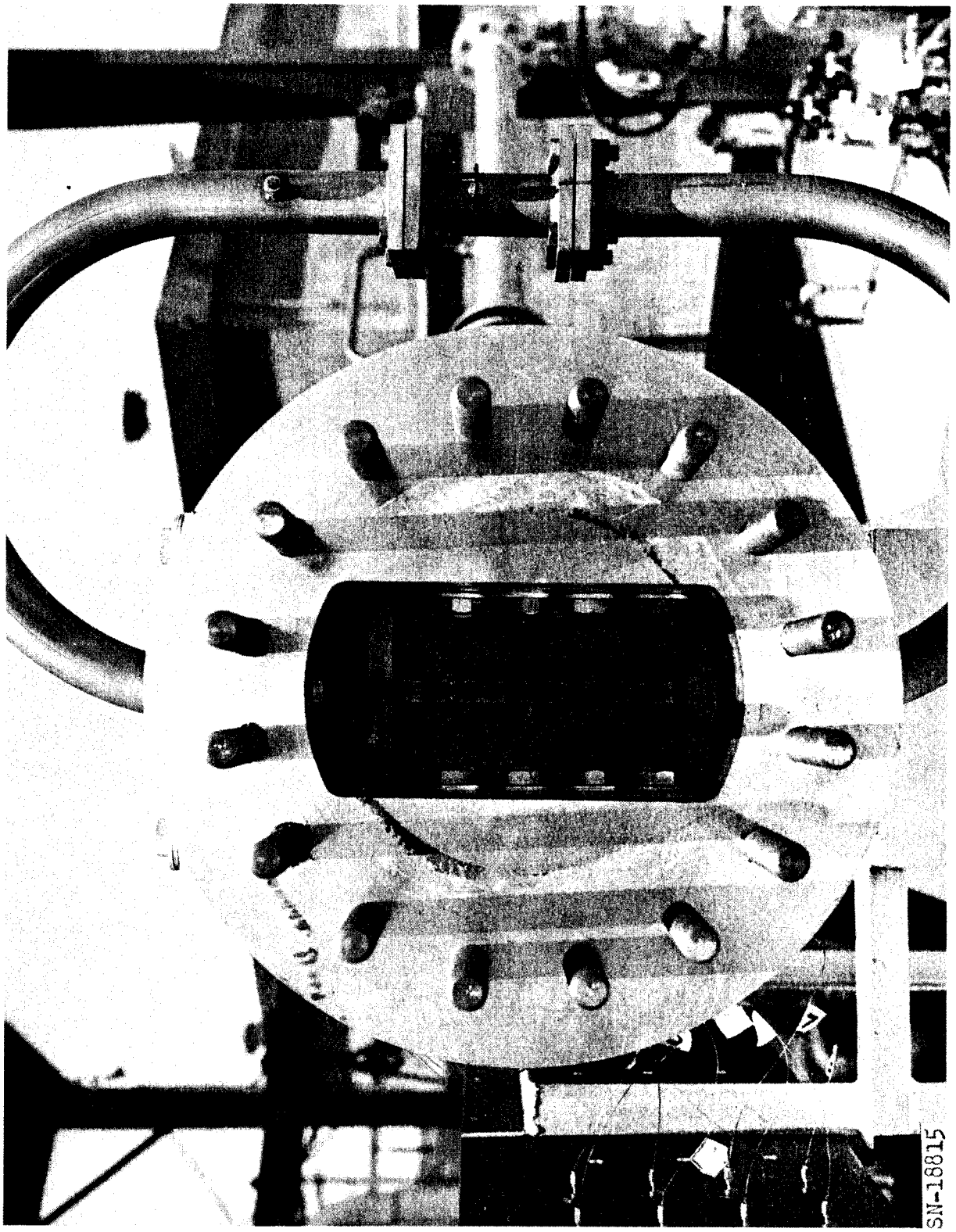

Fig. I-14.

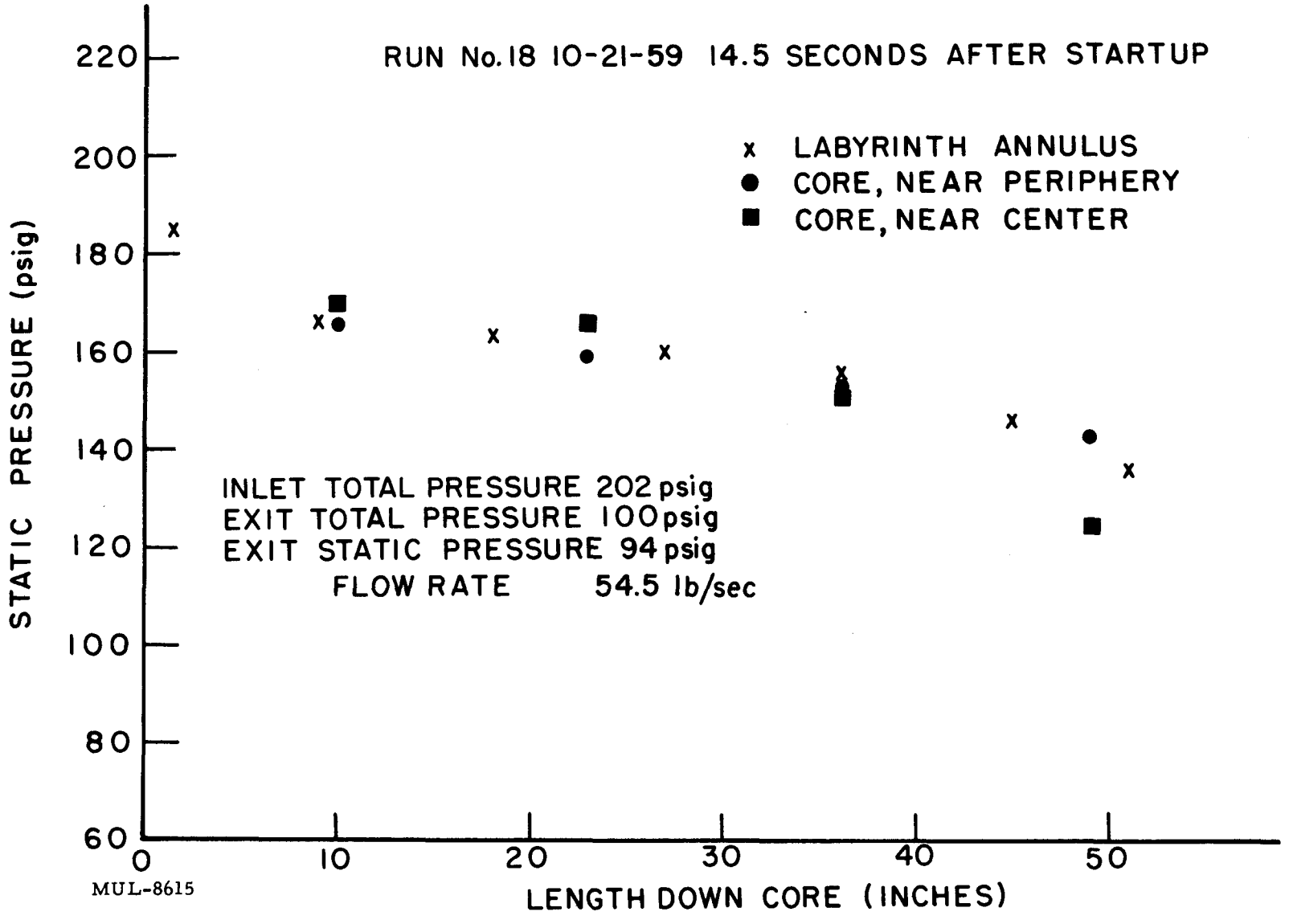

Fig. I-15. Graph of static pressures from a typical test.

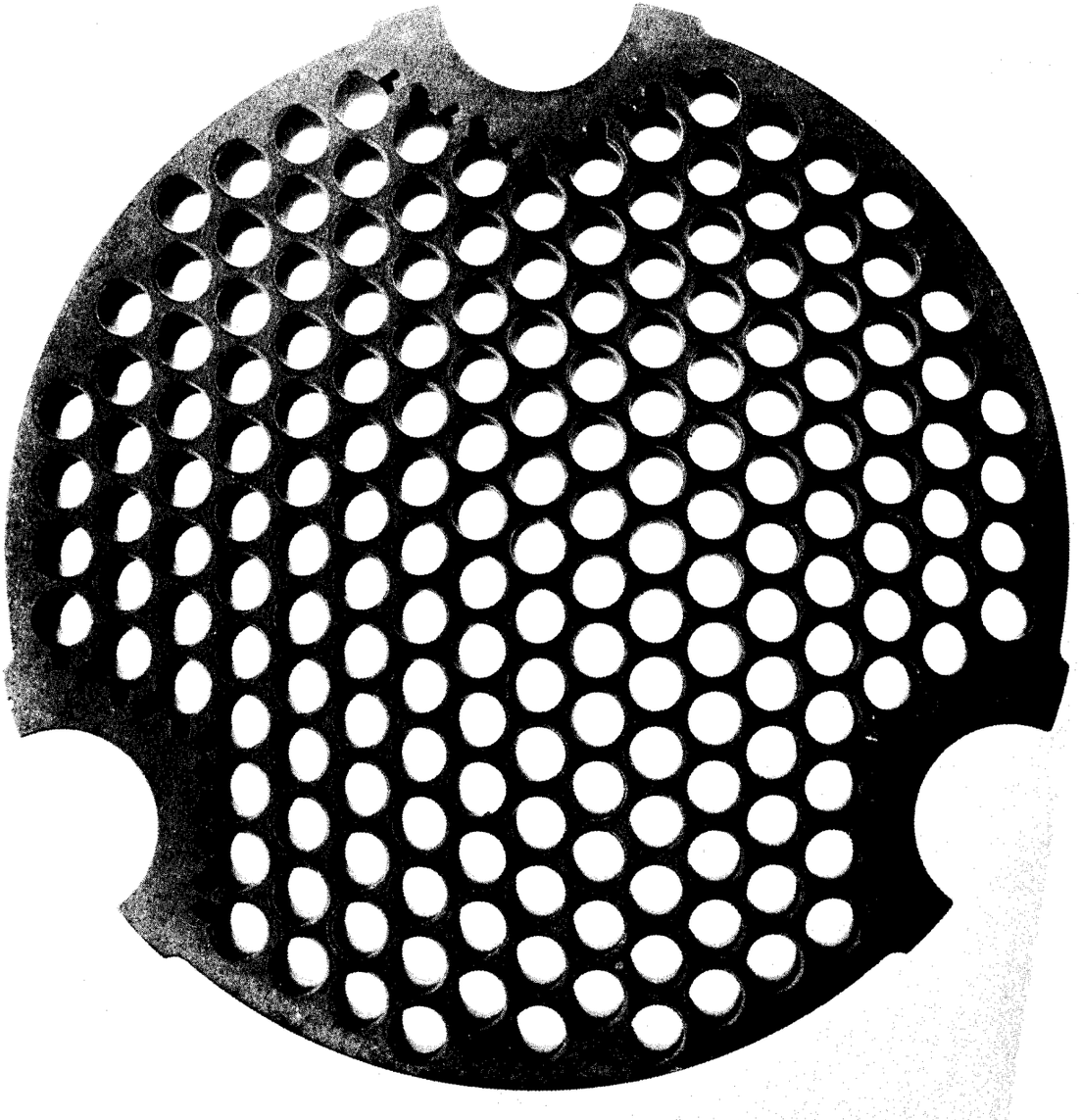

Fig. I-16.

SN-18313

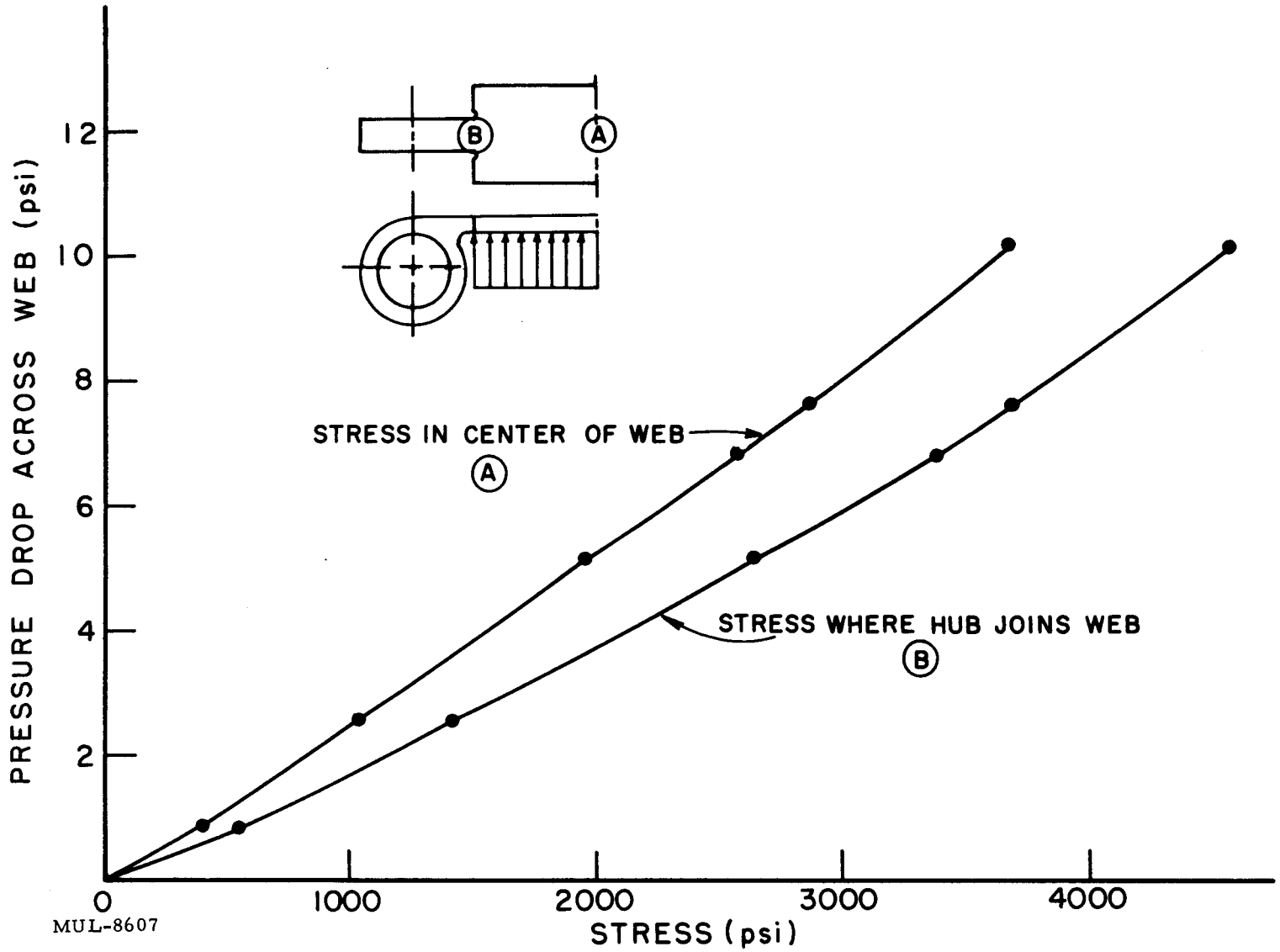
PRESSURE DROP ACROSS WEB (psi)
12
10
8
6
4
2
0
1000
2000
3000
4000
STRESS (psi)
B
A
STRESS IN CENTER OF WEB
A
STRESS WHERE HUB JOINS WEB
B
MUL-8607

Fig. I-17.

2. Short Module Damping Evaluation

The Tory II-A design uses small hexagonal fuel elements of relatively short lengths within a containing framework. There is a network of restraining links or webs which effectively separate the reactor core into smaller units.

The tolerances applied to the pieces of the core provide some clearance and consequent relative motion. This rubbing motion undoubtedly provides internal damping. To ascertain the magnitude of this damping, it was decided to construct a test fixture to evaluate these characteristics over the frequency range of the Tory II-A test bed.

A short module assembly (approximately 12 in. long) has been fabricated and assembled. This test item is slated for numerous tests, the first of which is the damping evaluation. The test fixture consists of a cantilevered beam of variable length which has relatively little damping of its own. The "tare" damping of the system will be measured by substituting a simple solid dummy module.

3. Shroud-Snubber Test

Summary. The shroud vibration model was tested on the Engineering Test Section shake table. The purpose of the test was to evaluate the snubber design and to provide knowledge concerning the shroud-snubber dynamic system. The first series of tests showed that the existing snubber design was not adequate in limiting the amplitudes of the shroud; further the results indicated that impact feedback was a most serious problem. A second series of tests were made with a revised snubber model. The tests proved that this model was far superior in dynamic performance. The snubbers are now in the process of redesign, predicated on these results.

The Model. The cantilever shroud is acted upon in two ways at its free end. The first is dynamic action between the core and the shroud through the elliptical springs. The second is action between the shroud and the pressure vessel through the snubbers which are corrugations on the pressure vessel.

To include a core and springs was beyond the scope of this test. The shroud-snubber system is, however, easily simulated. The shroud was scaled down to 12 in. while leaving the static deflection (and hence the dynamic response) the same. On the mass at the end of the shroud were located knife edges which were adjustable in the vertical direction. Between the knife edges

was located a leaf spring held cantilevered from an adjustable support. Clearance between the knife edges and the spring represented clearance between the shroud and the snubbers. Adjustment of the spring in the longitudinal direction changed the spring constant of the snubber model (Fig. I-18).

In the final series of tests, the spring was covered with a folded array of ceramic bat and the knife edges were replaced by square jaws.

Test Details. Vibration accelerometers were located on the model base, the model support, and on the mass. Strain gauges were located on the tube and on the spring. In all tests the driving force was 1/2 g. Frequencies between 20 cps and 80 cps were swept in 2 minutes and all 5 instrument readings were recorded on a photographic strip chart with keyed-in time reference. The chart speed was 1 in./sec.

The following tests were run on the Engineering Test Section shake table (Table I-5).

TABLE I-5

SERIES I

Test No.	Clearance	Spring distance (in.)	Remarks
10A			No spring
10B	0.002	1/2	
10C	.005	1/2	
10D	.010	1/2	
11A	.002	1	
11B	.005	1	
11C	.010	1	
11D	.000	1	
11	.005	1	4 layers of electrical tape on spring
12A	.002	1-1/2	
12B	.005	1-1/2	
12C	.010	1-1/2	
12D	.000	1-1/2	
13A	.002	2-1/2	
13B	.005	2-1/2	
13C	.010	2-1/2	
13D	0.000	2-1/2	

(continued)

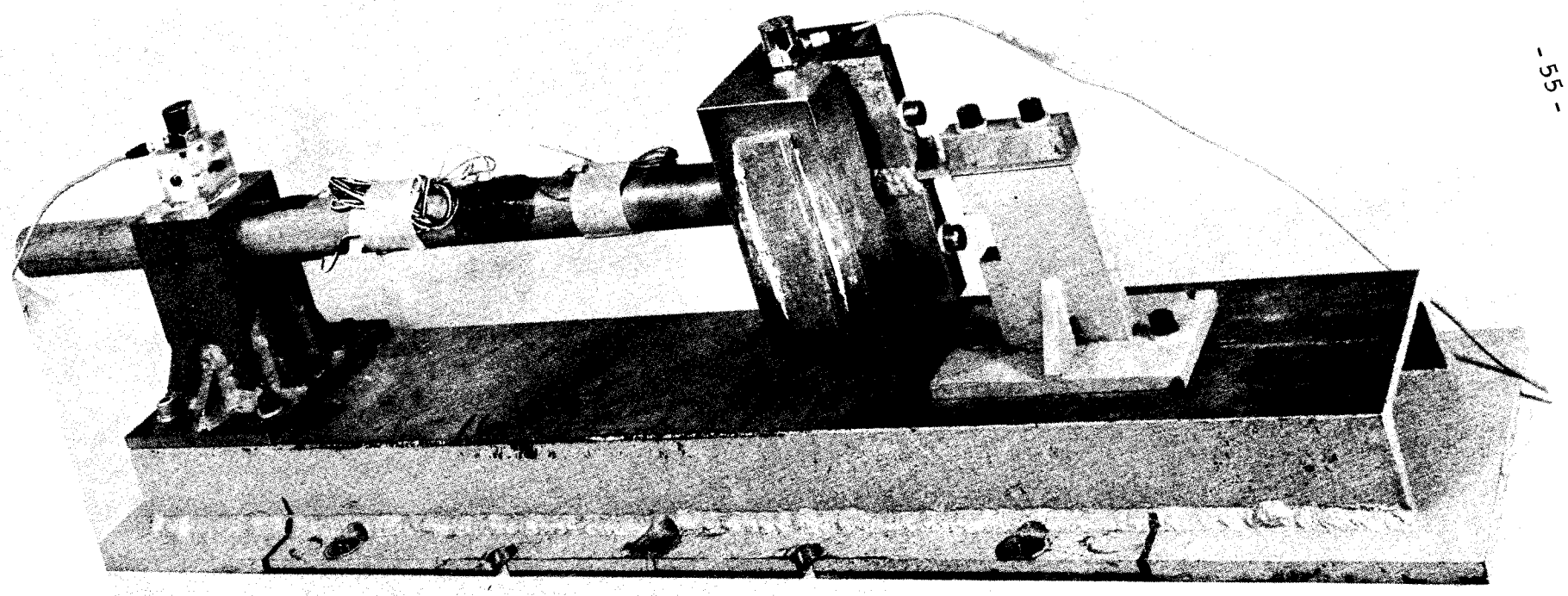

Fig. I-18.

SN-16645

TABLE I-5 (continued)

SERIES II

Test No.	Clearance	Spring distance (in.)	Remarks (square jaws on all tests)
14A	0.002	1/2	
14B	.000	0	2 layers of ceramic bat on spring – tight
14C	.000	0	2 layers of ceramic bat on spring – loose
14D	.000	1/2	2 layers of ceramic bat on spring – tight
14C	0.000	1/2	2 layers of ceramic bat on spring – loose

Test 10A with no spring gave results as would be predicted in calculations. A resonance at 42.5 cps was observed as compared with the calculated 45 cps value for the shroud. The discrepancy is accounted for in the fact that the weight on the end of the model was greater than it should have been. Strain gauge information in this test indicated that failure would most certainly occur if the driving frequency was held at 42.5 cps for any length of time.

The tests with the bare spring at various spring rates and clearances (Tests 10B through 13D) proved interesting. In all cases where there was initial clearance between the spring and the mass, high frequency "chatter" was fed back to the model support. In addition the spring proved to be ineffective in limiting shroud amplitudes.

When the mass reached fairly large amplitudes, the oscilloscope showing the trace of the accelerometer on the base of the model indicated high frequency impact feedback, and appeared as follows:

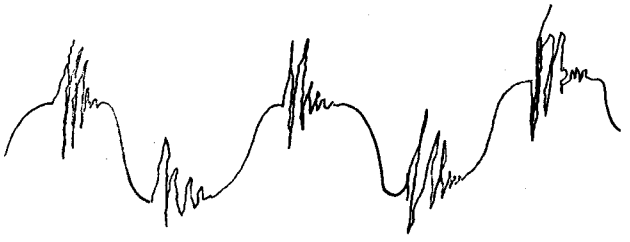

The maximum transient accelerations were sometimes 10 times that of base driving force. On several of the runs the test went "off the air" due to the high level of transient feedback.

The accelerometer located on the weight sometimes registered accelerations as high as 15 g. The shroud would reach these high amplitudes and then suddenly drop to a very low level of vibration. This is consistent with nonlinear theory (see next paragraph) as is the fact that the frequency at which the peaks occurred decreased with decreasing spring constant.

In the tests in which there was no initial clearance between the shroud and the spring the impact feedback disappeared. The accelerations observed were also lower than in the cases where there was clearance.

After evaluating these results it became obvious that the present system had two faults: (1) even with small clearances the shroud could have large dynamic stresses due to the amplitudes near resonance, (2) the impact feedback could be detrimental to the shroud support members. It was decided to revise the simulated system by wrapping the spring with a ceramic bat and replacing the knife edges by square jaws.

The accelerations of the weight were maintained at a constant level throughout the vibrational range (20 - 120 cps) and the signal from the base of the model remained a clean 1/2 g throughout.

Calculations. A complete analysis of the model dynamic system, while interesting, is not the present concern. Only simplified calculations are given to indicate the performance of the model as compared to the actual system and to show why certain phenomena were observed.

A. Free shroud (model)

$$f_n(1) = \frac{1}{2}\frac{3EIg}{L^3 M} = 43.1$$

$E = 30 \times 10^7$ lb/in^2
$I = 1000$ in^4
$L = 12$ in.
$M = 7.1$ lb

$f_n(1)$ (Data) = 42.4
$f_n(1)$ (Shroud) = 44.5

B. Shroud with no clearance (model)

$$K_{system} = K_{shroud} + K_{spring}$$

$$f_n \text{ system} = \frac{1}{2\pi}\sqrt{3g\,(K_{sh} + K_{sp})}$$

Spring length (in.)	f_n (system)	f_n (observed)
2-1/2	51	46
1-1/2	70.5	64
1	110	92
1/2	289	160

The discrepancy between the calculated and observed natural frequencies may be accounted for by the fact that the "joint" between the mass and the spring is not a true material joint (see Fig. I-19). This lowers the observed f_n due to vibration in other degrees of freedom.

C. Shroud – spring with clearance

Were it not for the fact that impact is a significant factor in this dynamic system, we could easily represent the system by the following curve, where a sudden drop from the high to low amplitudes can occur between points "a" and "b" (see Fig. I-20). This sudden drop was indeed observed (Figs. I-21 – I-23).

However impact also occurs as stated. One could say that the curve is imposed upon the previous force-deflection curve. An impulse function imposed on the system will produce decaying transients of a high frequency in the system. This was observed in the tests.

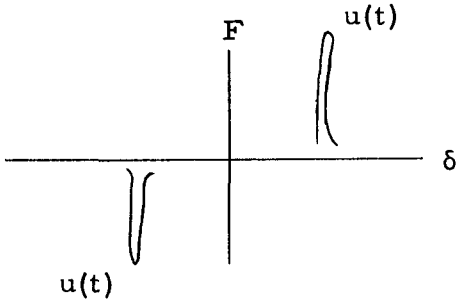

Conclusions.

(1) The corrugation system will not limit shroud amplitudes near driving frequencies of 40-50 cps.

(2) The impacts occurring drive large forces to the shroud support.

(3) The new design should have small static clearances between the shroud and the pressure vessel.

(4) A soft "bat" – preferably canned – located on the pressure vessel should help in the end shroud region.

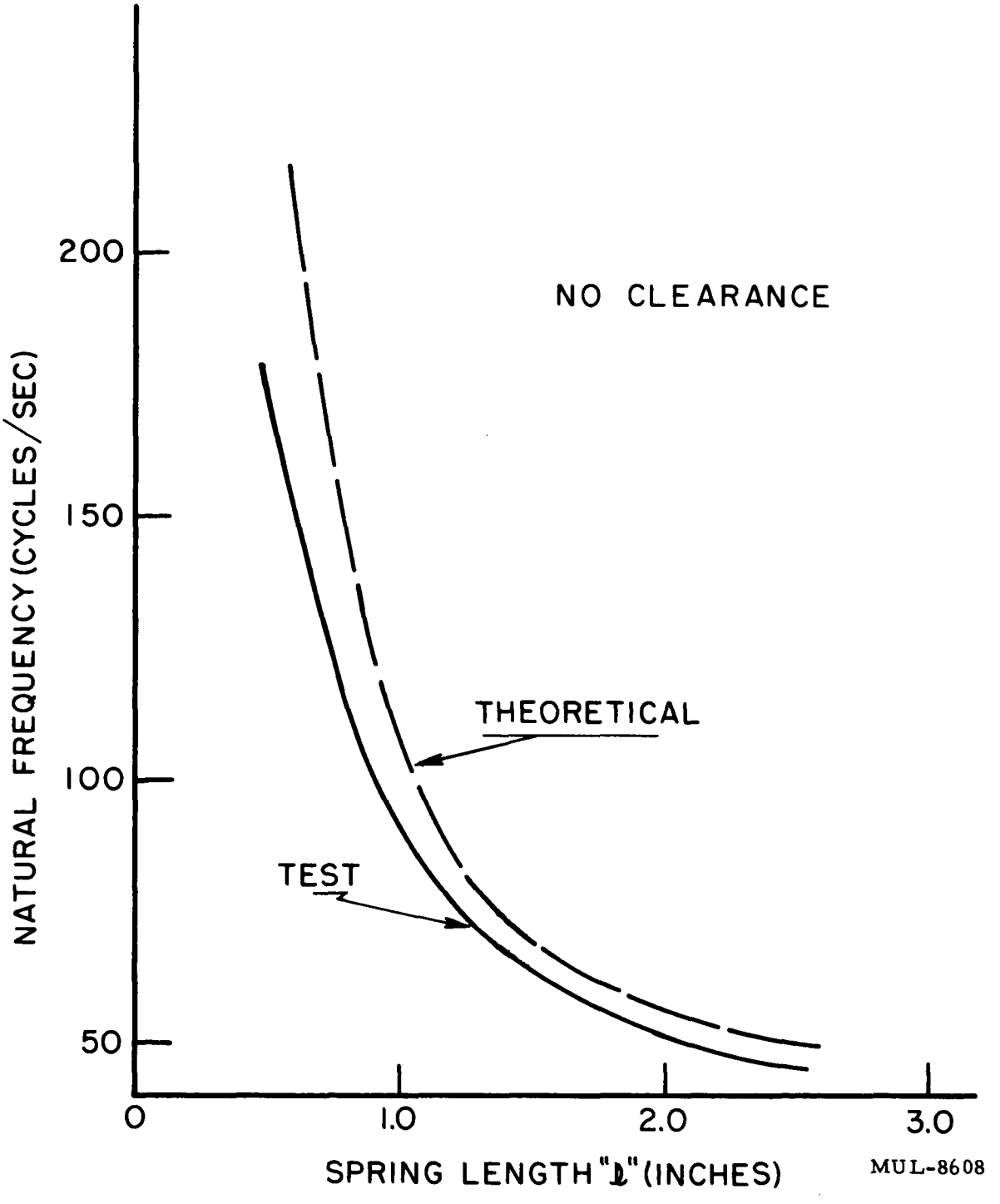

Fig. I-19. Natural frequency vs spring length.

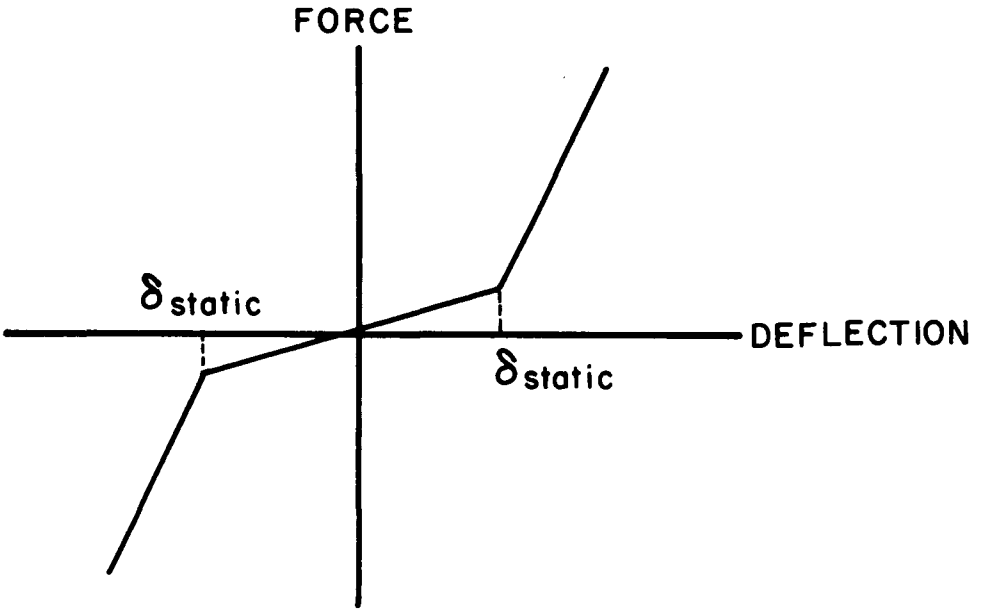

THE RESPONSE OF THE SYSTEM THEN LOOKS LIKE

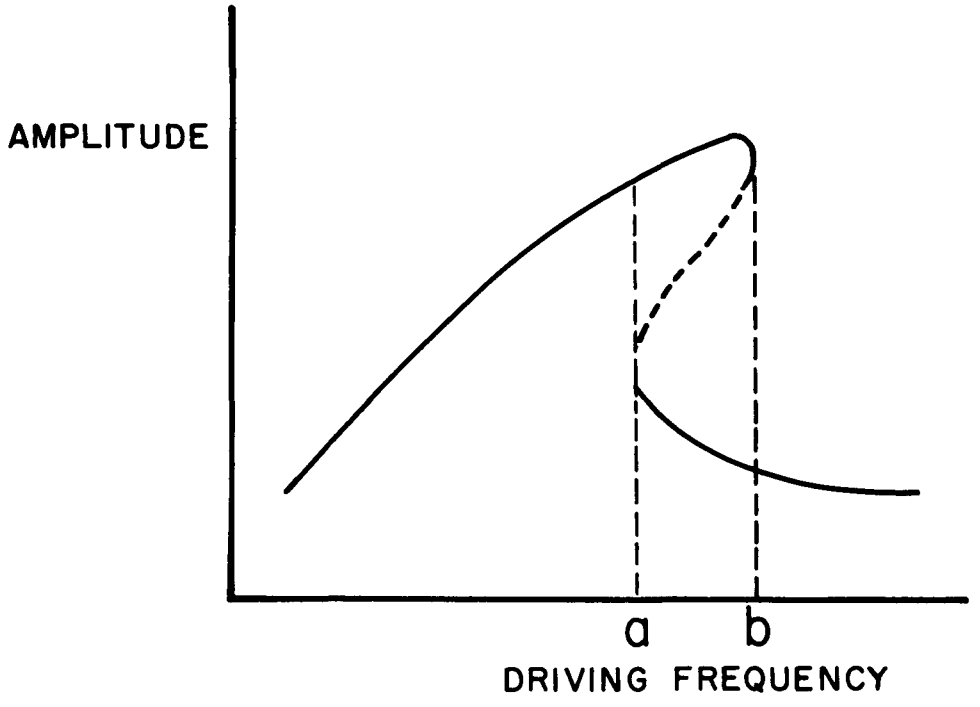

MUL-8609

Fig. I-20.

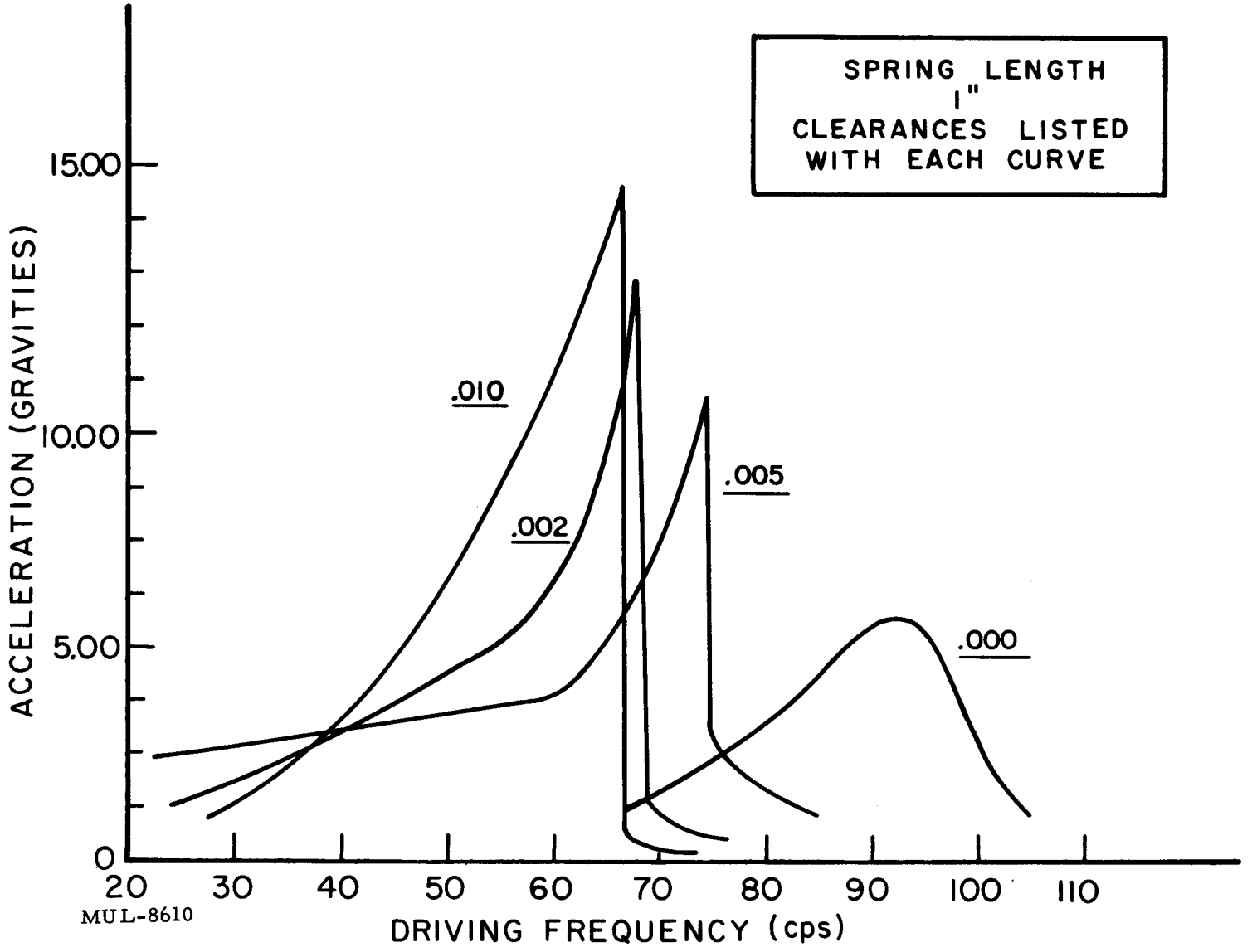

Fig. I-21. Acceleration of mass vs driving frequency.

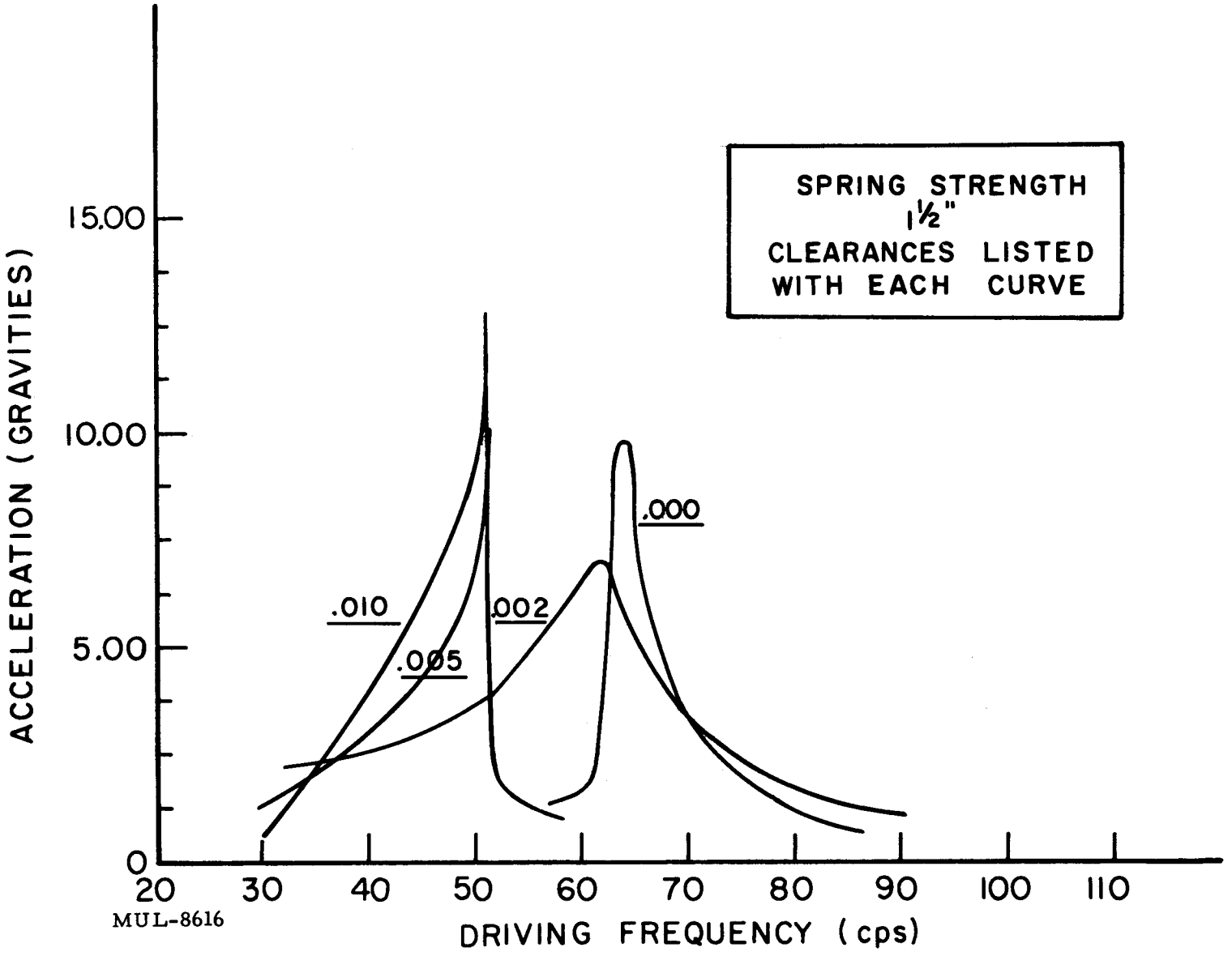

Fig. I-22. Acceleration of mass vs driving frequency.

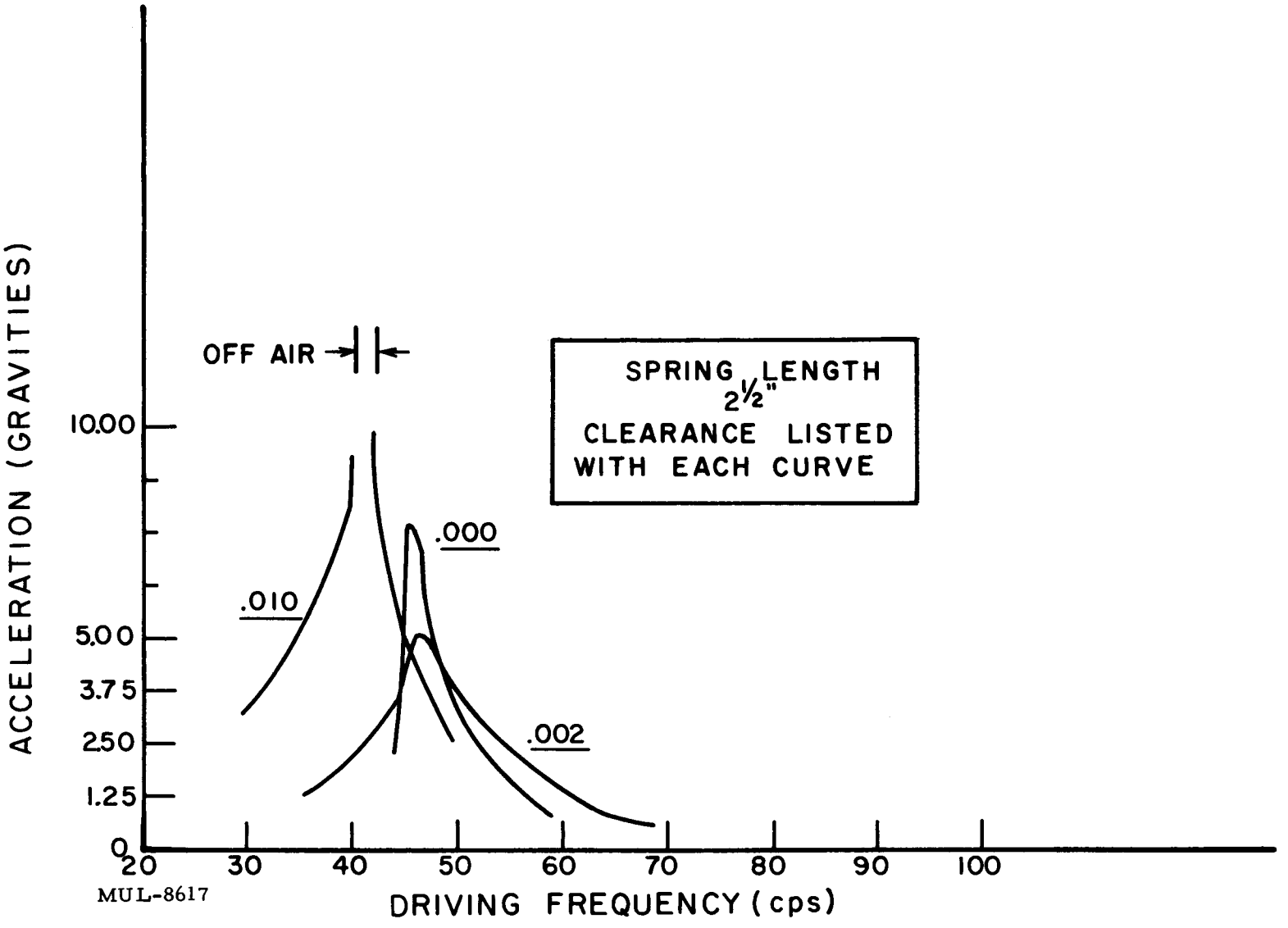

Fig. I-23. Acceleration of mass vs driving frequency.

4. Core Vibration Model

The model (Fig. I-24) was a dynamic simulation of the Tory II-A core. The test item was a 28-in.-long set of thin rods linked with aluminum sheet containing ceramic tubes and surrounded by a thin-walled steel tube. The assembly is at present undergoing vibration testing. Resonances at 20 to 40 cps and 190 cps have been found. Snubbers have not been used on this test to date.

5. Compression Test on Fuel Elements

The purpose of this test was to demonstrate the ability of a fuel element to carry a longitudinal compressive load on unsquare ends at elevated temperature.

A beryllia fuel element with one end truncated at 89° was placed in a Marshall furnace between two alumina loading columns, as shown in Fig. I-25. The specimen was heated to a temperature of 2450°F and loaded to 10 lb, which corresponds to a pressure drop across the core of 128.2 psi. The load was held for two hours and then released. The test was repeated for a fuel element at loads of 20 and 30 lb, corresponding to 246 and 385 psi pressure drop, respectively.

The fuel element loaded to 10 lb showed some chipping on the truncated end as shown in Fig. I-26.

D. Graphite Reflector Tests

1. Permeability and Conductivity of Graphite

The purpose of this test was to develop a plastic coating to seal the cooling passages in the Tory II-A reflector.

Certain epoxy resins were selected by the Chemistry Division. Spectroscopic analysis eliminated those too sensitive to radiation.

Water at 25 psig and 200°F was forced through graphite specimens coated with these resins. Thermal conductivity tests were run on the coatings shown to be superior in the permeability tests to make certain that the coating would not interfere with the function of the cooling passages.

The specimens were then exposed in the LPTR (Livermore Pool Type Reactor) to a radiation history equivalent to the reflector life. Permeability tests were then repeated to determine whether radiation damage had changed permeability.

The coating selected is composed of the following:

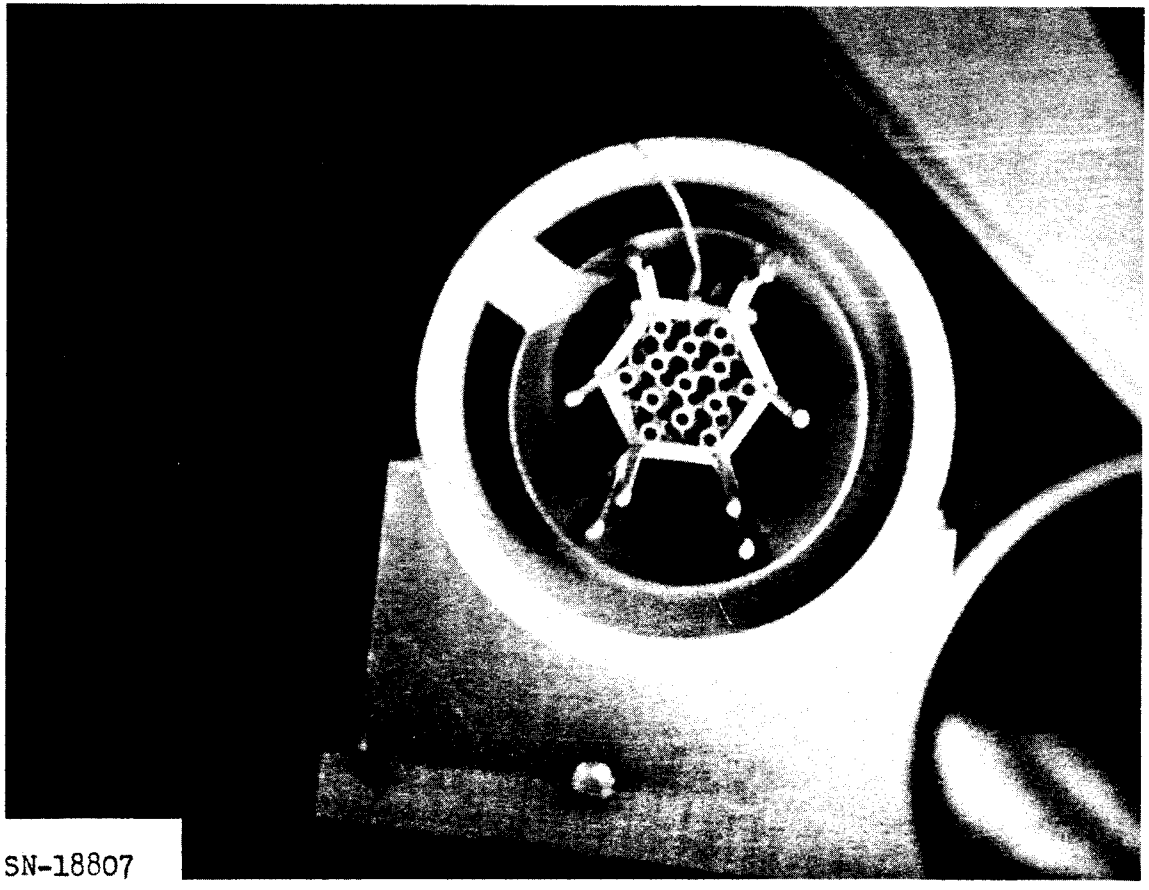

SN-18807

Fig. I-24. Core vibration model.

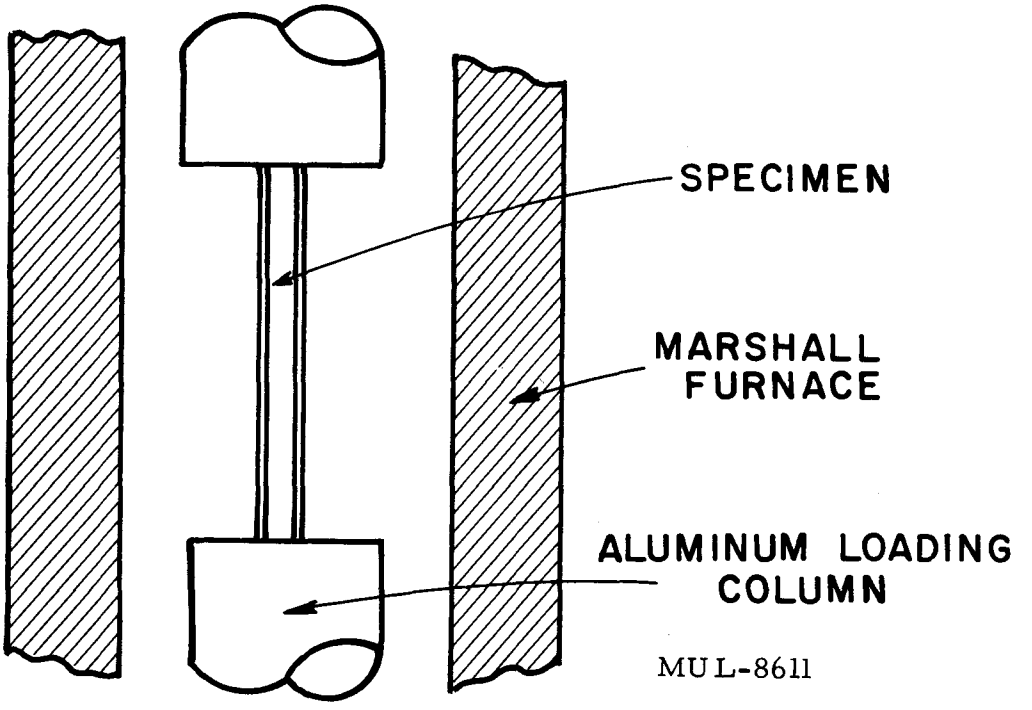

Fig. I-25. Test setup.

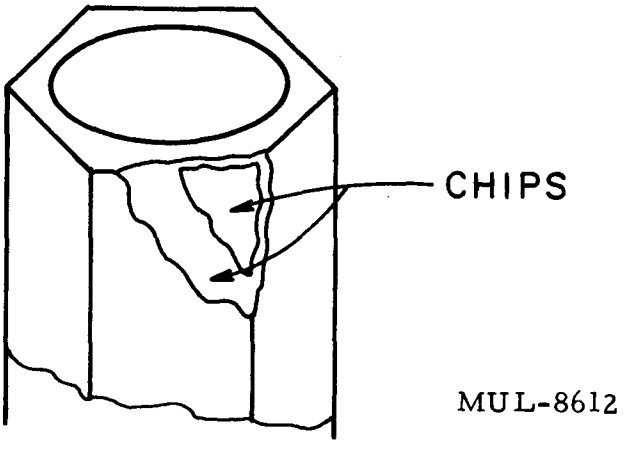

Fig. I-26. Chipped specimen.

Compound	% by wt	Source
332 LC	15.62	Dow Chemical Co.
n AEC	6.25	Jefferson Chemical Co.
X-11	46.87	Shell Chemical Co.
Toluene	31.25	-------

This material gave zero leakage at room temperature and at 200°F both before and after radiation. It has the lowest chlorine content of any of the compounds studied and in effect the lowest radiation sensitivity. A coating of this material on a 2-in.-thick specimen decreased the thermal conductance only 5%.

2. Graphite Thermal Stress

There are three purposes for this series of tests. The first is to determine whether the reflector graphite can withstand a gradient of 200 to 300°F across a partially restrained wall. The second is to determine whether it can stand this when cycled 25 times. Finally, it is desired to determine whether the rate of heat generation can be changed sufficiently rapidly to rupture the graphite due to internal boiling.

These tests are currently in progress. Specimens have withstood a gradient equivalent to 1000°F across an unrestrained wall and to 500°F across a completely restrained wall (on the basis of calculated elastic stresses).

One specimen has been cycled at this level 25 times without fracturing, but there are visual indications that some cracking occurred during the last few cycles.

3. Platinum Alloy Strength Tests

Introduction. These tests were conducted to ascertain if wires of either of the three alloys would perform satisfactorily as tensile members (wires) for use in holding together parts of a high temperature strain gage to operate at temperatures to as high as about 2800°F in air. In addition, it was borne in mind that the data might indicate a conceivable interest in materials like these for structural or control element materials in reactors.

Summary of Results. Short-time tensile tests were performed on 0.010-in.-diam. wire having the following compositions:

1. pure iridium
2. 30% iridium-platinum
3. 40% rhodium-platinum.

The wires were resistively heated and ultimate tensile strength was measured for three different temperatures. Times to rupture for stresses lower than ultimate tensile strength were also measured. Changes in weight after heating for one hour at 1690-1700°C were measured. No strains were measured.

While the methods employed were rather crude, they appeared adequate for the purposes.

Specimens and Equipment. The specimens were all 0.010-in.-diam. wire obtained from a commercial supplier. The alloys were cold drawn. The iridium was hot drawn.

The loads were applied by suspending a small "bucket" (lower half of a polyethylene bottle) from the wire and filling the bucket with lead shot to the particular weight required or desired. Resistance heating was accomplished with a 25 amp variable transformer fed by a constant voltage transformer. Temperatures were measured with a "micro-optical pyrometer."

Results.

Short-Time Ultimate Tensile Strength

Alloy	Temp (°C)	Ult. tensile strength (psi)
Pure Ir	1450	24,600
		25,600
	1570	25,200
		25,100
		17,900
	1690	19,800
		22,200
30% Ir-Pt	1450	20,100
		19,800
	1570	18,300
		14,400
	1690	11,800
		12,800
40% Rh-Pt	1455	15,900
		16,400
	1580	9,100
		9,100
	1700	10,600
		9,900

Stress-Rupture Data

Alloy	Temp (°C)	Stress (psi)	Time to failure
Ir	1690	2,800	60 min – no break
	1450	22,700	18 sec
		19,900	1 min, 27 sec
		17,100	4 min, 0 sec
		15,700	4 min, 27 sec
30% Ir-Pt	1690	11,000	2 sec
		10,100	8 sec
		9,200	4 sec
		8,100	32 sec
		7,200	5 sec
		7,200	20 sec
		5,800	2 min, 40 sec
		5,800	23 sec
		5,100	2 min, 10 sec
		4,400	2 min, 43 sec
		3,700	3 min, 15 sec
		1,640	42 min
	1450	12,900	28 sec
		10,100	57 sec
		8,600	2 min, 42 sec
		7,200	4 min, 21 sec
40% Rh-Pt	1700	1,640	11 min
	1455	12,900	4 sec
		10,100	11 sec
		7,200	1 min, 2 sec
		5,900	2 min, 28 sec
		4,400	6 min – no break

1-Hr Oxidation Data

Alloy	40% Rh-Pt	30% Ir-Pt	Ir
Temp (°C)	1700	1690	1690
Wt before (g)	0.0677	0.0869	0.0989
Wt after (g)	0.0655	0.0809	0.0799
Wt change (g)	0.0022	0.0060	0.0190
% loss of wt	3.2	6.9	19.2

The Ir wire measured 0.0072-in. min diam after the test, indicating 0.0014 in. loss from the surface.

Discussion and Conclusions. The two obvious inconsistencies in the tensile strength data (one low strength of Ir at 1570°C, the low values of strength for Rh-Pt at 1580°C) may be explainable on the basis of strain rates. No attempt was made to control the strain rates quantitatively. No explanation

is offered for the several inconsistencies in time to failure for the stress-rupture data.

4. BeO Flexure Tests

The purpose of this test is to determine the modulus of rupture at elevated temperatures of standard prisms of beryllia from various sources and fabrication techniques.

The blocks are tested at 2200°F and 2400°F with a platen rate of 0.02 inch per minute in an inert atmosphere (either helium or nitrogen). A diagram showing the loading geometry is given in Fig. I-27.

This test is being performed under contract by Aerojet-General Corp. in Azusa, Calif. Results for the Beryllium Corporation hot-pressed, Brush hot-pressed, and Brush cold-pressed are tabulated in Tables I-6, I-7, and I-8. Yet to be tested are National Beryllia hot-pressed, cold-pressed, and slip cast; UCNC – Y-12 hot-pressed and Coors cold-pressed.

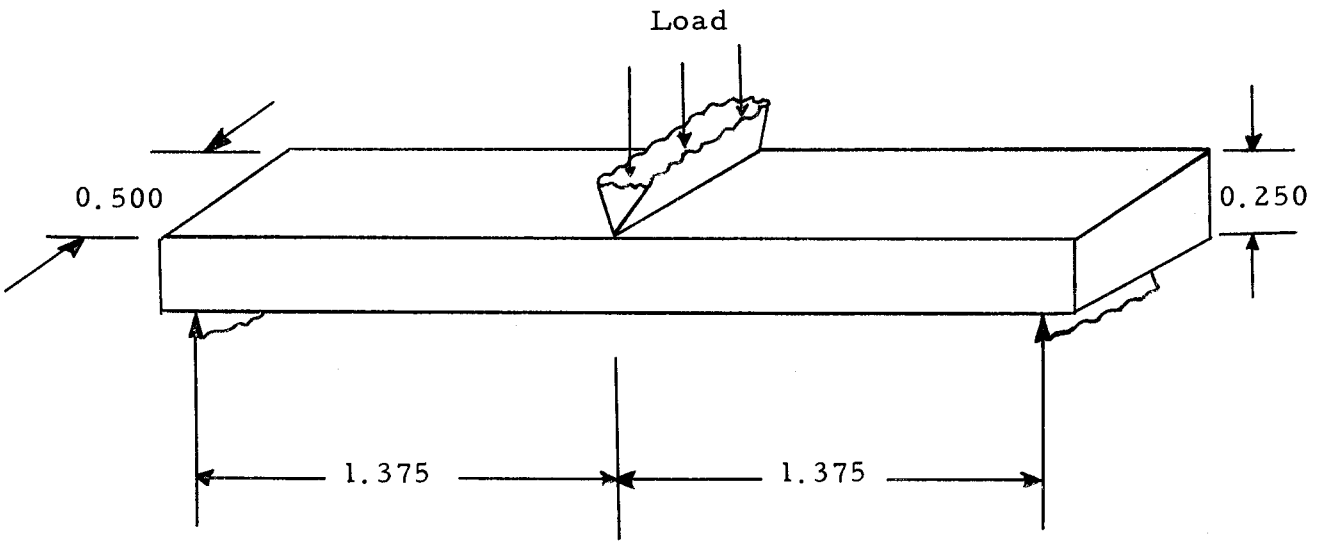

Fig. I-27.

TABLE I-6. DATA FROM TESTS ON BeO SPECIMENS

Beryllium Corporation, Hot-Pressed (Dark)

Specimen No.	Temperature (°F)	Modulus of rupture (psi × 10^4)
4	75	2.51
13	75	2.89
5	2200	2.46
7	2200	2.33
14	2200	2.38
15	2200	2.51
16	2200	2.62
17	2200	2.50
1	2200	2.50
6	2200	2.10
2	2240	1.85
3	2275	2.17
19	2390	2.17
8	2400	1.98
9	2400	1.93
10	2400	2.00
18	2400	2.09
20	2400	2.06
21	2400	1.94
25	2410	1.94
22	2445	1.71
23	2445	2.02
11	2600	1.47
12	2600	1.59
24	2795	1.22

TABLE I-7. DATA FROM TESTS ON BeO SPECIMENS

Brush, Cold-Pressed (Light)

Specimen No.	Temperature (°F)	Modulus of rupture (psi × 10^4)
1	75	1.26
4	75	1.68
8	1285	1.45
7	2190	0.82
2	2200	0.87
5	2200	1.01
17	2200	0.97
9	2210	0.74
19	2210	0.87
10	2220	0.88
11	2220	0.83
12	2220	1.01
21	2220	0.69
3	2400	0.73
6	2400	0.78
13	2400	0.56
15	2400	0.81
23	2400	0.76
25	2410	0.73
16	2420	0.85
20	2420	0.62
14	2430	0.99
18	2435	0.83
22	2645	0.72
24	2985	0.38

TABLE I-8. DATA FROM TESTS ON BeO SPECIMENS

Brush, Hot-Pressed (Dark)

Specimen No.	Temperature (°F)	Modulus of rupture (psi × 10^4)
26	75	1.63
29	75	1.84
37	1265	1.97
40	2165	1.65
35	2190	1.59
27	2200	1.68
30	2200	1.86
34	2200	1.80
39	2200	1.86
41	2200	1.68
38	2210	1.85
36	2240	1.44
33	2255	1.85
45	2390	1.51
28	2400	1.42
32	2400	1.61
43	2400	1.34
46	2400	1.32
47	2400	1.65
48	2400	1.34
42	2420	1.48
44	2435	1.30
49	2465	1.61
50	2865	1.19
31	No data (broken by accident)	

Maximum-Load Determinations. All the specimens that were tested broke in the normal fashion under the loading point. The specimens did not weaken appreciably when the temperature was raised from ambient to 1400°F; in fact, in one case (the hot-pressed Brush samples) there appeared to be a slight increase in strength. Further investigation of this area of the curve is warranted.

Specimen-Failure Observations. All the specimens (except Brush No. 4) that were fabricated by cold-pressing broke by stress-relieving crack formation without separation, as described in an earlier report.[1]

Samples made by hot-pressing failed by normal brittle fracture. Severe creep was observed in the Brush cold-pressed specimens that were tested at 2645 and 2985°F.

Test Vehicle. A group is responsible for the complete test vehicles with the exception of the reactor core and the reactor control servo system. The outline drawing, Fig. I-28, shows major components. The fabrication agency is shown on the drawing by the symbols associated with each component coded as follows:

LRL – Lawrence Radiation Laboratory
ACFI – ACF Industries, Inc.
TMC – The Marquardt Corporation

The status of the ACFI test vehicle activity on November 11 is shown in Fig. I-29.

[1] Aerojet-General Report L3595-01-3, October 1959, p. 2.

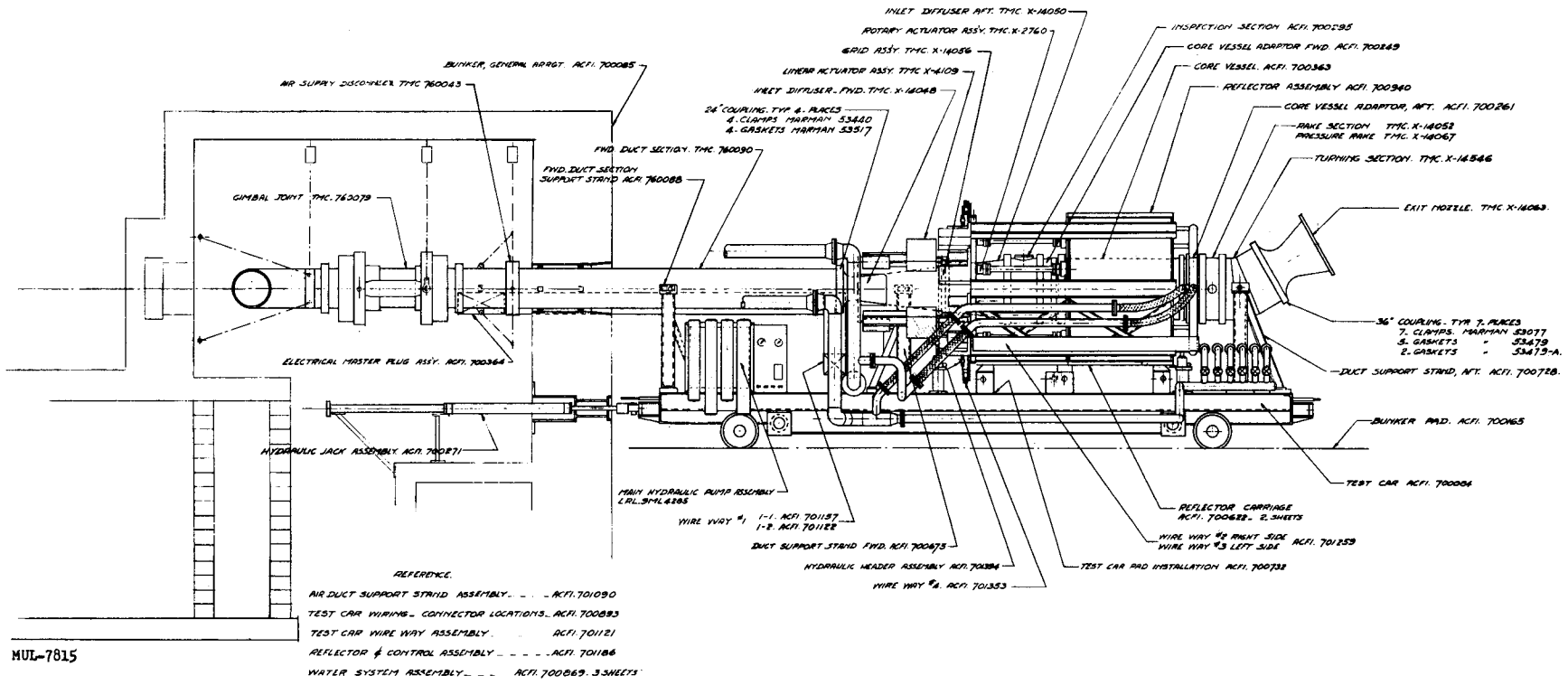

Fig. I-28. Tory II test vehicle and bunker appurtenances.

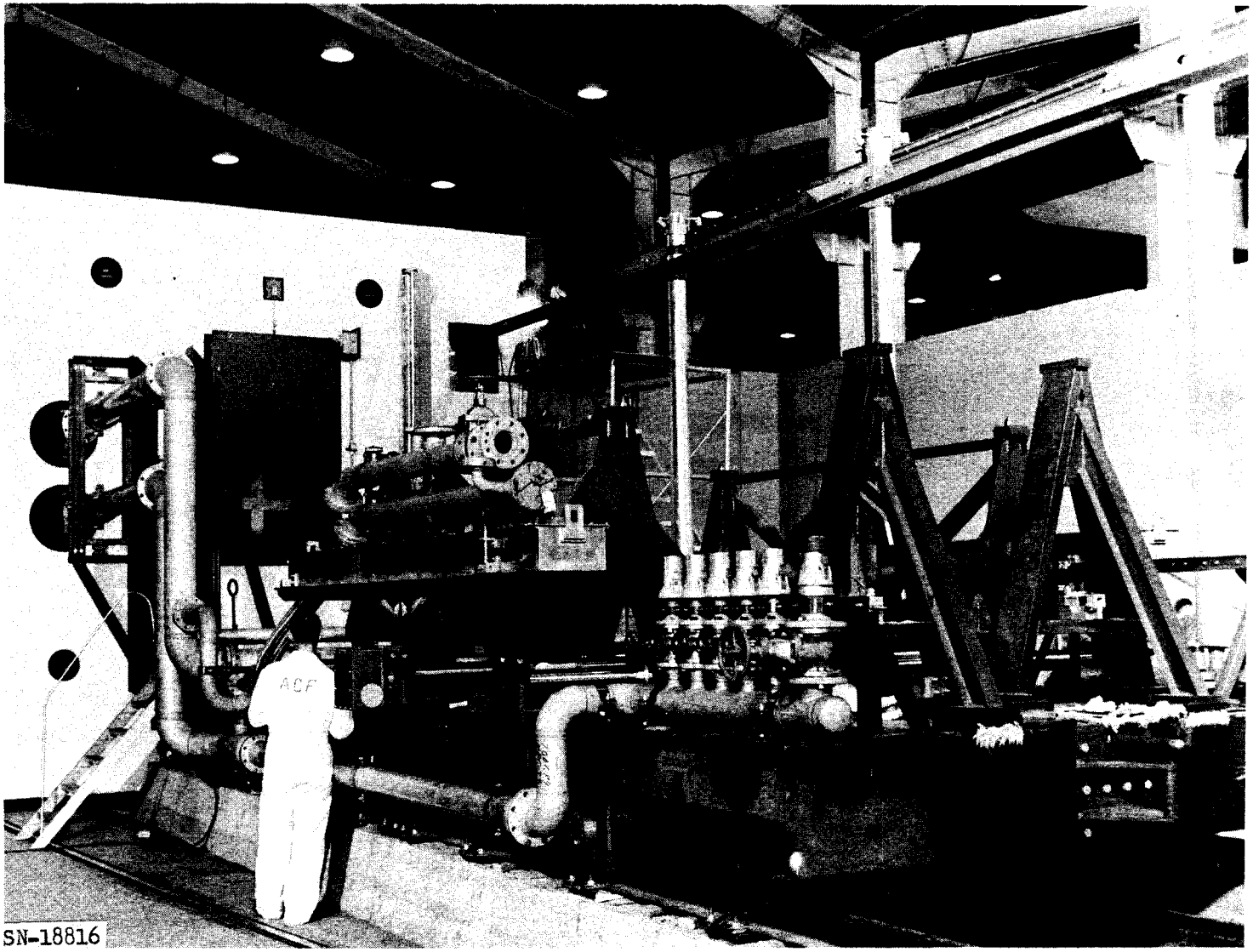

Fig. I-29.

CHAPTER II. MATERIALS DEVELOPMENT AND PILOT PLANT ACTIVITIES

SECTION I. PROCESS AND MATERIALS DEVELOPMENT

I. CERAMICS

A. Materials Studies

1. Pure BeO Preparation and Properties

BeO pieces prepared from $Be(OH)_2$ precipitated by the ammonia process using oxygen as the carrier gas and half molar NH_4Cl as the electrolyte were generally denser than UOX grade pieces sintered under the same conditions.

The 2 kg of BeO equivalent $Be(OH)_2$ was made by mixing together 55 batches of the hydroxide precipitated, filtered, and dried as similarly as possible. The method involves ammonia precipitation of the $Be(OH)_2$ from a 10-liter water solution of 300 g $BeSO_4 \cdot 4H_2O$, 300 g NH_4Cl, and 10 g E.D.T.A. The NH_3/O_2 stream is bubbled into the solution at 1000 cm^3 per min/4000 cm^3 per min until the slurry reaches pH 8.5. The hydroxide is vacuum filtered and dried. When the 55 batches were accumulated, they were ball-milled dry using sintered BeO rods. This accomplished the mixing as well as the breaking up of the precipitate for subsequent washing. The hydroxide was water-washed until it was apparently $SO_4^=$-free and then it was dried and set aside for air calcining.

To check purities and variations in the above processes and operations, samples of various batches were taken at intervals and submitted for $SO_4^=$ analysis, partial spectrographic cation analysis, and electron microscopic examination. Three washed, three unwashed, and two UOX oxide samples were sintered at 1750°C in hydrogen for three hours along with three samples of BeO obtained by the air calcination (1000°C for four hours) of a supplier's $BeSO_4 \cdot 4H_2O$. The analyses and densities thus far obtained are given in Table II-1.

It appears that the solvent water used in making the unwashed calcined hydroxide contains cation impurities, especially Na and Si. The calcined sulfate made the densest and purest samples.

TABLE II-1

Sample No.	Sample	Sintered Piece Density (g/cm^3)	Sintered Piece % Theo. density	Partial chemical analysis (ppm) Al	B	Ca	Cu	Fe	Mg	Na	Si	SO_4
35-0-1	Calcined sulfate	2.956	98.3									
35-0-2	Calcined sulfate	2.955	98.3	<10	5	5	<5	2	20	<100	40	--
35-0-3	Calcined sulfate	2.959	98.4									
35-1-1	Unwashed calcined hydroxide	2.916	97.0									
35-1-2	Unwashed calcined hydroxide	2.901	96.5	<10	n.d.	10	10	10	40	300	100	--
35-1-3	Unwashed calcined hydroxide	2.913	96.9									
35-2-1	Washed calcined hydroxide	2.933	97.5									
35-2-2	Washed calcined hydroxide	2.929	97.4	--	--	--	--	--	--	--	--	2900
35-2-3	Washed calcined hydroxide	2.935	97.6									
UOX-1	As purchased oxide	2.916	97.0									
UOX-2	As purchased oxide	2.925	97.3	50	n.d.	<20	2	50	40	<10	100	2400

2. Sintered BeO – Petrographic Study

We are studying the effect of sintering time in H_2 on the microstructure of BeO. Estimated grain sizes for four samples of thin-walled tubes sintered in hydrogen for 5, 24, 50 and 100 hours at 1725°C are:

Sample No.	Sintering time (hr)	Grain size (μ)
192	5	20-80; max 105-135
122	24	35-135; max 150-200
194	50	100-200; max 330-360
148	100	100-250; max 280-350

From these figures, it appears that after 50 hours, the grain size has nearly reached a maximum. Even more striking than the increase in grain size are the changes in textural features in these samples. (See Figs. II-1 and II-2.)

The effect of increased sintering time may be summarized:

(a) Grain size increases for about the first 50 hours, then remains approximately constant for the next 50 hours.

(b) The preferred orientation of the c-axes parallel to the axis of extrusion, which is present after 5 hours sintering apparently persists unchanged.

(c) Marked textural changes take place: Grains of beryllia develop straight sides and square corners, approaching a tabular shape flattened in the c-direction; pores are entrapped within the grains, and grain boundary porosity is decreased and/or consolidated into fewer, larger pores.

To determine the effect of elevated temperatures on the microstructure of pure BeO, samples of the above were also heated in air at 1650°C for 20 hours. No optically perceptible differences occurred. Presumably, air heating at lower temperatures would also show no changes.

3. Fuel Retention and Stability: $BeO-UO_2$

a. Phase Stability in U_3O_8 Region

A high density H_2-fired tube (BeO + 10% UO_2) was tested in dry air at 700°C and 900°C. At these temperatures UO_2 oxidizes readily to U_3O_8. It is conceivable that surface cracking could occur as UO_2 is oxidized. This in turn would expose more UO_2 to oxidation and cause premature failure of the tube.

The total weight change in the sample was almost negligible after 55 hours at 700°C and 80 hours at 900°C (0.03% loss). Had all the UO_2 oxidized to U_3O_8 the weight gain would have been 0.4%. The fact that a weight loss occurred instead of a gain is unimportant in light of the small percentage

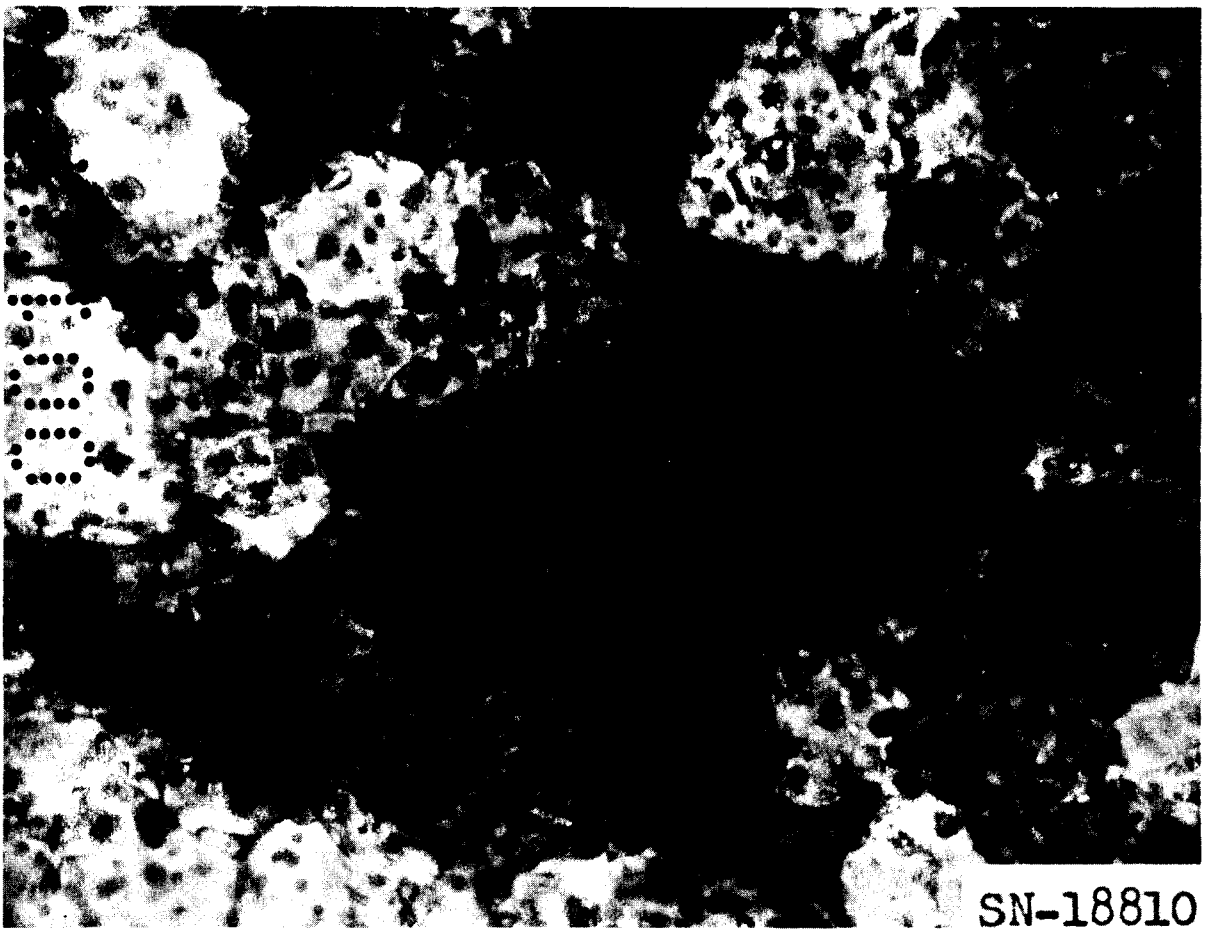

700× X-Nicols

Fig. II-1. Unfueled beryllia sintered 5 hours, showing rounded or irregular grains, and evenly distributed porosity. Large dark area in the center of the photograph is a single crystal of beryllia. Dark gray spots are pores.

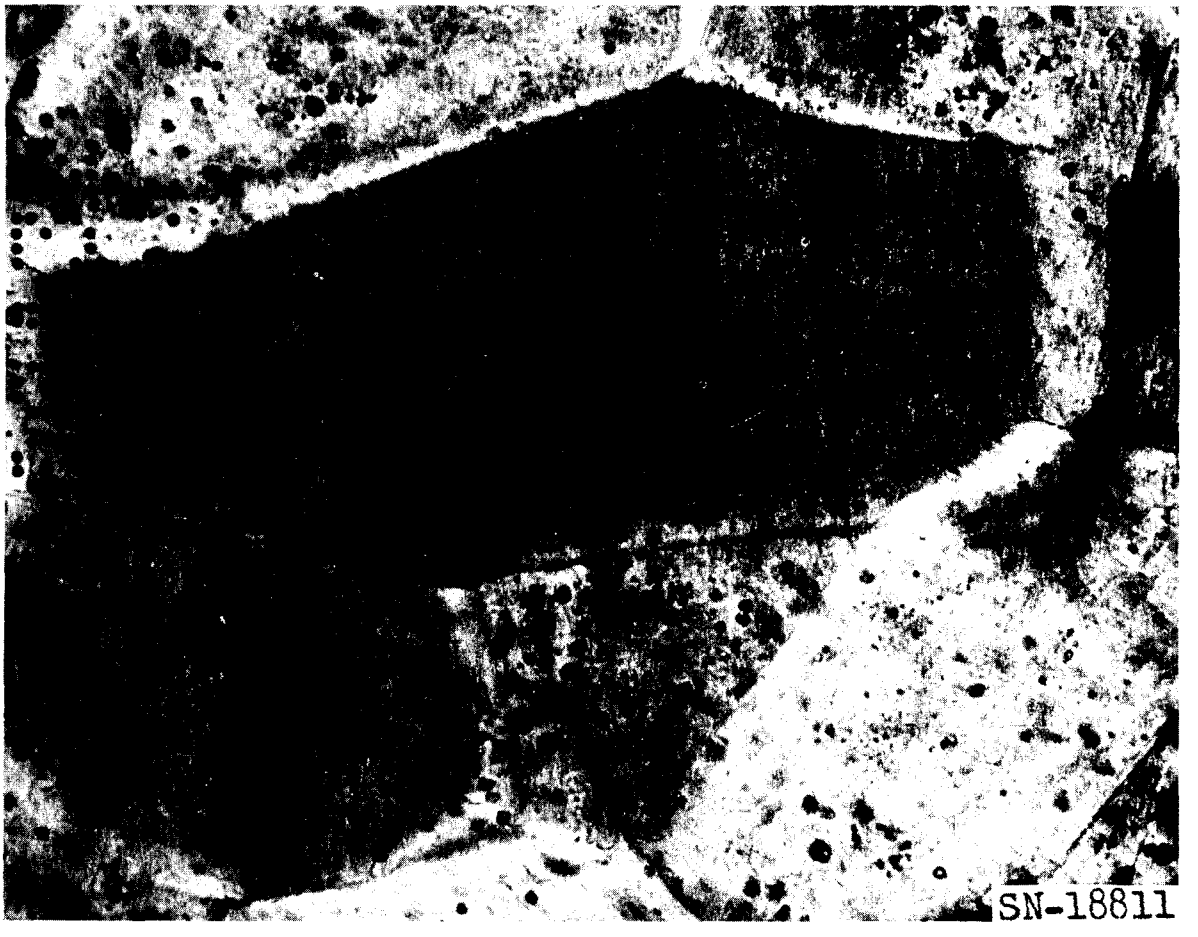

400×

X-Nicols

Fig. II-2. Unfueled beryllia, sintered 100 hours at 1800°C, showing planar grain boundaries and sharp corners, clusters of fine pores of rectangular outline, elongated parallel to the c-axis, and one large beryllia grain, elongated normal to the c-axis. Dark spots in the outer part of the grain are larger pores.

change, which shows that UO_2 oxidation in the temperature range of 300°-900°C is not significant.

b. Thermal Cycling

We are assessing the effect on tube strength and fuel retention of temperature cycling through the U_3O_8 stability region. To insure initially sound tubes, x-ray and Zyglo inspection were used. Tubes with 98-99% theoretical density were chosen. Five tubes each of unfueled, 5% UO_2, and 10% UO_2-BeO were cycled as follows:

1. From base temperature to 2500°F in approximately 2 hours and held for 1-1/2 hours.
2. Cooled to 1250°F (about 5-6 hours) and held 1-1/2 hours.
3. Cooled over night (ca. 13.5 hours to ca. 500°F). On weekends, cooled to room temperature.

This is considered one cycle. Tubes were removed after 2 cycles, 6 cycles, and 10 cycles and will be removed after 15 cycles.

Thus far through 10 cycles there has been no visual cracking in the tubes. The changes in density were:

	Unfueled		5 w/o UO_2		10 w/o UO_2	
No. Of cycles	Before cycles	After cycles	Before cycles	After cycles	Before cycles	After cycles
2	2.9391	2.9381	3.0897	3.0882	3.2269	3.2242
6	2.9419	2.9418	3.0904	3.0896	3.2273	3.2239
10	2.9418	2.9406	3.0875	3.0848	3.2288	3.2177

Note the excellent reproducibility in initial densities. After the pieces are run for 15 cycles, all pieces will again be subjected to Zyglo and x-ray prior to modulus of rupture tests.

c. Phase Changes During Oxidation (U_4O_9)

A black-colored region appears and progresses inward from exposed surfaces during loss testing of dense BeO-UO_2 in air. The color change from brown to black is due to oxidation of the UO_2. In a sample that had been held in air for 4 hours at 1525°C the black oxide was identified by x-ray diffraction as U_4O_9, an f.c.c. phase more dense than UO_2.

Results are given in Table II-2 for x-ray diffraction measurements at increasing depths in this sample (CA-181) which was made by iso-static

pressing and sintering in hydrogen. A core cut from a disc of the same fuel body after loss testing of the disc in air for 4 hours at 1525°C is shown in Fig. II-3. Figure II-4 shows the same appearance in an extruded and H_2-sintered tube of BeO-UO_2 sectioned after 4 hours in air at 1525°C.

Low fuel loss rate is related to this slow oxidation behavior. Earlier high-loss-rate material was oxidized throughout the test specimens after the same test exposure.

TABLE II-2. X-RAY DIFFRACTION ANALYSIS OF OXIDIZED BeO-UO_2

Specimen: CA-181. 3% UO_2-BeO, sintered in H_2 at 1650°C for 5 hours. See Fig. II-3.

	Lattice parameter, angstroms (estimated precision ± 0.002)	
	UO_2	U_4O_9
	a_0 f.c.c.	a_0 f.c.c.
After H_2 Firing		
Internal region	5.474	
Outer surface	5.474	
1/8"-thick disc after 4 hours in air at 1525°C		
Position:		
Surface (black)	---	5.445
1/64 inch in (black)	---	5.445
1/32 inch in (black)	---	5.445
3/64 inch in (black)	---	5.445
3/64 inch in (brown)	5.473	---
1/16 inch in, center of specimen, (brown)	5.471-5.473	---

Oxidation penetration studies have also begun on 3/8-in.-diam solid rods. These specimens contain 10 w/o UO_2 and were sintered in hydrogen at 1725°C for 5 hours. Sample densities are 98-99% theoretical. They are being tested in 5 l/min dry air flow at 1525°C. Exposures at 5 and 20 hours

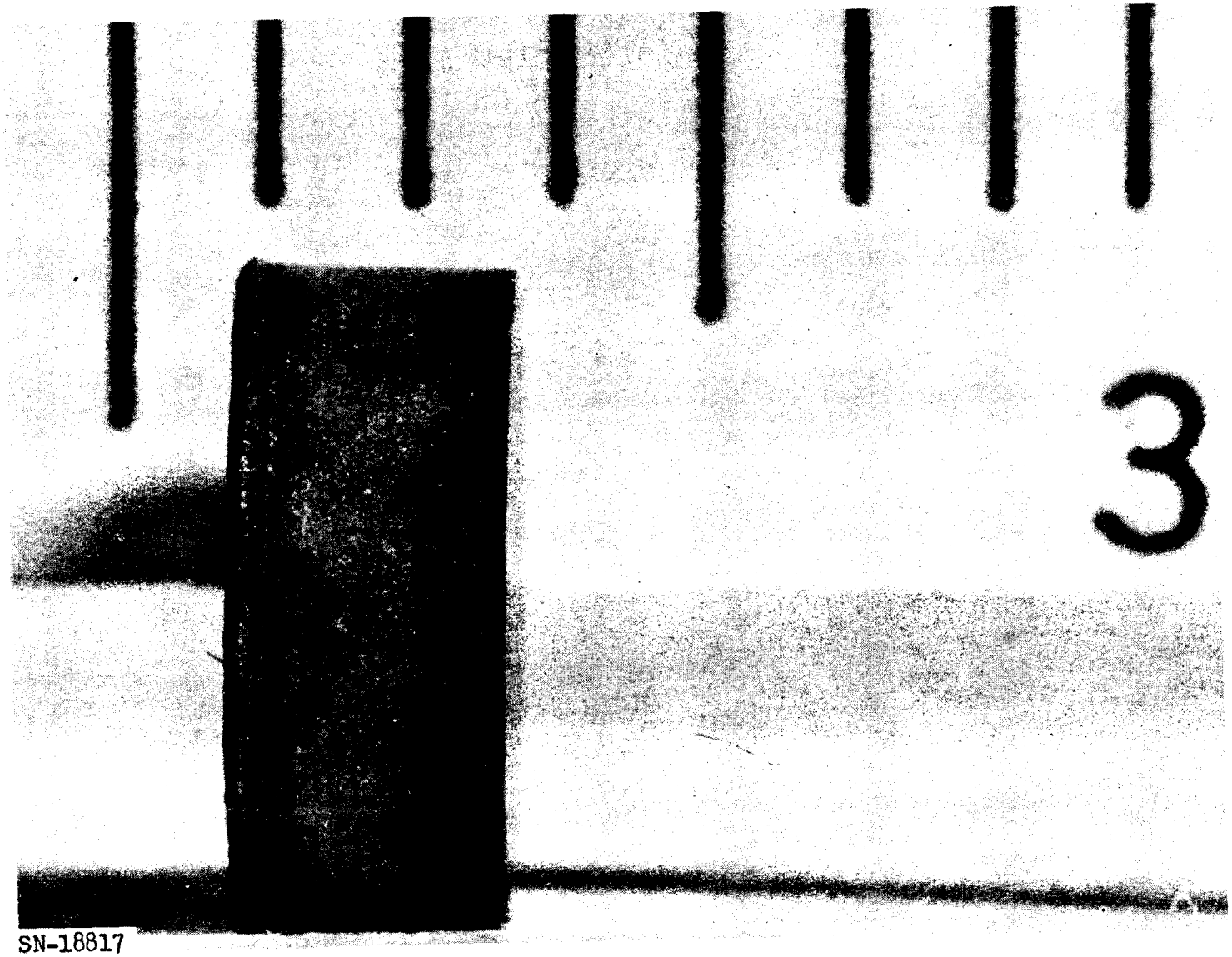

Fig. II-3.

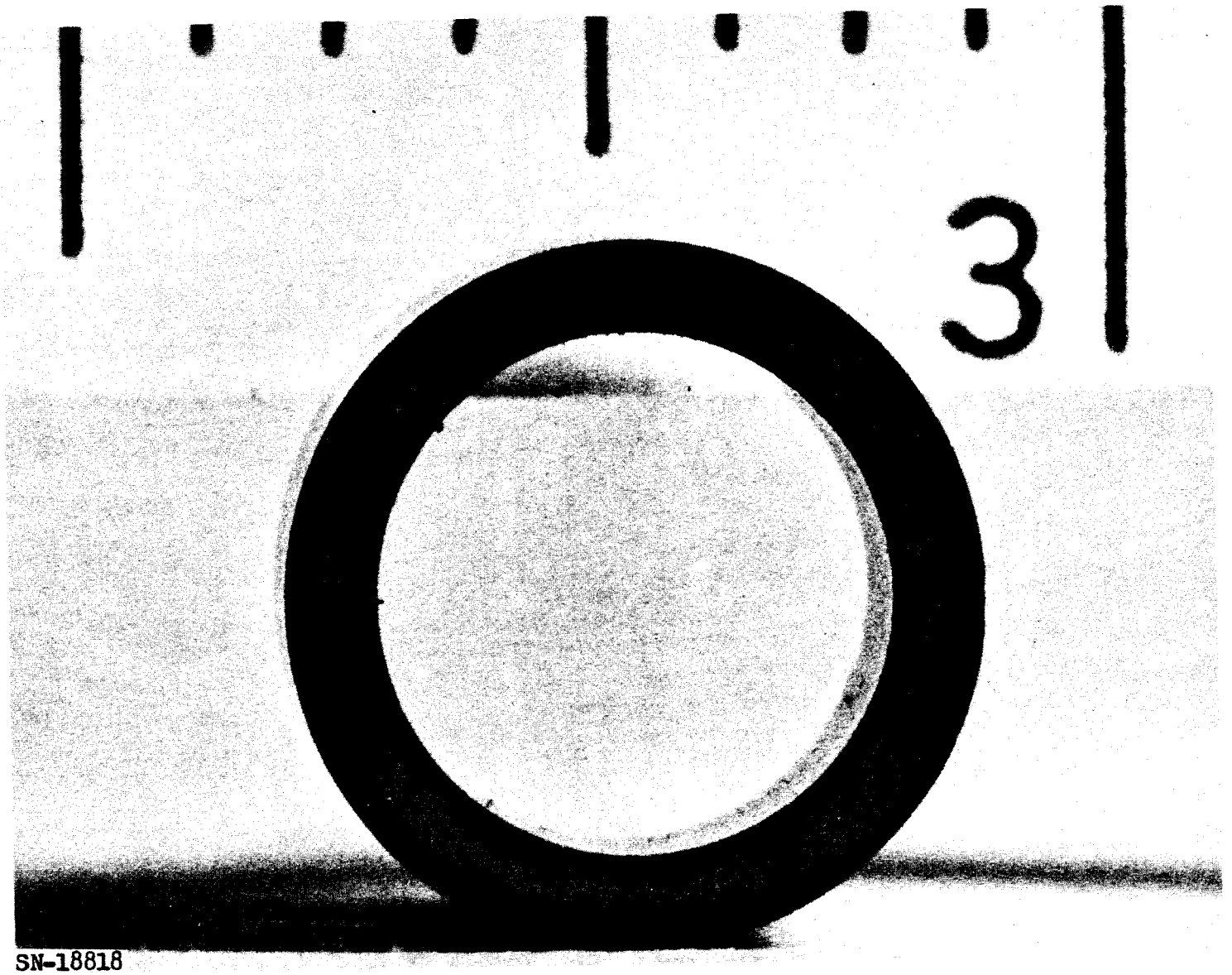

Fig. II-4.

show a small outer zone of darkening (UO_2 brown → U_4O_9 black) which is probably less than 0.01 in. thick, indicating very low penetration rates.

Further microstructural observations of phase changes are described below.

d. Atmosphere Effects (He and Air)

Weight loss data were obtained for two pair of BeO-UO_2 tubes in flowing dry gas streams at 1650°C, one pair in tank helium and one in air (ca. −40°C dew point) to indicate whether fuel loss rates would tend to become equal and therefore possibly limited by the same rate mechanism, independent of atmosphere. The tests were continued for 20 hours. Density and weight data were obtained by removal of the samples from the furnace at 1 to 4 hour intervals.

The loss rates in air, although gradually decreasing with time, were always greater than those in helium. In the 16 to 20 hour interval, the rate in air was 6 times that in helium. The inherent loss in He may be still less; the samples were gradually removed from the furnace to air while hot to avoid severe thermal shocking. We would expect some surface loss to occur under these conditions. Microscopic study of thin sections (see below) also show marked differences between samples from the two atmospheres.

Figure II-5 shows these results and corresponding changes in volume and density. Volume of both pairs of samples decreased by approximately 1% during the first 8 to 12 hours. There was little change thereafter. Values plotted are averages of the pair values. Deviations of loss between pairs were less than 10% of the mean with one exception.

The BeO-UO_2 tubes were 2 in. long by 5/16-in.-diam, contained 10 w/o UO_2 and were extruded from Mix V-18. They were heated in hydrogen for 5 hours at 1725°C. Densities ranged from 3.19 to 3.21 g/cc before loss testing. Thin section observations are summarized below:

	Initial condition	After 20 hours at 1650°C	
		In helium	In air
BeO grain size, μ	10-20	10-20	20-55
UO_2 grain size, μ	0.5-1	1-2	2-8
Color, macroscopic	Brown	Black* throughout	Black throughout
Color of uranium oxide grains, microscopic	Gold	Gold	Black

* Actually, thin sections from He exposure were olive in transmitted light, while similar samples from air exposure were black.

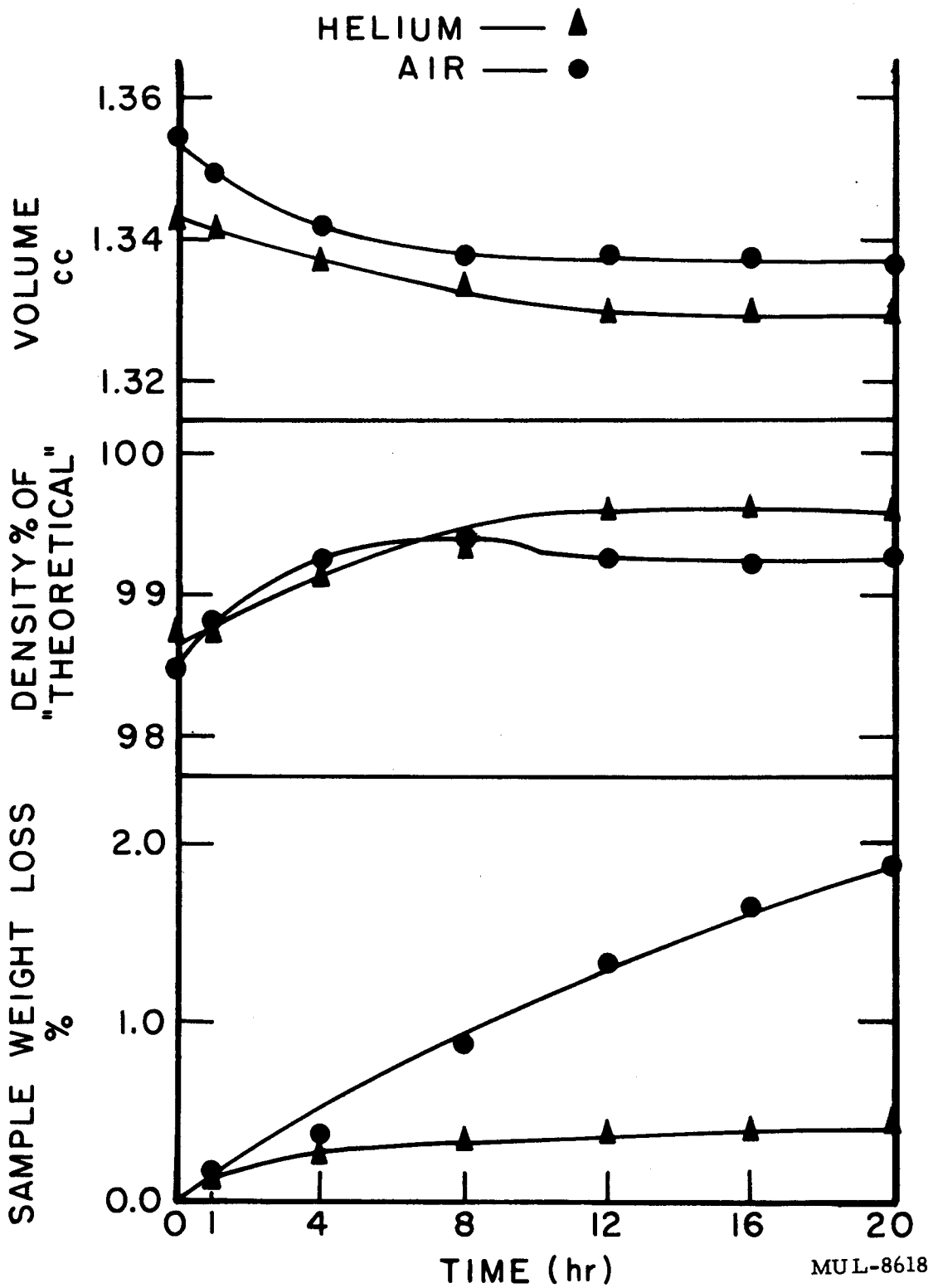

Fig. II-5. Atmosphere effects.

Evidently grain growth of the UO_2 and BeO was considerably more marked in air than in helium. The macroscopic black color in the helium-heated sample is not explained yet. The gold uranium oxide grains indicate UO_2 is still present. Further work will be done on this problem.

e. Fuel Loss Studies

(1) Analysis of Loss

Fuel loss determined by weight change was compared with that determined by wet chemical analysis. The loss studies were made at 1650°C for 20 hours with 5 l/min dry air flow. The tubes were high density 10 w/o UO_2 (Batch V-18).

	Percent UO_2 loss	
Sample No.	By weight change	By chemical analysis
1	5.17	7.44
2	4.72	5.99
3	6.89	8.41
4	6.37	7.19
5	7.22	7.81

The slightly higher losses by chemical analysis are consistent with the hypothesis that two opposing factors contribute to weight change. The major one is weight loss of UO_2 by volatilization as UO_3; the minor one is weight gain by oxidation of UO_2 to U_4O_9. The latter reaction would account for no more than 1.5% weight change based on the urania initially present, and generally much less.

(2) Effect of Fuel Loading

Studies of fuel retention as a function of fuel loading are nearly complete. Tests were run at 1650°C, 1525°C and 1260°C, for 20 hours with 5 l/min dry air flow. (See Table II-3.) Weight changes at 1260°C are extremely low, and thus precision is poor. Note that, e.g., for 10% UO_2 the % total weight changes are 1/10 those listed. Thus losses due to volatilization (if they exist) are obliterated by weight gains due to oxidation to U_4O_9, and both of these effects are extremely small.

TABLE II-3. % LOSS OF UO_2 BY WEIGHT: 20 HOURS

% UO_2	1260°C	1525°C	1650°C	Remarks (1650°C results)
5	----	----	6.4/6.7/15.6	High value suspect
10	+0.18/0.14/ 0.09/0.09/ 0.35	2.6/2.5/2.4/ 2.7/2.2	7.7/9.5/8.6/ 7.3/15.1	High value tube showed irregularity in fuel distribution by DXT analysis after test.
12.5	+0.36/0.28	4.0/4.9	12.7/11.7	
15	+0.19/+0.36	5.6/4.4	14.4/20.9	20.9% tube showed defect in DXT analysis after test.

Note: A "+" preceding a value indicates % weight gain based on UO_2 content.

Figure II-6 shows the fuel losses of 5 specimens with time. These specimens are V-18's, 10 w/o bodies fired in H_2 at 1725°C with 5-hour soak. One tube was cut into 3 pieces, one each for 1650°C, 1525°C and 1260°C loss study.

Data on various tubes at 1525°C are in good agreement. The range of these values is given by the I-bars on the plot, covering 4-5 points each. The loss rate is parabolic, i.e., loss rate decreases with time in the interval measured.

The 1650°C data show much poorer agreement on portions cut from the same tubes. The apparent increase in loss rate with time may not be real. Further data will determine this. In any case it should be noted that 1650°C is considered primarily an accelerated test temperature, and is far above any contemplated temperatures of reactor core operation.

DXT analysis of these tubes prior to test showed relatively uniform UO_2 distribution over the length of the tube. (Maximum deviation 1.5% of average loading. Most tubes showed no measurable variation.) Further DXT work after fuel loss testing showed higher loss at the front of the tube, i.e., at the air inlet to the furnace, which gradually decreased over the length of the tube. Apparent flaws or irregularities in several tubes were evidenced by sudden dips in the concentrations on DXT plots.

(3) Effect of H_2 Sintering Time

Fuel retention has been determined as a function of microstructure, achieved by varying sintering time in hydrogen.

Specimens of Mix V-18 (10% UO_2) which had been sintered for 5, 24, and 100 hours at 1725°C, were examined petrographically. Grain sizes (estimated) are in Table II-4.

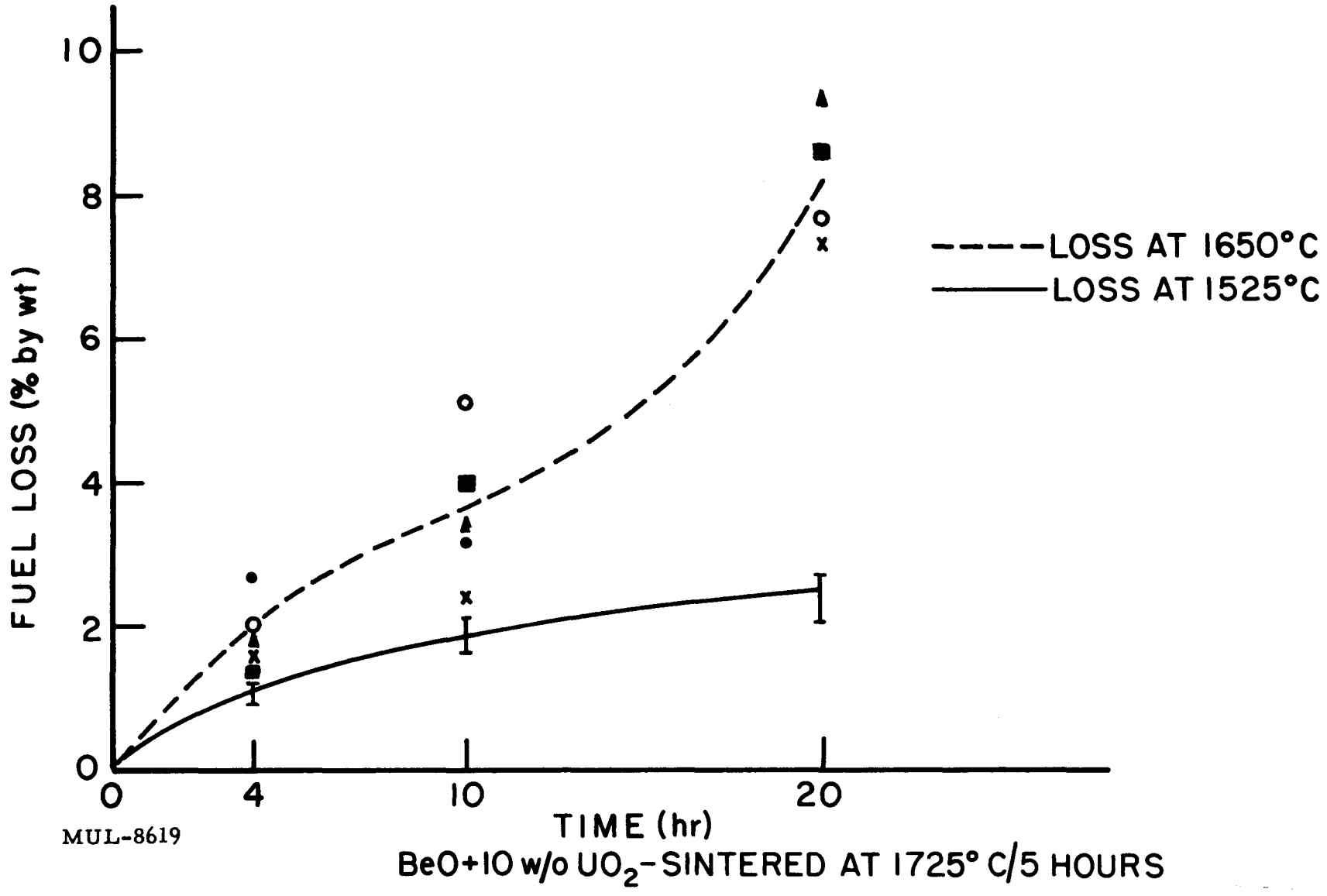

Fig. II-6. Fuel loss vs time. 10% UO_2-BeO.

TABLE II-4

Sample No.	Sintering time (hr)	Density (g/cc)	Grain size BeO (μ)	Grain size UO_2 (μ)	Distribution of urania
Mix V-18					
113	5	3.226	10-20	< 1	Evenly distributed
119	24	3.240	20-45	2	Tend to concentrate at G.B.
149	100	3.25	25-50 max 100	1-9	Concentrate at G.B.
Mix 116					
112	5	3.197	10-25	1	Tend to concentrate at G.B.
118	24	3.220	20-45	3-5	Concentrate at G.B.
150	100	3.2205	35-85 max 115	1-9	Concentrate at G.B.

Note the increasing density, BeO grain size, UO_2 grain size and increasing tendency for UO_2 to migrate from an evenly distributed mixture in the BeO to one primarily concentrated at the grain boundaries. Unlike the unfueled BeO, the BeO grains in these samples still have rounded or irregular outlines without straight sides or sharp corners. There is very little porosity apparent.

Fuel loss as a function of sintering time in hydrogen is plotted in Fig. II-7. Note that loss decreases as sintering time in hydrogen increases from 5 to 24 hours. The data are less clear from 24 to 100 hours. The specimen which showed increased fuel loss at 100 hours was contaminated with Mo crystals on one surface. We have observed in the past that BeO-UO_2 bodies contaminated with Mo failed to densify and thus had high losses.

Microstructures of these specimens after loss-testing at various temperatures in air are summarized in Table II-5. Three zones are observed:

1. An outermost colorless selvedge from which UO_2 is lost.
2. An intermediate black zone (oxidized to U_4O_9 presumably, see below).
3. An innermost, apparently unchanged brown UO_2 zone.

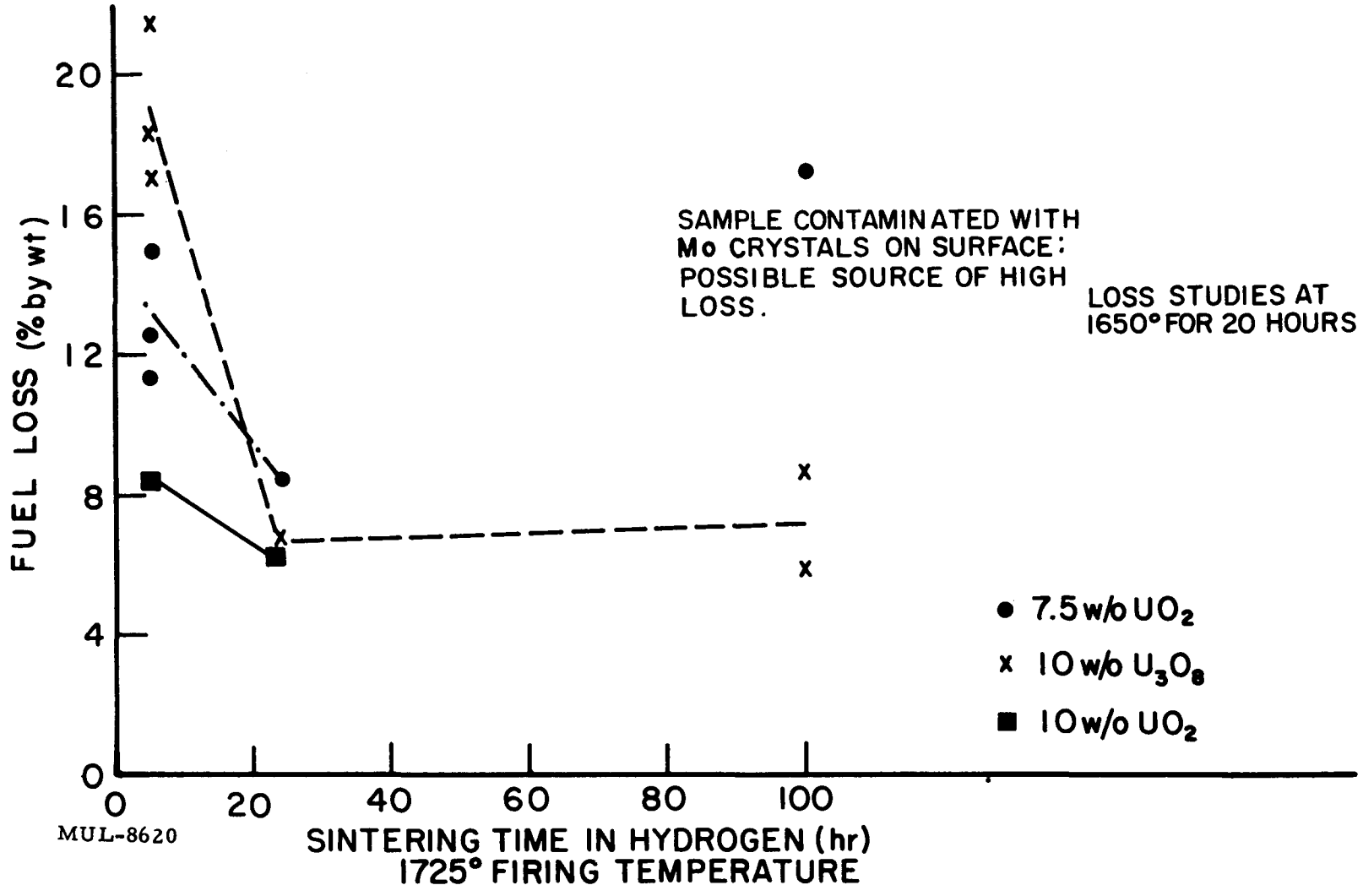

Fig. II-7. Fuel loss vs hydrogen sintering time.

Depths of zones 1 and 2 decrease with increased H_2-sintering time or decreased air firing temperature. BeO grain size increases somewhat during air firing, but not markedly. Urania grains increase appreciably in size and tend to move from interior of grain to boundaries.

TABLE II-5

Mix	Sintering time (hr)	As sintered	Fired in air 20 hours at: 1260°C	1525°C	1650°C
		Grain size of BeO (μ)			
V-18	5	10-20	10-20	10-20	20-30
V-18	24	20-45	20-45	20-35	20-35
116	5	10-25	14-45	20-35	20-35
116	24	20-45	20-45	25-55	25-45
		Grain size of urania along grain boundary (μ)			
V-18	5	1*	1*	2-4	1-5
V-18	24	2	2-6	2-5	2-6
116	5	1	1-5	3-9	3-8
116	24	2-5	2-5	2-12	2-10
		Depth of penetration (μ) of black zone/of colorless zone			
V-18	5	---	135/0	Complete/10	Complete/35
V-18	24	---	20-30/0	180/10-20	300-340/20-60**
116	5	---	60-150/0	Complete/30-50	Complete/80-110
116	24	---	35-70/0	140-180/50**	Complete/35-65

* In these samples UO_2 was evenly distributed through grain rather than concentrated on grain boundaries.

** Zone not entirely colorless. Some black urania grains retained.

The interface between the black and brown zones are straight and fairly sharp (within 1-2 BeO grain diameters) for firing temperatures of 1525 and 1650°C. In three of the four tubes fired at 1260°C, however, the interface is poorly defined and irregularly shaped. Its position seems to be controlled by imperfections and possible microcracks in the tube. There are broad irregular transition regions in which most of the urania along grain boundaries is black, but gold urania grains are retained in the interiors of the beryllia

grains. It appears that the mechanisms of oxygen diffusion and reaction in the sample at 1260°C are different from those at 1525 and 1650°C. At 1260°C, oxygen penetration seems to be more closely controlled by grain boundaries and discontinuities in the sample, while at the higher temperatures, the penetration is pervasive.

Another study examined the effect of "incomplete" H_2 firing on subsequent oxidation in air (Fig. II-8). The cylinder from which this sample was taken had been isostatically pressed and H_2-fired for only 1 hr at 1715°C. A thin disc cut from the cylinder after 4 hours in air at 1515°C was black on all surfaces. Subsequent removal of a layer from one face exposed the photographed surface. The oxidation rate was clearly more rapid in the central region than near the circumference, where an unoxidized brown zone still appears. An interpretation is that effects during the H_2 firing which result in lower fuel loss progress inward radially and were only partly accomplished. It is not clear yet whether the effect is a chemical one (e.g., reduction of non-stoichiometric UO_{2+X} to a reduced UO_2 by means of H_2) or simply a densification of the BeO-UO_2, decreasing diffusion rates of oxygen into the matrix. More extensive x-ray diffraction will be taken to clarify this point.

(4) Effect of Ball Milling

The effect of ball milling on fuel retention was examined. The batch was prepared by milling the BeO-aqueous uranyl nitrate slurry with excess NH_4OH for 24 hours, 200 mesh screening, drying, and preparing specimen in the standard manner. The results are plotted as Fig. II-9 and are tabulated below.

	Density (g/cc)	Loss, o/w UO_2 20-hour test at: 1650°C	1525°C
Milled material	3.1878	9.01	4.39
	3.1818	9.51	3.75
Standard precipitation	3.2250	8.28	2.50

The density of the milled batch is lower by about 1% than the density of standard prepared material, (consistently through the 30-sample batch) and the losses are approximately 1.5% higher. Note that the loss rates appear to decrease with time even at 1650°C.

(5) Effect of U_3O_8 Addition

To determine the effect of adding U_3O_8 powder to BeO instead of the usual diruanate precipitation, samples of BeO 10 w/o UO_2 as U_3O_8 were

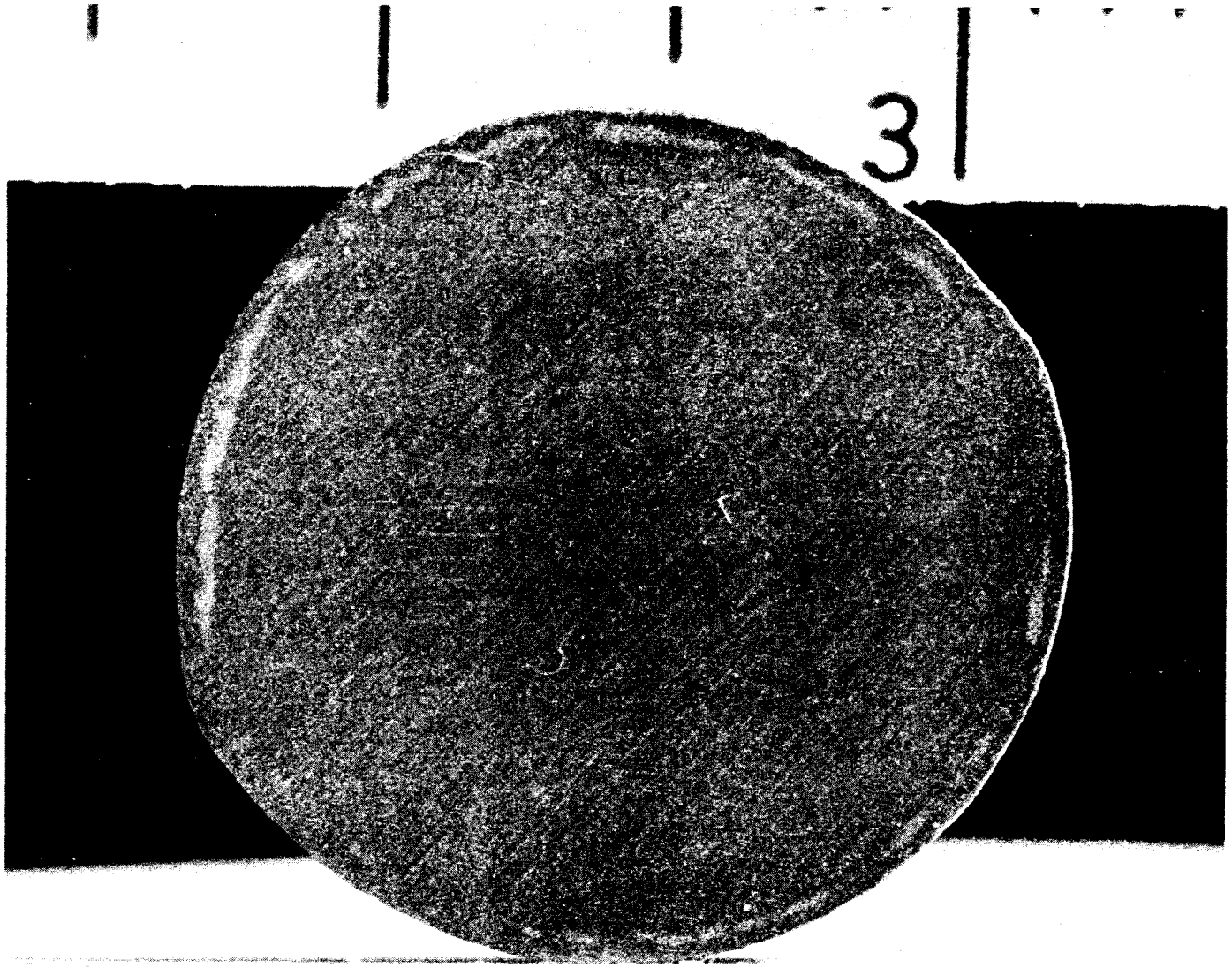

SN-18819

Fig. II-8.

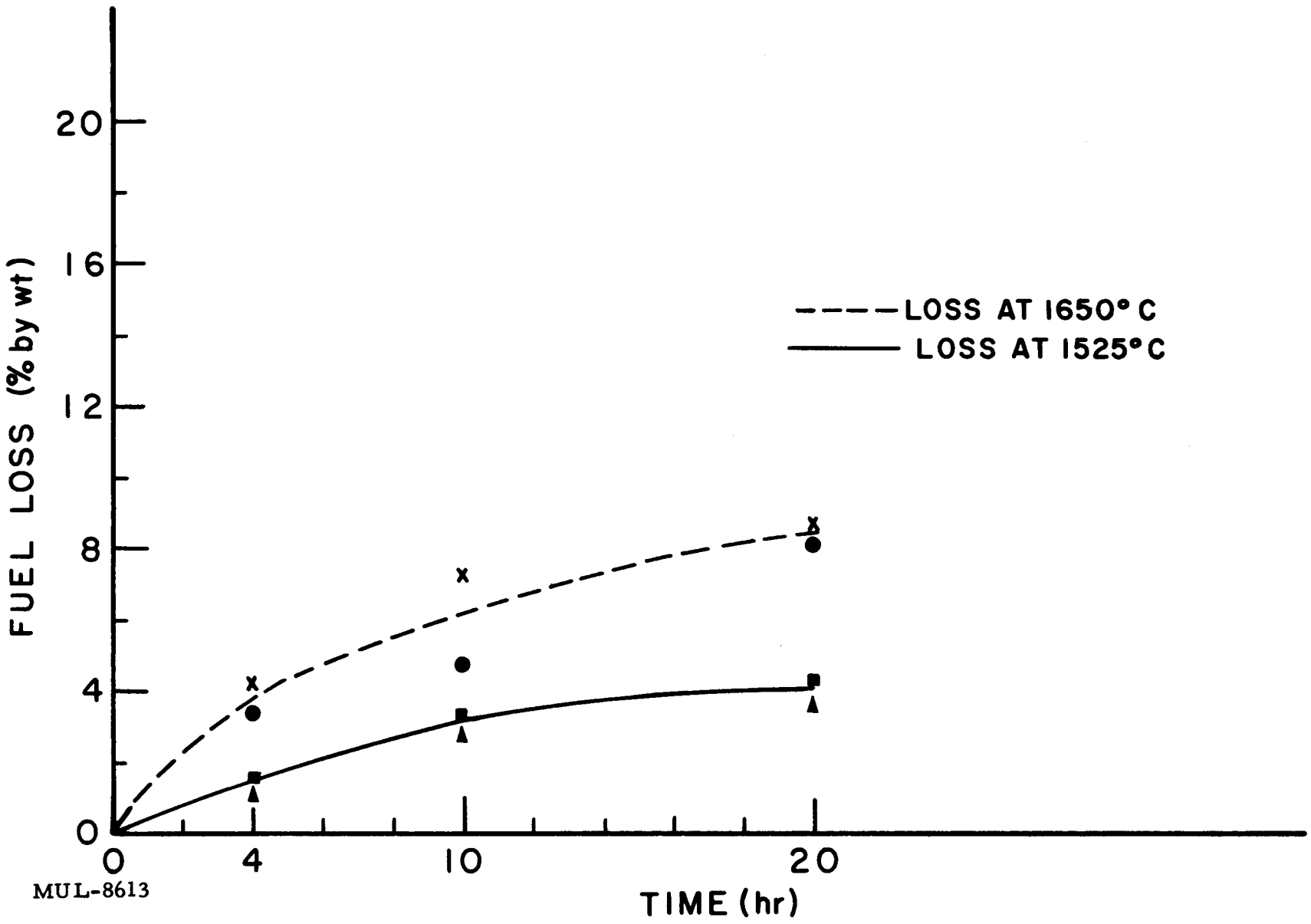

Fig. II-9. Fuel loss vs time. Ball-milled 10% UO_2-BeO.

made (Mix 116). The U_3O_8 was obtained by converting Mallinckrodt UO_2 in air at 475°C for 24 hours (confirmed by x-ray diffraction). The samples were sintered at 1725°C for 5, 24, and 100 hours.

Figure II-7 shows the fuel losses vs the H_2 sintering time; losses are compared with our standard diuranate-prepared specimens. It is of interest to note that as the soak time reaches 24 hours, the loss approaches that of the standard material.

Petrographic comparisons are made with the conventional material in Tables II-4 and II-5. In the sintered specimens, UO_2 grain sizes are larger for the U_3O_8 mix (No. 116) after 5 and 24 hours' sintering, but seem to approach those of the standard mix (V-18) after 100 hours. Also at the shorter sintering times, the urania in Mix 116 has a greater tendency to concentrate in grain boundaries rather than randomly. These observations are consistent with the coarser aggregation of U_3O_8 powder than diuranate precipitated from solution.

During oxidation tests (Table II-5), the urania grains of Mix 116 remain larger than those of V-18 under comparable oxidation conditions. Finally, penetration of the colorless and black oxidation zones are deeper in the 116 mix. These observations are consistent with the higher fuel losses for the 116 mix compared to the V-18 one.

One fact clearly emergent from the data is that concentration or urania in the grain boundaries alone does not per se cause higher fuel loss. Note that concentration of urania in boundaries does become more pronounced as hydrogen sintering times increase from 5 to 24 hours, yet fuel losses decrease in this interval, perhaps due to reaction with the hydrogen and/or increased densification of the body.

(6) Effect of Grinding

Since fuel elements may have to be ground to finished tolerance, the effect of surface grinding on fuel loss was examined. The tubes used for this test were 10 w/o UO_2 (density 99% of theoretical), which had been fired at 1725°C for 5 hours in H_2.

Specimen No. 1 was severely gouged during hand grinding. Specimens No. 2 and 3 were ground on a lathe and although much smoother, still had wheel patterns. After grinding, Specimen No. 3 was annealed at 1725°C for 1 hr in hydrogen. Measurements of 15 points with a micrometer indicated no dimensional changes during annealing. Weight loss during annealing was only 0.04%.

		% UO_2 loss by weight 1650°C/4 hr
1. Severely gouged pieces	(duplicate)	12.8, 12.0
2. Surface ground	(duplicate)	9.7, 9.5
3. Surface ground, annealed in H_2 at 1725°C/1 hour	(duplicate)	5.3, 5.1
4. Control (not ground)	(5 samples)	2.0 ± 0.6

There seems to be a real effect of grinding on fuel loss at 1650°C. The improvement effected by the 1-hr annealing is apparent; the effect of longer anneal times will be studied. Further tests are indicated on tubes ground smoother on production grinding facilities when the latter are enclosed.

4. System BeO-UO_2

a. Phase Diagram Study: Be-O-U

The phase diagram of Be-O-U warrants further study because of some unusual behavior observed in sintering and in x-ray diffraction. BeO-UO_2 sinters much more readily than BeO alone, and the lattice parameter of UO_2 in BeO-UO_2 is larger than that of pure UO_2. No evidence of solid solution or compound formation appears in the literature.

In an effort to achieve intimate mixing at temperatures below possible decomposition (other alkaline earth uranates are reported to decompose at 1100°C), Be and U were fused as nitrates and then decomposed in air.

The mixtures that have been prepared and other pertinent information are listed in Table II-6. (See page 100 for table.)

In summary two items seem significant.

1. A second unidentified phase occurring in the 99 m/o BeO-1 m/o UO_2 mixture may be a Be uranate or an Mg uranate. The latter is likely in view of alkaline earth impurities.

2. In the 50 m/o BeO-50 m/o UO_2 mixture x-ray analysis did not show the presence of BeO. It is not likely that 50 mole % (8.5 w/o) could have been lost in the decomposition process.

b. Electrical Conductivity of BeO-UO_2

Two samples of BeO-5% UO_2 have been cycled to 1440°C twice, to measure their resistivity as a function of temperature. The two cycles of one sample are shown in Fig. II-10, and the second sample gave essentially the same results for each cycle. All cycles used a dry-air atmosphere. The samples had previously been heated to 800°C in air to bond the electrodes.

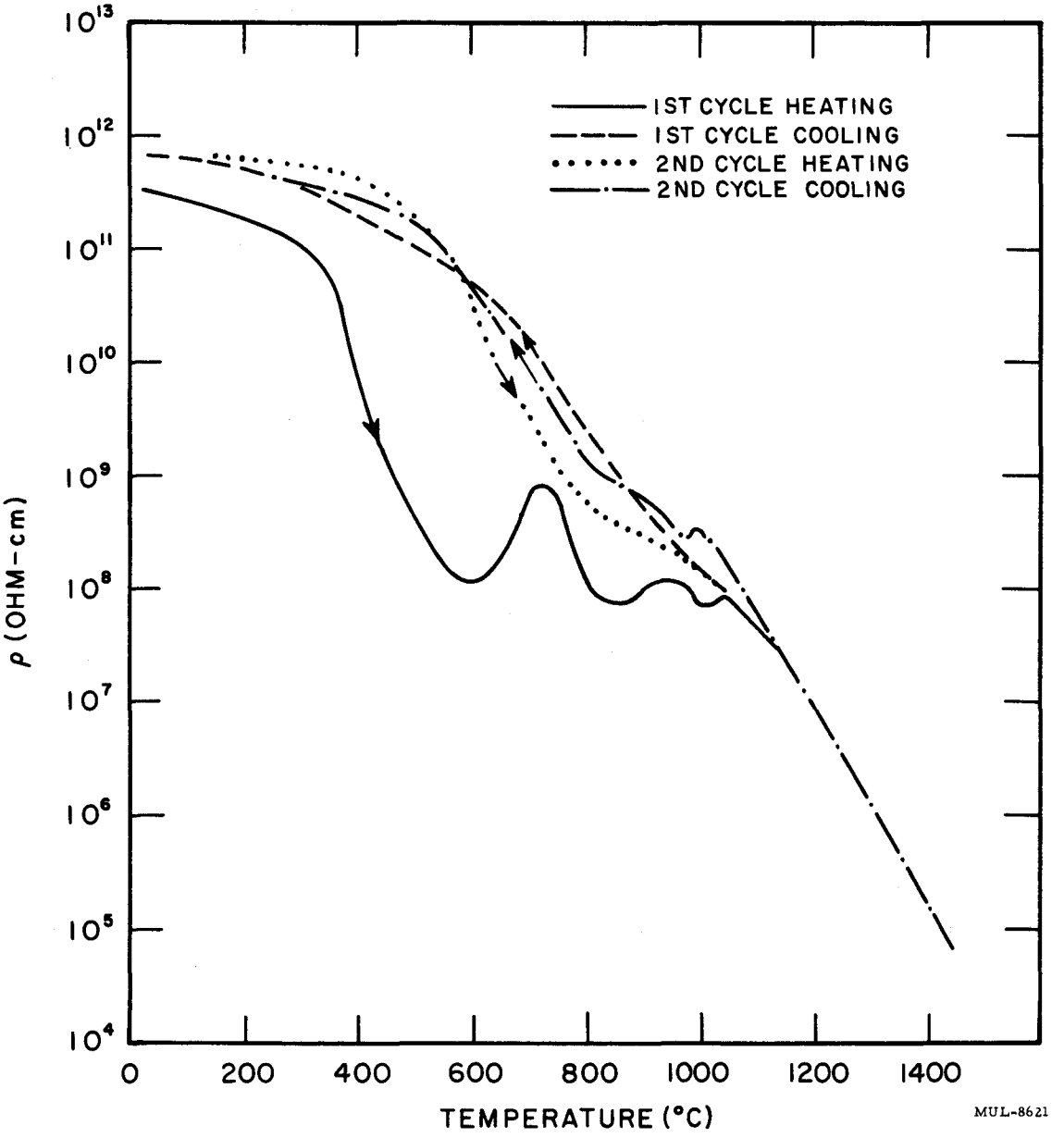

Fig. II-10. Resistivity vs temperature of BeO-5% UO_2.

TABLE II-6

Mole ratio BeO/UO_2	Temperature of decomposition °C	Decomposed color	X-ray analysis
99/1*	900	Cream-white	Good BeO pattern present. No U_3O_8, $CaUO_4$, $MgUO_4$ present. Strong lines from second unknown phase present. D_{hkl} = 5.91, 3.34, 3.16. The second phase could be MgU_2O_6 which is reported to have the fluorite structure of UO_2.
50/50	500	Red-orange	Powder pattern was poorly developed due to poor crystalline development.
50/50	900	Black	Good U_3O_8 pattern but no second phase. Conspicuous absence of BeO pattern.

*Confirmed by chemical analysis after air-ignition. Spectrochemical analysis of the fused mass: Mg, 1%; Ca, 0.03%; Al, 1%; (Fe, Mn, Si, B), 1%.

An electrometer was used to measure the voltage drop across a known variable resistance which was in series with the sample. By knowing the total potential of the circuit the resistance of the sample may be calculated. The first sample was 11/16 in. diam and 0.4 in. thick with platinum electrodes on each face. Two-mil platinum foil was bonded to the $BeO-UO_2$ with platinum paste and the composite fired to 800°C.

For both samples the heating curve for the first cycle was different from the cooling curve between 25 and 1150°C. The second-cycle heating and cooling curves followed closely the first-cycle cooling curve. This would indicate that an internal change in the material takes place around 600°C in an air atmosphere, but is not reversible when some temperature between 800 and 1400°C is reached.

5. Be-B System

The BeB_2 sample prior to test had been sintered in argon at 1675°C to 70% theoretical density. No oxidation was observed up to 900°C. Weight changes from 900°-950°C are listed in Table II-7 and are plotted in Fig. II-11. The data indicate that the buoyancy and convection disturbances were not

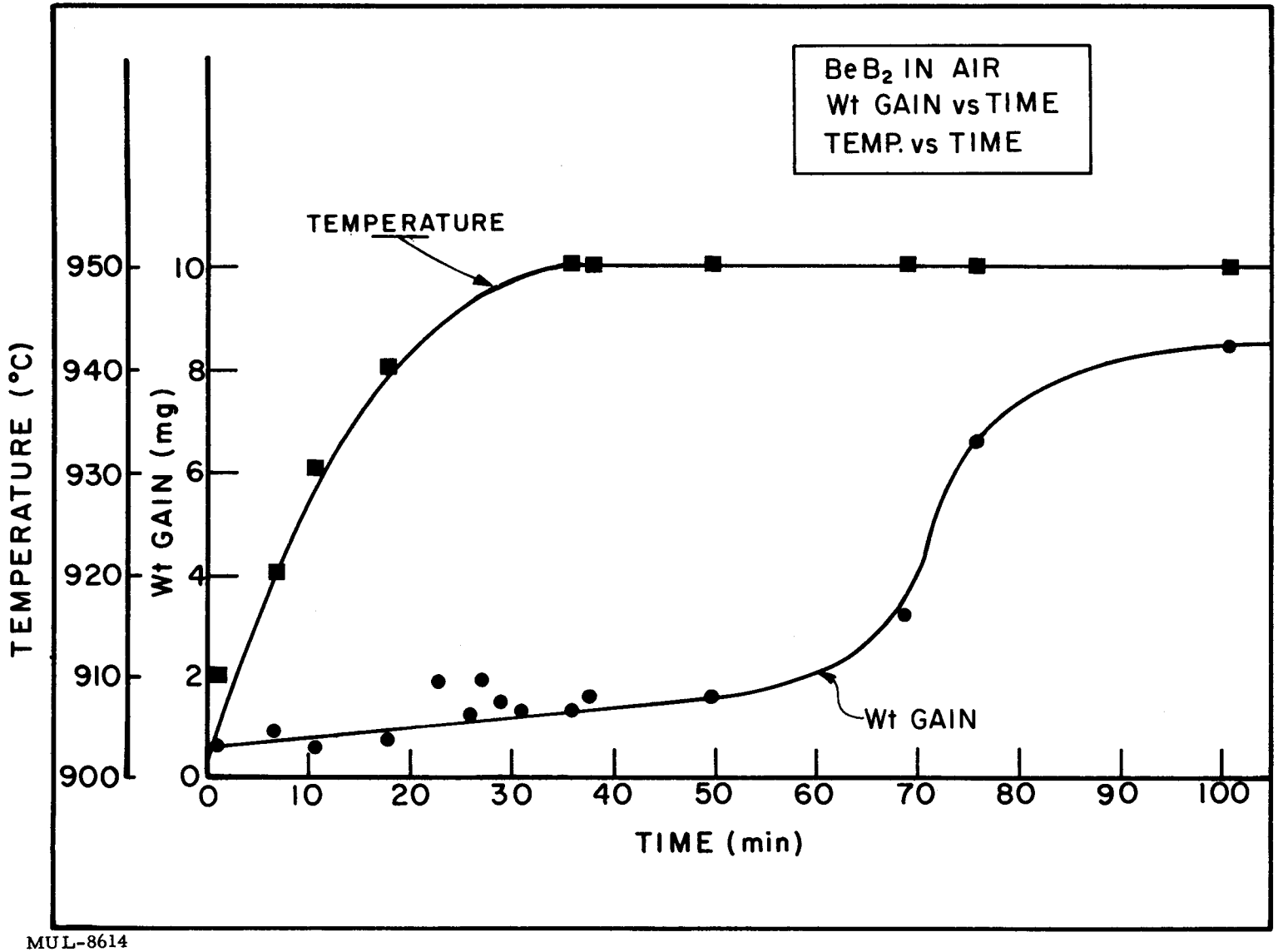

MUL-8614

Fig. II-11. BeB_2 in air. Weight gain vs time, and temperature vs time.

significant relative to the oxidation process once constant temperature (950°C) had been reached. The rate curve shown in Fig. II-11 is a parabolic type indicating that some reaction product is forming and acting as a diffusion barrier to further oxidation. Unfortunately, the data are not extensive enough to show conclusively that the reaction product will continue to protect.

The hardness data have been refined through observation at a higher magnification. The new hardness data are shown in Table II-7. The BeB_2 and the red crystal phases have among the highest hardnesses observed in compounds.

TABLE II-7

Be/B ratio	Melting pt. (°C)	X-ray identification	Hardness identification (Mag.) (1200X)
6/1	1100	Two phases:	
		Be	704 ± 25 (HKN-20)
		Unknown δ phase	1500 ± 50 (HKN-50)
2/1	1400	Two phases:	
		Be_2B	2350 ± 75 (HKN-50)
		Unknown δ phase	Too little to measure
1/2	1750-1950	Two phases:	
		BeB_6	2577 ± 75 (HKN-100)
		BeB_2 (?)	3181 ± 100 (HKN-100)
1/6	1950	BeB_6	2588 ± 75 (HKN-100) (500X)

Note: Some red crystals of microscopic size which condensed on the side of the BeO crucible showed very high hardness: 4377 ± 240 (HKN-50).

6. Coated Graphite

The silicon-coated graphite program has been discontinued for the present. The work indicates that moderately large samples can be coated without cracking or spalling.

The most successful sample of the program was a solid cylinder 4 in. in diam and 2.4 in. high. This sample lasted 665 hours at 1350°C in air and did not fail catastrophically.

Two cylinders with 127 holes 0.200 in. in diam were also coated. The purpose of these samples was to determine if a graphite base plate for Tory II-C

could be coated. The first sample cracked between the outermost holes and the circumference of the cylinder, a distance of 5/32 in. The minimum hole distance to the circumference was increased to 3/8 in. in the second sample. The second sample coated completely and was free of cracks. However, the sample failed in 1 hr at 1350°C in air. The failures were caused by pin holes on the outer circumference of the sample which one expects would be the easiest surface to coat. The failures were probably due to "over-oxidation" of this surface during the procedure to botain the proper oxidation in the many small holes.

A 3-in. sphere proved to be the easiest shape to coat. This sample was not tested.

The graphite used in this coating work was Grade A which has some undesirable features for coating work. The main disadvantage is that the depth of penetration of the coating into the graphite is greater in a radial direction than in an axial direction. It is probable that a more uniform grade of graphite would permit still better coating results.

B. Mechanical Properties

1. Thermal Stress (Process and Materials Development Section)

During the current quarter, thermal stress data have been obtained on pure BeO at 600, 800, 1000, and 1200°C. The data are listed in Table II-8 and plotted against temperature in Fig. II-12. Sample firing histories are also described. The time to obtain the desired power in the heater is of the order of 20 sec. Preliminary calculations indicate that the stresses are imposed in times of 10 sec, at 1000°C, and less at lower temperatures, so that the ΔT is established before failure occurs.

The thermal stress resistance of BeO decreases with increasing temperature, which is to be expected if the material is behaving elastically. Above 1000°C the stress resistance may be increasing again due to plastic behavior, but the data are not sufficient to state this with certainty. The fiber stress at failure calculated by averaging thermal stress parameters (R') at each temperature is roughly constant (except at 1200°C) and approximates known modulus of rupture for BeO (see Table II-8). Note that the scatter in R' is rather large, so the significance of constant fiber failure stress is questionable.

The type of fracture appears to be more severe in these higher density specimens than in the lower density ones reported previously; cracks propagate across the length of the specimen and in some cases radial cracks appear.

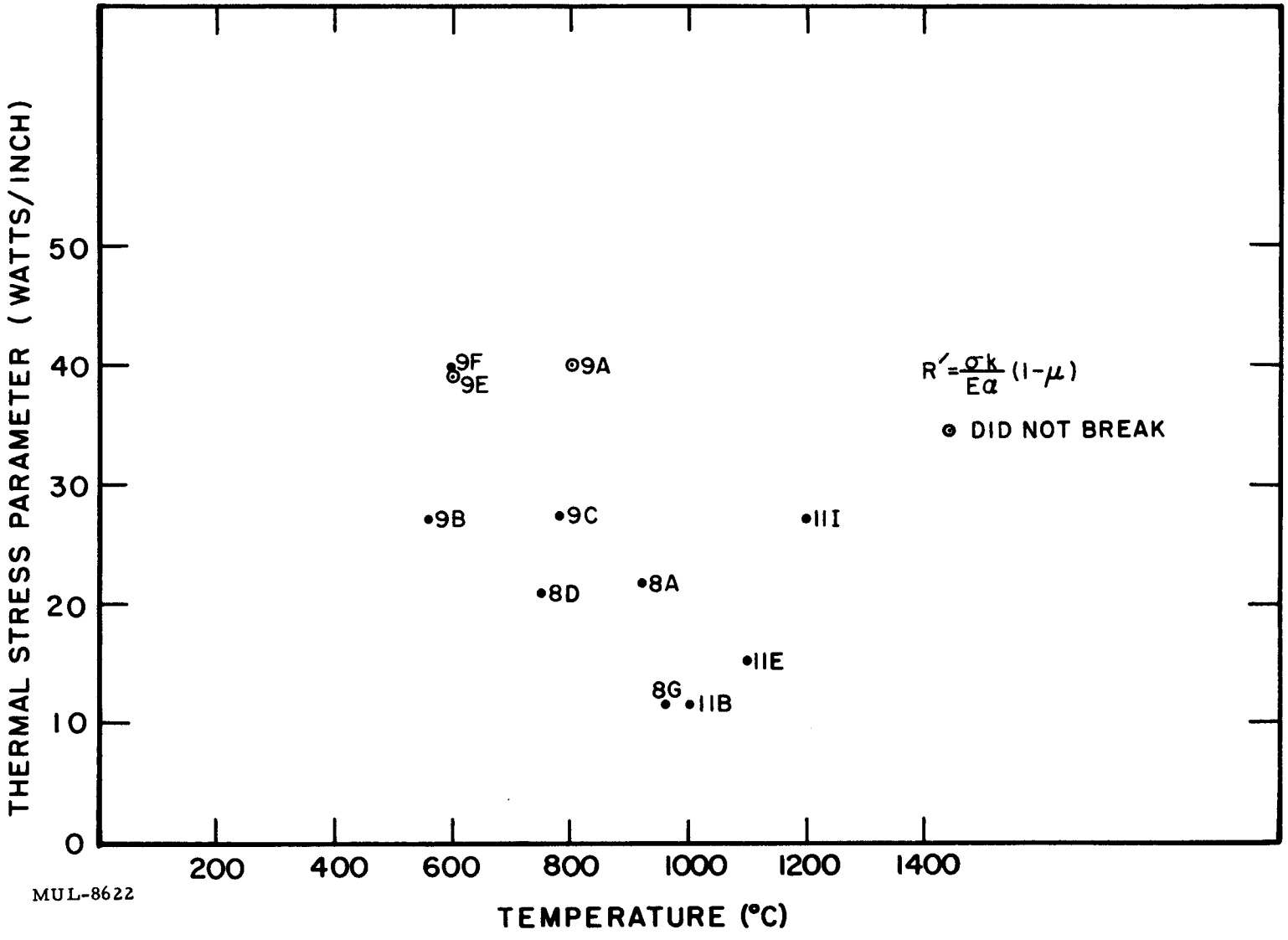

Fig. II-12. Thermal stress parameter vs temperature.

Samples are generally cycled up and down in power and temperature to incrementally reach the point at which failure occurs. The effect of this cycling on the measured stress resistance will be studied, since a reverse residual stress would bias the data and could increase the power required to cause failure.

TABLE II-8. THERMAL STRESS RESISTANCE OF PURE BeO

Sample No.	Failure temp.	ρ (g/cm^3)	P_f (watts/in.)	ΔT_f (calc.) (°C)	R_f' (watts/in.)	Average σ_f (psi)
9E	--	2.93	>567*	104	39.0	
9F	600	2.93	583	106	40.0	19,400
9B	560	2.92	392	95	27.0	
8D	750	2.92	297	72	21.0	
9C	780	2.93	400	98	27.5	22,300
9A	--	2.93	567*	137	>40.0	
8G	960	2.91	167	97	11.8	
8A	920	2.93	320	51	22	15,100
11B	1000	2.94	>167	83	<11.8	
11E	1100	2.95	223	85	15.5	18,600
11I	1200	2.95	400	150	27.5	35,400

* Did not break

R_f' = thermal stress parameter = $\frac{\sigma \rho k}{E a}(1-\mu)$

Sample Histories:

Sample batch	Sintered in hydrogen	
	Time (hr)	Temp (°C)
9	8	1800
8	5.5	1750-1800
11	14	1800

2. Compressive Creep

Hot Pressed BeO. The results of creep tests run on supplier's hot pressed G.C. Grade BeO are given in Table II-9.

These results for creep are up to 6 times higher than the results of similar tests performed on specimens hot pressed by another corporation using "High Purity Grade" BeO reported last quarter. Petrographic examination of samples of the two grades of BeO, BB-GC-4 (GC grade) and BC-BH-31 ("High Purity"), after creep testing showed that the specimen hot pressed from GC had pores distributed throughout the grains and at the grain boundaries while the specimen hot pressed from High Purity had few pores in the grains

and most of the porosity at the grain boundaries (see Fig. II-13). These data indicate that the porosity distribution can have a large effect on the creep properties of BeO since the other measurable characteristics of the specimens, purity, density and grain size, are approximately equal.

TABLE II-9

Specimen*	Density g/cc	Density % theo.	Test Temp (°F)	Test Load (psi)	Test Time (hr)	Total strain (in./in.)	Constant strain rate (%/hr)
BB-GC-3	2.84	94.5	2300	1000	22.2	0.0087	0.04
BB-GC-3			2400	1000	17.2	0.0255	0.15
BB-GC-3			2500	1000	1.5	0.0066	0.46
BB-GC-3			2600	1000	0.68	0.0085	1.25
BB-GC-3			Total		42.0	0.0513	
BB-GC-4	2.96	98.5	2400	1000	16.4	0.0125	0.072
BB-GC-4			2500	1000	4.0	0.0120	0.244
BB-GC-4			2600	1000	2.2	0.0129	0.59
BB-GC-4			2700	1000	1.2	0.0140	1.16
BB-GC-4			Total		25.1	0.0525	

*Both specimens were preconditioned for 12 hours at 2850°F in air before testing.

One specimen, BC-BH-37, hot pressed from "High Purity" BeO was tested at different stress levels and constant temperature, 2500°F. The specimen had a density of 2.84 g/cc (94.3% theoretical) and had been preconditioned for 12 hours at 2850°F in air before testing. The results are given below.

Load (psi)	Time (hr)	Total strain (in./in.)	Constant strain rate (%/hr)
500	12.7	0.0045	0.043
750	10.4	0.0059	0.057
1000	16.8	0.0137	0.080
1250	8.0	0.0084	0.100

In this range, constant creep is linear with stress (Fig. II-14), and gives a stress factor of 8.0×10^{-5} %/hr/psi.

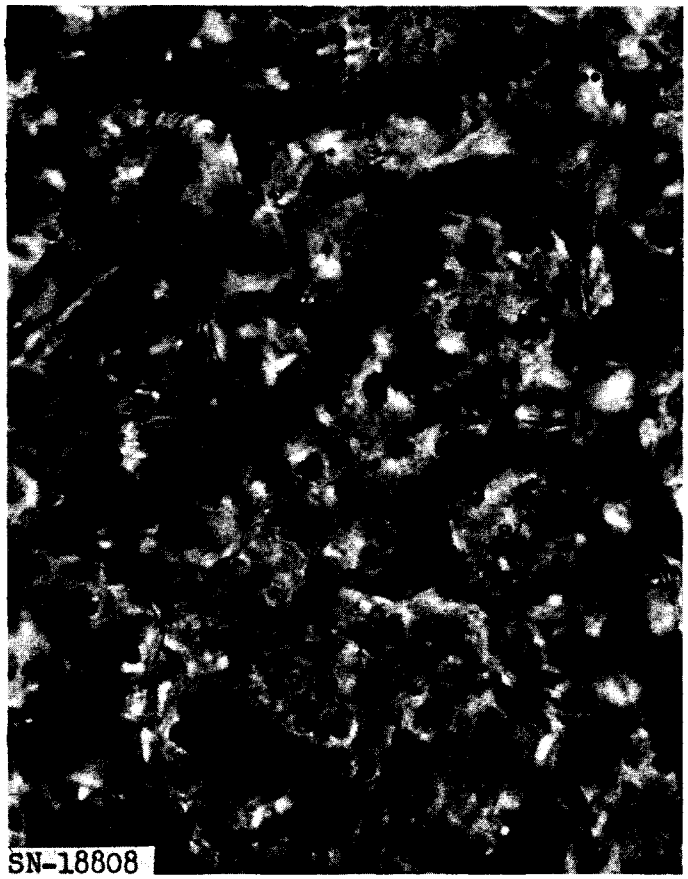

BB-GC-4
1500×, plane polarized light

BC-BH-31
1500×, plane polarized light

Fig. II-13.

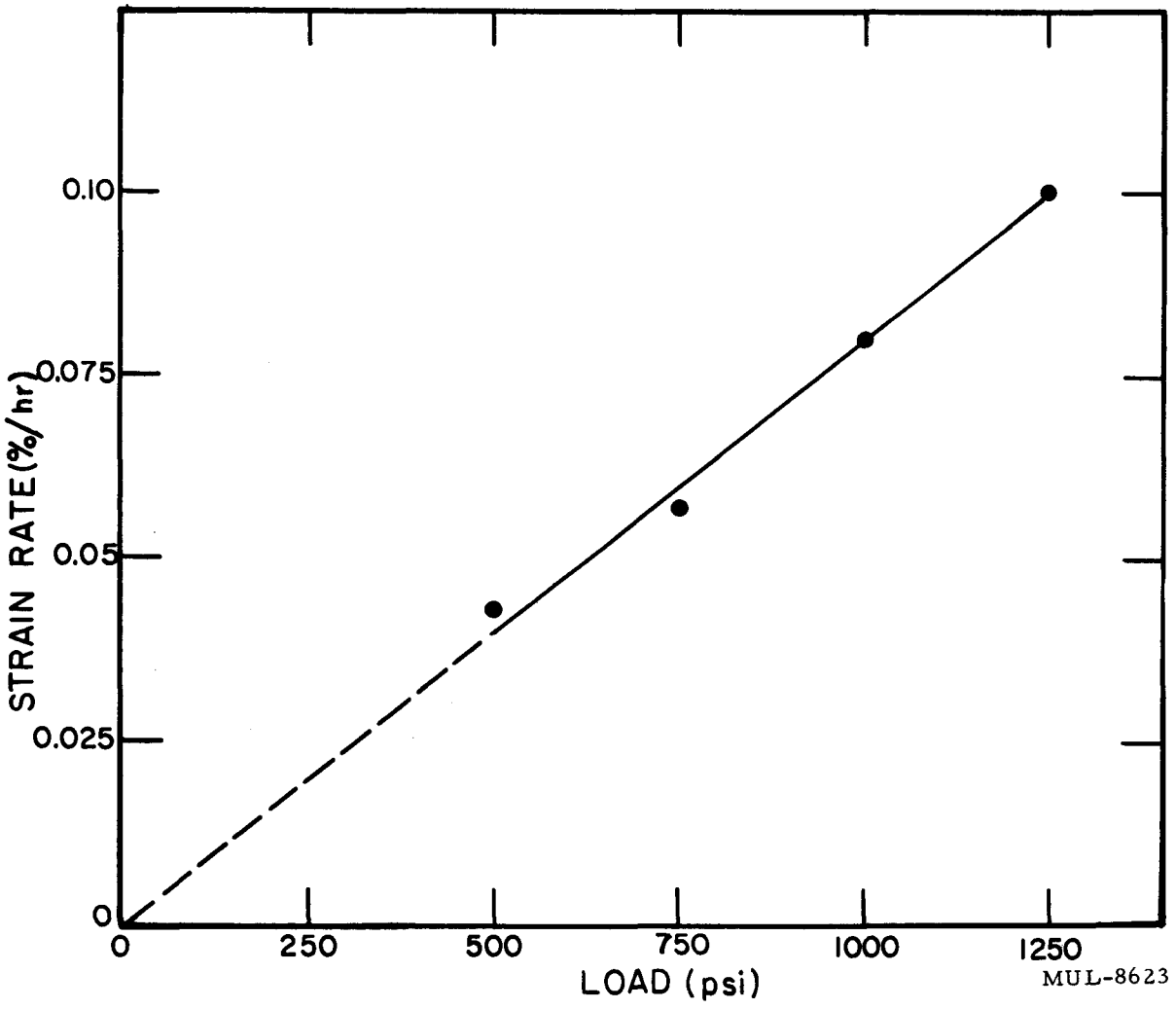

Fig. II-14. Creep rate vs load, BeO at 2500°F.

Extruded BeO. The results of creep tests run on specimens extruded by LRL from supplier's UOX Grade BeO are given below in Table II-10. Both BeO and BeO-UO_2 specimens were tested.

TABLE II-10

Specimen*	Density g/cc	Density % theo.	% UO_2	Test Temp (°F)	Test Load (psi)	Test Time (hr)	Total strain (in./in.)	Constant strain rate (%/hr)
1E98-2	3.06	94.2	10	2500	1000	10.0	0.0227	0.22
1E98-4	2.94	90.7	10	2500	1000	5.2	0.0512	0.84
4E105-1	3.16	99.4	7-1/2	2500	1000	11.0	0.00076	0.0027
7X115-1	2.94	97.7	0	2500	1000	29.3	0.00054	<<0.001
7X115-3	2.95	98.1	0	2700	1000	28.8	0.00031	0.00057
7X115-3	2.95	98.1	0	2800	1000	141.8	0.0175	0.0077

*Specimen 1E98-2 was preconditioned for 2 hr at 2850°F in air before testing; the others received no preconditioning.

Specimens 4E105-1, 7X115-1 and 7X115-3 which are high density, 98-99% of theoretical, gave the lowest values of strain rate that we have measured to date or have seen reported in the literature for BeO. In fact they are almost at the lower detectable limit of our apparatus.

Petrographic examination shows that there is a preferred orientation of the c axis parallel to the extrusion direction. All compression tests have been made with the compression parallel to the extrusion direction. It is planned to run tests with the compression perpendicular and at 45° to the extrusion direction.

Air Apparatus. Room temperature modulus of rupture tests have been made on pure BeO and 10% UO_2-BeO, to check out the apparatus. The calculated outer fiber stress for pure BeO in two tests were 21,000 and 26,000 psi, and 31,000 psi for the 10% loaded BeO.

3. Coefficient of Friction

The following static coefficient of friction measurements were made at room temperature to aid in the design of copper clamp-on grips for BeO tensile specimens:

Contact surfaces	Contact pressure	Coefficient of friction
BeO vs Cu	500	0.31 ± 0.02
Pt coated BeO vs Cu	500	0.33 ± 0.01
Ag coated BeO vs Cu	400	0.40 ± 0.01

The BeO used was hot pressed, 95% theoretical density.

C. Construction and Planning

Fuel Element Fabrication Facility (Building 192-C)

The status of equipment to perform operations in Building 192-C is as follows:

Raw Material Supply and Storage. Thirty containers of Oy nitrate have been received and are now in storage in the vault in Building 102.

The transfer hood, sampling devices, and storage tank have been completed and leak-checked using water at 25 psi pressure. The storage tank has been calibrated and working charts made. The BeO storage bins, gloved box, and hoppers are completed and ready for use.

Measuring, Mixing, Filtering and Drying Equipment. The Oy nitrate solution measuring tank and all its components are completed and have been checked for leaks. The tank has been calibrated and working charts made. The BeO weigh box and scales are ready for use. The BeO batch containers are being fabricated. The mix boxes, filter boxes, and dryer boxes are completed. All pipe lines have been leak-checked and a number of batches of MgO have been slurried in order to check out the mixing pot action, the filtering efficiency, and the dryer operation. These units have performed satisfactorily using MgO and filter runs are planned using tuballoy precipitated on BeO, following the same procedures which will be used in actual production. It is planned to take batches thus prepared through the entire process through extrusion and sintering of samples. A method for preforming the filter tubes is being developed. The method of seating the filter papers in the basket has been changed from water immersion to spray in order to decrease contamination on the outside of the basket. A safe storage rack on casters has been completed which will take the surge from the dryer.

Blending and Pugging Equipment. The equipment in this section has been completely installed and initial runs using unfueled BeO are being made. A moisture balance has been installed in a box to determine the total free moisture of the filter cake from the dryers prior to the blending and pugging process. Equipment (mixers, scales, etc.) is being purchased for binder preparation and a work bench has been set up to handle this operation.

Storage Area. The "always safe" shelf arrangement for storing and aging mixed batches prior to extrusion has been erected beneath the extruder platform. A Butler building for storing in-process material has been constructed.

Extruder-Conveyor-Dryer System. All components of this system have been completed and tubes of straight BeO have been extruded under actual operating conditions. A heat balance study of the conveyor-dryer was made and current production is being made under modified conditions of uniform temperature gradient along the conveyor. A rack for storing tubes subsequent to burn-out and prior to sintering has been constructed.

Hydrogen Kiln. The entire operating schedule of this furnace has been revised since the initial run, and numerous safety devices have been installed. A shakedown run for this kiln to 600 °C was made without incident.

Liquid Waste Disposal. Installation of the waste tank system has been completed and operation has been proven. Two-wheel liquid-waste trailers have been received and pressure checked, and are ready for use.

Reclaiming Process. The reclaiming silo is being completed. Electrical wiring is completed and the lucite sides installed.

Analytical Control Area Hoods. This equipment is completely installed and the area is ready for use.

II. PLASTICS

Graphite Coating

During the operation of the Tory II-A reactor water is circulated through the graphite as a cooling medium. A coating was required which makes the graphite impervious to water. The coating selected:

1. Should not reduce the graphite thermal conductivity appreciably.
2. Should be nearly impervious to water from room temperature to 96 °C at 25 psi pressure.
3. Should have good bond strength.
4. Should be resistant to radiation damage.

Table II-11 gives the formulations for the various coatings. Leakage of water through the graphite had to be less than 0.13 mils/min/m^2. The two best coatings (Nos. 187 and 198) were chosen on the basis of zero water penetration, non-measurable coating thickness, negligible effect on thermal conductivity of the graphite, and ease of application.

TABLE II-11. FORMULATIONS OF GRAPHITE COATINGS.

Coating No.	332 LC Dow	ERL 3794 Bakelite	332 Dow	Versamid 140	n-amino ethyl piperizine	Toluene	X-71 Shell	Gen. Elect. SR-53	Laminac 4128	MEK	Benzoyl peroxide	Laminac Promoter No. 400	Copon No. EA-200	Copon Activator	Dehydrative No. 22	Genamid 250	Genamid 310
176	X			X													
177	X			X		X											
178	X				X		X										
179	X				X	X	X										
180	X				X												
181	X				X	X											
182								X									
183	X				X	X	X	X									
184	X			X		X		X									
185	X																
187	X				X	X	X										
194									X	X							
195						X			X	X							
196									X		X	X					
197						X			X		X	X					
198													X	X			
199															X		
200	X															X	
201	X																X
202	X																X
203	X															X	

Thermal conductivity is obtained by determining the temperature difference (ΔT) across the coated sample for a given heat flow and fixed geometry. Table II-12 lists ΔT's which are inversely proportional to conductivities. Conductivities were measured near 99°C and at 22°C to represent the temperature range of interest.

TABLE II-12

Average Temperature 99°C						
Coating No.	No coating	187A	187B	187C	187D	198
No. of coatings	--	1	2	3	4	1
ΔT °C	29.6	29.3	30.5	30.8	28.7	28.5
Average Temperature 22°C						
Coating No.	No coating	187A	187B	--	--	198
No. of coatings	0	1	2			1
ΔT °C	7.3	6.7	7.0			7.8

Table II-13 gives the results of water penetration for both hot and cold water at 25 psi. Note that a number of the coatings met the penetration requirement.

Resistance to radiation damage was determined under conditions simulating the Tory II-A conditions. After irradiation the coatings maintained their resistance to water penetration.

The final coating selected (187) gave the desired properties, i.e., good radiation resistance, low water penetration, good thermal conductivity and ease of application. The final formula is:

	Weight %
Dow low-chlorine epoxy resin No. 332 LC	15.62
n-amino ethyl piperizine	6.25
Toluene	31.25
Shell Chemical Co. epoxy resin X-71	46.87
	99.99%

TABLE II-13. FLOW RATES OF DISTILLED WATER THROUGH A 1.50-INCH DIAMETER SPECIMEN OF COATED GRAPHITE 1/4-INCH THICK

Specimen†	Flow rate, ml/min.*	
	Cold (70°F)	Hot (200°F ± 15°)
176	2.28	0
177	1.30	0.01
178	0.067*	0.0067
179	0.267*	0.0033
180	1.39	0
181	0.10*	0
182	3.00	5.62
183	0.33*	0
184	0.133	0
185	1.00	0.93
186 (No Coating)	3.15	3.64
187	0	0
194	0	0
196	0	0
197	0	0
198	0	0
199	5.22	5.00
200	0.40	0
201	1.11	0
203	0	0

* Flow rates so marked are in drops/min.

† Specimen 196 was noticeably soft at 200°F. Specimen 176 was damaged after the test.

SECTION II. THERMAL FRACTURE OF BERYLLIUM FUEL ELEMENTS (BLOWPIPE)

Tubular beryllia specimens, about the same size as the Tory II-A fuel elements, are subjected to high temperatures and high thermal stresses in the Blowpipe apparatus. A specimen is heated by thermal radiation from a graphite heater surrounding it. The heat is removed by forced convection cooling at the inside surface, using helium.

One hundred thirty-seven tests have been performed to date. Thirty eight of the tests performed since the last quarterly report have been with specimens having densities of 98% or higher and 10% uranium by weight.

The tests have been of three types:

1. Rapid start, rapid stop, 5-minute duration, single-cycle, various stresses and temperatures;

2. Same except 10 stress cycles applied to each specimen, and the same stress and temperature for all tests;

3. Same except single-cycle, test times of 1, 2, 4, 8, and 16 minutes, all tests at approximately the same stress and temperatures.

Tests of Types 1 and 2 were to obtain statistics on damage, as were all previous tests. Tests of Type 3 were to obtain data on residual stresses. The evaluation of these data is incomplete.

The results of the Type 2 tests (10 cycles) are listed below. This limited amount of data indicates that the degree of damage is somewhat worse with 10 stress cycles than with 1.

Specimens Cycled 10 Times

Thermal stress parameter, $\frac{\sigma k}{E\alpha}$ = 23 to 30 w/in.

Inside surface temperature = 1860 to 2050°F

Five tests, damage as follows:

No damage	1
Mild "	3
Severe "	1

The results of the Type 1 tests performed to date on specimens of 98% density or greater are shown in Fig. II-15. The ordinate is the thermal stress parameter, $\sigma k/E\alpha$, which represents the severity of the test. The thermal stress generated in the fuel elements of Tory II-A at design conditions is shown by the curve. The degree of damage is indicated by the symbol ◯ for no damage, ⌒ for one or two cracks, and for more severe damage.

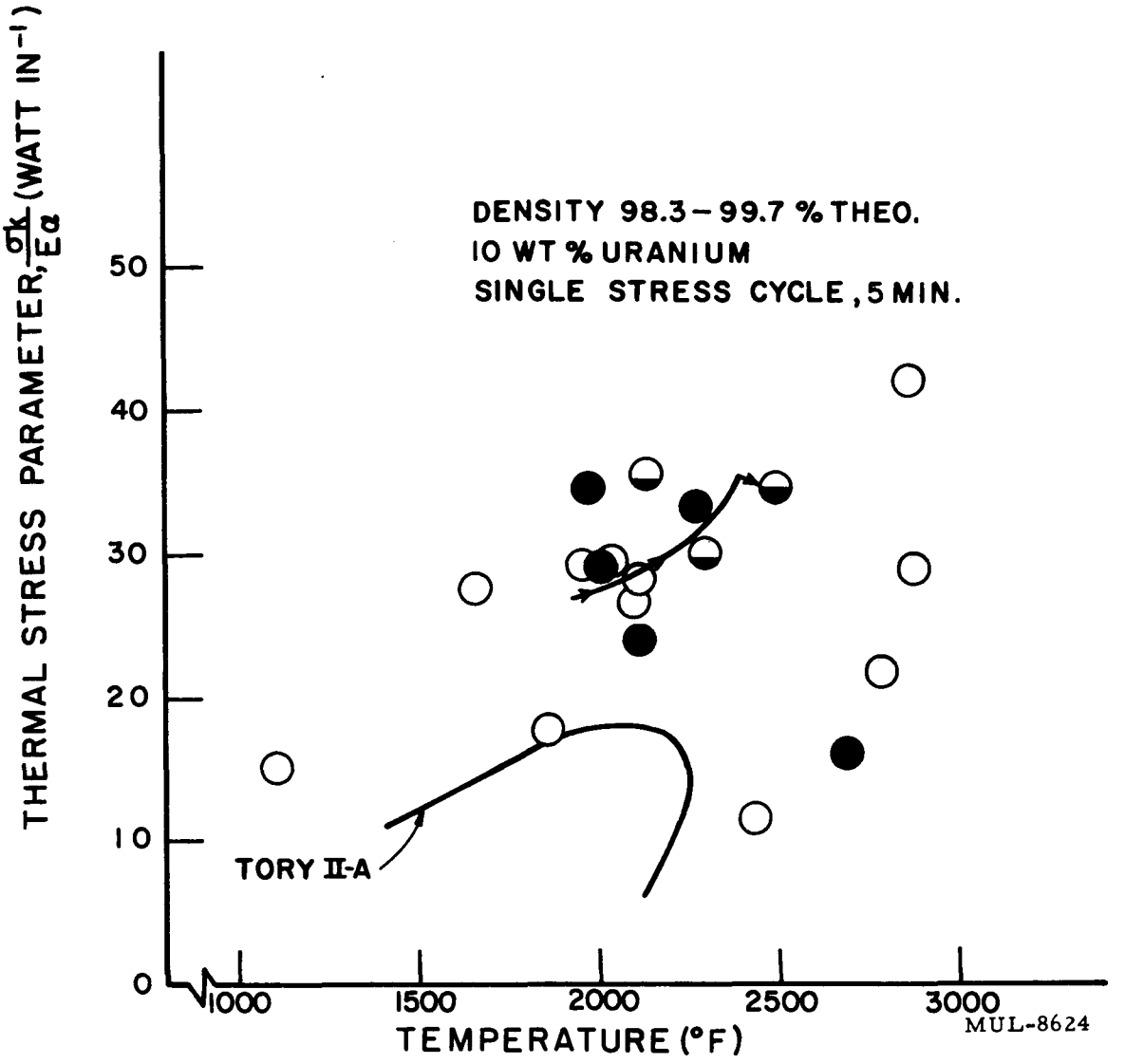

Fig. II-15. Blowpipe thermal fracture tests.

Theoretical studies have indicated that although our comparison of Tory II-A conditions and the test conditions is based on elastic theory, the comparison is still valid if considerable inelastic action occurs. Other studies have shown that the thermal stresses in the hexagonal fuel element are at most 5% higher than in an equivalent round tube on which the "Tory II" curve in Fig. II-15 is based.

The previous conclusion, that " 'failure' seldom occurred when the Tory II-A conditions are not greatly exceeded" seems to still be justified except that "failure" may be too strong a word; "substantial damage" might be better. "Failure" in the sense of actual breaking of the specimen has occurred only a few times, usually only under very severe conditions.

SECTION III. GENERAL CHEMISTRY

I. ANALYTICAL AND SUPPORT ACTIVITIES

A. Wet Chemical Analysis

A beryllium box line for the analysis of uranium in BeO prior to sintering has been completed, and is located in Bldg. 154D. The line consists of a balance box for weighing the sample, a furnace box for igniting the sample to the oxide, and a hood for dissolving the sample. A titration box houses an automatic titrator which follows the reduction of U^{VI} to U^{IV} by Cr^{++} ion, and which allows the titration of the reduced uranium with either primary standard permanganate or ceric solution. All controls are outside the box.

Methods have been developed for the determination of Mg and Al in BeO-UO_2 sintered pieces.

B. Emission Spectroscopy – Spectrographic Determination of Impurities

The spectroscopic method for the determination of impurities in BeO has been further refined to increase the sensitivity for certain elements. Examples of present detection limits are: B - 0.5 ppm, Cd - 2 ppm, Ni - 1 ppm, Cr - 1 ppm.

C. Electron Microscopy

Fractography. BeO-UO_2 pieces fractured by thermal stress have been examined by the electron microscope. The method enables one to determine whether fracture occurs by propagation along grain boundaries or if the cracks cut across the grains. It is hoped to relate the mechanism of fracture to fabrication variables.

Cathodic Etching. Cathodic etching (ion bombardment) is being used to enhance the differentiation between grains in BeO and BeO-UO_2 ceramics for viewing with an optical microscope.

D. Air-Borne Beryllium Monitor

A two-channel direct-reading spectrometer has been constructed for the spectrographic determination of air-borne beryllium. The instrument is mobile and consists of a monochromator modified by addition of a focal curve and two photomultiplier tube assemblies, a spark generator, photomultiplier tube power supply, and integrator-amplifier. Air is sampled through a 3/8-in.-diam filter disc, which is then glued to one of the electrodes and sparked. The instrument is capable of readily detecting 0.05 micrograms of beryllium. The reference spectral line has not been fixed. A more linear integrator-amplifier of wider range is under construction; on its completion the final calibration of the instrument will be made.

E. Phases Present in Supplier's Fueled Tubes

Several samples of supplier's tubes were received and subjected to x-ray analysis. These tubes contained CaO in roughly the same concentration as UO_2. Upon exposure to air at 1200°C for several hours, the tubes had cracked and turned from black to yellow. X-ray powder patterns showed the presence of $CaUO_4$ in all specimens after testing, where only CaO and UO_2 were found in untested pieces. The expansion accompanying the phase change resulting from the oxidation of the UO_2 is doubtlessly responsible for the destruction of the piece. The reason for such rapid oxidation of the CaO-containing tubes is not clear.

II. MATERIALS DEVELOPMENT

A. Beryllides

During the current period, 100 g of preparations of the powders of $NbBe_3$, $NbBe_2$, Nb_3Be_2, $TaBe_{12}$, and Ta_2Be_{17} were prepared. These compounds, together with available supplies of $ZrBe_{13}$, $NbBe_{12}$, and Nb_2Be_{17} are being used to establish sintering conditions. Rods 1 cm in diameter and up to 10 cm long are compacted by isostatic pressing to 70% theoretical density. The pressed rods are then heated in BeO or Ta containers to various temperatures under 1/2 atm argon. Results to date indicate that sintering begins at approximately 1450°C for most of these compounds with Ta compounds requiring the highest sintering temperatures.

B. Transition Metal Aluminides

The transition metal compounds with aluminum are a class of compounds which recently have aroused interest as potential high temperature materials. Some aluminides have melting points above 2000°C and several show excellent oxidation resistance up to 1500°C.[1] A few aluminide systems such as the Mo-Al, Ti-Al, Ni-Al, and Zr-Al systems have been extensively investigated.

Since the aluminides are in many ways similar to the beryllides and since one of the most promising of the beryllide systems is the Nb-Be system, it seemed reasonable to investigate first the Nb-Al system.

In the Nb-Al system three compounds have been reported: $NbAl_3$ (ref. 2), Nb_2Al (refs. 1, 3), and Nb_3Al (ref. 1). $NbAl_3$ is reported to have good

---

[1] R. M. Paine and A. J. Stonehouse, WADC-TR-57-240, Pt. II.

[2] M. Hansen, Constitution of Binary Alloys (McGraw-Hill, New York, 1958) p. 118.

[3] C. R. McKinsey and G. M. Faulring, Acta Cryst. 12, 701 (1959).

oxidation resistance to 1370°C. Modulus of rupture, hardness, and hot impact strength are also reported for this compound.[1]

An oxidation test specimen of $NbAl_3$ was prepared by hot pressing in a 1/2-in. graphite die at 1400°C and 1500 psi for 10 minutes. The resulting rod was 94% theoretical density and could be cut easily on an SiC cutting wheel. Oxidation tests in still air at 1350°C gave the following results:

Time	Wt gain
0.50 hr	1.16 mg/cm^2
17.13 "	4.66 "
86.30 "	7.95 "

A wt gain of ~7 mg/cm^2 corresponds to one mil metal consumed.

X-ray powder diffraction pictures of a number of other preparations show that no compound containing more Al than $NbAl_3$ exists in the system. The compound Nb_3Al has been prepared in pure form.

C. Thermal Conductivity Measurements

An apparatus has been constructed and is currently being developed for measurement of the thermal diffusivity of rod-shaped specimens. The method used is to contact a rod approximately 1 cm diam and 3 cm long against an isothermal heat source, then measuring the resulting temperature rise at the cold end of the specimen. The method has proven excellent for obtaining relative values, but further refinement is required before absolute measurements of high accuracy can be made.

D. Coatings on BeO

A test was performed for PMD on uncoated specimens to determine how fuel loading and percentage theoretical density affect the rate of attack by water vapor. Specimens ranging from 97.8-99.67% theoretical density and 0-10% UO_2 were tested 4 hr at ~1560°C and 1 atm water vapor. The attack rate could not be correlated either with respect to fuel loading or with percentage theroetical density.

E. Coatings on Molybdenum

If molybdenum and its alloys could be protected from oxidation at high temperatures, their many excellent mechanical properties would be very useful for Pluto applications. A possible means of obtaining oxidation resistance

[1] See Paine and Stonehouse, on preceding page.

would be to completely cover the surface of the metal with oxidation-resistant $MoSi_2$. A process now under study is the application of the coating by electrophoretic plating. This method has been reported to give even, coherent and dense coats on many materials.

The coatings obtained thus far, however, have failed to protect the molybdenum from air oxidation at 1100°C. This failure is thought to be due to an inability to obtain uniform coats, or to achieve coats of high density. Further work will be carried out to see if the difficulties can be resolved; if not, other methods of coating will be tried.

F. Effect of Irradiation on Thermal Conductivity of Fueled BeO

There has been some concern that exposure to irradiation doses as large as those contemplated in a Pluto mission would seriously decrease the thermal conductivity of the BeO-UO_2 fuel elements. Indeed, earlier work by Hunter (TID-66) showed this effect, but the work was done at a much lower temperature than that required in Pluto design.

During the last quarter two high temperature irradiations have been made on BeO-6% (by wt) OyO_2 samples to look for any change in the thermal conductivity due to fissions in the material. Both experiments were done at ~1325°C; the first to a total dose of 9.5×10^{17} nvt, the second to a total dose of 9.5×10^{18} nvt. The thermal diffusivity of each specimen was measured before and after irradiation. The data are given below, and are compared with the earlier work done at a lower temperature.

This work				Hunter (TID-66)			
nvt	kw-hr/cm^3	T°C	R/R_0	nvt	kw-hr/cm^3	T°C	R/R_0
9.5×10^{17}	0.7	1310±20	1.0	--	0.7	750	1.2
9.5×10^{18}	7.0	1335±20	1.1	--	7.0	750	4.3

R and R_0 are thermal resistivities after and before irradiation, respectively.

The effect at 1325°C is thus quite small. Since the larger irradiation is equivalent to a Pluto flight of ~10 hr, radiation effects on the thermal conductivity will cause no difficulties at this temperature.

Further work contemplated includes irradiations in oxygen atmosphere to detect any effect on the oxidation rate of UO_2, and also the effect of irradiation on UO_2-BeO at temperatures intermediate between those of this work and those of Hunter.

CHAPTER III. HOT BOX

A hot, non-nuclear test of the air-cooled graphite reflector installation was conducted during the first half of the week ending October 3. The installation is considered satisfactory. The core was heated to 1000°F in 10 hr, the reflector reaching about 225°F. With the cooling air off, the reflector heated up to 800°F in about 6 hr, the core being 950°F at that time.

Cold nuclear runs with the reflected core were conducted the remainder of the week. The reflector covers the east and west side (Fig. III-1). The first core assembled contained 12 in. of BeO in the north and south halves, and was subcritical by an estimated Vane No. 4 worth, or about 10 fine vanes. One inch of BeO was added to the north and south halves, and the assembly was then 0.6 fine vane supercritical (with all vanes out and source in). The two fuel foils in slot SW-3 were removed remotely by the foil retraction system, and found to be worth 0.4 fine vane. Six oralloy activation ribbons were placed vertically in SW-3 (the fuel was left out of this slot) and two ribbons were placed horizontally in NE-3.5 through the east reflector and core half about 10 in. below the top of the core. This assembly was supercritical by 0.23 fine vanes. Transient studies gave an average worth of $0.82 for the fine vane. The reactor was placed on a period, with no vane motion for several minutes. The power level vs time is plotted in Fig. III-2, from which the period was calculated as 105.4 sec. Using this period and the corresponding portion of the fine vane worth, the total vane worth was determined as $0.89 from the period-reactivity graph (Fig. III-3). This graph is a plot of the asymptotic period resulting from insertion of the corresponding reactivity. Data for this curve were taken from DANE code results.

The oralloy ribbons were irradiated for 1 hr at a power of about 1 watt. A plot of the relative activation of the horizontal ribbons is shown in Fig. III-4. The activation in the reflector is depressed with respect to that in the core by about 12% fairly uniformly by self-shielding (based on ZOOM code spectrum calculations).

Figures III-5 and III-6 are plots of the relative activation vertically through the core. The general shape agrees with that for the bare core (UCRL-5699). The solid lines are not calculated cosines but just drawn by eye. A tendency of the experimental data to show a steeper slope at the top of the core than at the bottom indicates that the real distribution is not a true

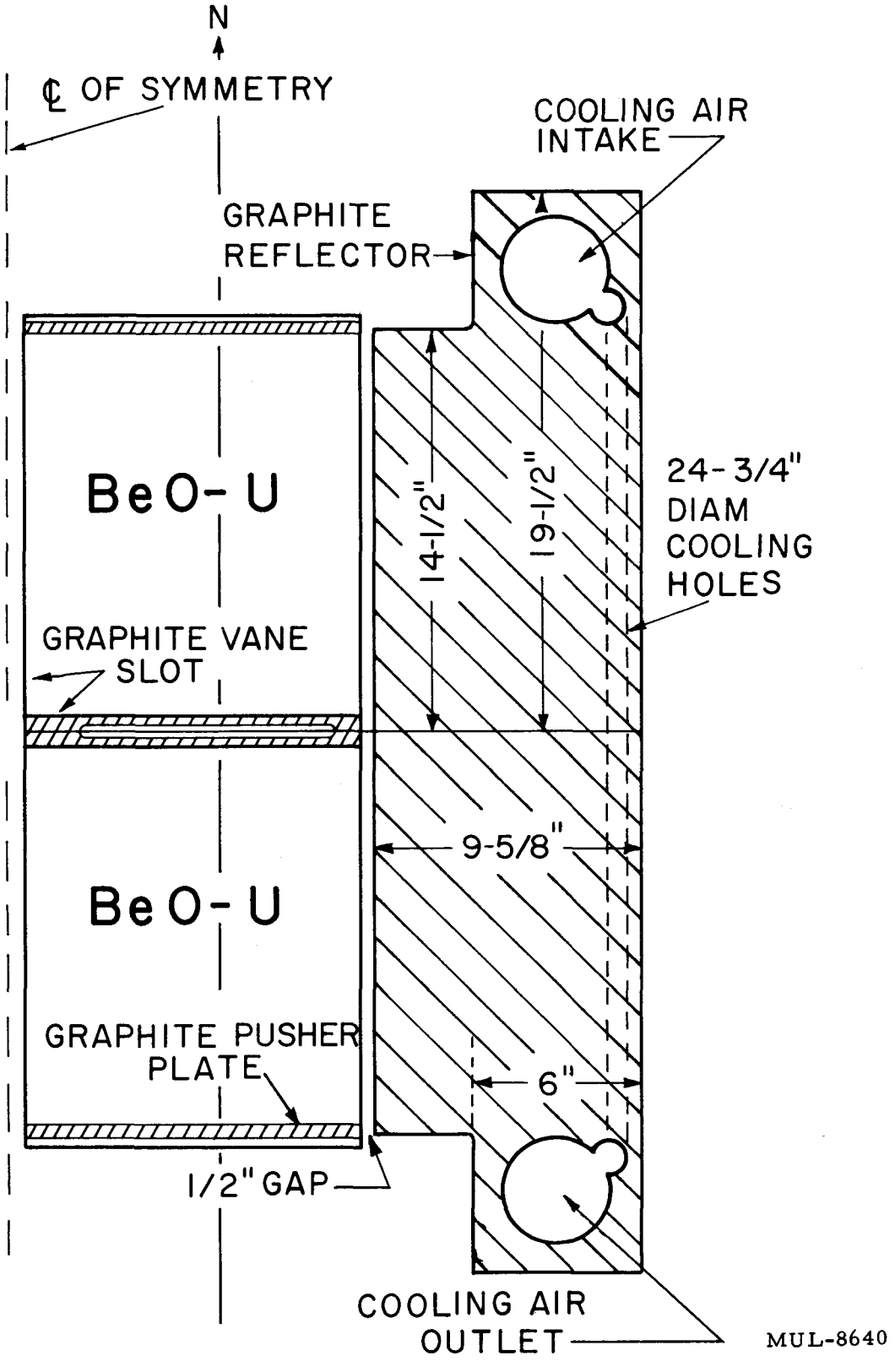

Fig. III-1. Scale drawing of reflected core.

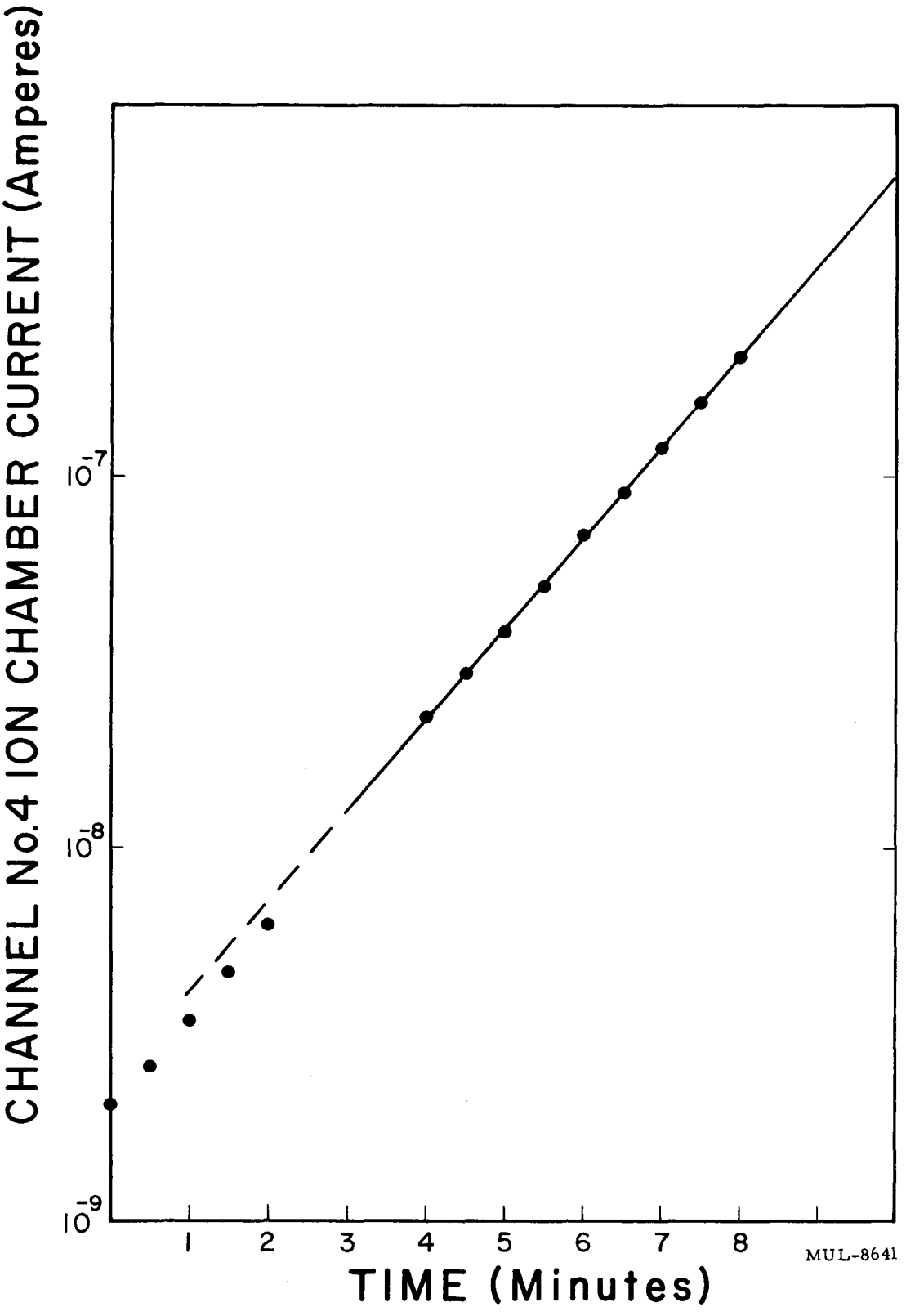

Fig. III-2. Reactor period during rise to power (Oct. 2, 1959). τ = 105.4 sec.

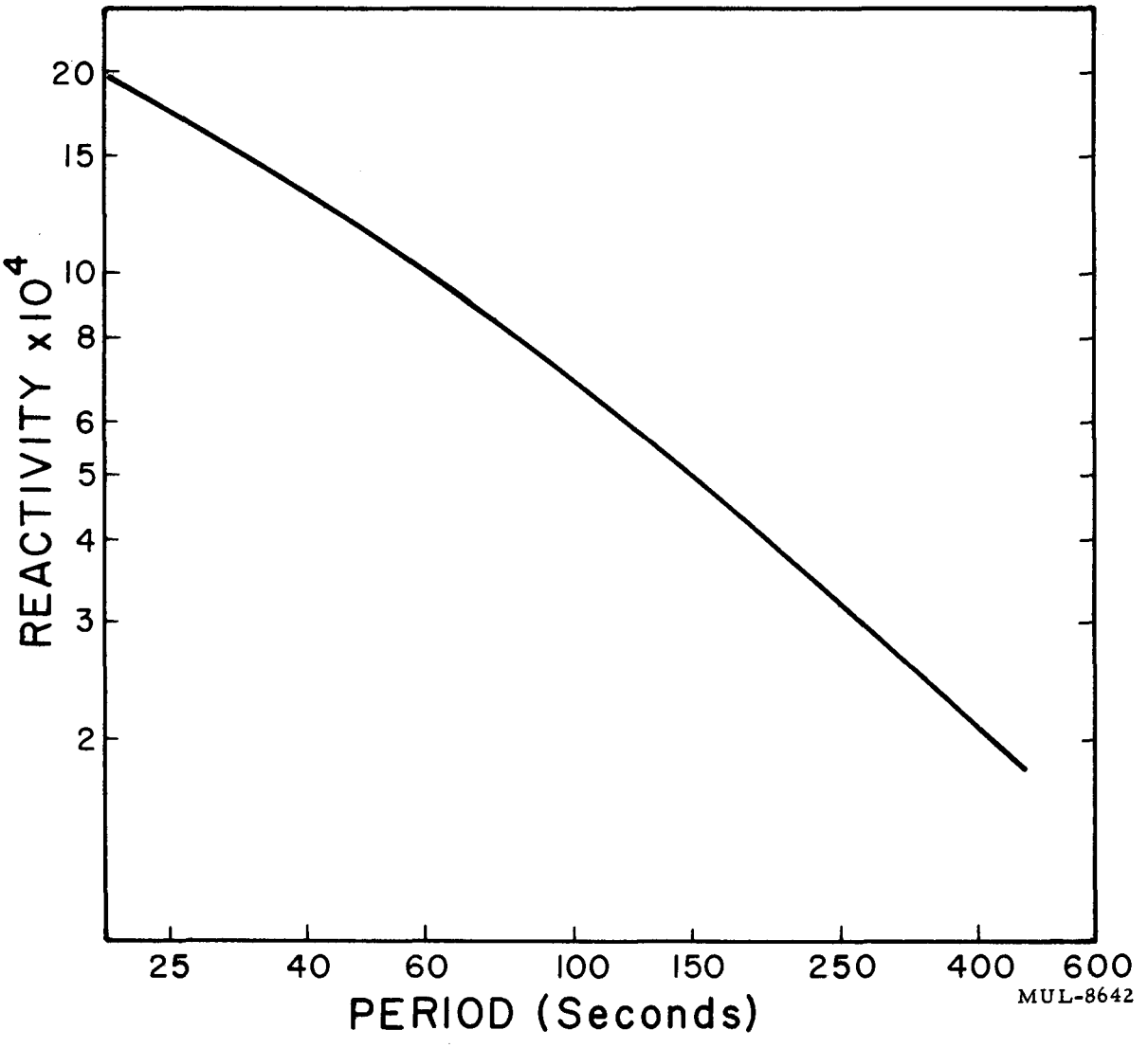

Fig. III-3. Reactivity for $\beta = 0.006872$ from DANE code.

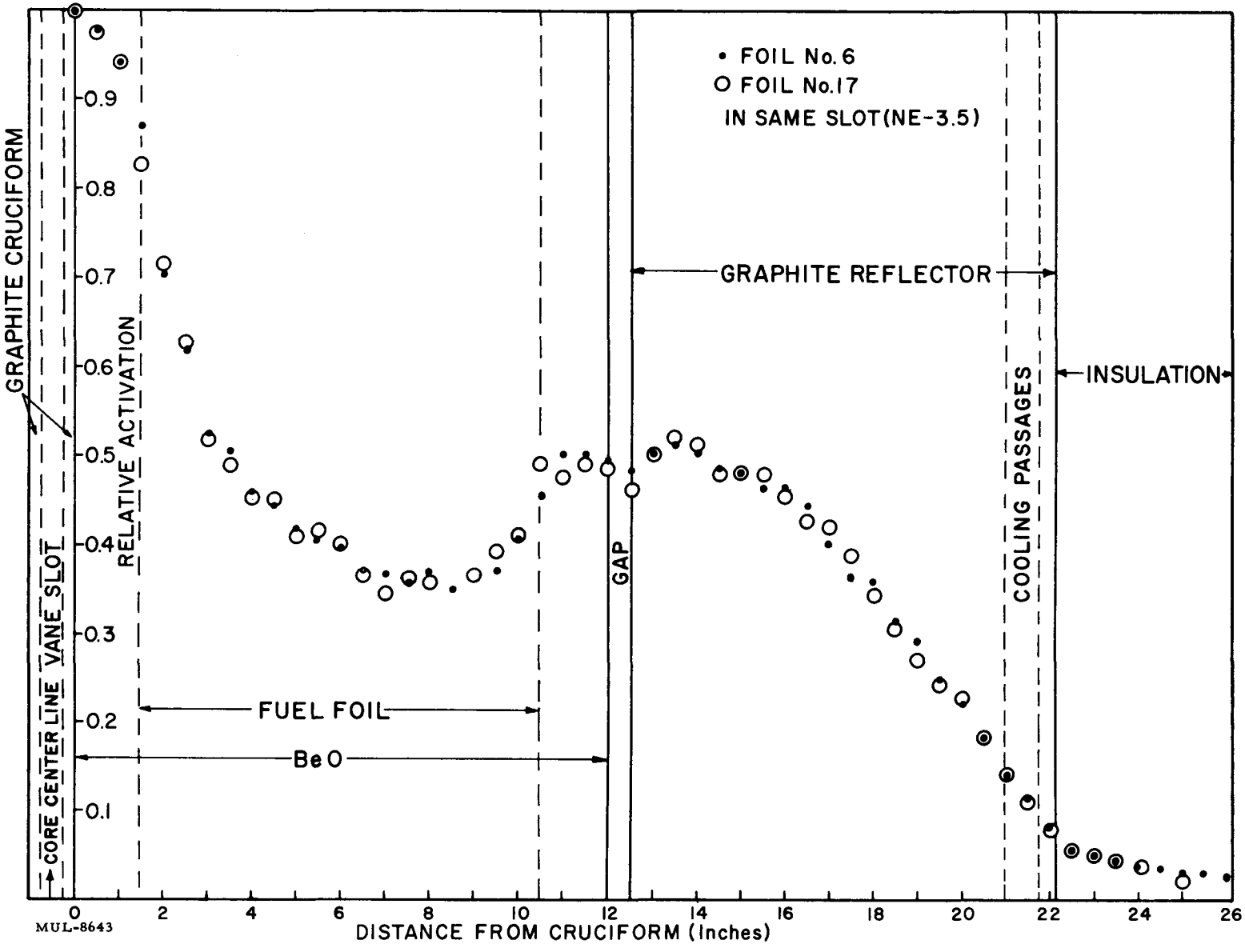

Fig. III-4. Activation run of Oct. 2, 1959. (Horizontal trace).

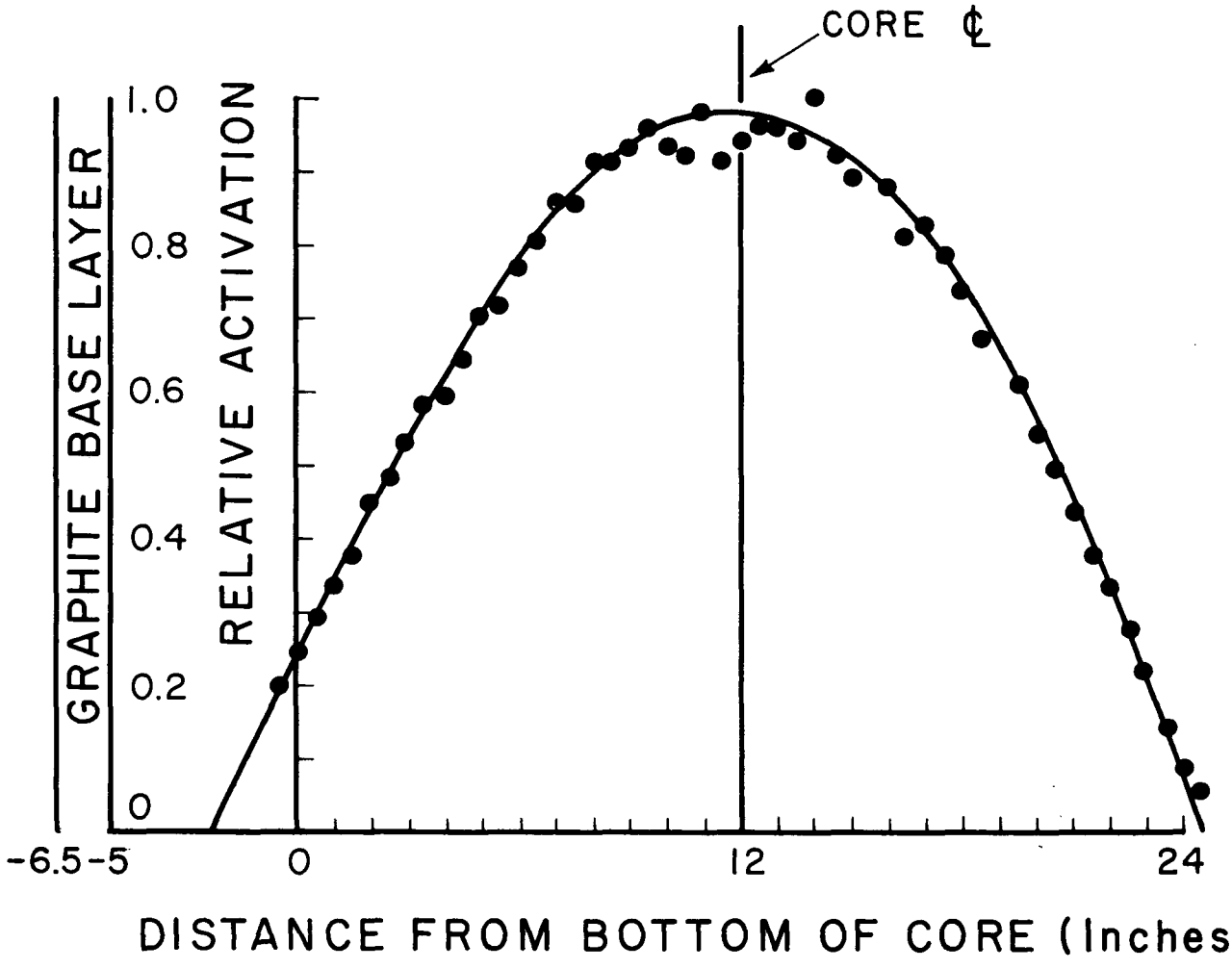

Fig. III-5. Vertical flux plot (10-2-59). Ribbon No. 16. MUL-8644

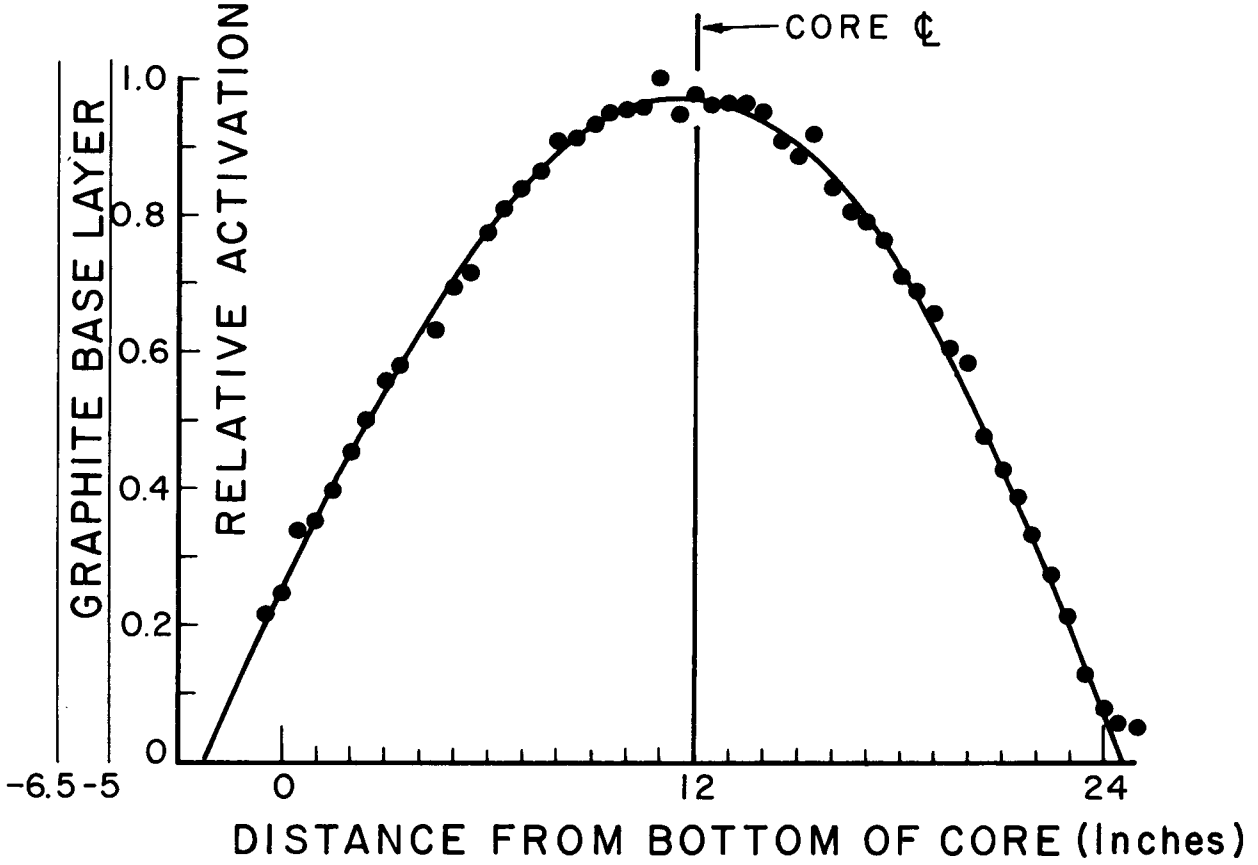

Fig. III-6. Vertical flux plot (10-2-59). Ribbon No. 5. MUL-8645

cosine. This leaning of the distribution, seen to a small extent in the bare activation experiment, is possibly attributable to the reflection from the base layer, low-mass-table, and floor. The extrapolation length at the bottom of the core is now 2.3 ± 0.2 in.; at the top, 0.5 ± 0.2 in. Revised extrapolation lengths for the bare BeO experiment are 1.7 ± 0.2 in. and 0.4 ± 0.2 in. at the bottom and top of the core, respectively. The reflector in the present case, by reducing neutron loss in the E-W direction, could enhance reflection from the base layer. In addition to the graphite base layer common to bare and reflected cores, the latter has 420 in^3 of graphite supporting the reflector. This is in the form of six 2 × 3 × 5 in. and six 2 × 4 × 5 in. blocks.

Table III-1 is a summary of the results obtained during the week.

TABLE III-1

Core length*	Inches BeO N	Inches BeO S	Super-criticality fine vanes	Source worth fine vanes	Fine vane worth (dollars)	SW-3 fuel worth fine vanes	Vane No. 4 worth fine vanes	Temp and Date
$27\frac{1}{16}'' \pm \frac{1}{16}''$	12	12	Sub-critical	--	--	--	--	21.7°C 10/1/59
$29\frac{1}{4}'' \pm \frac{1}{16}''$	13	13	0.592	0.159	--	0.410	10.0	20.7°C 10/1/59
$29\frac{1}{4}'' \pm \frac{1}{16}''$	13	13†	0.233	0.144	0.86 0.79 0.82 0.82	--	9.9	16.5°C 10/2/59

*Includes pusher plates.

†Fuel removed from SW-3.

Revisions have been made in the description of the bare hot critical assembly in the previous quarterly report. The assembly, and its shorter cold companion are reduced to the simplified geometry shown in Fig. III-7. The respective dimensions are given in Table III-2. The height is modified according to the revised extrapolation length at the bottom of the core.

TABLE III-2

T (°F)	ℓ (in.)	w (in.)	h (in.)	ρ_{BeO} (g/cm^3)	ρ_{gr} (g/cm^3)
90	33.67	26.20	25.10	2.711	0.87
950	36.19	26.23	25.20	2.695	0.87

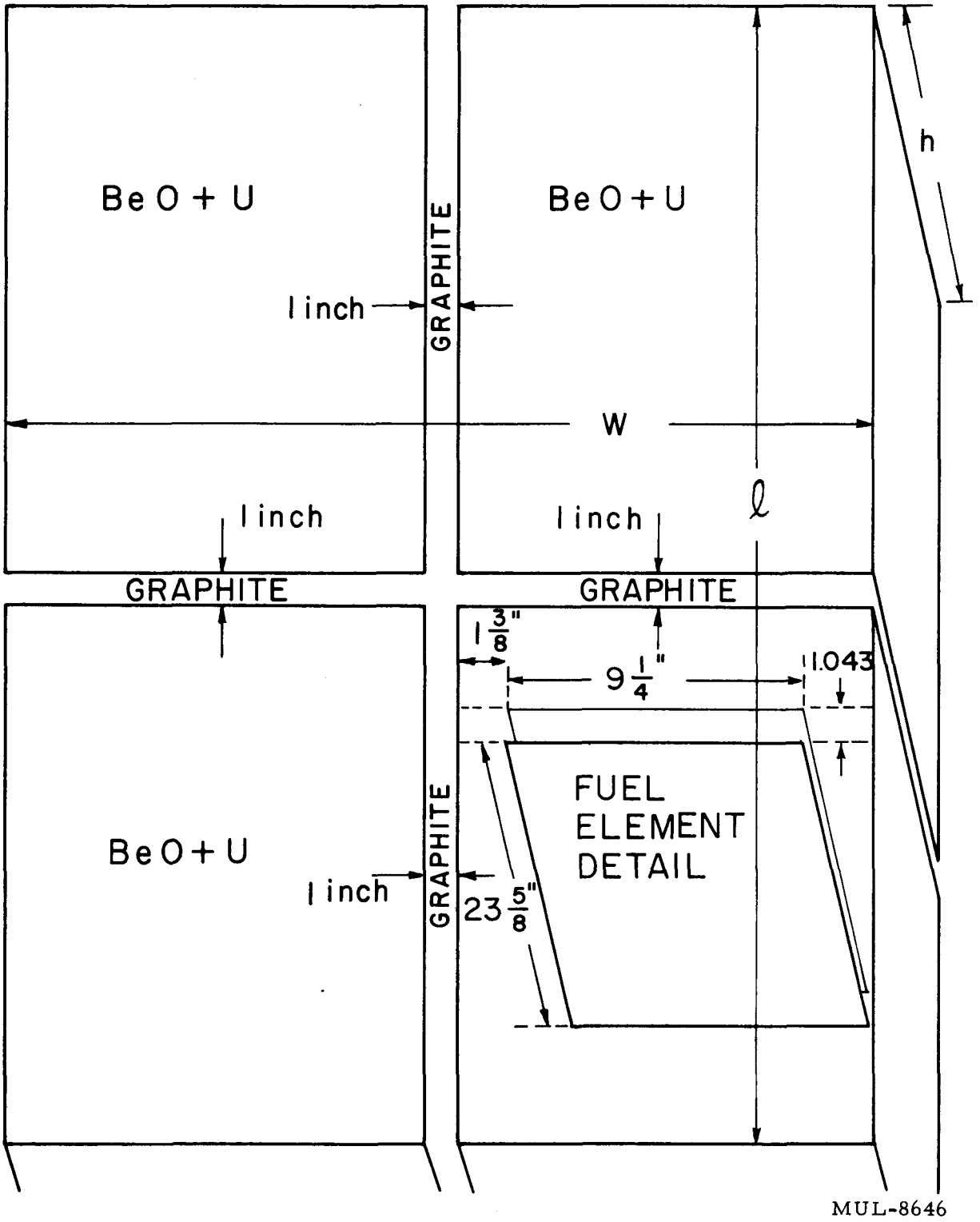

Fig. III-7. Reduced bare BeO assembly.

The fuel elements (detail in Fig. III-7) are effectively 0.004-in.-thick oralloy (93.2% U^{235}) encased in type 347 stainless steel envelopes. The oralloy foils actually occupy only 8.69-8.75 inches of the fuel element width and 22.905-22.930 inches of the fuel element length. (Actually an "element" is a pair of two 2-mil packaged foils.) The average oralloy mass per element is 245.2 g and the average stainless steel weight per element is 210.6 g. A flux-weighting of the actual individual masses of the fuel elements gives an average oralloy mass per element of 257.8 g. The arrangement of the fuel elements starts with one against the graphite cruciform in each quadrant. The room-temperature assembly had 62 fuel elements and the high-temperature assembly had 66 fuel elements. The resultant BeO/U^{235} ratio in both cases was about 565:1, averaged over the quadrants.

Several cold nuclear runs were made during the week of October 12 with the graphite reflected BeO core. The main objectives required prior to the elevated temperature run were: 1) to determine the worth in fine vanes of an incremental inch in core length for both the standard core and one with fuel foils moved to the outer edge of the core; 2) to determine the cold critical length of the latter type core; and 3) to obtain a flux plot in the horizontal direction through the core and reflector for the modified core. The results appear in Table III-3. It is seen that the cost of moving all fuel foils to the outer edge of the BeO is about 2.95 inches increase in core length. The worth of the fine vane appears to have decreased by a few cents, while the worth of Vane No. 4 in fine vanes has increased from about 10 fine vanes to 13.3 fine vanes. The effect on the horizontal flux is seen in Fig. III-8 (compare Fig. III-4). The flux in the BeO "island" is about four times the average flux in the remainder of the core.

The week of October 19 to 23 was devoted to the elevated temperature run for the BeO-core – cooled-graphite-reflector assembly. The main purpose of this run was to determine the comparative size of the temperature coefficients of reactivity for the two systems: hot-core-cold-reflector and hot-core-hot-reflector. The extrapolated temperatures of criticality for the two systems were 1085 ± 10°F and 1115 ± 10°F, respectively. Results in detail are given in Table III-4.

The 9-1/4-inch-wide fuel elements were moved outward in the 12-inch-wide slots between the BeO blocks so that they occupied the part of the core immediately against the reflector. This arrangement emphasizes the boundary

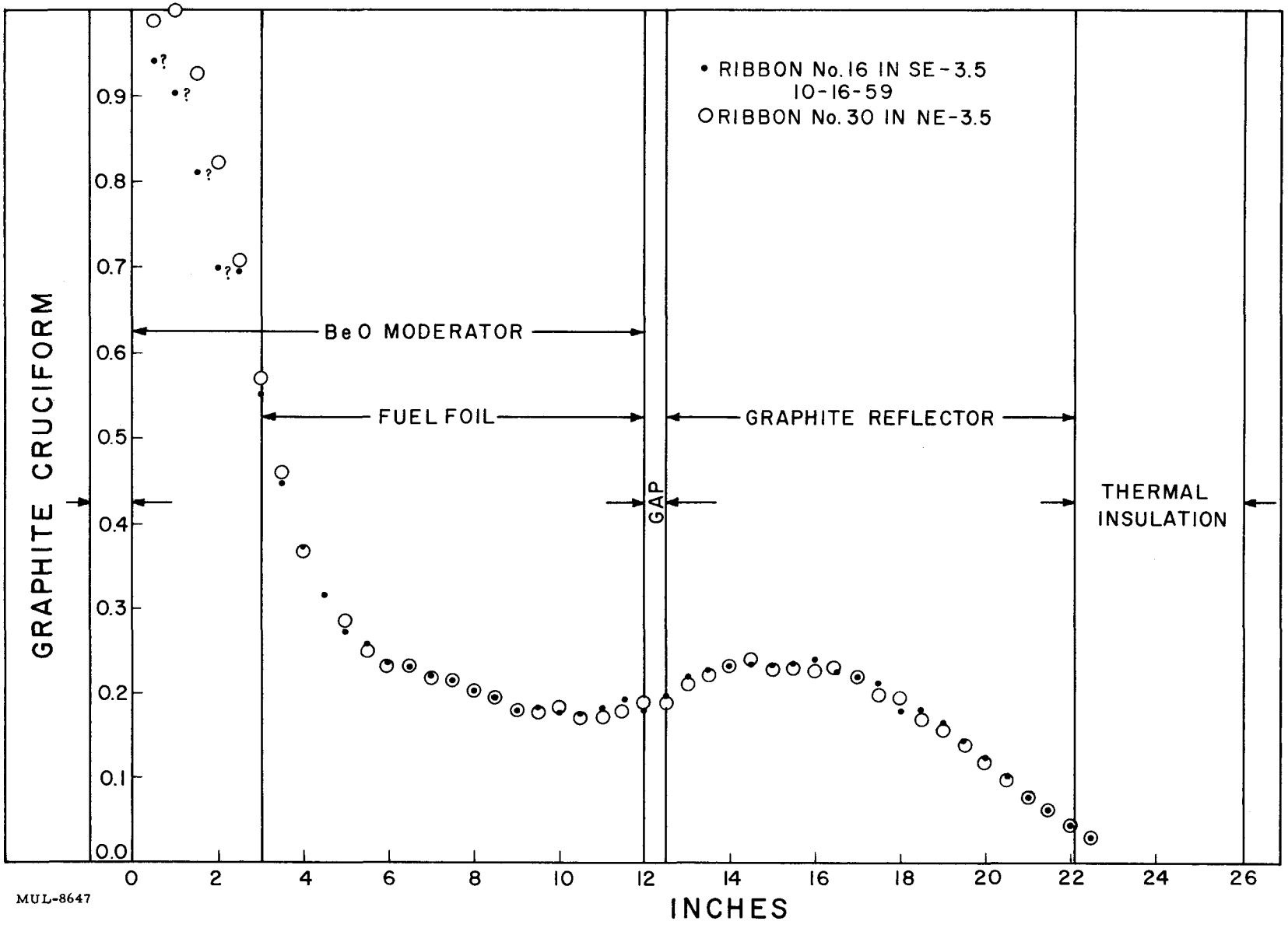

Fig. III-8. Relative activation vs horizontal distance.

TABLE III-3

Date and Temp	Overall length (includes graph. pusher plates)	Inches BeO N	Inches BeO S	Super-criticality, fine vanes (Source In)	Vane 4, worth fine vanes	Fine vane worth (dollars)	Source worth fine vanes	Remarks
10-13-59 22.2°C	$30\frac{3}{8}" \pm \frac{1}{32}"$	13	14	3.82	10.0	---	0.046	1. Source lower limit switch assembly came apart – part remained in core. 2. Comparison with assembly of 10-1-59 gives 1" BeO = 3.2 f.v.
10-13-59 22.2°C	$29\frac{10}{32}" \pm \frac{1}{16}"$	13	13	0.89	9.0	---	0.099	1. Comparison of 10-13-59 crits gives 1" BeO = 2.93 f.v. at 13". 2. Part of source assembly remained in core.
10-14-59 20.6°C	$29\frac{10}{32}" \pm \frac{1}{16}"$	13	13	0.90	9.1	---	0.140	1. Source lower limit switch assembly repaired.
10-14-59 20.8°C	$29\frac{10}{32}" \pm \frac{1}{16}"$ †	13	13	Sub-critical	---	---	---	1. All fuel foils moved to outer edge of BeO core. Multiplication indicates assembly about 2" BeO subcritical.
10-15-59 23.0°C	$31\frac{18}{32}" \pm \frac{1}{16}"$ †	14	14	Sub-critical by 1.15 f.v.	13*	---	---	
10-15-59 23.3°C	$31\frac{31}{32}" \pm \frac{1}{16}"$ †	14	14-1/2	Sub-critical by 0.22 f.v.	---	---	---	1/2" BeO = 0.93 f.v. at 14".
10-16-59 23.3°C	$32\frac{15}{32}" \pm \frac{1}{16}"$ †	14	15	0.615	13.3	$0.785 - Ch 1 $0.784 - Per. $0.842 - Ch 4	0.195	1/2" BeO = 0.835 f.v. at 14-1/2".

* Doubtful figure due to low count rate.

† Fuel foils moved to outer edge of BeO.

TABLE III-4

SUMMARY OF RESULTS: WEEK OF OCTOBER 19-23, 1959

T_{core} (°F)	T_{refl} (°F)	T_{amb} (°F)	L (in.)	N, S (in. BeO)	Supercrit. (fine vanes)	Vane 4 (fine vanes)	Source (fine vanes)	Fine vane ($)	Fine vane (in. BeO)	Date (1959)
74	---	---	32 15/32	14, 15	0.62	13.3	0.195	0.785 0.784 0.842	0.60	10-16
77	---	---	32 14/32	14, 15	0.71	13.0	0.163	0.900 0.948 0.781 0.764	near top near bot	10-19
77	---	---	34-1/2	15, 16	3.92	9.45	0.165	0.705 0.677 0.724	0.62	10-20
425	165	770	"	"	2.66	---	---	---	---	10-20
645	200	850	"	"	1.54	---	---	---	---	10-20
875	205	910	"	"	0.90	---	---	---	---	10-20
945	220	1130	"	"	0.52	---	---	---	---	10-20
990	225	1175	"	"	0.33	---	---	---	---	10-20
1055	215	1065	"	"	0.12	---	0.23	0.775 0.793	257°F	10-21
1110	960	1022	"	"	0.01	---	---	---	265°F	10-21
1095	960	960	"	"	0.01	---	---	---	---	10-21
1040	975	975	"	"	0.30	---	---	---	---	10-21
770	820	840	"	"	1.23	8.18	---	---	---	10-21

between fueled core and cooled reflector, but creates an "island" of about 3 in. of unloaded BeO on each side of the N-S graphite cruciform arms. An activated oralloy ribbon fission traverse through the reflector for the room temperature assembly is shown in Fig. III-8.

Before the heating cycle was started the supercriticality of the basic assembly with all vanes out, 14 in. BeO North and 15 in. BeO South (Table III-3, crit of 10-16-59) was redetermined. Then 2 in. of BeO were added, 1 at each end, to compensate for the negative temperature coefficient of reactivity, and the supercriticality of this assembly at room temperature was determined. The reactivity worth of the fine vane for these two assemblies was determined with transient studies.

As the core was heated, supercriticality measurements were made at 425 and 645°F without slowing down the rate of heating. At 875°F the core temperature was leveled to give a good intermediate point. Quick points were then taken at 945 and 990°F before the core was leveled at the top point of 1055°F with the reflector at 215°F. At this temperature, the reactivity worth of the fine vane was determined by a transient study, and a 1-hour activation run at about 0.5 watt was made. The activation ribbons could not be withdrawn, however, due to friction in the guide tubes, so they remained in the assembly.

The cooling for the reflector was stopped and the reflector allowed to rise up to the core temperature. During this heating time the source container became soldered in position due to the temperature and could not be withdrawn for any further transient studies.

With the core at 1110°F and the reflector at 960°F a supercriticality evaluation was made. The core was allowed to cool to 1095°F and another point was taken. Finally, the core was leveled at 1040°F with the reflector about 975°F and a 1-hour activation run at about 10 watts was made. This high power was chosen so that the oralloy ribbons would still have enough activity to count when the oven would be opened about 13 hr later. The shutdown from the 10-watt run was made by inserting a small amount of negative reactivity. The decay in neutron flux was recorded for about 1/2 hour to observe the effect of delayed photoneutrons from the beryllium.

The temperature of the core was leveled at 770°F with the reflector at 820°F for the final supercriticality measurement.

The temperature coefficient of reactivity for the cold reflector assembly is only very slightly more negative than that for the hot reflector assembly. The values are – \$0.30/100°F and – \$0.29/100°F, respectively. The difference in extrapolated critical temperature is only 30 ± 15°F at 1100°F. Figure III-9 shows the variation in supercriticality (in fine vane units) with temperature. Straight lines fit the results satisfactorily. Separation of nuclear and geometry temperature coefficients has not been made. For comparison the total temperature coefficient for the bare BeO core (with same loading) is – \$0.48/100°F, composed of – \$0.35/100°F nuclear temperature coefficient and – \$0.13/100°F geometry temperature coefficient (UCRL-5699).

The reactivity worth of the fine vane appeared to decrease by about 10% with the total increase in temperature. An uncertainty of about 20% in the determination of the fine vane worth was noticed in the run of Oct. 19 in which two transient studies were performed: one with the fine vane almost fully inserted and a second with the fine vane almost fully withdrawn. The observed difference in worth might be attributable to a deviation in the real vertical flux distribution from the assumed cosine. It should be noted that an uncertainty in fine vane position of the smallest indicator division, ± 0.1 in., gives an uncertainty in the worth of up to 15%.

The position of the vanes must be corrected for the thermal expansion of the supporting rods. For those times when the heating or cooling rate was high and the difference between gas temperature and core temperature was large, the position correction was made using the oven ambient temperature determined by unused thermocouples hanging outside the core. Using the core temperature gave definitely erroneous results, as could be expected.

The activation ribbons were in slots passing horizontally through the core and reflector in the west-east direction in positions NE 7, NE 3.5, SE 3.5, and SE 7. Both the two inner ribbons (in the 3.5 positions) were disturbed in the first pulling attempt so they were partially out of the core for the second high-temperature activation run. The full hot-core, hot-reflector fission traverse records, Fig. III-10, were obtained from the outer positions. The room temperature activation run (shown as a dashed line in Fig. III-10) was made with two ribbons in NE 3.5 and SE 3.5 (Fig. III-8). The comparison between the results for the hot run from the ribbons in the "7" positions with the partially withdrawn ribbon in SE 3.5 is shown in Fig. III-11, showing little dependence of the fission traverse results on distance from E-W core axis.

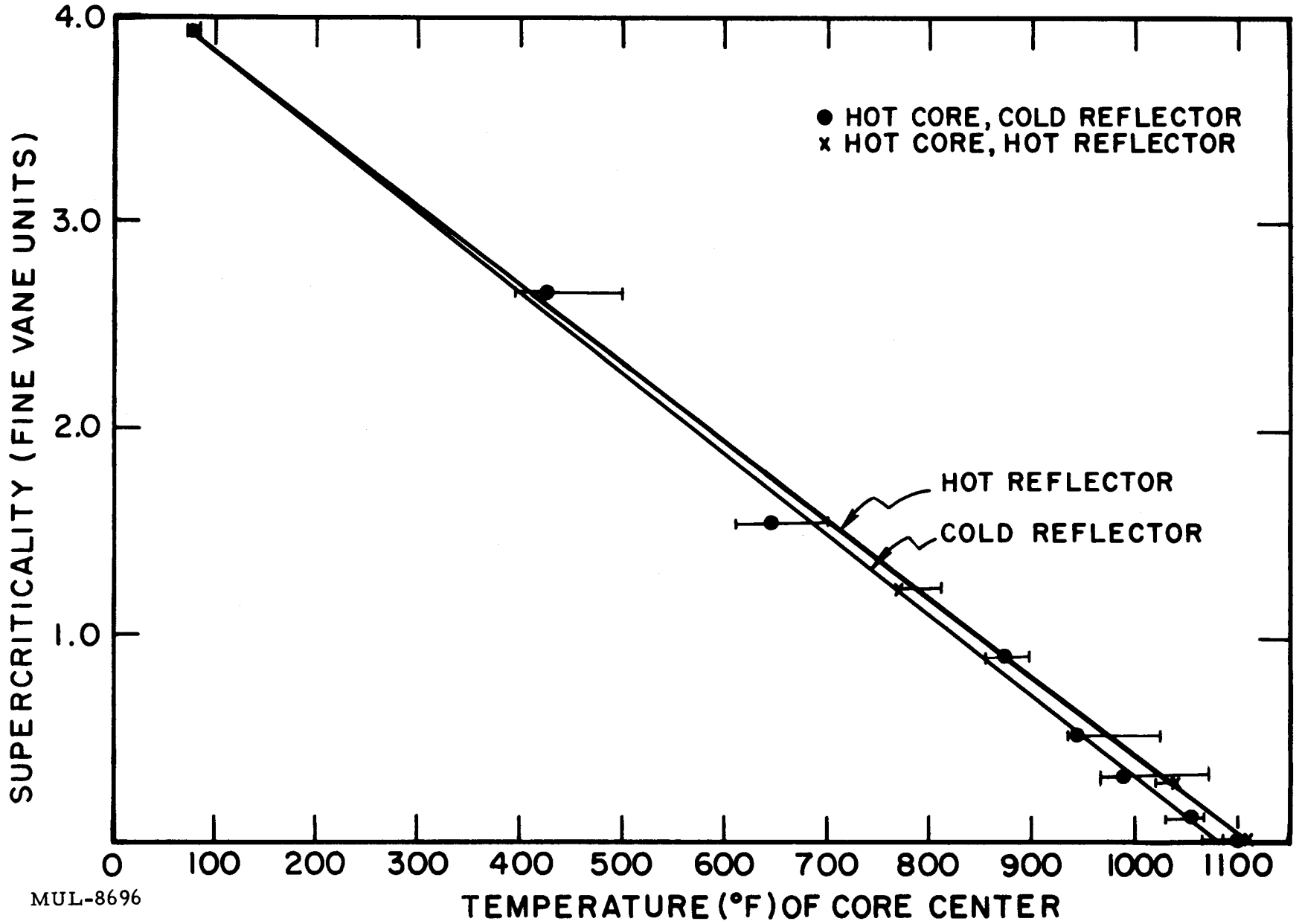

Fig. III-9. Supercriticality vs temperature.

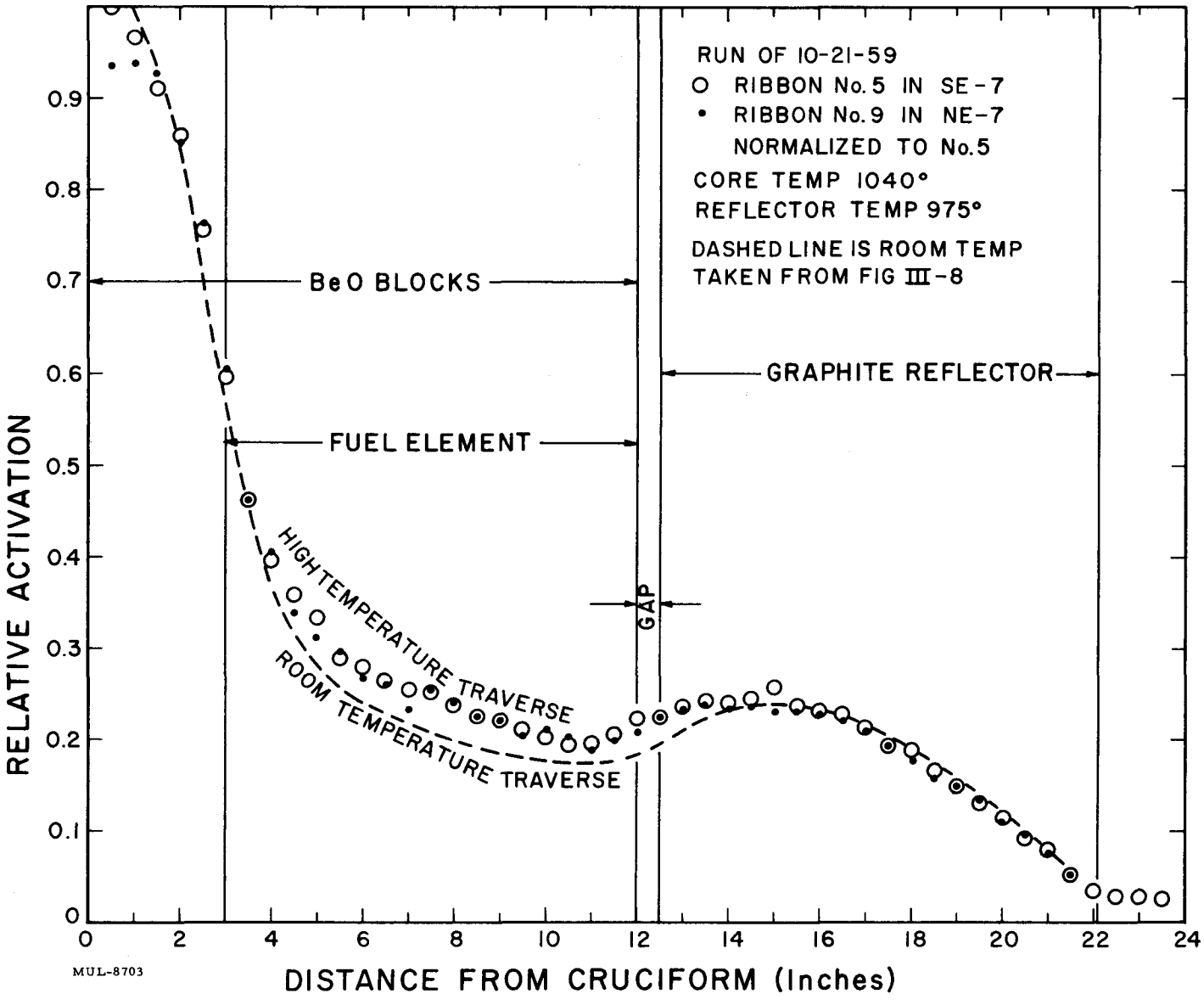

Fig. III-10. Fission traverse for hot-core, hot-reflector.

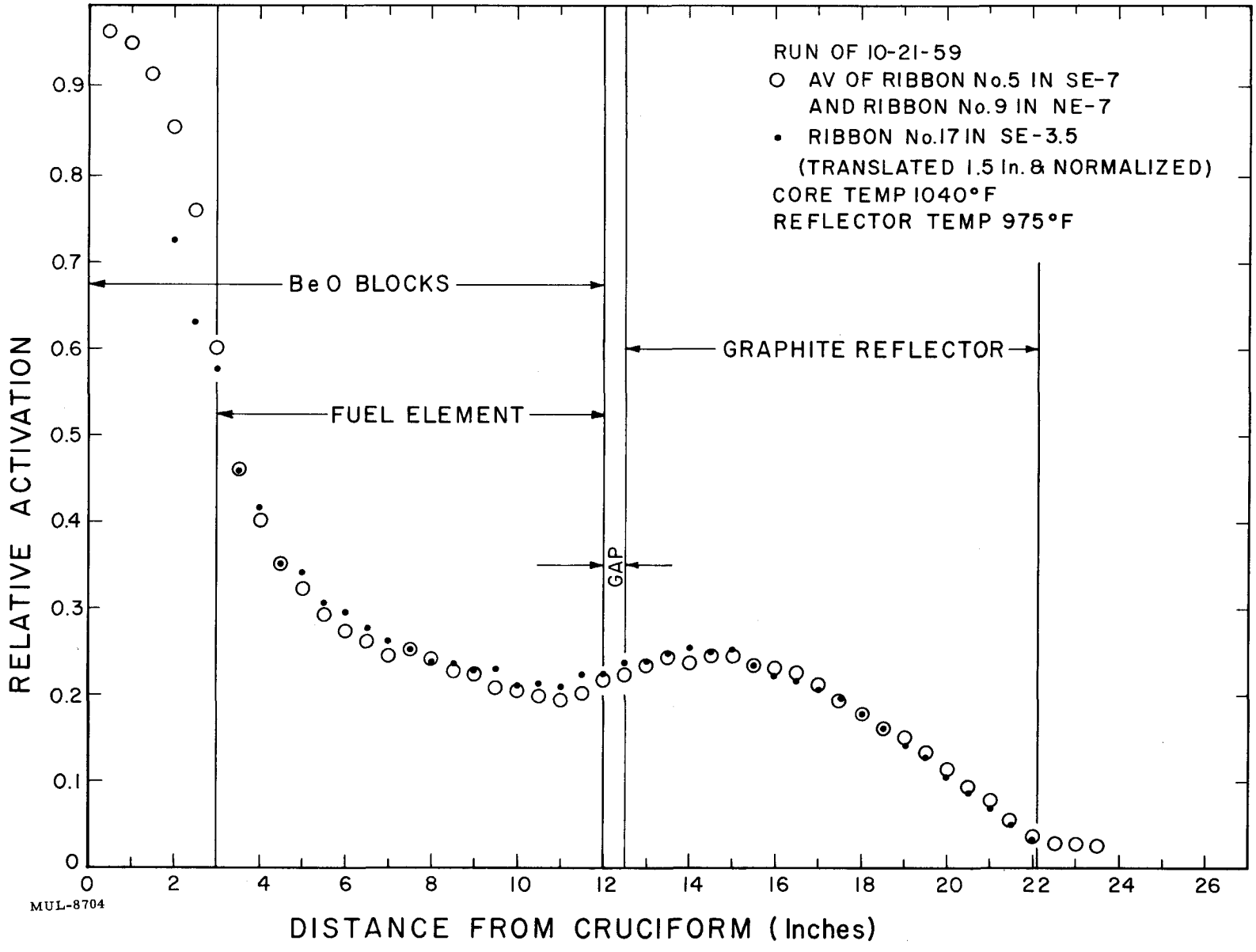

Fig. III-11. Comparison of traverses in position 3.5 and positions 7.

It is seen in Fig. III-10 that the difference between the room temperature traverse and the 1040° core, 975° reflector traverse is mainly a decrease in the depression of the flux in the fuel foil at high temperature.

The decrease in neutron flux with time after the 10-watt run is shown in Fig. III-12. It is seen that the decrease is clearly asymptotic to the decay in gamma-activity (dashed line, normalized for comparison) for those gammas above the threshhold for neutron production from beryllium. The decay in the gamma-activity was obtained from Perkins and King (Nuclear Sci. and Eng. 3, 726, 1958).

The experiments were centered about a high-temperature run in which the assembly with the cooled graphite reflector and BeO core with staggered fuel elements was examined. Specific experimental results are shown in Table III-5.

Preliminary experiments were concerned with determining the super-criticality of the basic core, measuring the worth of an additional inch of BeO in fine vane units, and conducting an activation run to record the power distribution through the reflector at room temperature.

In the high-temperature run, determination was made of the super-criticality variation with temperature of both the hot core-cold reflector and hot core-hot reflector systems, and an activation run was made for each at the highest core temperature to determine the effect on power distribution of the change in reflector temperature.

Discussion

In the previous cooled-reflector hot run the two fuel elements in the slot between BeO blocks were both moved out to the core edge to emphasize the hot-core cold-reflector boundary. By doing this, a central island of 3 inches of unloaded BeO on each side of the N-S cruciform was created. The neutron flux (actually fissions per uranium atom) was about four times as high in the island as in the reflector shown in Fig. III-10, so that the moderating effect of the reflector might have been reduced. In order to eliminate this island the fuel element pair was split and one element was moved to the inside of the box against the cruciform. In effect, half the fuel was removed from the outer 3 inches of the previous core and put into the inner 3 inches. The first result was that about 4 inches less BeO was required to bring the assembly to criticality. A further comparison of the two fuel-element arrangements is given below.

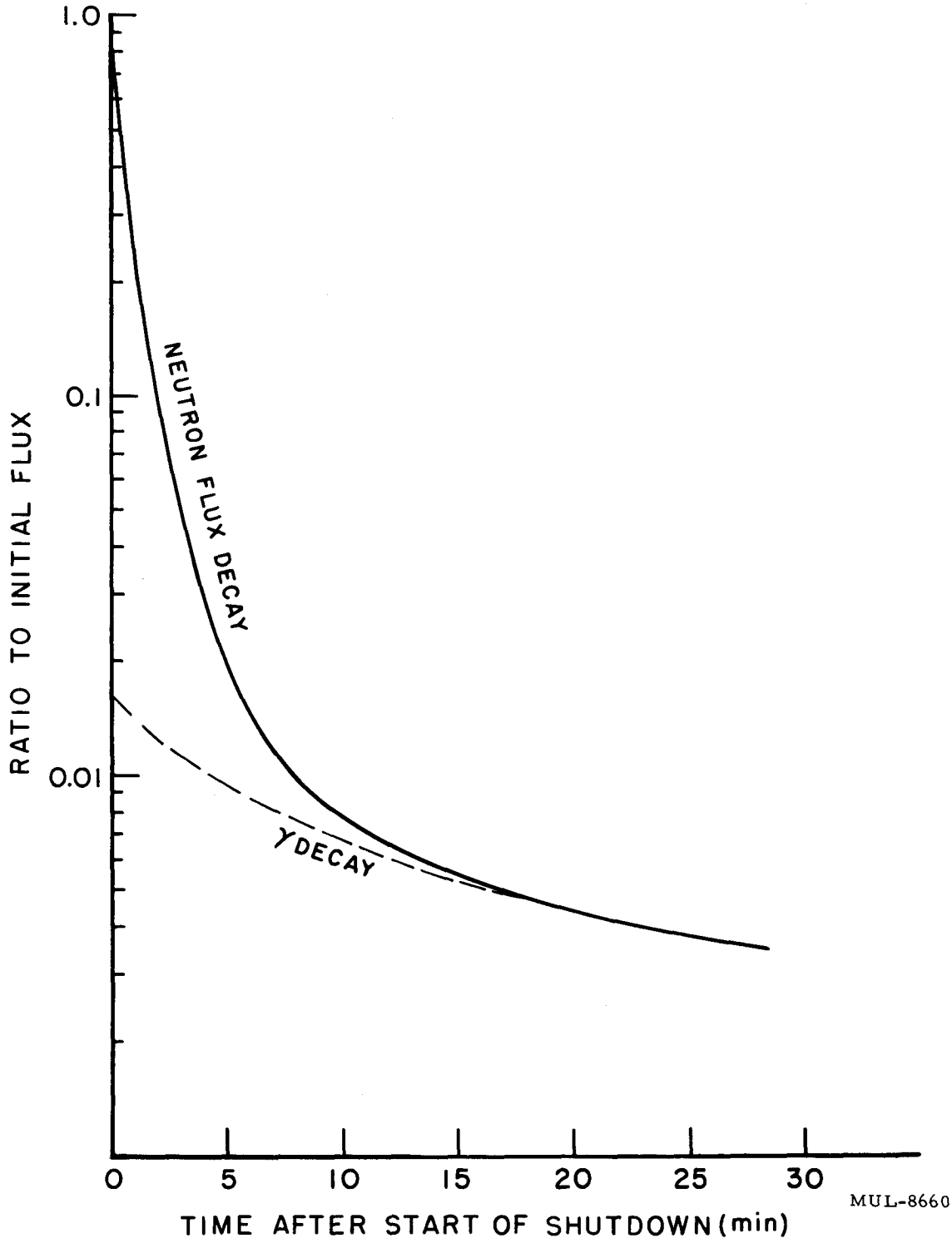

Fig. III-12. Shutdown from ~ 10 watt activation run (Oct. 21, 1959). (Insertion of $0.35 negative reactivity in 10 sec).

TABLE III-5

SUMMARY OF RESULTS: PERIOD OF OCTOBER 26-NOVEMBER 20, 1959

T_{core} (°F)	T_{refl} (°F)	T_{amb} (°F)	L (in.)	N,S (in. BeO)	Supercrit. (fine vanes)	Vane 4 (fine vanes)	Source (fine vanes)	Fine vane ($)	Fine vane (in. BeO)	Date (1959)
52	---	---	29-5/16	13, 13	3.12	9.0	---	---	---	10/30
52	---	---	28-5/16	13, 12	0.49	9.5	0.09	0.84 0.88	0.38	10/30
55	---	---	28-5/16	13, 12	0.48	9.7	0.11	0.79	---	11/2
54	---	---	28-1/4	13, 12	0.39	9.3	0.10	0.82 0.89	---	11/3
56	---	---	30-1/4	13, 14	6.18	9.40	0.08	0.58 0.62 0.58 0.62	0.345	11/3
435	160	895	"	"	4.35	(8.73)	---	---	---	11/4
595	175	990	"	"	3.53	(8.45)	---	---	---	"
735	160	725	"	"	2.65	8.13	0.10	0.81 0.93	---	"
935	205	1100	"	"	1.66	(7.85)	---	---	---	"
1025	215	1105	"	"	1.30	7.41	---	---	---	"
1060	215	1115	"	"	1.13	7.75	---	---	---	"
1110	230	1160	"	"	0.96	7.80	---	---	---	"
1153	235	1170	"	"	0.84	7.86	---	---	---	"
1161	235	1170	"	"	0.81	(7.80)	---	---	---	"
1177	230	1177	"	"	0.75	8.00	0.12	---	---	"
1185	200	1180	"	"	0.72	7.80	0.09	0.83 0.86	---	"
1240	1235	1200	"	"	0.56	8.27	0.13	0.71 0.72	---	11/5
1050	985	690	"	"	1.68 ?	7.96	---	---	---	"
990	960	940	"	"	1.41	7.10	0.22	0.64 0.69 0.64 0.67	---	"

	Fine vane	Vane 4	Source
Fuel elements at edge	$0.78 ± 0.12; 0.61 in. BeO	13.0 f.v.	0.17 f.v.
Fuel elements staggered	$0.75 ± 0.20; 0.36 in. BeO	9.5 f.v.	0.10 f.v.

The results of the room temperature activation run at about 0.5 watt for 1 hr are shown in Fig. III-13. It can be seen that flux in the reflector is now much higher. Unfortunately the agreement between the two activation ribbons is not as good as hoped for, and another room temperature activation run will have to be made.* It is felt that the results from ribbon No. 16 (the lower points) are probably erroneous since the counts at the welds, every 3 in. seem to be improper.

For the high-temperature run 2 in. of BeO were added to the south half of the core to compensate for the decrease in reactivity with temperature. During heating, the supercriticality was followed without slowing the heating rate by taking quick points at 435, 595, 935, 1025, etc. At 735°F, the heating rate was interrupted and the core temperature was leveled for a good intermediate determination of the supercriticality, vane 4 worth, and fine vane worth. At the higher temperatures, the heating rate is so gradual that good readings may be taken without stopping. At the highest temperature, 1185°F, with the reflector still at about 200°F, the worths of vane 4 and the fine vane were determined, and a 1-hr activation run was made at about 0.5 watt with the activation ribbons being removed with only partial success. More than 10% of the initial cold supercriticality obtained from the additional 2 in. of BeO still remained at this high temperature. A definite curvature of the supercriticality versus temperature curve is seen; the temperature coefficient decreases at higher temperatures. Any possible systematic change in fine vane worth with temperature was much smaller than the uncertainties. The best extrapolation to the just-critical temperature is made with a straight line on a supercriticality vs log temperature plot as in Fig. III-14. The temperature of criticality is 1400 ± 50°F. The total temperature coefficient of reactivity varies from $0.39/100°F between room temperature and 700°F to $0.26/100°F at 1200°F with an uncertainty in the values of about ± 10%.

An interesting feature of this run is the smooth decrease in vane 4 worth with temperature from 9.4 fine vanes at room temperature to 7.8 fine vanes at 1185°F. For those temperatures at which the vane 4 conversion to fine

*See note at the end of this Chapter.

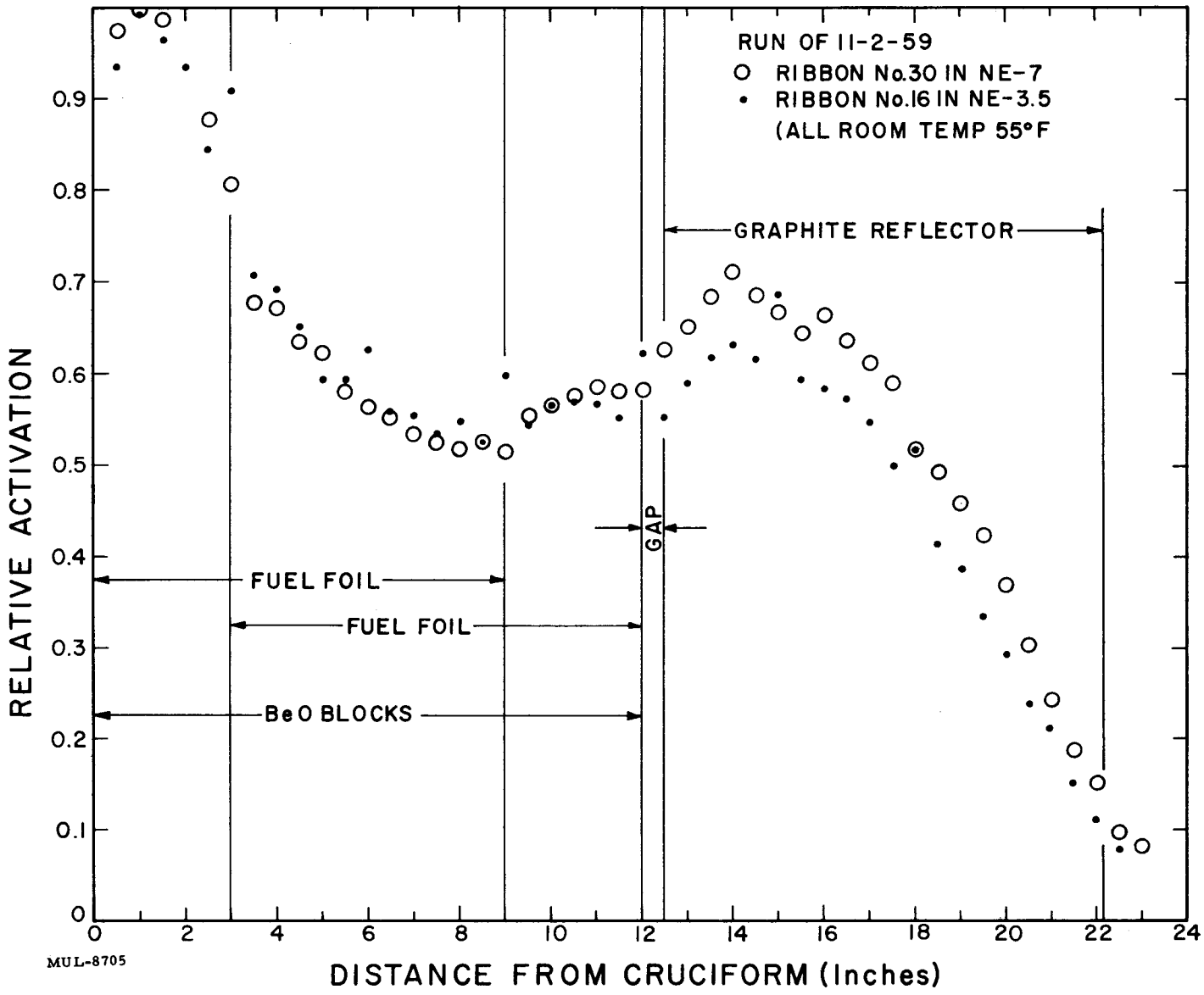

Fig. III-13. Activation run of 11-2-59.

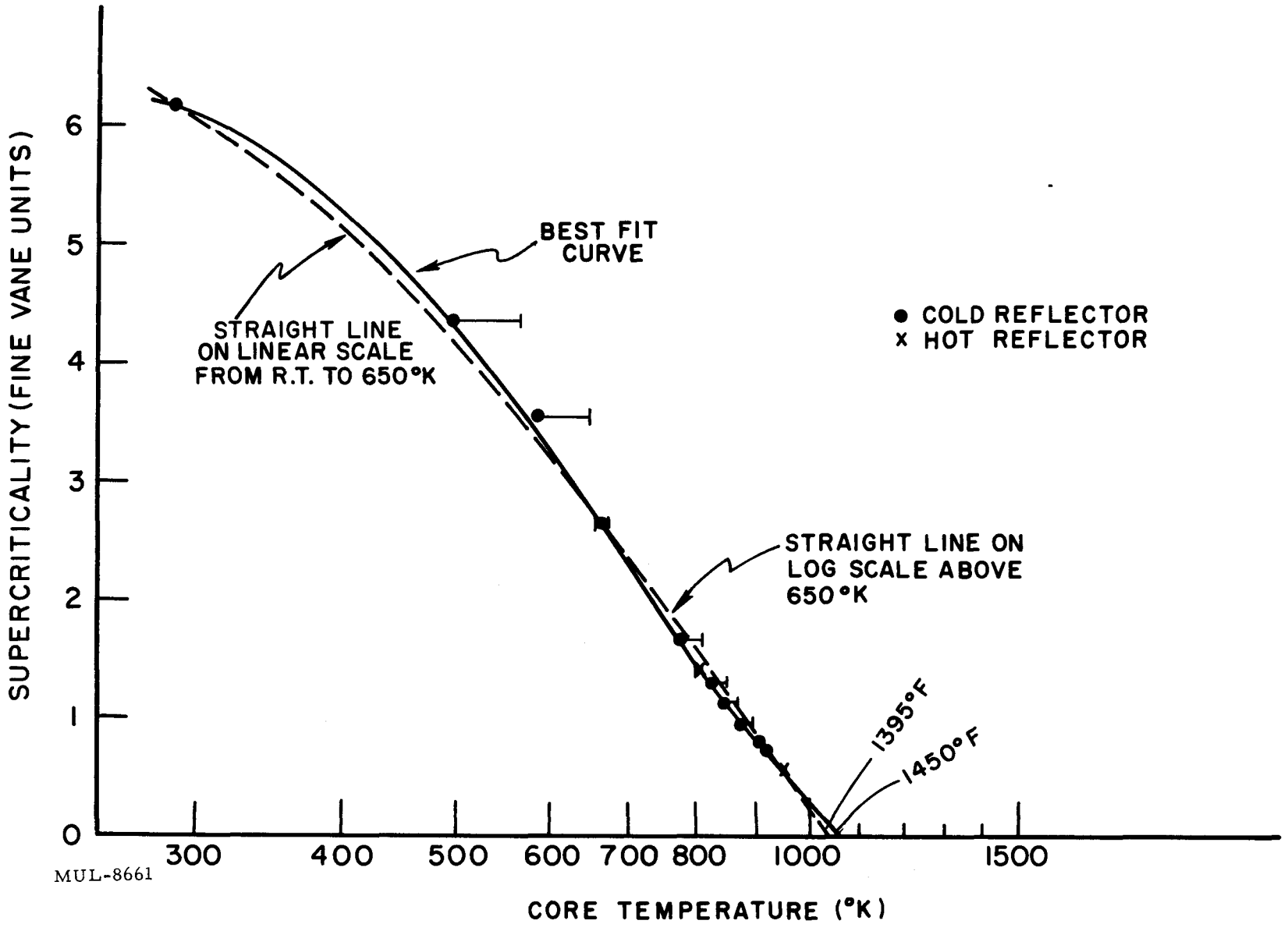

Fig. III-14. Supercriticality vs temperature for run of Nov. 4-5, 1959.

vanes was not measured, a linearly interpolated value (in parentheses in Table III-5) was used to determine the supercriticality in fine vane units.

The reflector cooling was stopped and the reflector was allowed to warm up to the core temperature which had increased in the meantime to 1240°F. The supercriticality, vane 4 worth, and fine vane worth were determined, and an activation run was made at about 5 watts for 1 hr. A small amount of negative reactivity was inserted at the end of the run and the decay in power was recorded to give information on the neutrons from delayed gammas (Fig. III-15). The ribbons jammed in the wall feed-through during removal, but were successfully removed when the cooling cycle was started and the feed-through flange could be safely unbolted.

The cooling of the assembly was stopped and the temperatures of the core and reflector were leveled off just below 1000°F for a good, intermediate and final determination of the supercriticality of the hot-core, hot-reflector configuration. The supercriticality points of the all-same-temperature curve fall so close to the cold-reflector curve that no sensible difference can be seen. The temperature of criticality is probably the same as the previous 1400° within 30°F with no indication that it is smaller or larger. The temperature coefficient of reactivity is the same as for the cooled-reflector within the uncertainty of measurement.

Full fission traverse records were obtained from only one ribbon in each of the high-temperature experiments. A useable partial record was obtained on a second ribbon only in the cold reflector experiment. The results of the high-temperature activation runs are shown in Fig. III-16.

Since the core was made up of 13 blocks North and 14 blocks South, the E-W centerline of the core was displaced about half an inch from the E-W centerline of the reflector. If the neutron flux were tied rigidly to the core and reflector extremes, a fission traverse in the E-W direction would be disturbed by the nonconcentricity of the two flux distribution. For the ribbons in the NE-7 and SE-7 positions a disparity of about 12% in the relationship between the flux in the core and the flux in the reflector could exist. Some of the disparity in the room temperature traverse (Fig. III-13) and the disagreement between the NE-7 and SE-3.5 ribbons in the cold reflector traverse (Fig. III-16) might be explained by this off-center effect. Another room temperature activation experiment is planned to clear up this problem.

Note: This repeat experiment was performed December 1 and the results support the disparity suspicions to a large extent.

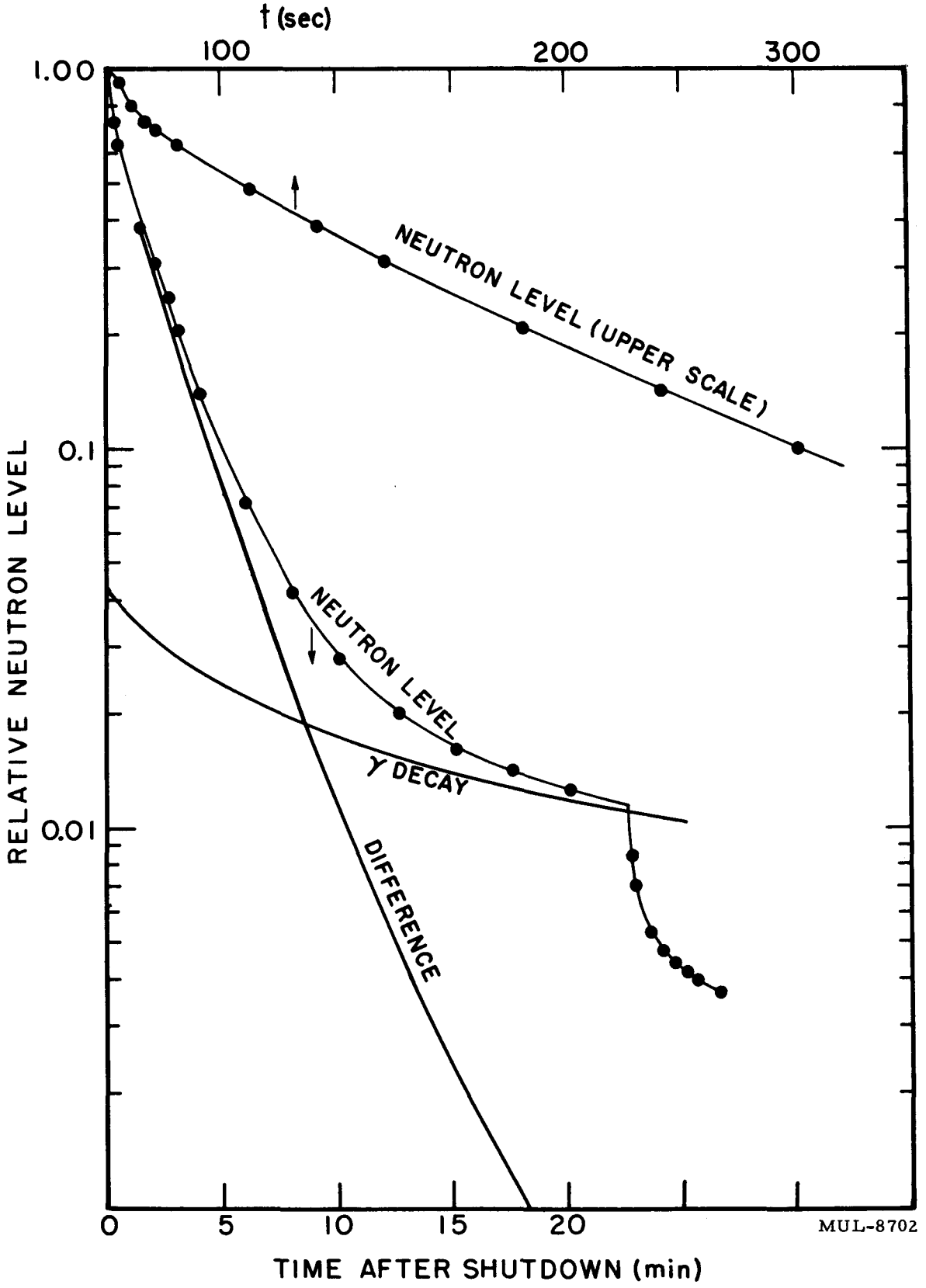

Fig. III-15. Shutdown from ~5 watt run on Nov. 5, 1959. (Insertion of $0.12 negative reactivity in 10 sec).

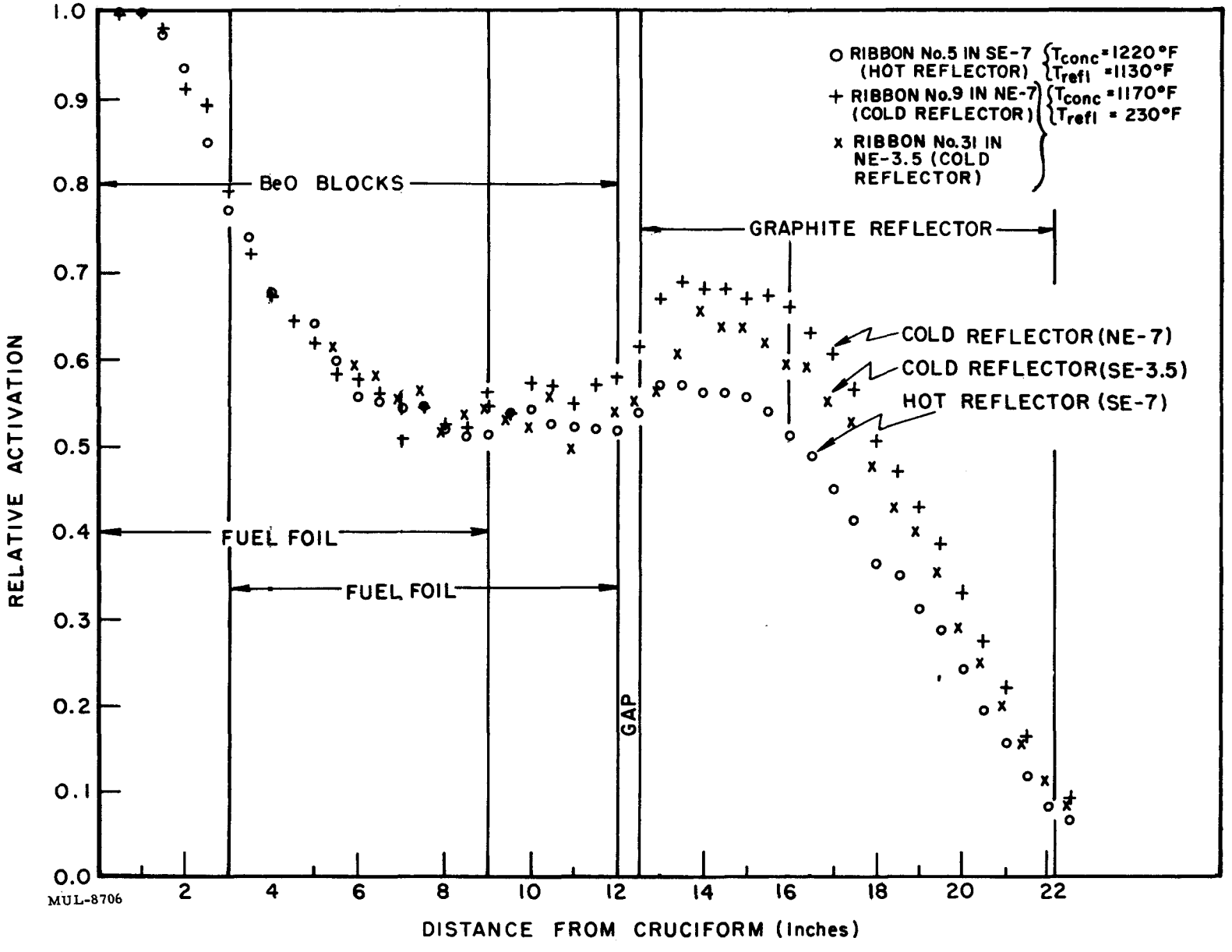

Fig. III-16. Cold- and hot-reflector fission traverses. Run of Nov. 4-5, 1959.

CHAPTER IV. TORY II-C

SECTION I. NEUTRONICS

Further ZOOM calculations have been made on the lightly reflected Tory II-C type reactor having an axial length of 51 inches and a core temperature of 1700°K. The reactor description and methods of calculation were presented in the last quarterly report.

Three families of curves have been made which involve changes in critical mass and reactor radius. These are for a bare core, a core having a 2-in. reflector, and a core having a 4-in. reflector. They are shown as Figs. IV-1, IV-2, and IV-3. In each family the porosity of the core has been varied (holding the reflector porosity at 0.05). Figure IV-4 shows how critical mass varies with reactor porosity, using two reactor radii and a 4-in. reflector.

In Figs. IV-5 and IV-6 a porosity was chosen for reactors having critical masses of 50 and 100 kilograms respectively. Relative power was then plotted against the relative core radius for cores having 0, 2 and 4-inch reflectors.

Figures IV-7 and IV-8 are similar to IV-5 and IV-6 except that reactor radius has been held constant while porosity is varied.

Since molybdenum is a possible structural metal for high temperature applications, several problems have been formulated involving molybdenum in the core. Molybdenum has some high resonance absorption peaks in the epithermal region (40 to 800 electron volts). All resonance absorption has been placed in the ZOOM code in the neutron energy range between 31.7 and 100 ev. When foils of molybdenum are used in the reactor the neutron absorption is dependent on the thickness of the foil because of self-shielding effects. In Fig. IV-9 a base reactor containing 1% by volume of 20-mil-thick molybdenum foils was adjusted to obtain criticality. The thickness of the foil was then changed and the volume percent adjusted (at the expense of moderator) to bring the reactor back to criticality. The thicker foils required a lower resonance absorption cross section per unit thickness by an amount determined by critical experiments.

The 20-mil-thick molybdenum foil was used in Figs. IV-10 and IV-11 to show how core porosity suffers when 1% by volume of this foil is used. All points shown are for critical systems. A continuous curve has been drawn for the reactors having a 2-in. reflector, and points indicating displacement in the reactor having a 4-in. reflector are shown.

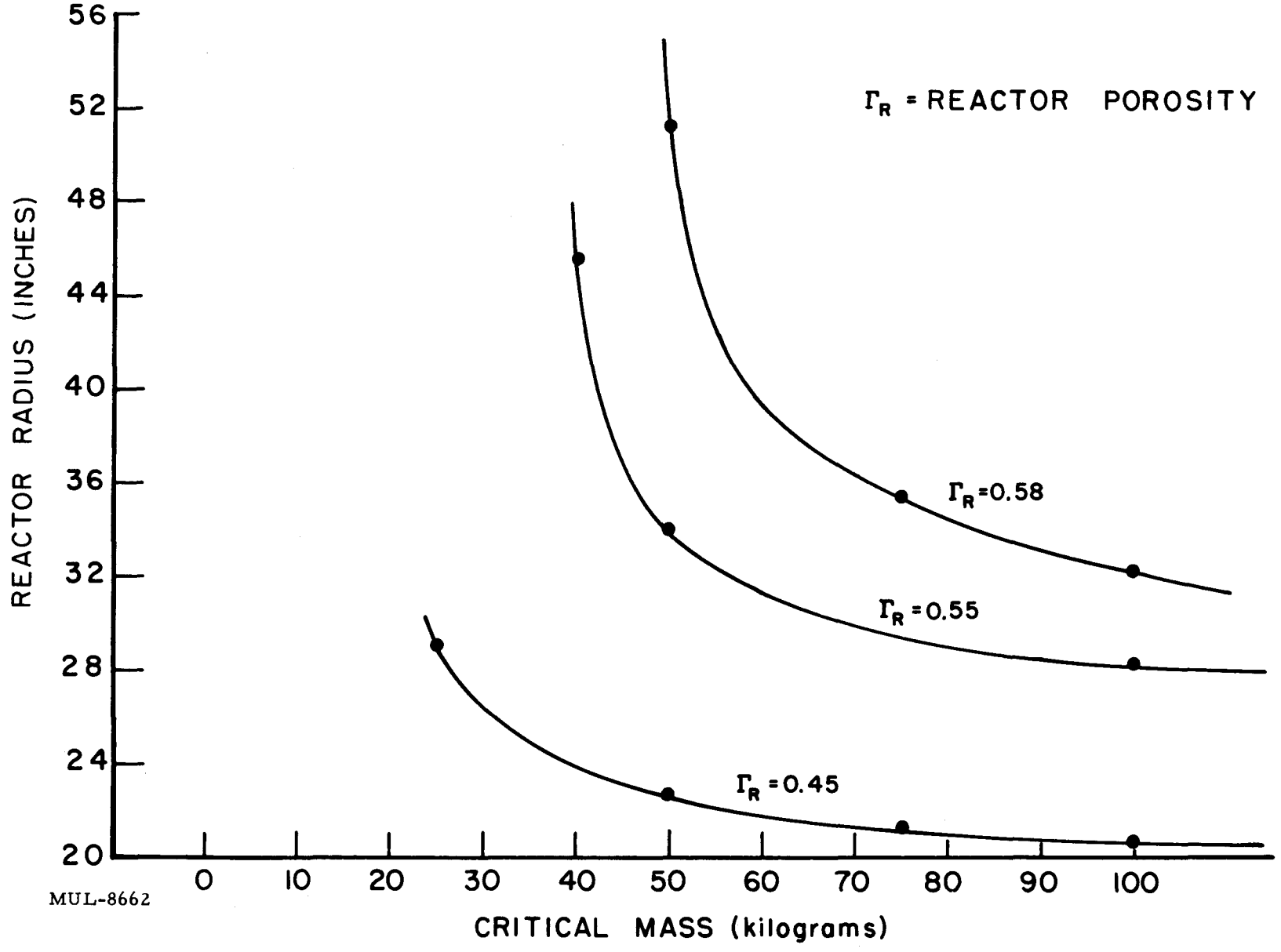

Fig. IV-1. Critical mass vs reactor radius for no reflector.

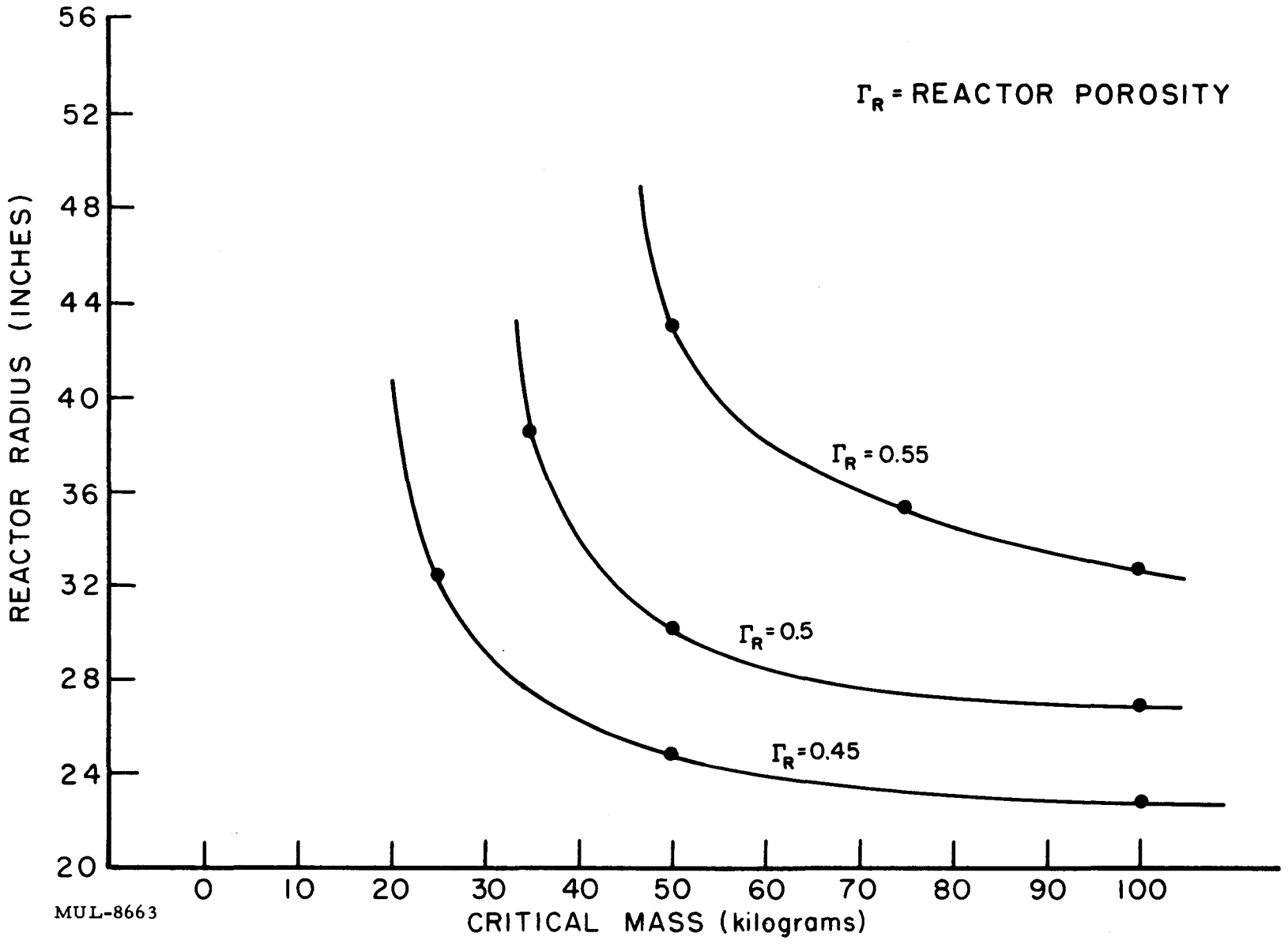

Fig. IV-2. Critical mass vs reactor radius for a 2-in. reflector.

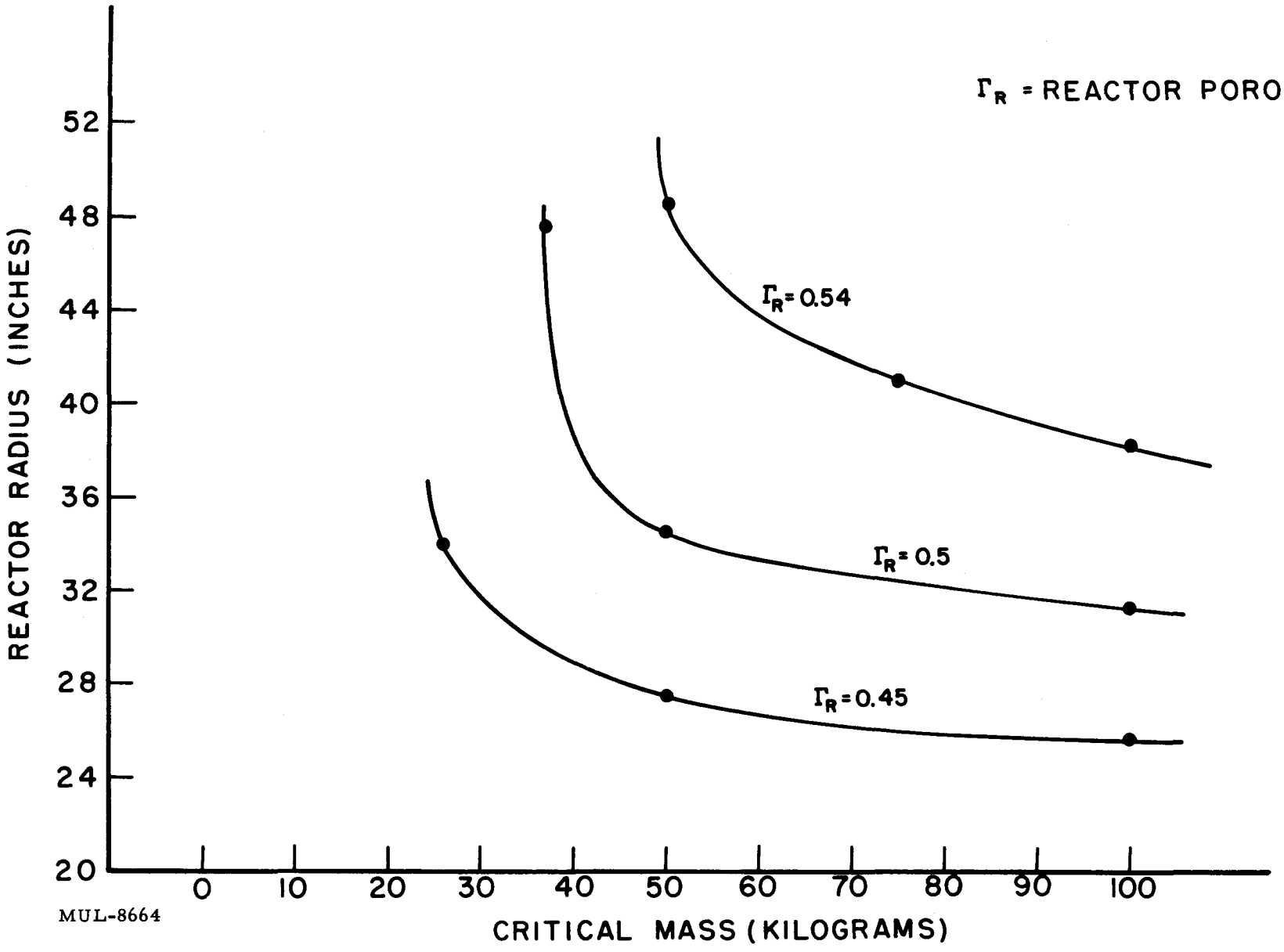

Fig. IV-3. Critical mass vs reactor radius for a 4-in. reflector.

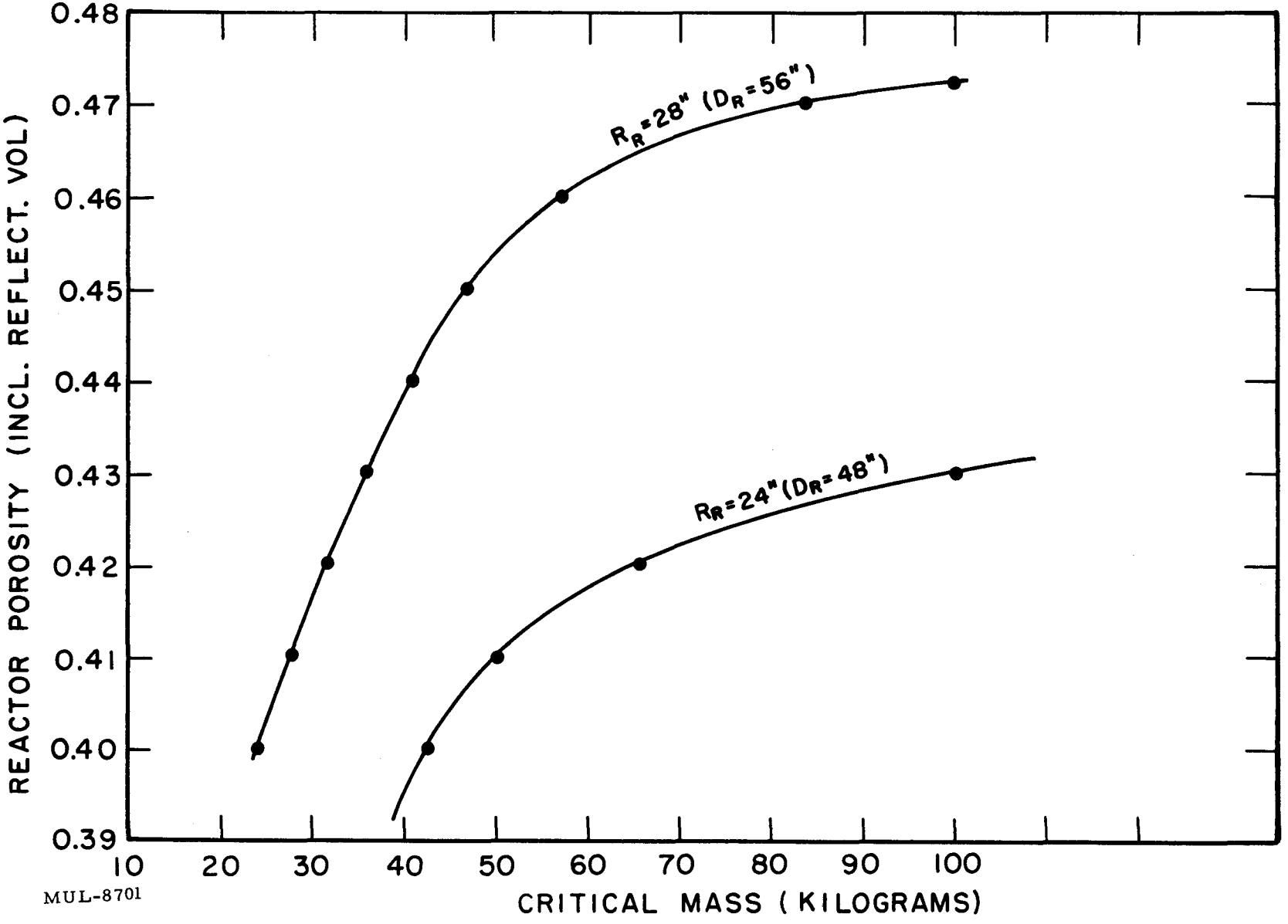

Fig. IV-4. Reactor porosity vs critical mass for a 4-in. reflected system of 48 in. and 56 in. diameters.

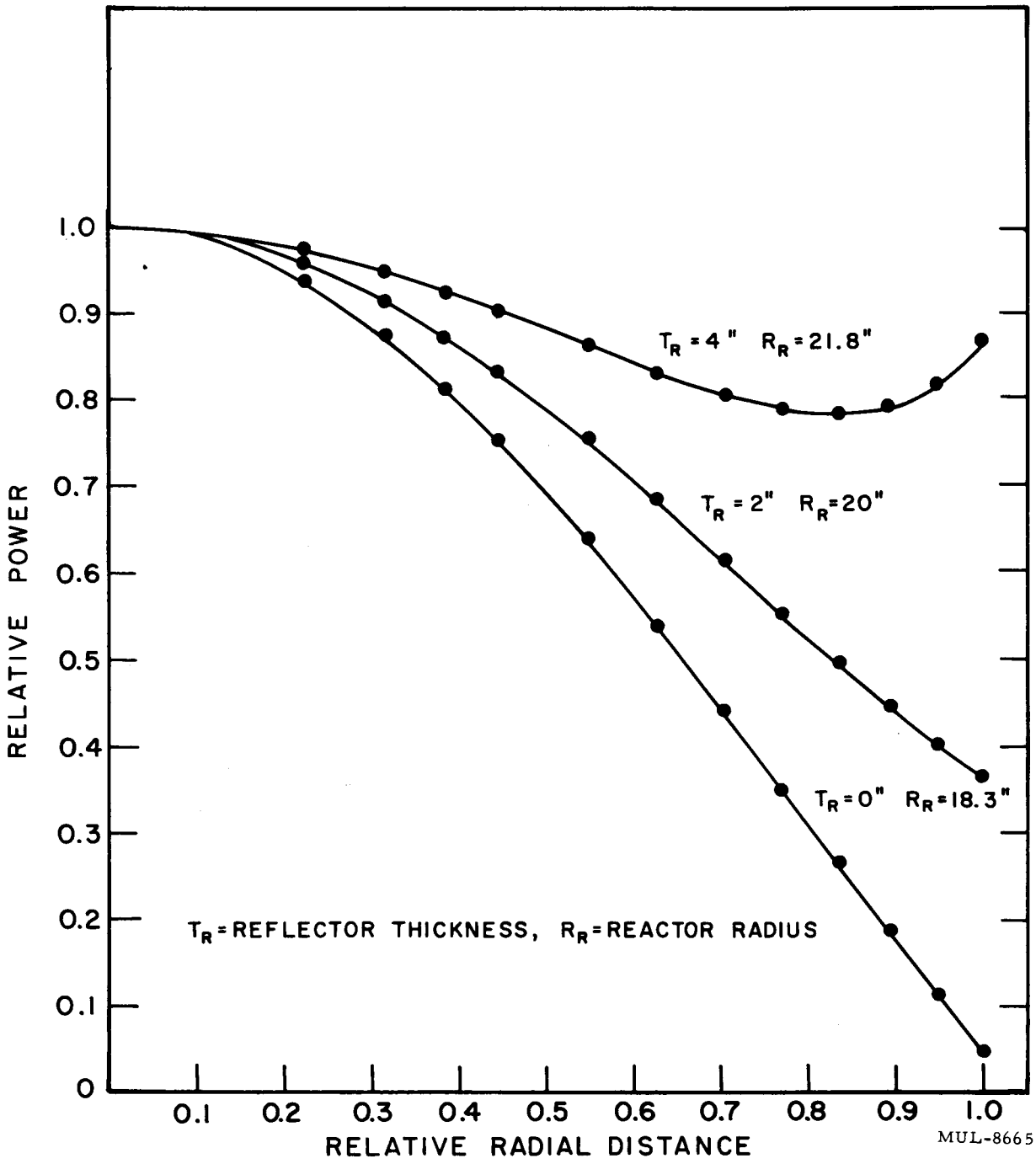

Fig. IV-5. Relative power fraction vs relative radial distance for constant reactor porosity (0.38) and critical mass = 50 kg.

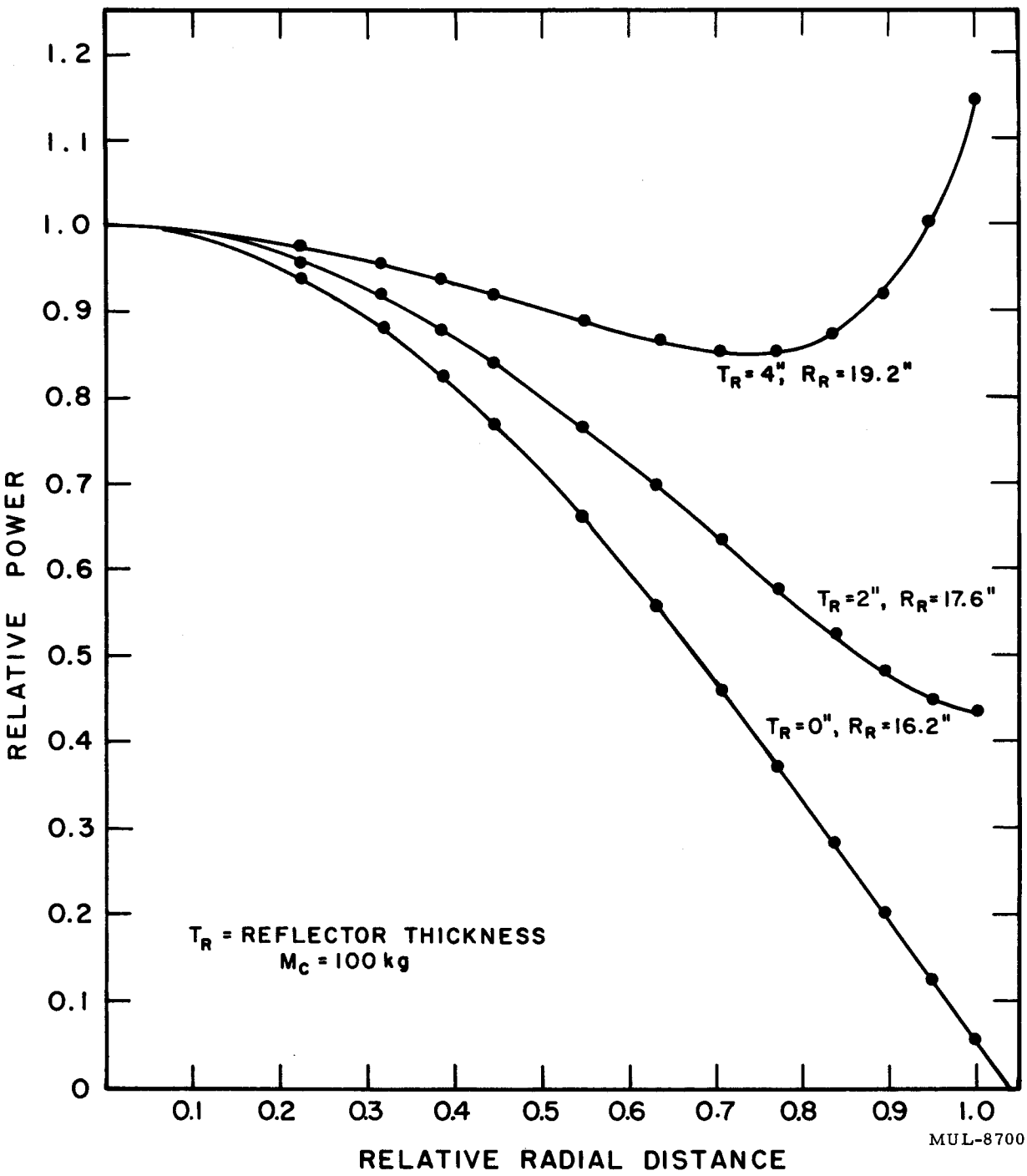

Fig. IV-6. Relative power fraction vs relative radial distance for constant reactor porosity (0.36) and critical mass = 100 kg.

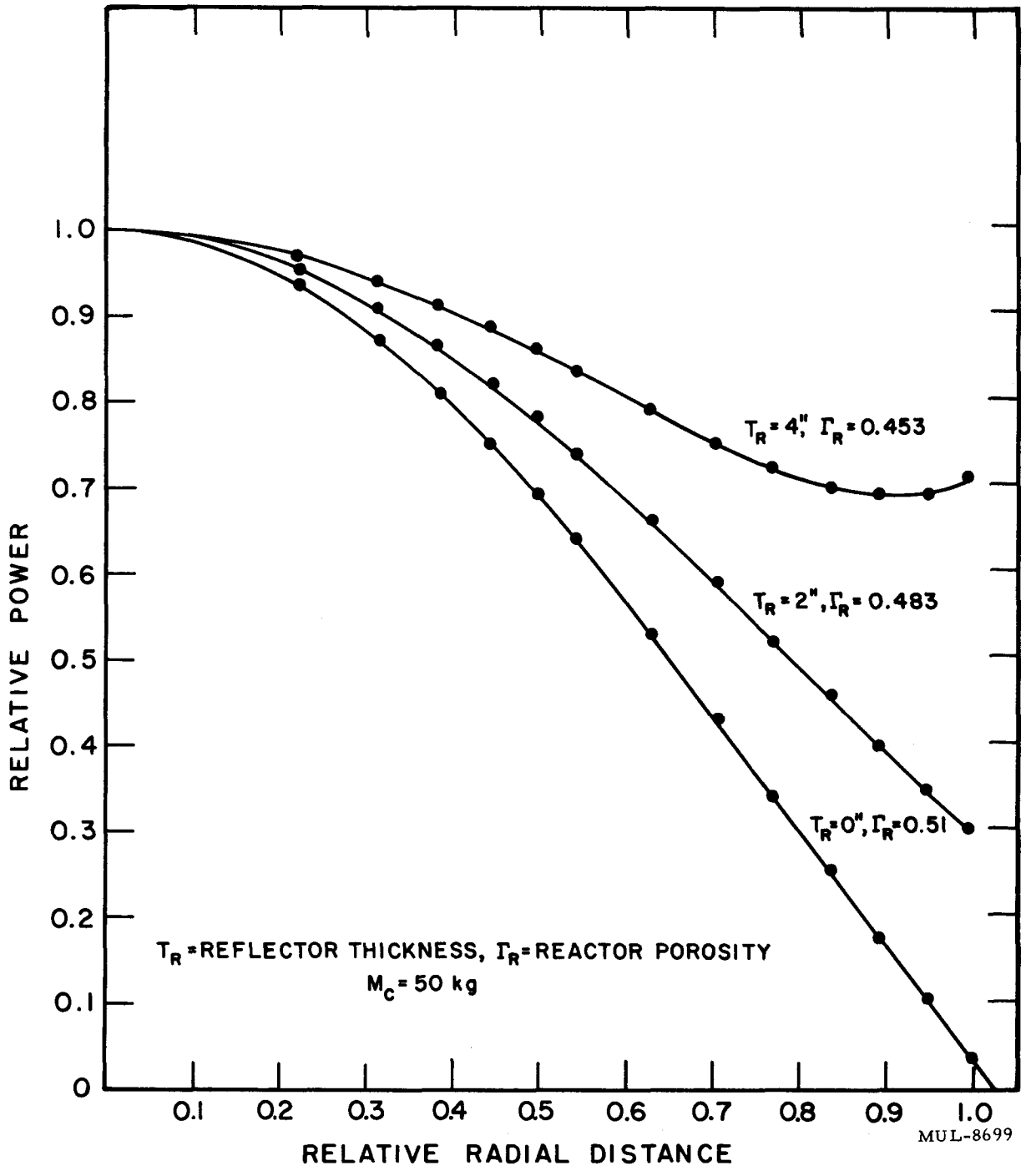

Fig. IV-7. Relative power fraction vs relative radial distance for constant reactor radius (28 in.).

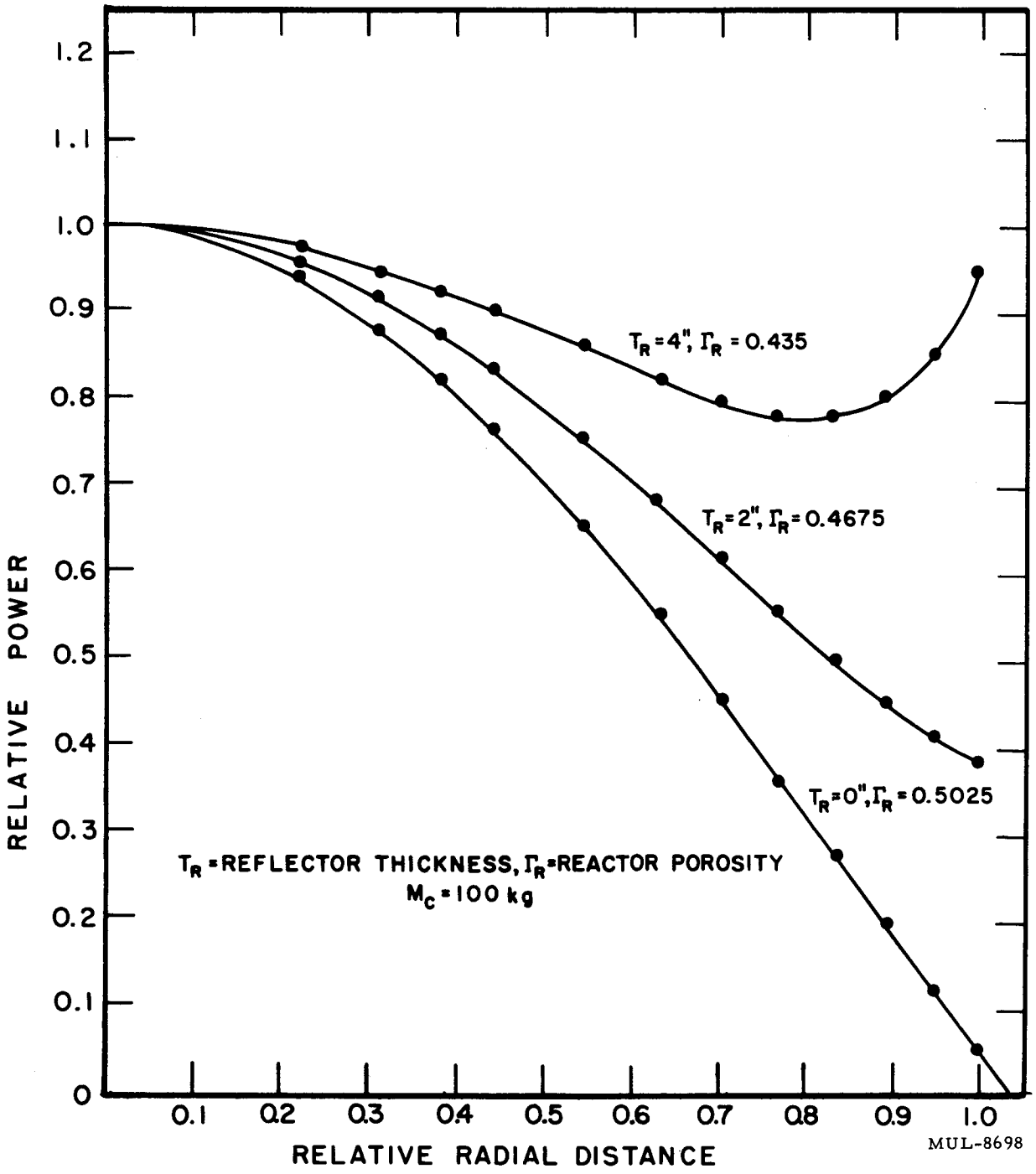

Fig. IV-8. Relative power fraction vs relative radial distance for constant reactor radius (24 in.).

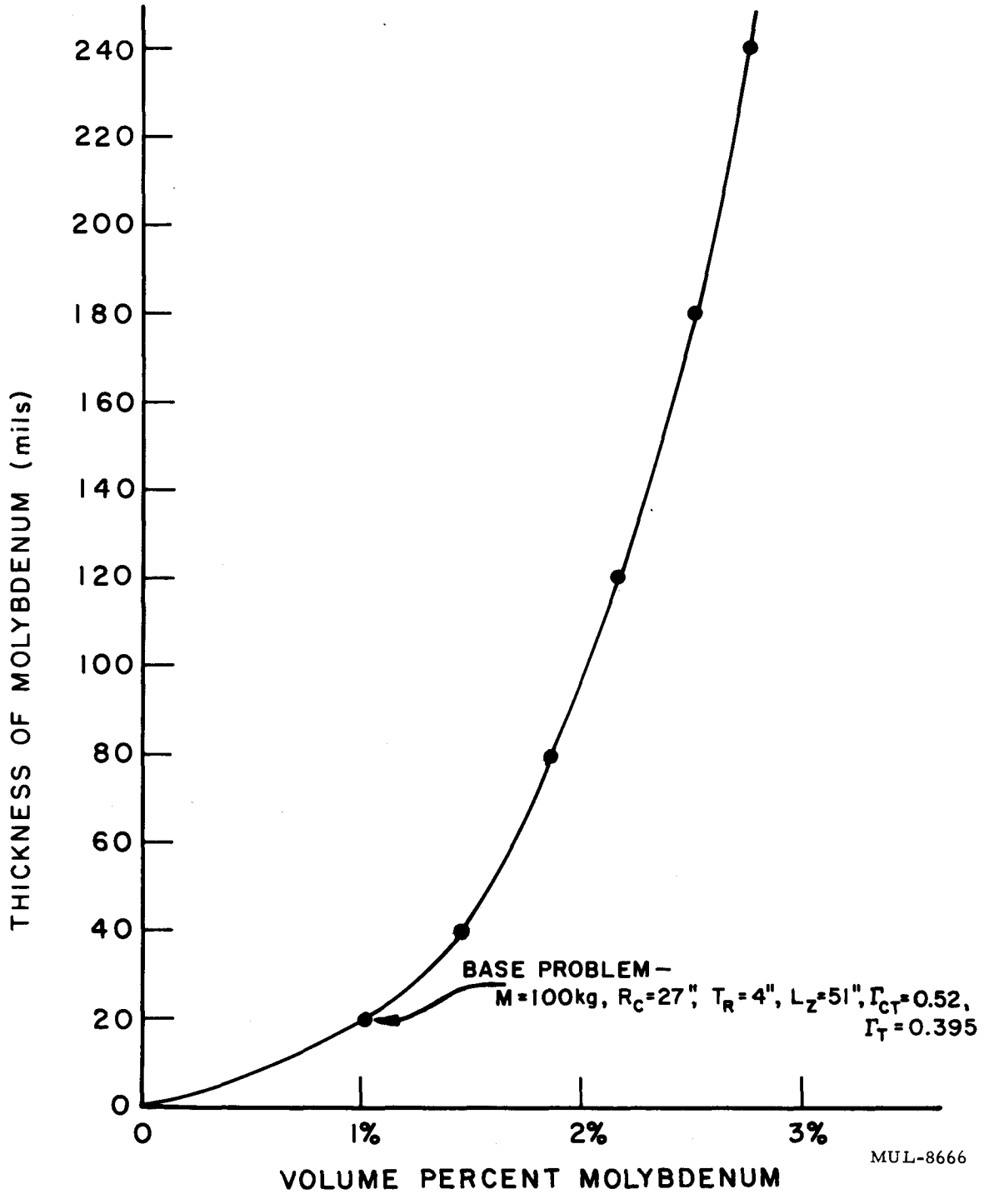

Fig. IV-9. Thickness vs volume percent of hot molybdenum foils for critical systems.

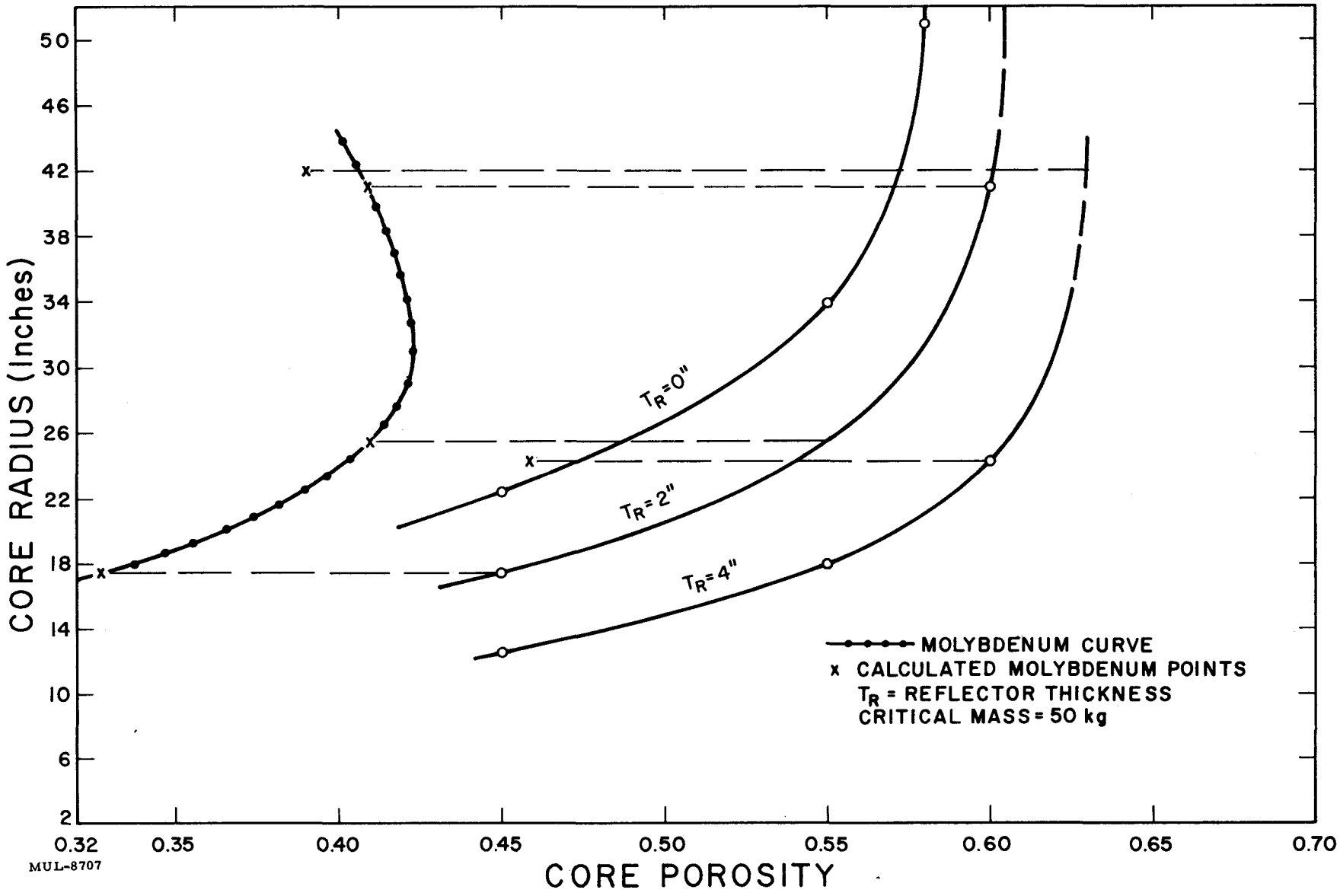

Fig. IV-10. Core porosity vs radius, showing displacement due to 1% by volume of molybdenum foils of 20-mil thickness.

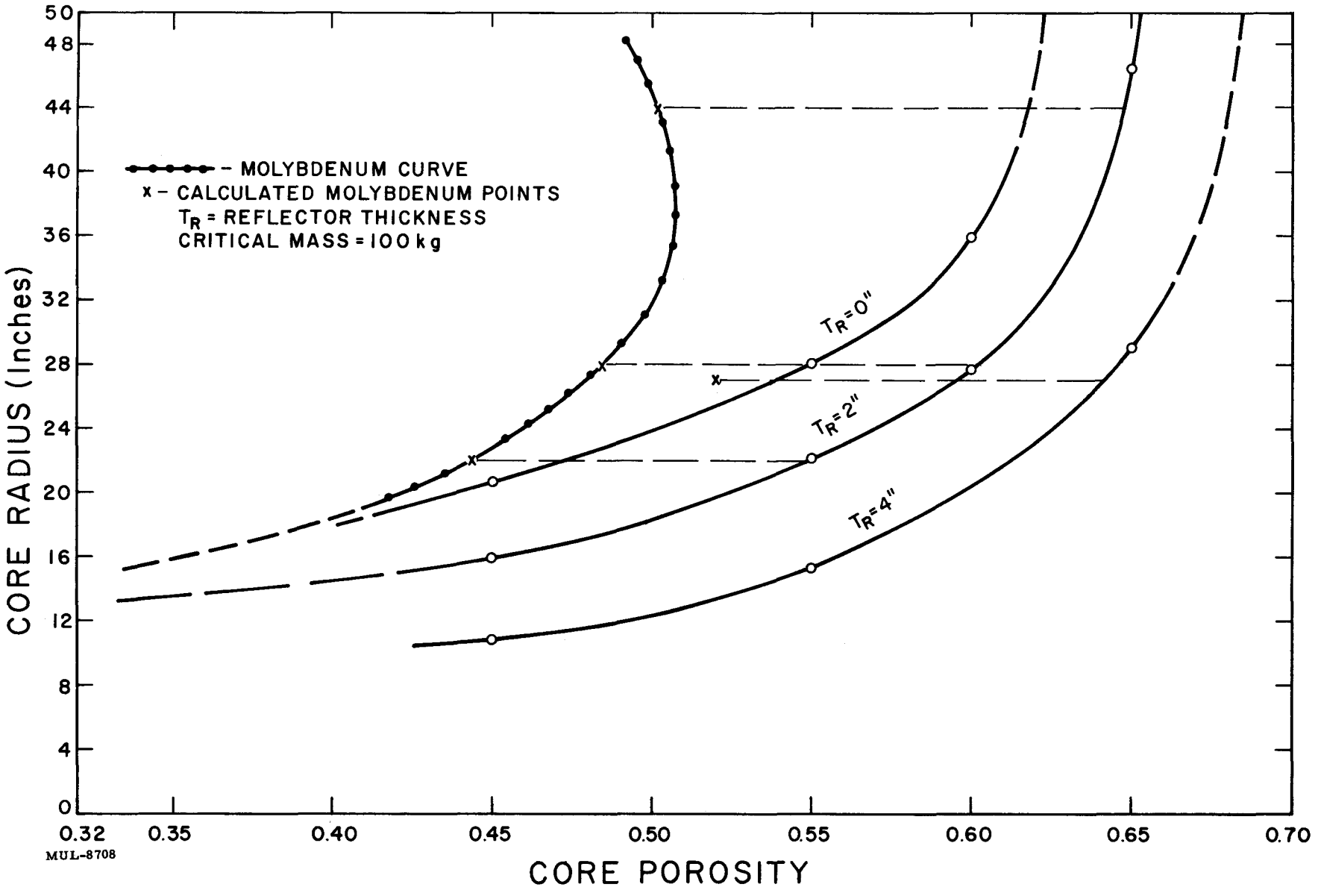

Fig. IV-11. Core porosity vs core radius, showing displacement due to 1% by volume of molybdenum foils of 20-mil thickness.

UCRL-5829

SECTION II. CONTROLS

Pneumatic Actuation System

The Model 40T room temperature pneumatic actuation system was delivered to LRL. The system included a Nike-type, single-stage, 4-way servo-valve, gear-motor pneumatic actuator, rotary potentiometer, and a multi-stage transistorized ac amplifier which serves as the comparer as well as the power stage for the servo-valve.

There were several difficulties encountered with the system as delivered:

(1) The system static stiffness (force-to-displacement ratio at the load) was much lower than expected. This was due to the low pressure gain of the Nike servo-valve which is a single-stage valve. The contractor is presently developing a 2-stage valve which will increase the static stiffness by a factor of about 100. Also, the stiffness can be improved in future valves by employing lag-type dc compensation around the dc operational amplifier. This could not be done with the present amplifier because it is an ac amplifier and not an operational type.

(2) The system exhibited a steady-state jitter or limit cycle which has a frequency of about 4 cps. The jitter has not yet been corrected but is known to be caused by the transistorized ac amplifier which has both 400 cps and 60 cps power supplied to it. The latter is used for dithering the valve and load.

(3) There was considerable 400 cps noise present throughout the system, preventing meaningful measurements of the system characteristics. This trouble was corrected by using dc excitation on the feed back potentiometer (rather than 400 cps).

Aside from the above-mentioned difficulties (which are principally electronic in nature), the actuator appears to have considerable promise. It is very simple; at the time of delivery it was completely disassembled and reassembled in less than 30 minutes. It uses no lubrication and appears to be quite rugged. It has had about 10 hours total operating time with only one shutdown, which was for realignment of the end-bearing cylinder. The starting and running friction level increased from 1 lb to 7 lbs during the first 8 hours; after realignment of the end-bearing cylinder, the friction level returned to its original values of 1 lb.

The high-temperature prototype actuator, Model 60, is presently being tested by the contractor in the 500-600°F temperature range. The test cell is maintained at this temperature as well as the air used for actuation. The

Model 60 is very similar to the Model 40T in design; however, graphite surfaces are used on the side plates to eliminate metal-to-metal contact. During high-temperature tests an increase in actuator friction level has been generally noted; however, no jamming or severe wear has been observed.

A standard, linear differential transformer has been purchased by the contractor for evaluation at 1000°F for possible use as a position transducer.

Development of a 2-stage servo-valve for use at 1000°F is proceeding satisfactorily. The proposed valve will use a flapper first stage which in a previous development project has been proved capable of operation to 1200°F.

Radiation-Resistant Log Power Amplifier

During this reporting period, three different methods of getting log power indications were studied and one method was selected for development. The three methods considered were: (1) transistorized log amplifier, (2) servo log amplifier, (3) ceramic or vacuum-tube log amplifier. The first method offered ideally small packaging and good accuracy but was the least radiation tolerant, requiring considerable shielding. Method 2 offered the best conformity and lowest drift but involved numerous relays and many moving parts. It would also have the largest volume and the lowest frequency response of the three methods considered. Method 3 was felt to be most promising and was selected for development. It involves state-of-the-art components, can be packaged neatly, has adequate band width and should be quite radiation tolerant. The most difficult problem here was finding a pentode with a good log characteristic over the specified four decades. By trial and error with a number of selected commercial tubes the contractor has found several tubes with good log characteristics over six decades and it appears that they can successfully meet our range specifications.

SECTION III. ENGINEERING

TORY II-C REACTOR DESIGN ANALYSES

A. Tory II-C Reactor Design Studies

Four reactor design concepts are currently being investigated for Tory II-C application. These may be classified according to the method of reacting axial and lateral reactor loads. These methods are depicted in Fig. IV-12 and are discussed below.

ALIKE. Axial loads are reacted at the coolant inlet end of the reactor, using an arrangement of longitudinal tie tubes, modular base plates, and a transverse monolithic support structure attached to the missile air frame at the reactor inlet.

The strength of each tie tube in bending is utilized to transmit lateral loads to both ends of the reactor and thence to the missile air frame. Structural ceramic (BeO) links within the reactor divide the reactor into modular regions and transmit lateral loads to the tie tubes.

The ALIKE reactor concept is identical to the Tory II-A core design.

INTEGRAL. Axial loads are reacted in the same manner as in the ALIKE reactor concept. Solid tie rods are used in lieu of hollow tubes. The tie rods are located in clearance holes in a "tightly packed" reactor and therefore sustain only negligible lateral loads due to their own weight. The ceramic reactor parts are in intimate contact with each other and an insulated reactor shell. The reactor shell exerts an elastic (or plastic) clamping action on the reactor parts. The reactor shell transmits lateral loads to the missile air frame at each end of the reactor.

TRAY. Axial and lateral loads are reacted at several stations along the length of the reactor, using a system of radial sheet metal "beams" contained in a circular "tray" which is attached to the missile air frame or an intermediate pressure shell. Several trays are used. Each tray is loaded only by the volume of the reactor associated with its own gross volume.

DOME. Axial loads are reacted at the coolant exit end of the reactor by a dome which spans the missile diameter. The dome is supported on an insulated ring attached to the missile skin. Lateral loads are reacted in the same way as in the INTEGRAL concept. No metallic structural components are required within the reactor.

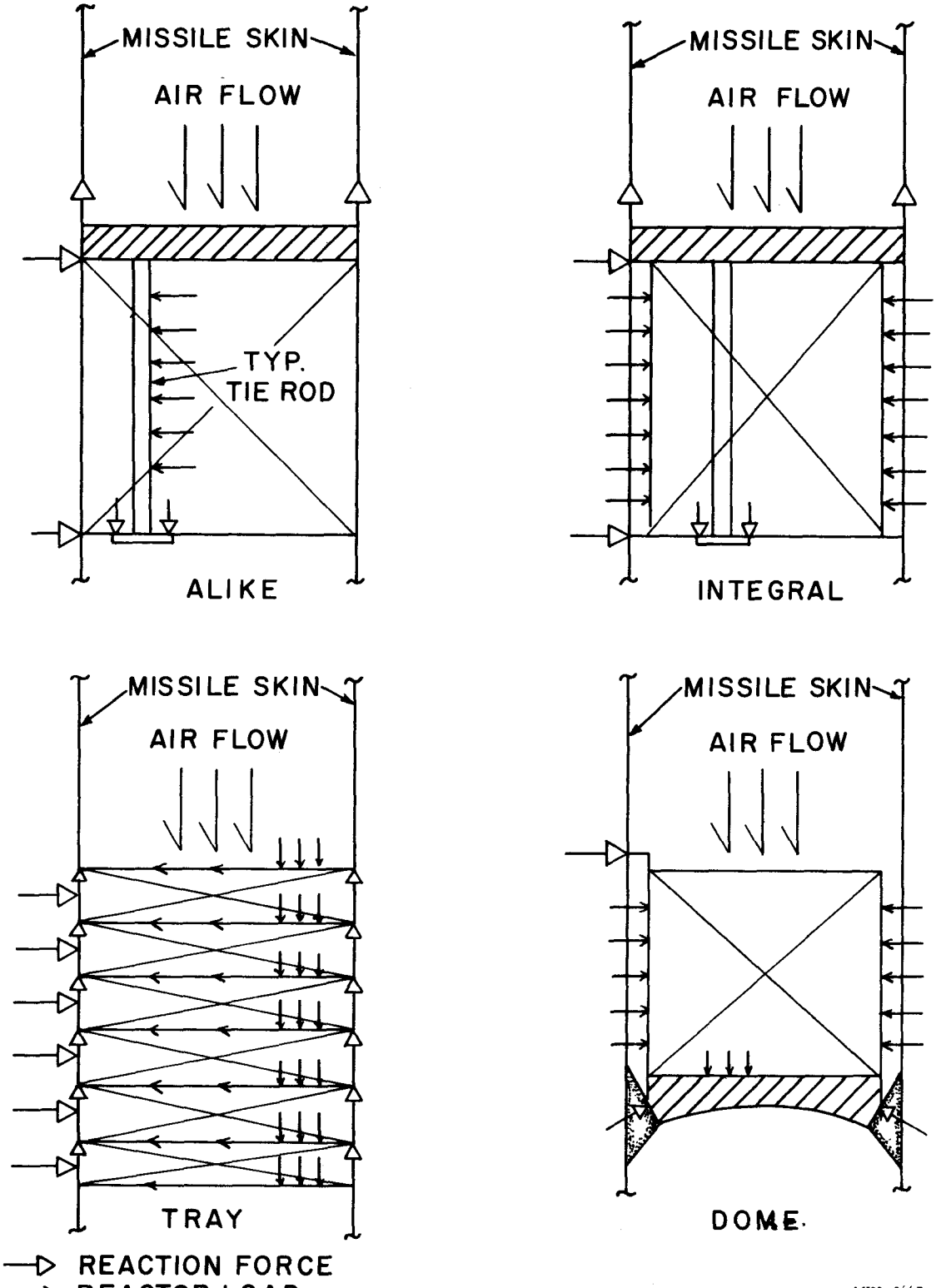

Fig. IV-12. Tory II-C reactor design concepts.

Characteristics of the structural metal used within these reactors can be compared in a general manner. For the purpose of comparison a 52-in.-diam reactor is assumed. Other conditions are given in Sec. B.

Metal Volume Requirements

It is desirable to have as little metal in the reactor as possible to reduce critical mass and minimize fuel retention problems. A preliminary estimate of cross-sectional area of metal required in each of the reactors being considered is given in Table IV-1.

TABLE IV-1

COMPARISON OF METAL PARAMETERS FOR 52-IN.-DIAM REACTORS

Reactor	Metal cross-sectional area (in^2)	Ratio of metal surface area to metal volume (in^{-1})	Typical metal thickness (in.)	Metal distribution related to importance (See Sec. I-D)
DOME	0	--	--	--
INTEGRAL*	7	21	0.190 diam	Favorable
ALIKE	29	32	0.060	Favorable
TRAY	32	49	0.060	Unfavorable

* Values of the parameters for INTEGRAL reactor are average, based on the use of 252 tie rods whose maximum diameter (at the hot end) is 0.25 in. See Sec. B.

Both INTEGRAL and TRAY reactors would probably use a molybdenum alloy in the aft 0.6 of the reactor. A nickel alloy (more economical of neutrons than molybdenum) would be used in the forward 0.4 of these reactors.

In the ALIKE reactor an efficient coupling for these two metals is more difficult to conceive since the coupling would have to transmit bending moment as well as tensile loads. These tie tubes would most likely be made only of one material (molybdenum).

Ratio of Metal Surface Area to Volume

For the cross-sectional areas of metal given in Table IV-1 the corresponding surface areas have been calculated. The ratio of metal surface area to metal volume is given in Table IV-1.

A high ratio of metal surface area to volume, per se, leads to easier cooling of the metal. However, unfueled BeO is most likely associated with the metal arrangement in proportion to absolute metal surface area; therefore,

a low ratio of metal surface area to volume may be desired. For other reasons (ceramic shapes available, incidental void, etc.), this ratio is essentially fixed for the TRAY and ALIKE reactors. The ratio may be varied considerably in the INTEGRAL reactor by use of more, smaller rods, or by use of rods with cross-shaped rather than circular cross sections.

Typical Metal Thickness

Typical metal thicknesses are indicated in Table IV-1. Thicker metal sections have greater self-shielding and therefore absorb less neutrons than an equivalent volume of thinner metal sections.

Metal Distribution

The longitudinal distribution of metal within the reactor is given for the INTEGRAL reactor in Fig. IV-13. Radial distribution is constant.

The longitudinal distribution of metal within the reactor for the TRAY reactor is constant. The radial distribution is shown in Fig. IV-14.

Both longitudinal and radial metal distribution in the ALIKE reactor are constant.

Since the central portion of the reactor is a region of high importance, metal distributions have been indicated in Table IV-1 as favorable if constant or increasing at the boundary; the distribution is termed unfavorable if it decreases at the boundary.

Conclusions

Based on these considerations of metal volume, thickness, distribution, and surface area-to-volume ratio, the order of superiority of the reactors studied is the same as their order of listing in Table IV-1. Because each reactor concept has other individual characteristics the overall order of superiority of the reactors being studied cannot be stated at this time.

B. INTEGRAL Reactor

The INTEGRAL reactor employs solid molybdenum alloy tie rods of optimum cross-sectional area to react the pressure drop load of air flow through the reactor. Solid tie rods have the advantages over hollow tie tubes of easier fabrication and easier application and inspection of oxidation protection coatings. By using a reasonable number of rods, thermal stress is unimportant. Lateral loads are reacted in the ceramic core directly to an external containing shell; the bending strength of the tie rods is not utilized.

It is shown below that for reasonable assumptions of reactor conditions, the INTEGRAL reactor contains 1/3% by volume of 1/2% Ti-molybdenum

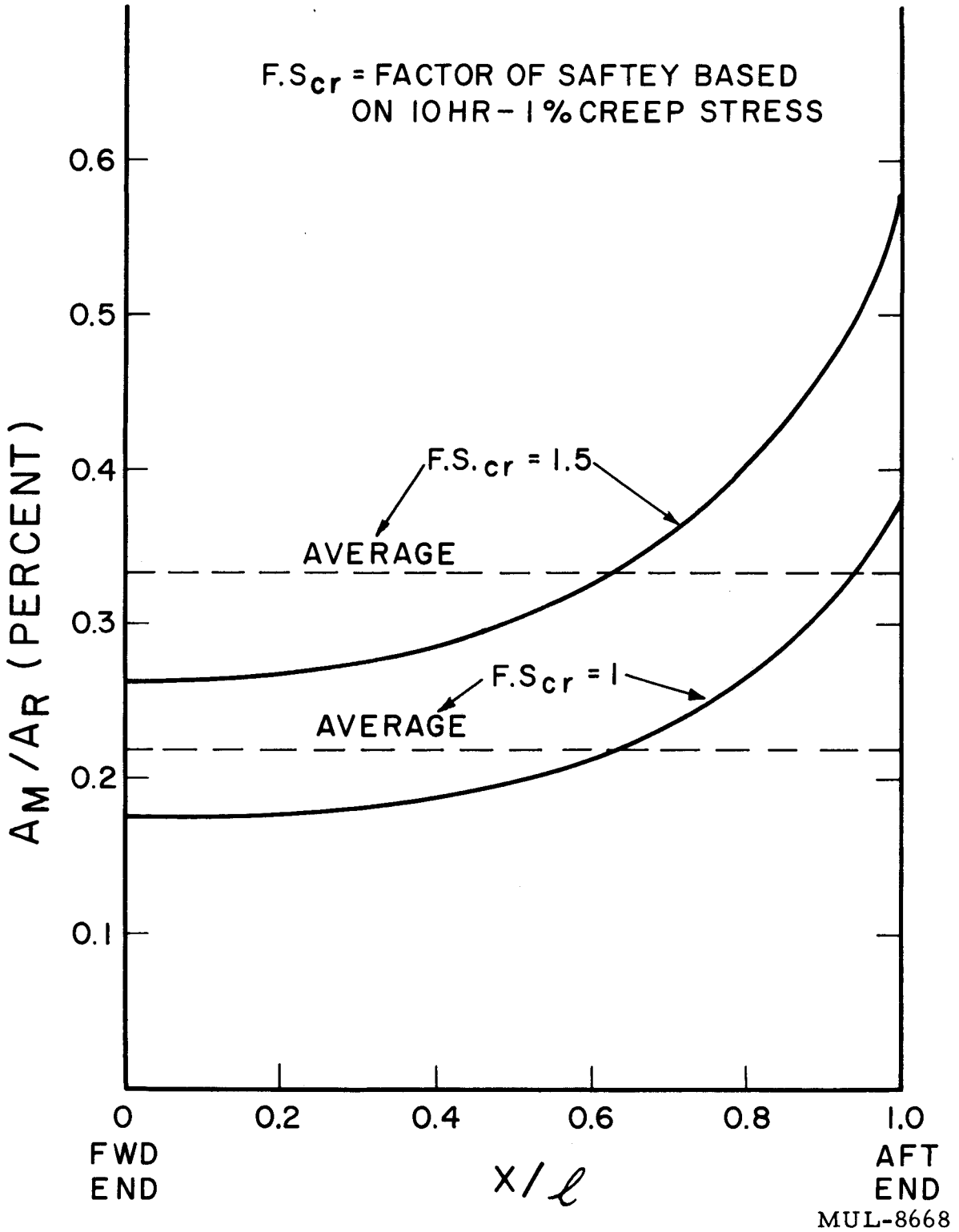

Fig. IV-13. Longitudinal variation of metal fraction in INTEGRAL reactor.

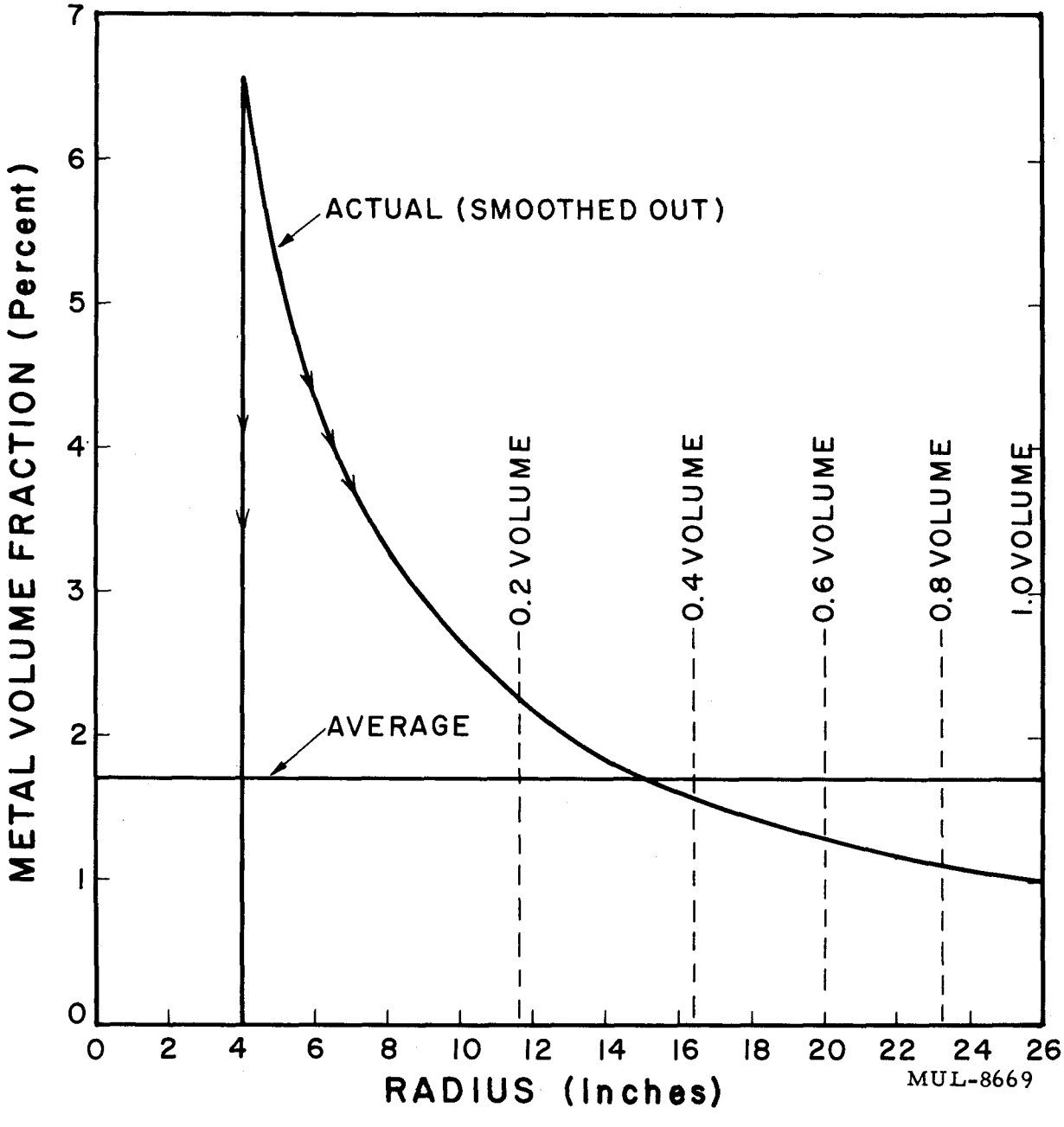

Fig. IV-14. Radial distribution of metal in TRAY reactor.

alloy. Use of Hastelloy R-235 at the cold end of the reactor can reduce the molybdenum content by 1/3.

The following ground rules and reactor conditions are specified:

(1) Metal temperature increases linearly in the reactor from 1200°F to 2000°F (at all reactor radii).

(2) Overall reactor length, L = 54 in.

(3) Overall reactor diameter, D = 52 in.

(4) Pressure drop through the core, P = 141 psi.

(5) Factor of safety (based on 10 hr-1% creep strength), $F.S._{cr} = 1.5$.

(6) Neglect axial and lateral flight loads and vibration.

(7) Neglect thermal stress in sizing components, but consider thermal stress separately.

Analysis

Material Strength

Because only meager creep data is available on Hastelloy R-235, the analysis of the tie rods is based on the use of molybdenum throughout their length. General statements will be made regarding the transition of molybdenum to Hastelloy in the tie rod.

Three data points for 1% creep in 10 hr for stress-relieved 1/2% Timoly alloy were obtained from Ref. 1 as well as a curve of yield strength for 0.1% offset.

The yield strength curve permits a conservative estimate of 1% creep strength at 1200°F. The data are tabulated in Table IV-2, normalized to the creep strength at 1200°F and plotted in Fig. IV-15.

TABLE IV-2

Temp (°F)	Stress for 1% creep in 10 hr ($\times 10^{-3}$, psi)	Normalized creep stress ratio	0.1% offset yield stress ($\times 10^{-3}$, psi)	Normalized yield stress ratio
1000	--	--	87.0	1.07
1200	81.0*	1.00	--	--
1600	70.5	0.87	77.0	0.95
1800	56.5	0.70	--	--
2000	36.5	0.45	--	--

* Estimated

[1] Battelle Memorial Institute, report No. DMIC-MEMO-14, April 1959.

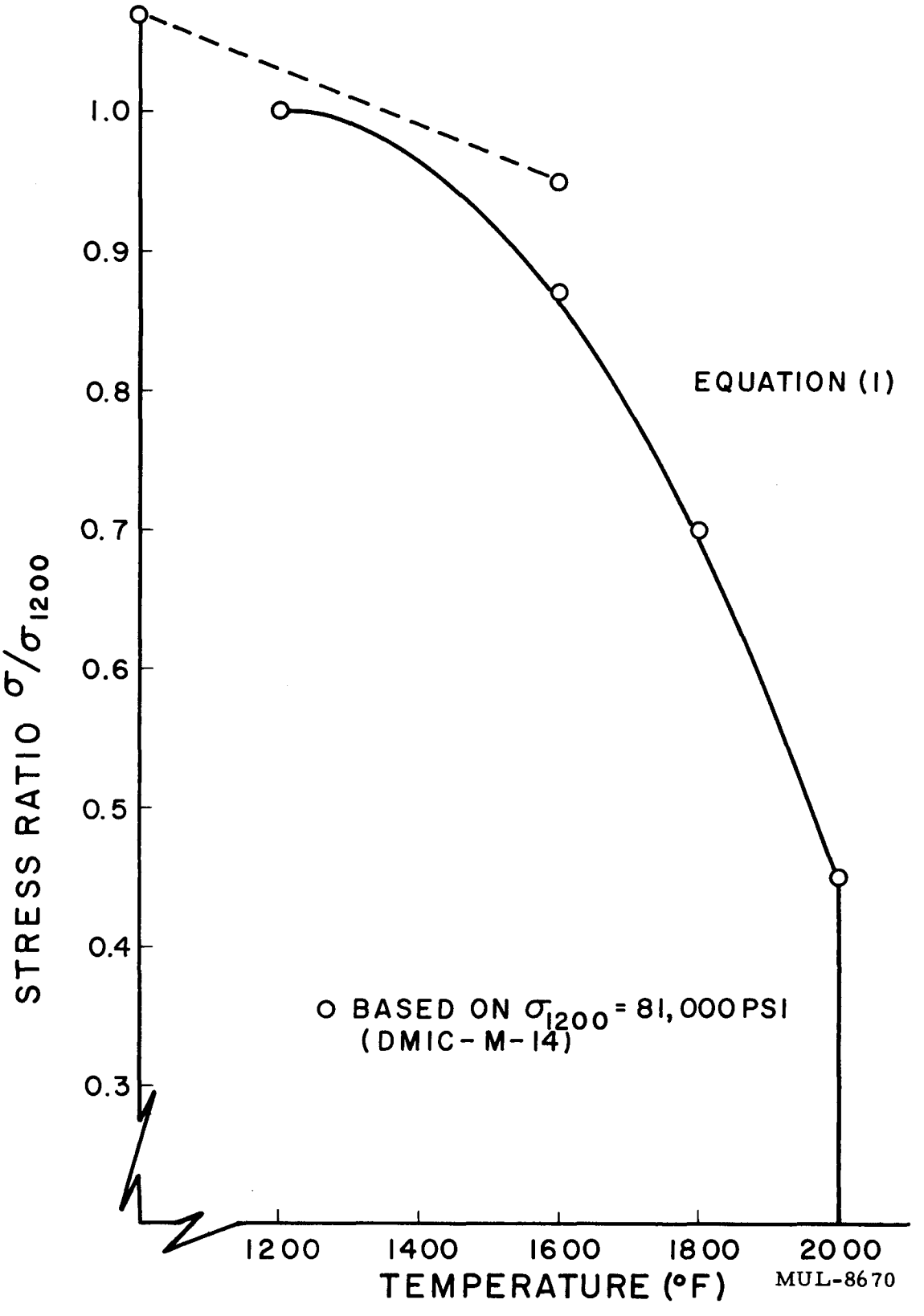

Fig. IV-15. Stress ratio for 1% creep in 10 hr for 1/2% Ti-Mo alloy vs temperature.

The creep data, together with the estimated creep at 1200°F, are very well described in the temperature range 1200°F $\leq$ T $\leq$ 2000°F by the parabola given by Eq. (1). This equation is also plotted in Fig. IV-15.

$$\frac{\sigma}{\sigma_{1200}} = 1 - \frac{0.55\,(T - 1200)^2}{64 \times 10^4}\,, \tag{1}$$

where σ is the 1%-10 hr creep strength at temperature T, and σ_{1200} is the corresponding strength at T = 1200°F.

Metal Area Requirements

Under the assumptions given above, the longitudinal temperature distribution is given by:

$$T = 1200 + 800\,x^*\,,$$

where

$$x^* = x/L\,. \tag{2}$$

The required area of metal, A_M, in the reactor is given by

$$A_M = \frac{P}{\sigma}\,, \tag{3}$$

where σ is given by Eq. (1) and P is the steady load due to the pressure drop over the reactor area, A_R:

$$P = \Delta P\, A_R\,. \tag{4}$$

The ratio of metal area to reactor area from Eqs. (3) and (4) is,

$$\frac{A_M}{A_R} = \frac{\Delta P}{\sigma}\,. \tag{5}$$

Substituting Eqs. (1) and (2) in (5) we have

$$\frac{A_M}{A_R} = \frac{\Delta P}{\sigma_{1200}} \quad \frac{1/2}{1 - 0.55\,x^*}\,. \tag{6}$$

Equation (6) gives the longitudinal distribution of metal in the reactor and is plotted in Fig. IV-13 for factors of safety of 1 and 1.5 based on creep strength, using the values:

$$\Delta P = 141 \text{ psi}$$

$$\sigma_{1200} = 81{,}000 \text{ psi.}$$

The total volume of metal, V_M, contained in the reactor volume, V_R, is given by

$$\frac{V_M}{V_R} = \int_0^{x^*} \frac{A_M}{A_R}\, dx^*\,. \tag{7}$$

Substitution of Eq. (6) in (7) and integration gives

$$\frac{V_M}{V_R} = \frac{\Delta P}{0.55\ \sigma_{1200}} \left[\frac{1}{2\ (1.35)} \ln \frac{1.35 + x^*}{1.35 - x^*} \right] . \qquad (8)$$

Note that V_M/V_R is equivalent to the average metal cross-sectional area fraction in the reactor. With $F.S._{cr} = 1.5$, the mean metal area fraction for the reactor from Eq. (8) is 1/3%. The longitudinal distribution is favorable from a neutronic standpoint. For a reactor with dimensions given above, the actual volume of metal in the reactor is:

$$V_M = \frac{V_M}{V_R} \quad A_R \quad L$$

$$= \frac{10^{-2}}{3} \quad \frac{\pi}{4} \quad (52)^2\ (54)$$

$$= 382\ \text{in}^3 \text{ of Moly alloy}$$

$$\equiv 140\ \text{lb of Moly alloy.}$$

Use of Hastelloy

If Hastelloy is used for the "cold" end of the tie rod, the Moly content in the reactor is reduced. The cumulative content of Moly in the reactor, measured from the front end, is plotted in Fig. IV-16. If Hastelloy were used to $x^* = 0.4$, then about 1/3 of the Moly could be eliminated.

The joining of the two materials could be made in the manner shown in Fig. IV-17. At $x^* = 0.4$ the 1% creep in 10-hr strength of Hastelloy R-235 is roughly 1/2 that of 1/2% Ti-moly. The dimensions indicated by the sketch in Fig. IV-17 are based on rough calculation using the latter consideration and 252 tie rods. Additional analysis is required to determine optimum transition location and coupling method.

Number of Tie Rods

The number of tie rods used to provide the total area indicated by Fig. IV-13 is determined by considering:

1. Base plate size
2. Incidental void fraction
3. Tie rod temperature
4. Thermal stress in rod.

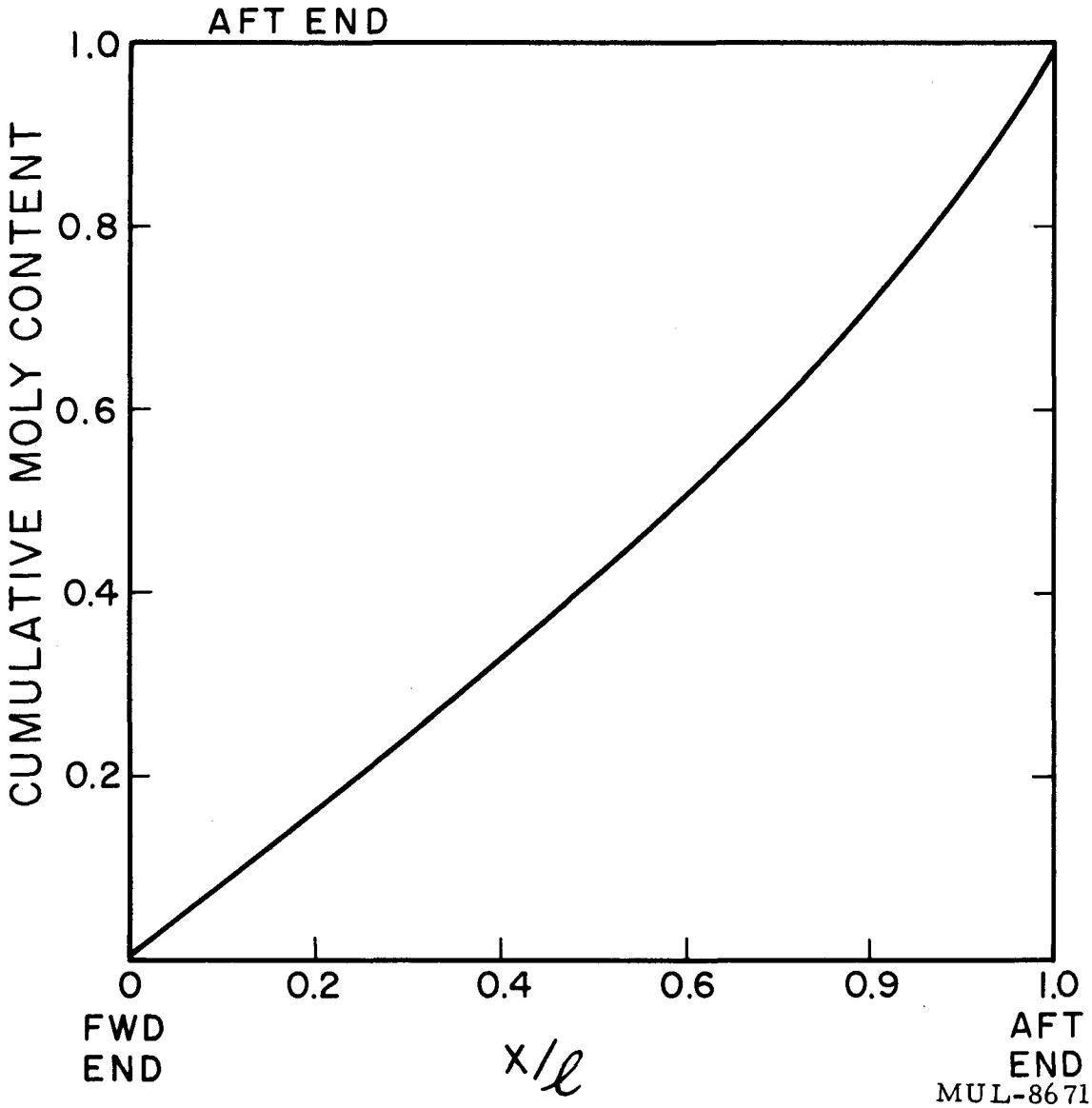

Fig. IV-16. Cumulative molybdenum alloy content vs position in reactor (INTEGRAL reactor).

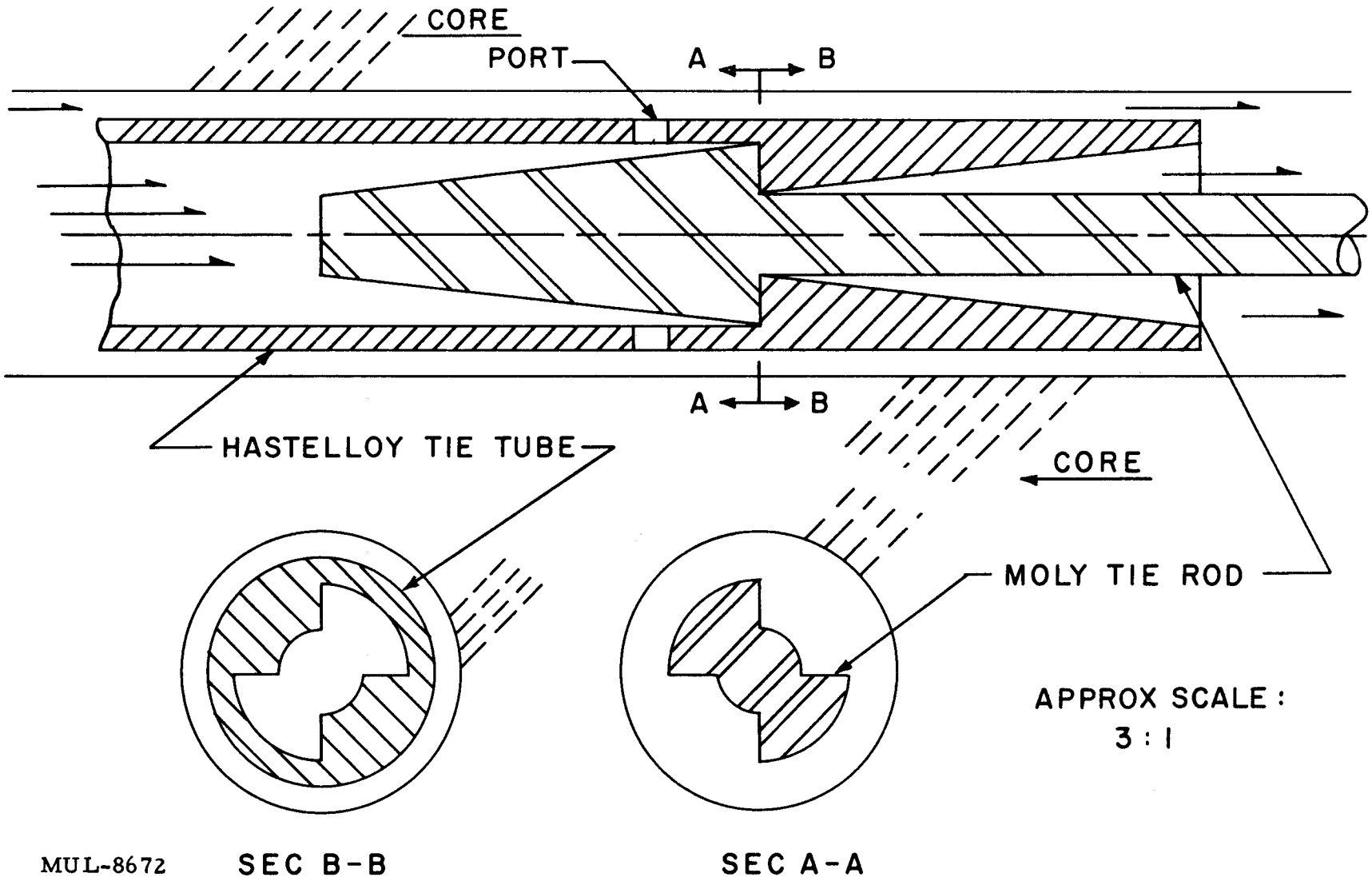

Fig. IV-17. Molybdenum-Hastelloy coupling at $x^* = 0.4$.

The number of tie rods can vary over a considerable range. Pending investigation of items 2 and 3 above it appears that 252 rods would be reasonable from the standpoint of items 1 and 4. Note that this number of rods is only slightly greater than one would have in an ALIKE reactor.

The number of tie rods, N, vs diameter, d_H, of tie rod at the hot end of the reactor for $F.S._{cr} = 1.5$ and D = 52 in. is:

$$N = \frac{15.7}{d_H^2} \quad . \tag{9}$$

The diameter of the tie rod at any given station is:

$$d = \left[\frac{\left(A_M/A_R\right)_{d_H}}{\left(A_M/A_R\right)_H} \right]^{1/2} \quad . \tag{10}$$

Equations (9) and (10) and Fig. IV-13 provide the relations given in Table IV-3.

TABLE IV-3

Hot end rod diam (inch)	Number of tie rods	Cold end rod diam (inch)
0.10	1570	0.067
0.15	698	0.100
0.20	394	0.133
0.25	252	0.167
0.30	175	0.200
0.35	128	0.234

Thermal Stress

The limits of thermal stress in a tie rod will now be calculated. Assume that 252 tie rods are used and that the internal heat generation is uniform.

The upper limit of thermal stress will result from considering a high-power density in the tie rod. The lower limit will result from considering a low-power density. Rough extrapolation of early Tory II-A heating calculations yields 12 and 6 Mw/ft^3 in the tie rods for high-power density (at center of reactor) and low-power density (at ends of reactor), respectively.

For uniform power generation, the maximum thermal stress (at the surface) in a solid cylindrical rod is given by

$$\sigma_{ZZ} = \sigma_{\theta\theta} = \frac{\alpha E P_{str} a^2}{8k(1-r)} , \qquad (11)$$

where

α = inst. coef. of thermal exp., F^{-1}

E = modulus of elasticity, psi

P_{str} = structural heating rate density, Btu/hr ft^3

a = radius of rod, ft

k = thermal conductivity, Btu/hr ft °F

r = Poisson's ratio

σ_{ZZ} = longitudinal stress, psi

$\sigma_{\theta\theta}$ = tangential stress, psi.

The material property group $\left[\frac{E\alpha}{k(1-r)}\right]$ based on Climax Molybdenum Co. data is tabulated in Table IV-4 for temperatures corresponding to 1/4 length intervals of the reactor. The rod radius is calculated from Eq. (10) for the case:

D = 52 in N = 252 $F.S._{cr} = 1.5$.

The resulting thermal stress, using Eq. (11) is also tabulated in Table IV-4 for the two structural heating rates considered.

TABLE IV-4

T (°F)	x^*	$\frac{E\alpha}{k(1-r)}$ (psi-ft-hr-Btu^{-1})	a^2 ($\times 10^4$, ft^2)	$\sigma_{ZZ} = \sigma_{\theta\theta}$, psi: High limit ($P_{str}$=12Mw/$ft^3$)	$\sigma_{ZZ} = \sigma_{\theta\theta}$, psi: Low limit ($P_{str}$=6Mw/$ft^3$)
1200	0	3.33	0.486	766	383
1400	0.25	3.40	0.503	808	404
1600	0.50	3.48	0.567	930	465
1800	0.75	3.54	0.708	1180	590
2000	1	3.58	1.08	1826	913

Fig. IV-18 shows the upper and lower thermal stress limits as a function of x^*. The broad band between the two curves indicates the probable stress due to power density variation along the reactor longitudinal axis. It is seen that the thermal stress in a solid 1/2% Ti-molybdenum alloy is only about 1000 psi.

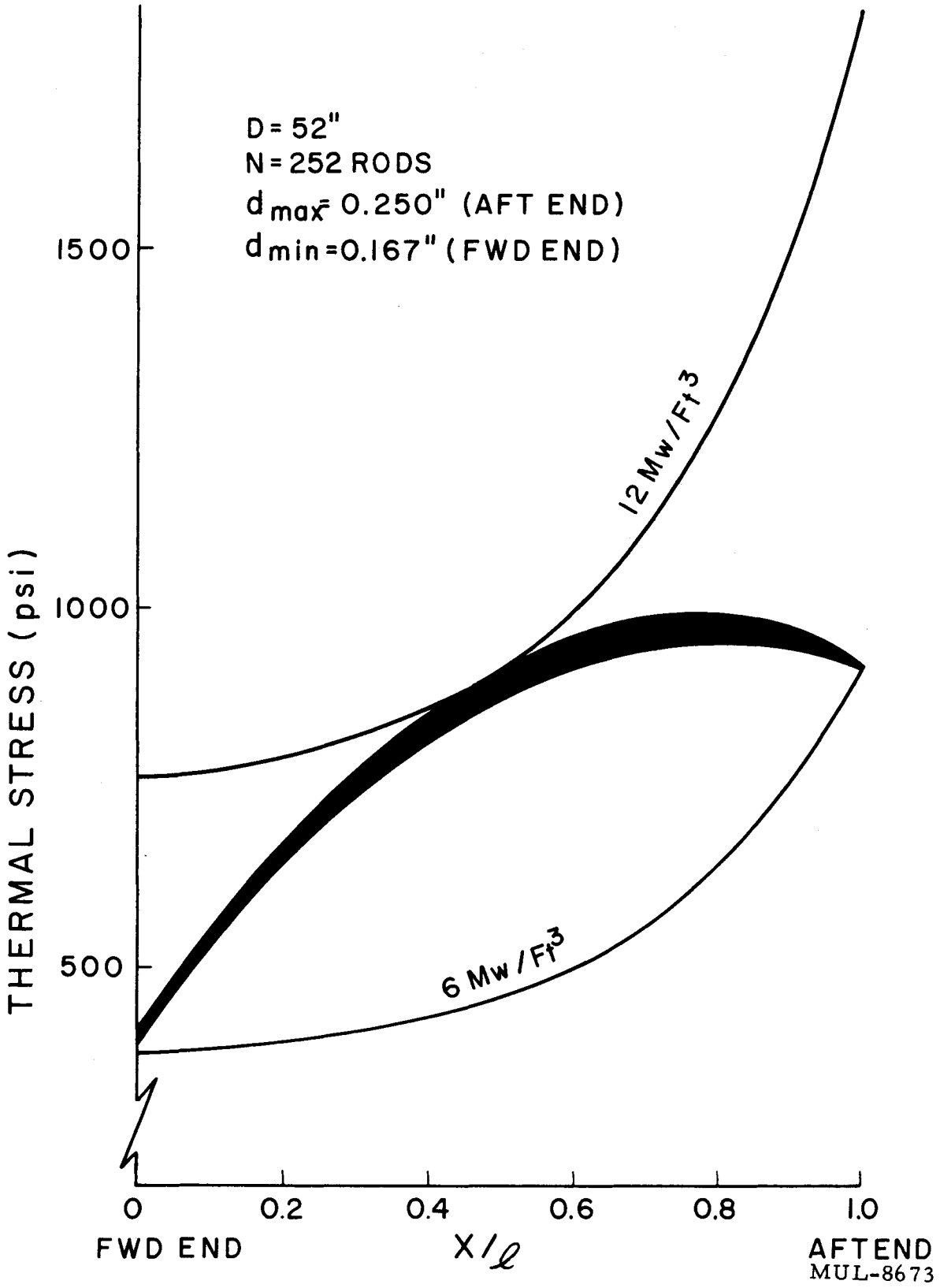

Fig. IV-18. Thermal stress in tie rod vs position in INTEGRAL reactor.

C. Tray Core Design

The tray core design evolved from considering three demanding requirements for mechanical support of a ramjet missile core. One of these is that the axial pressure-drop loads and transverse missile "g" loads be simultaneously reacted. Secondly, differential thermal expansions between core components must be accommodated without restraint. The third requirement is that the air-borne core be supported within the smallest possible airframe diameter.

With regard to the first two requirements, each tray reacts the axial pressure drop and transverse "g" loads at the pressure duct through flexible support tabs. By being flexible these tabs can allow differential expansion between tray and pressure duct within acceptable stress limits for the tab material. The requirement for support within the minimum airframe diameter is fulfilled in the tray design by utilizing the airframe pressure ducting directly to react axial pressure-drop loads within the core. The tray scheme for core support joined with the concept of integrating airframe and reactor will result in the smallest practical airframe diameter surrounding the core.

Material Choice

The condition that tray metal would eventually be used at reactor cooling air temperature guided the choice of sheet metal materials. The range of temperature for Tory II-C cooling air indicates two sheet materials for tray fabrication. Below 1600°F a superalloy would be used. Above 1600°F a molybdenum alloy would be used.

There are three superalloys with adequate strength and creep resistance for tray service at 1600°F. Of these, R-235 was chosen because it is least objectionable neutronically. Also, our experience with this alloy for the Tory II-A shroud proved it to be easily fabricated. R-235 is commercially available.

For service at 1600°F and above, Tory II-C trays will be made from the 1/2% titanium alloy of molybdenum. This alloy has adequate strength and creep resistance to 2100°F. A wide interest in this sheet material over the past decade has produced a large background of fabrication experience which can be applied to the Tory II-C tray component. A new alloy is in a semi-commercially available status. This is the 0.45% Ti+0.07% Zr alloy now being evaluated in the McDonnell-General Electric development program. It extends the useful strength temperature to 2500°F.

Successful oxidation protection systems for molybdenum sheet metal components operating at Tory II-C temperatures have been developed. Of these, the Inconel cladding system is considered to be the most reliable for tray application at present. The basic sheet would be clad with about 5% thickness of Inconel during rolling, and sheared edges will be sealed over during fabrication. The Inconel clad provides a tough, ductile, abrasion-resistant protection for the basic sheet. The favored temperature range for clad molybdenum is up to 2100°F.

Testing of an 18-in.-diam model tray of Hastelloy R-235 is complete. Instrumentation included 160 strain grids and 10 deflection gages.

In general, the test model proved that the tray structure is extremely rigid to pressure drop loading. This is because the compression edges of the radial webs are stabilized by the fuel blocks. At a load equivalent to the Tory II-C full flow pressure drop load, maximum tray deflection was less than 1/10th inch. Since diameter-to-depth ratio was preserved in the model, this is about the deflection that would be expected in a full scale tray. Failure was declared when one radial web began to tear at the outer joint. This failure occurred at a load equivalent to five times the Tory II-C full flow pressure drop load.

The strain gage data are considered reliable. They will be analyzed and used in the design of a 32-in.-diam test tray.

D. Conceptual Design for a Tory II-C Reactor Containing No Metal Parts

Introduction and Discussion

Use of a ceramic dome as the major structural element for the intended application is not new. Similar proposals are found in Refs. 1 and 2. Graphite dome-like structures have been considered for the Rover Project.[3]

An effort has been made to concentrate here on the items most affecting feasibility. Discussion of many details of the design, which it is believed do

---

[1] Oak Ridge National Lab., Oak Ridge School of Reactor Technology Reactor Design and Feasibility Problem, "Ceramic Jet Nuclear Power Plant", CF-56-8-202, Aug. 1956.

[2] Curtiss-Wright Corp., Quarterly Progress Report for Period Ending Sept. 30, 1956, Report No. CWR-445.

[3] R.B. Meuser and R.J. Vetterlein, A Preliminary Design Study of a Nuclear Rocket, UCRL-4779, Oct. 1957.

not affect feasibility, have been omitted. Dealing with the matter of feasibility, there is one area where the doubts are considerably graver than any other: i.e., the ability to sustain the very large (ca. 250,000 lb) loads produced by flow of air through the reactor. All serious design proposals require that this load be carried by structural elements which are at or near exit air temperature. Some proposals depend on coated molybdenum alloys as this structural material. The feasibility of the base dome design is dependent on sustaining the longitudinal load. The crucial dependence is on ceramic fabrication techniques and the structural integrity of a ceramic structural element rather than on a satisfactory molybdenum coating.

For inertial loads to produce forces as large as that associated with the pressure drop would require load factors of about 32 g. It is possible to transmit the inertial loads from the core through an insulating material to metal structure at temperatures tolerable to non-refractory metals.

Thermal stress in the fuel elements has been largely ignored because:

(1) The design appears to have good tolerance to thermally induced cracks.

(2) For the mission under consideration it is conceptually possible that power and temperature history, especially during the crucial launching phase, can be specified. These factors could have a very strong effect in reducing cracking due to thermal stress.

Since one of the main purposes here is to provide a basis for comparison with other designs, and since no differences in approach to the control problem for the several design proposals are now envisioned, no consideration is given to reactor control.

Base Dome Fabrication and Fuel Element Considerations

The self-bonded, dense SiC under consideration has strength and oxidation characteristics which are at least comparable with other ceramics.[1] The following factors appear to give it advantage over other ceramics from a manufacturing standpoint:

(1) Complex shapes can be formed cold in metal molds after which machining in the unfired state proceeds quite readily. It has been demonstrated that the forming can include making large numbers of closely spaced holes.

[1] E. Glenny and T.A. Taylor, The High-Temperature Properties of Ceramic and Cermets, Powder Metallurgy, 1958 No. 1/2.

(2) The shrinkage resulting from the firing operation is of the order of 1%. This is much less than that associated with the firing of most other ceramics of interest for this purpose, and it should result in dimensional control which is adequate without resort to grinding of the fired piece.

There is a possibility that silicon carbide bonded graphite would be more suitable for this purpose than the dense SiC. This material consists of particles of free graphite dispersed throughout an SiC body. It has better thermal shock resistance, but poorer strength and oxidation resistance.

In such a reactor, it is desirable, from the standpoint of assembly and reactor rigidity, to have fuel elements as large as possible. One limitation on size arises from flow-passage misalignments due to temperature differences in adjacent elements. This misalignment is approximately proportional to element size. Misalignments associated with elements which the A-I facility can make (hexagons about 5 in. across flats) appear to be completely acceptable. Single-hole elements have a wall thickness which is one-half that in multiple-hole elements, and consequently are more apt to encounter difficulties with crushing due to the restraining lateral forces. With tube elements, motions where the ends of the element act as a hinge appear to be kinematically possible. This is not so with plate-type elements.

In a core made of plate-type fuel elements and restrained against motion entirely from the outside, cracks due to mechanically and thermally induced stresses are almost certain to occur. However, the restraining forces will not tend to open up cracks which occur, but to maintain them closed in positive fashion.

Air Flow and Cooling Considerations

Reactor performance requirements lead to specification of the size of air flow passages in the core as well as the core porosity. These have been taken to be 0.25 in. and 55%, respectively. Maximum thickness of the SiC base dome is of the order of 15 in. Forming holes that have these proportions in the SiC base dome is quite difficult. In addition, pressure losses in these parasitic holes would be excessive. Consequently, it is proposed to duct the flow from several core flow passages into a single hole in the base dome. The porosity in the base dome would be approximately the same as that in the core, so that the Mach number is approximately the same in the base dome as at the exit of the core.

In order to avoid choking conditions it is required that the transition from core flow passages to the larger passage not reduce the available flow area. This can be done by having a "transition piece" between the core (containing small holes) and the base dome (containing large holes). Table IV-5 shows how diameters of the large hole vary with number of holes ducted together.

TABLE IV-5

No. of small holes manifolded	Small hole diameter (in.)	Large hole diameter (in.)
3	1/4	0.433
4	1/4	1/2
7	1/4	0.661

In order to maintain a side reflector temperature which is approximately the same as the core temperature, it is necessary to have a reflector porosity of approximately 5%. Where the base dome has parallel holes through it, it is necessary to duct the reflector flow through the base dome and into the region downstream of the reactor. Figures IV-19 and IV-20 show a way in which this might be done. It is apparent that it would be difficult to handle substantially increased reflector flow in this fashion.

Cooling of the metallic parts adjacent to the core (the conical ring supporting the base dome and the "girdle" providing lateral support) is accomplished easily if one assumes the availability of a material possessing reasonable compressive strength and low thermal conductivity. Average compressive stress on the material at the conical seat is of the order of 500 psi, whereas those adjacent to the girdle are of the order of 100 psi. In both cases it appears that the insulating material would be well confined. Stabilized zirconia or foamed SiC both appear to be adequate for these requirements. The temperatures obtainable in these metal parts appear to be easily consistent with commercially available nickel alloys.

Loads and Stresses (Other than in the Base Dome)

The proposed configuration consists of several thousand individual semi-elastic blocks supported on a single approximately rigid base and encased in a single sheet metal sleeve which undergoes yielding during the start-up phase. The entire assembly is pushed on from the inlet end (to insure stability). The

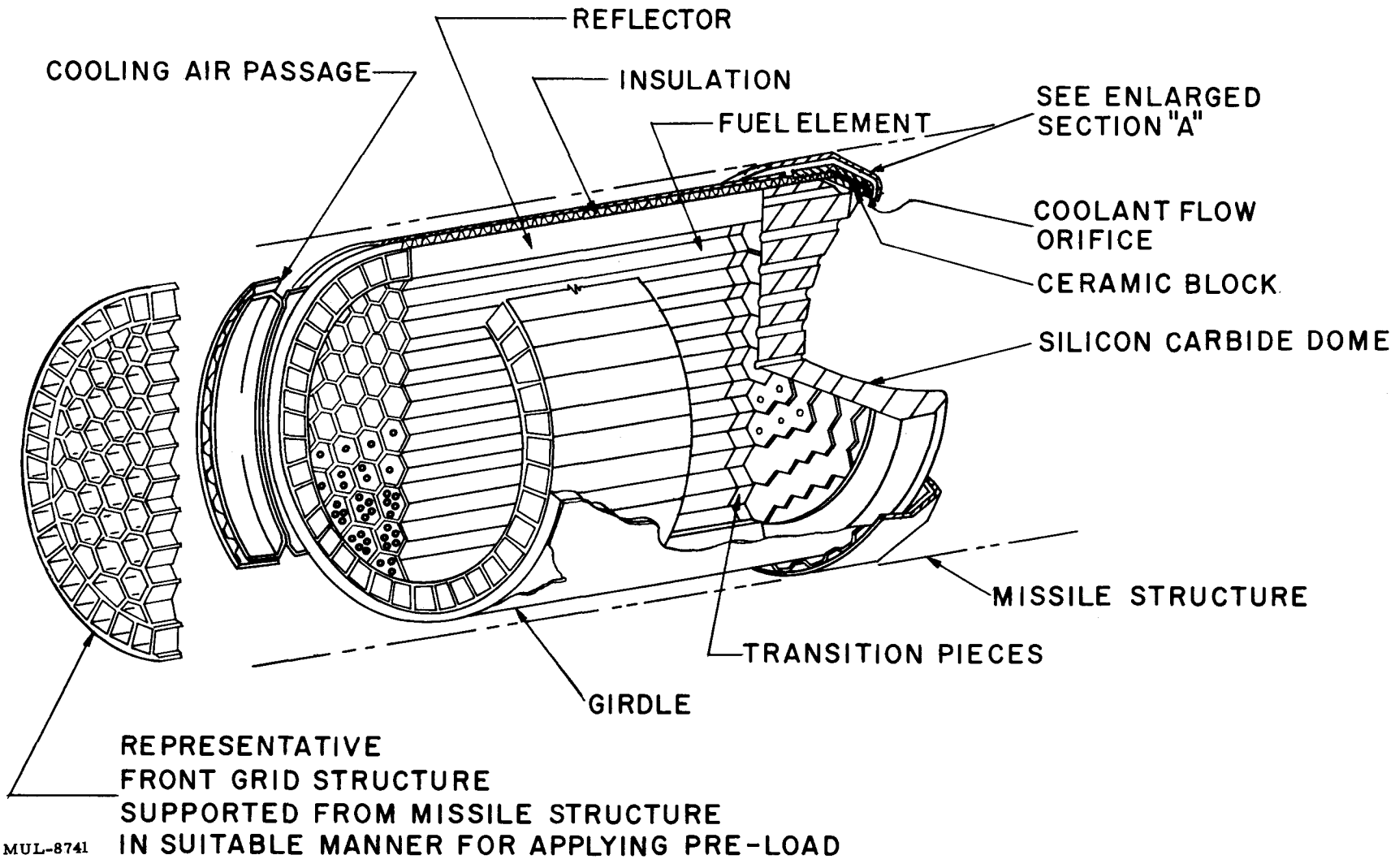
REFLECTOR
COOLING AIR PASSAGE
INSULATION
FUEL ELEMENT
SEE ENLARGED SECTION "A"
COOLANT FLOW ORIFICE
CERAMIC BLOCK
SILICON CARBIDE DOME
MISSILE STRUCTURE
TRANSITION PIECES
GIRDLE
REPRESENTATIVE FRONT GRID STRUCTURE SUPPORTED FROM MISSILE STRUCTURE IN SUITABLE MANNER FOR APPLYING PRE-LOAD
MUL-8741

Fig. IV-19.

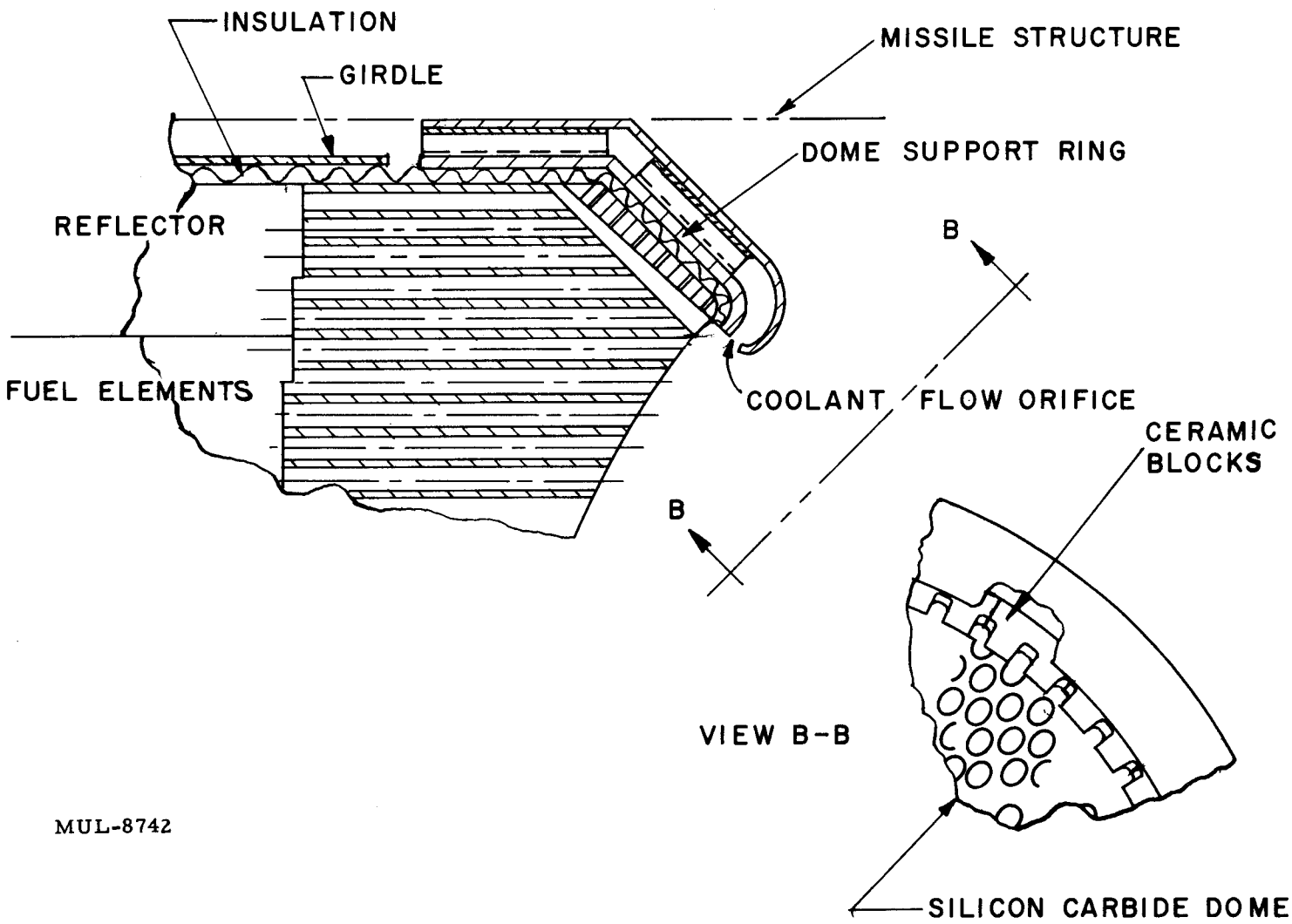

Fig. IV-20. Section "A" (see Fig. IV-19).

forces between the bodies are normal and frictional forces on all surfaces. Sources of stress are:

(1) Forces associated with flow through the core. These forces on the fuel elements are applied as shear forces on the flow-passage walls, and as pressure acting on the faces of the elements normal to flow. Since these are rather well distributed, they can be effectively treated as body forces.

(2) Body forces due to acceleration and gravitational attraction.

(3) The preload applied at the front of the core.

(4) Radially applied pressure caused by:

(a) The existence of essentially inlet pressure on the outside of the "plastic girdle" creating an inwardly directed differential.

(b) Tension in the "plastic girdle" caused by initial prestress and a tendency of the core to expand more on startup than the girdle.

It is practically impossible to specify an exact state of stress in the reactor. This fact should have no bearing on whether or not the design is used, provided crude but sufficient methods of analysis demonstrate its satisfaction of the required conditions. Despite the analytical difficulties there are strong intuitive arguments to favor supporting a core by forces arising from outside the core. In fact there appears to be a good possibility that the design would be adequate for a one-shot operation if the girdle had no strength at all in the usual sense of the word, but acted only as a pressure barrier. These stresses are:

(1) The forward preload, the pressure drop forces, and the radially applied forces tend to superpose a triaxial compressive stress on whatever other stresses may exist. Provided allowable compressive stresses are not exceeded, it is clear that stability of the stack of blocks can be insured by sufficiently high values of these external forces.

(2) These external forces (very modest in terms of compressive stress) originate either as air pressures or as loads supplied by metallic elements. Consequently there seems to be no question of feasibility. There is, however, a requirement for an insulating material adjacent to the metal structure which must sustain these low compressive stresses.

The following analyses deal with maintaining the integrity of the core. Consider a model consisting of slices having no bending stiffness but having compressive stiffness. Assume there is no friction between the slices (this will be discussed later). Such discs might be considered to consist of short

parallel rods, having no friction between them. This model appears more appropriate than a model consisting of plates having bending stiffness and extending across the entire reactor width because the proposed reactor may consist of small plates not capable of transmitting bending from one to the other. Let it be supposed that these discs are constrained from lateral motion by a sleeve which surrounds them. Such discs are acted upon by reactor loads. A disc is shown in Fig. IV-21.

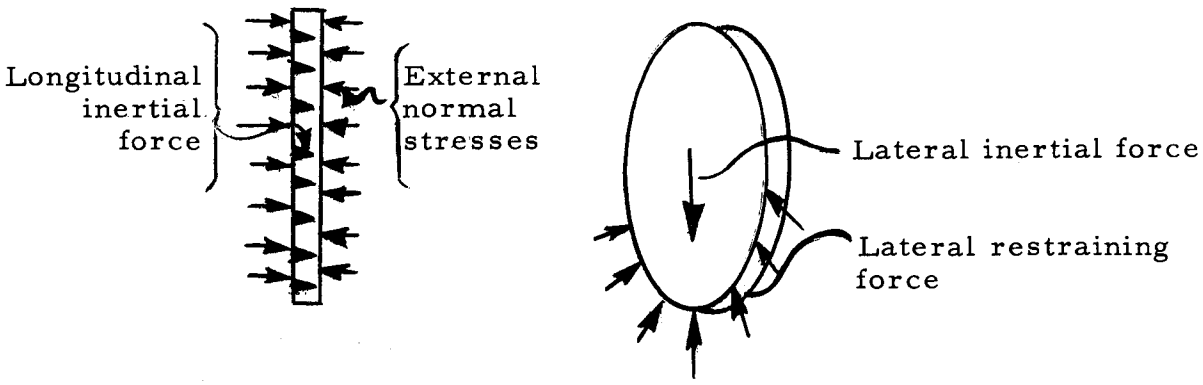

Fig. IV-21.

Consideration of several such discs makes it apparent that the external normal stresses (as referred to in Fig. IV-21) consist of the externally applied stresses at the front of the reactor plus the summation of the longitudinal inertial and pressure drop forces forward of the section in question. The lateral inertial forces have no effect upon longitudinal normal stresses. This conclusion is of questionable value in that it is wholly dependent on the assumption that there are no shear stresses transferred between the discs. In reality there are frictional forces between the elements.

If the core is supported laterally at both ends (Fig. IV-22), then it is reasonable to expect that the section with the greatest bending moment is the

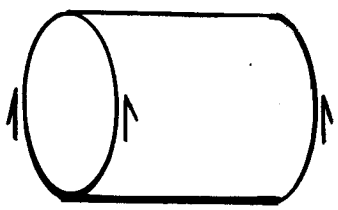

Fig. IV-22.

one with the most tendency for fuel elements to separate. However, that section has zero transverse shear on it, so that the anticipated stress situation should tend to be like that in the above model (deviating from that expected in an elastic solid).

The most useful purpose which the model discussed here may fulfill is to define upper limits on the shearing and bending strengths required of the girdle (i.e., the model ignores any shear and bending stiffness contributions from the stack of blocks – which surely exist). Let it be assumed that the "girdle" consists of a single layer of sheet metal 0.050 in. thick. The reactor diameter is taken to be 52 in. and its length to be 48 in. Its weight is approximately 8000 lb, and the lateral load factor is taken to be 5 g. The stress level is 2260 psi in the sheet.

The maximum shear occurs at a cross section near either end, and is equal to half the transverse load or 20,000 lb.

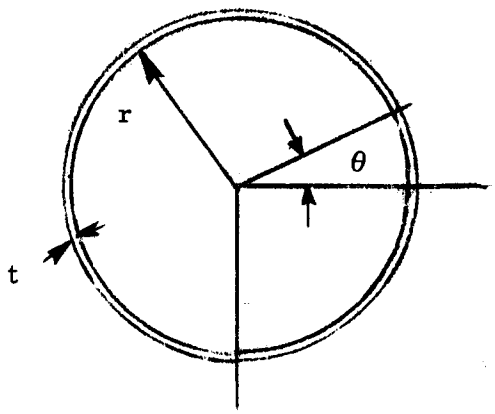

Fig. IV-23.

Assuming that the circumferential shear stress τ varies as cos θ (Fig. IV-23) (this follows assuming a displacement between adjacent slices), then it follows that the shearing stress is

$$V = 4\tau_m tr \int_0^{\frac{\pi}{2}} \cos^2 \theta \, d\theta = r\tau_m t\pi ,$$

where

$$\tau_m = \text{max shear stress} = \frac{V}{rt\pi} = \frac{20,000}{26 \times 0.05\pi} = 4900 \text{ psi}$$

V = shear force on the cross section

The "girdle" will be attached at the base dome end by having it fit closely over the base dome (Fig. IV-24) (perhaps an interference fit). The shear forces would then be transferred through the base dome to its support.

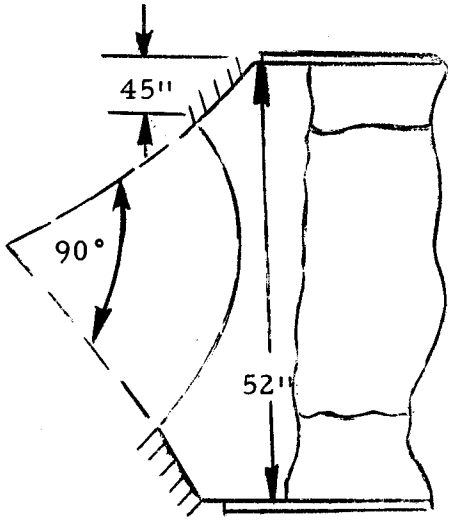

Fig. IV-24.

Assume that there is no friction between the base dome and the girdle and take the portion of the girdle surrounding the base dome as a free body as in Fig. IV-25. Since no friction is assumed, it is permissible to conduct a

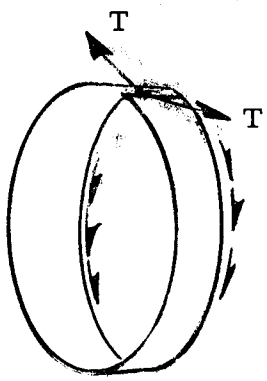

Fig. IV-25.

summation of forces in the circumferential direction. If it is assumed that the tensile force in the hoop-shaped piece (Fig. IV-25) diametrally opposite the cut section is zero (consistent with yielding or incipient motion), then it follows that the tensile force T = V/2 = 10,000 lb. Since the 5-g lateral load of interest here is of a transient nature, it appears reasonable to base its design on yielding considerations rather than stress rupture or creep strains. If an allowable stress of 30,000 psi is used, then a total cross-sectional area of 0.33 in^2 is needed.

Another approach to determination of the tendency of the core to open up on transverse cross sections is to consider the fictitious elastic beam having the same shape as the reactor. Assuming that the normal stresses on transverse cross sections are compressive and governed by the beam-column relation,

$$\sigma = \frac{P}{A} \pm \frac{Mc}{I} ,$$

then it should be possible to predict when the stresses change from compression to tension ($\sigma = 0$).

Expressed differently, the criterion to avoid tensile stress is that $P/A > Mc/I$. Figure IV-26 plots Mc/I for 5-g and 10-g transverse loads and P/A for a Tory II-A condition (assumed to be typical).

Actually the above approach is somewhat conservative because:

(1) Longitudinal normal stresses in the girdle are neglected, and these would develop to prevent or limit cracks opening.

(2) When rigid body motions of a pile of blocks necessary to open a crack substantially are considered, it is apparent that the condition required is that the resultant be outside the cross section.

During the launching phase the stresses associated with flow (P/A in Fig. IV-26) increase monotonically with time from zero. There are, however, inertial forces associated with boost acceleration which substitute in some measure for the flow-induced stresses above. For higher altitude flight (e.g., right after launching) the flow-induced stresses are reduced (compared to those of Fig. IV-26) in either of these cases, and if there is any tendency to separate on transverse joints then the data of Fig. IV-26 makes it clear that a modest preload on the front overcomes the tendency to instability.

The single-layer sheet metal "girdle" proposed here appears quite suitable for single flight operation. During the portion of launching where pressure differentials are low, the reactor tends to grow due to thermal expansion relative to the girdle. This condition will insure circumferential tension and a desirable stabilizing effect. After appreciable pressure differential has built up across the girdle, then these pressures in themselves can largely perform the stabilizing function just associated with the tensile force in the girdle. If there is a tendency (in flight) for the reactor to shrink relative to the girdle, the external pressure would cause a local wrinkling of the girdle and it should continue to perform its function satisfactorily.

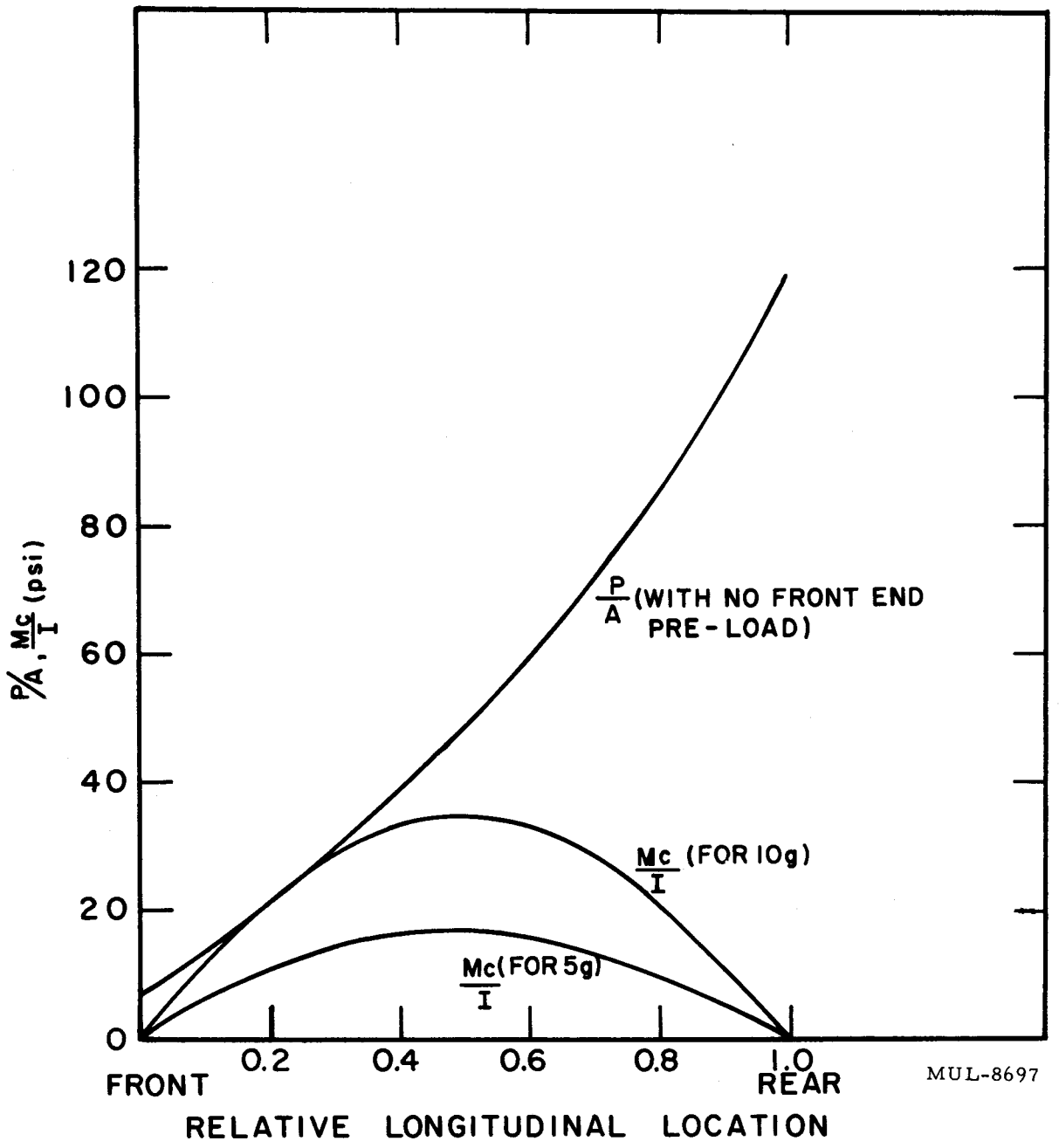

Fig. IV-26. Plots of Mc/I for 5-g and 10-g transverse loads and P/A for a Tory II-A condition.

It would be necessary, however, to shut down and restart test reactors. If the reactor were held at temperature while flow were reduced to zero, and then the reactor were cooled to ambient, a gap would develop between the reactor and the girdle. If, however, the flow were maintained while the reactor were cooled, the differential shrinkage associated with cooling would cause local wrinkling to develop as the inward differential pressure tends to put compression in the girdle. It is possible that repetitions of this procedure would cause intolerable cracking of the sheet metal. If that were the case then it would be necessary with a test reactor either to arrange to replace the "plastic girdle" periodically, or use an "elastic girdle," i.e., one configured somewhat differently such that radial forces are maintained for all conditions as a result of elastic strains.

As stated before, the foregoing analyses are crude. We will investigate experimentally the problems just discussed. Many of the answers needed can be categorized as dealing with the stability of stacks of appropriately shaped and loaded rigid bodies. The loads can be simulated by means of external pressures, inertial forces (centrifuge or drop table), and pressure drops through permeable bodies. These tests will be conducted on a reduced dimentional scale.

Calculations dealing with hoop tension in the base dome support ring reveal that a thickness of about 3/16 in. is adequate.

Stresses in the Base Dome

It is of interest to examine in general terms the stresses in an axially symmetric dome having no bending stiffness. This is done in Ref. 1 for domes having uniform thickness and acted on by gravity. The domes are oriented with gravity and the dome axis parallel, and with the concave side downward.

For the corresponding two-dimensional case (arch) there is only one form that permits equilibrium. That shape is the catenary. Any other shape requires bending moments as well as axial forces to insure equilibrium.

The situation is somewhat different in a dome. Analytically, circumferential normal stress and the normal stress perpendicular to the circumferential one can be treated as two variables (instead of one as in the arch). A consequence of this is that any axially symmetric dome is stable provided

[1] J. N. Goodier, Stresses in Domes and Crowns of Circular Kilns, J. Am. Ceram. Soc. 16, 220 (1933).

only tension and compression are permitted. If compression alone is permitted, then a rather large range of shapes is possible. Among these shapes are cones and surfaces of revolution defined by parabolas and catenaries, as well as caps of spheres where the included angle is less than 104°. Since in the proposed shape for a dome there are substantial differences from the idealized domes just discussed, the conclusions are apt to be of interest only for general guidance.

A logical method of arriving at the selected shape is presented below. A spherical cap permitting radial flow through the cap, as the only means of inducing load, would yield only compressive stresses (for the idealized case as above). However, in the case at hand the major load to be contended with is that induced by flow through the core and transferred by solid contact from the core. It is thus all longitudinal. A spherical surface is not very well adapted to receiving such a force. Consequently, it seems logical to make the upstream surface of the dome flat. Leaving the other surface of the dome spherical, it remains to select the relative proportions (thickness) and the included angle at the support. Since it is difficult to fabricate pieces containing holes with nonparallel axes, they should be parallel.

Three considerations govern selection of the included angle at the support. The base dome will grow substantially during start-up with respect to the support ring for the dome. If the included angle at the support is sufficiently small (determined by the coefficient of friction), sliding will not take place and high stresses will be induced in the support ring and the base dome. If, on the other hand, the included angle is too large, the piece requires an inordinately large depth. Also an "ideal" spherical dome where the included angle at the support is greater than 104° exhibits tension. In view of these, an included angle of 90° was selected. For this angle it can easily be shown that a coefficient of friction must be greater than 1 for a locking condition to exist.

For the geometry of the base dome, shown in Fig. IV-24, a pressure of 130 psi applied uniformly over the entire area of the flat section of the dome leads to a reaction pressure (p_r) of 410 psi (based on the entire conical area). Reference 1 discusses a perforated plate with webs which are thin with respect

[1] G. Horvay, The Plane-Stress Problem of Perforated Plates, J. Appl. Mech. 19, 355 (1952).

to the hole diameter. Applying the methods of this reference, the compressive stresses tend to be greater than those in the corresponding solid plate by a factor equal to the ratio of the hole spacing to the web thickness. For the selected proportions, this ratio is 0.811/0.151 = 5.37; this would lead to a compressive stress of 5.37 × 410 = 2200 psi.

Reported values of room temperature compressive strength of SiC vary from 150,000 psi (Ref. 1) to 250,000 psi (Ref. 2). Modulus of rupture values actually increase with temperature. At operating temperatures a compressive strength of 100,000 psi would exist. While the 2200 psi value represents idealistic assumptions as to stress distribution, it is doubtful that the deviation from "ideal" is sufficient to increase it to 100,000 psi.

The force caused by the 130-psi load is 276,000 lb. Considering that the weight of the core is 8000 lb, it appears clear that any compressive stresses caused by inertial forces are small compared with those produced by the pressure forces.

There is the possibility that thermally induced stresses in the base dome will cause cracking. One of the apparent advantages of a dome-shaped piece is that for most anticipated crack patterns the normal condition of compressive stress parallel to the lower surface would not cause the cracks to open, but rather to hold them closed.

A specific situation that might lead to thermally induced cracks occurs during start-up. The central portion of the base dome will be heated more rapidly than that part receiving flow from the reflector. This leads to circumferential tension in the outer portion of the base dome. It is proposed to saw shallow slots, as in Fig. IV-27, at several circumferential locations to predetermine the course of these cracks.

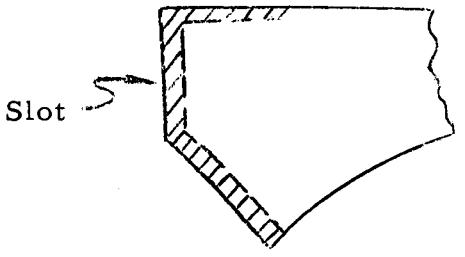

Fig. IV-27.

[1] L. M. Litz, Graphite, Carbide, Nitride, and Sulfide Refraction, Advance papers for the High Temperature Technology Conference held at Asilomar, Calif., Sept. 6-9, 1959.

[2] The Carborundum Co., unpublished literature on SiC.

Three alternatives with respect to the dome are:

(1) To make the dome of silicon carbide bonded graphite. This material is fabricated by processes similar to those for self-bonded SiC. It has lower mechanical strength but improved thermal stress resistance.

(2) To fabricate the dome of a number of tapered pieces which fit together brickwork fashion. However, the one piece approach may be preferable for the following reasons:

(a) Stress-induced cracks are able to transmit compressive stresses better than fabricated cracks.

(b) If an attempt is made to calculate the number and location of cracks which would occur and provide them in advance, it is likely that the estimate will be high. A fewer number of cracks in any structural element generally means greater redundancy and rigidity.

(c) Studies dealing with the possibility of reinforced ceramic aircraft wings concluded that the fundamental difficulty was that of transmitting high compressive stresses across manufactured joints in the ceramic.[1]

(3) It may be possible to cast such a piece. If so, holes with nonparallel axes would be preferable.

E. Tory II-C Materials Testing

Plaster Base Dome Tests

Tests of 12-in.-diam plaster domes having a cross section as in Fig. IV-28 have begun. The domes do not contain holes and are supported on the conical surface. They are loaded on the flat upper surface by water pressure acting through a rubber diaphragm.

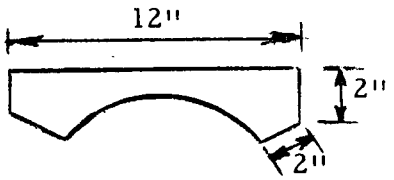

Fig. IV-28.

The objects of these tests are to observe the mode of failure and to compare the approximate level of compressive stress in the dome with compressive strength as determined from cylinder tests.

[1] F.R. Shanley et al., Prestressed Ceramic Structures, WADC-TR-54-75, Parts I and II.

So far three tests have been conducted. These have sustained water pressures of 650, 500, and 900 psi. Assuming that there is uniform compression in the dome leads to compressive stresses in the dome of about twice the water pressure. The cylinder strengths have not yet been determined. The compressive strength of plaster of paris is in the range of 2000 psi. Failures have generally been compressive, as evidenced by cracks intersecting the lower surface at an angle of about 45°, although a few tension cracks (intersecting the lower surface at 90°) have been observed. In general, failures are not sudden, and substantial deflection occurs with retention of load-carrying ability. The one sustaining the highest load did so at a deflection of 1/2 in.

Model Tray Test

The purpose of this test of a model of the ceramic-block in metallic-tray core concept is to:

(a) Determine the spider deflections due to various loads.

(b) Determine the mode of buckling and the buckling load.

(c) Determine the effects of clearance on deflection and/or buckling of side restraint clearances.

The test setup is as shown in Fig. IV-29. The test is currently in progress.

Transitions from Multiple-Hole Flow

The purpose of this test was to determine the pressure loss that occurs when the flow from seven close-packed tubes is collected into a single tube of area equal to that of the seven smaller tubes. Two transition sections were investigated.

The first region consisted of a close-packed array counterbored to the diameter of the large tube to a depth equal to one-half the diameter of this tube. The second region consisted of milled slots circumscribing each of the outer six small tubes and converging into the single tube at an angle of 30° to the tube axis.

The length of the single tube section downstream was 10 diameters.

This test has been completed and data reduction is presently in progress. Preliminary results indicate that:

(a) Pressure drops are twice as high at a given flow rate in the counterbored section as in the other.

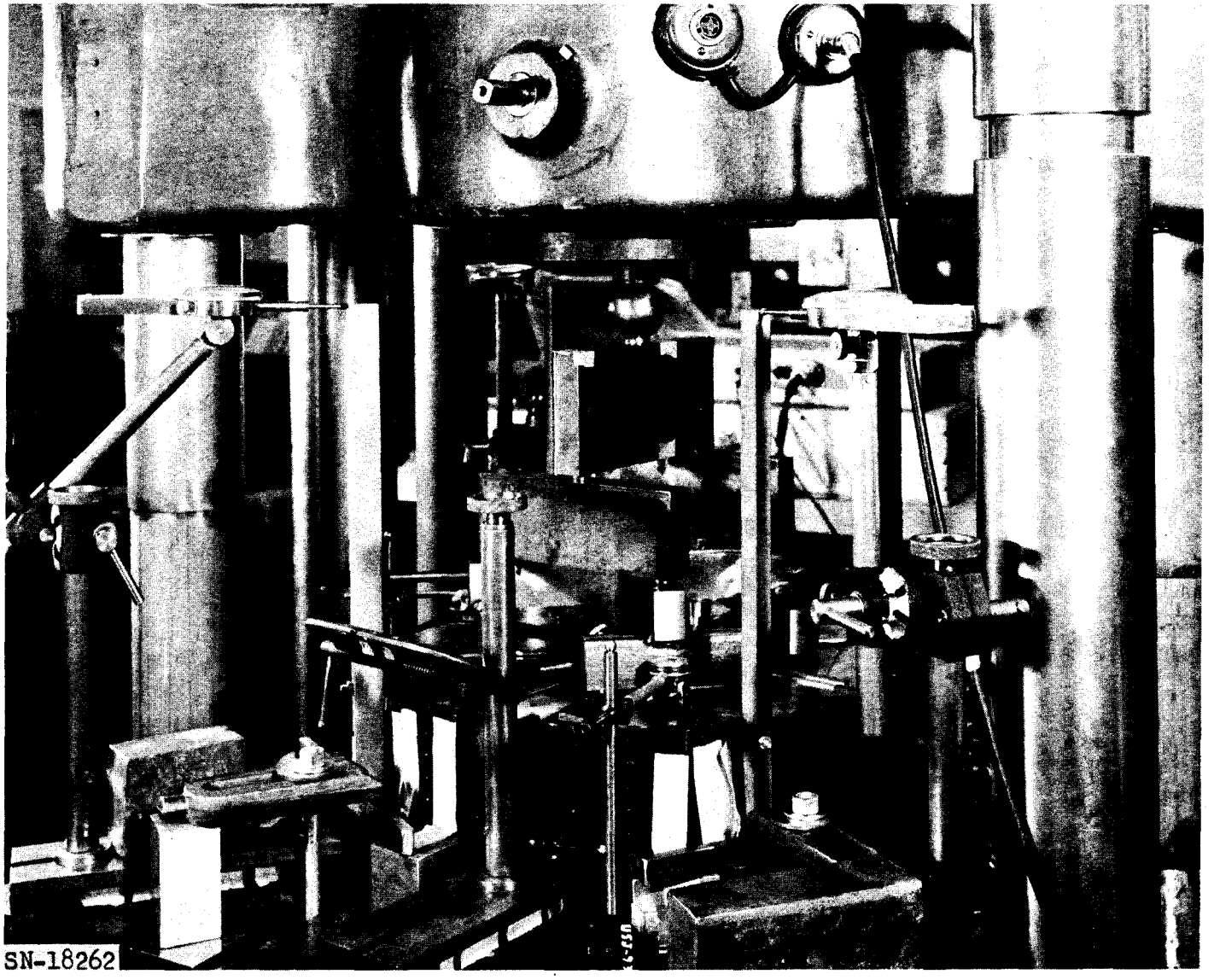

Fig. IV-29.

(b) Maximum obtainable Mach number at the point immediately preceding the transition section is approximately 0.45 in the counterbored case and 0.60 in the milled section.

(c) Maximum total pressure drop is on the order of 20% in the counterbored case.

Silicon Carbide Flexure Tests

Flexure tests were conducted on three types of silicon carbide bars. The types are hot-pressed SiC, the proprietary "KT" SiC, and silicon carbide bonded graphite (GRB). All three types were manufactured by The Carborundum Co. Table IV-6 summarizes the data.

TABLE IV-6

(All bars were tested on a 3-in. span with center loading)

Type	Approx. cross section (in.)	Temp (°F)	Modulus of rupture (psi)
KT	0.45 × 0.26	2100	23,200
			25,900
			18,600
		2500	19,400
			23,300
			22,100
Hot-Pressed	0.43 × 0.16	2100	55,700
			39,700
			60,000
		2500	43,000
			56,500
			57,800
GRB	0.45 × 0.16	2100	11,400
			10,900
			12,100
		2500	9,700
			13,400
			10,500

/md